EVALUATION OF MECHANICAL PROPERTIES OF TEXTILE CONCRETE SUBJECTED TO DIFFERENT ENVIRONMENTAL EXPOSURES

Siphila Wanjiku Mumenya

Thesis submitted for the degree of

DOCTOR OF PHILOSOPHY

at the

UNIVERSITY OF CAPE TOWN

2007

Declaration

I declare that the work presented in this thesis is my original work. I also affirm that this work has not been presented in this, or any other university for examination, or for any other purposes.

SIPHILA WANJIKU MUMENYA
2007

Abstract

Cementitious materials have been used for construction since ancient times and their properties are well documented and understood. The main limitation in these materials is their low tensile strength and inherently brittle type of failure which occurs due to cracking under tensile stress systems or impact loading, primarily due to the propagation of internal flaws. This has conventionally been compensated for by the use of steel reinforcement at the macro-level, and short discrete fibres at the micro-level. By appropriate addition of fibres to cementitious compounds, discrete cracks may be sufficiently bridged thus providing for some control to the fracture process and hence increasing the fracture energy.

Within the last decade, a new class of civil engineering materials referred to as High Performance Fibre Reinforced Cementitious Composites (HPFRCC) has been developed. As a subset in this new field, additions of polypropylene (PP) fibres, in the form of woven textile fabrics, have proved most successful as reinforcement to cementitious matrices, leading to the development of a novel composite material: so called "Textile Concrete" (TC). Although the strength and modulus of PP are not very high, careful design through the appropriate placement and high fibre volume fraction of a textile format, has led to sufficient strength and stiffness, while at the same time high toughness has been achieved. In particular the development of a fibrillated core fibre to which is attached an outer layer of ultrasonically welded, or bonded "fluffy" PP fibres, has been most successful, and is a unique feature. These outer fluffy layers provide excellent physical bonding characteristics to the cement matrix, thus overcoming the intrinsic hydrophobic nature and

otherwise weak matrix bonding of PP fibres.

In South Africa where TC has found ready application, the composite is produced from a fine grained cementitious matrix and a PP textile commercially known as CemForce. TC is not solely a South African concept and is gaining popularity in other parts of the world.

For long-term use and wide acceptance in the market place, a better understanding of durability and degradation susceptibility of TC is needed. Indeed, if ageing and the long-term performance of TC could be understood and accounted for in design, the composite could be a possible replacement for other forms of fibre cements. This aspect of durability performance of TC is the focus of this research.

This thesis contributes to the understanding of the effects of ageing on the mechanical performance of TC, and evaluation of the processes affecting its behaviour after exposure to different environments. This was achieved through mechanical characterisation of the matrix, fibres and their interface as well as the composite tensile behaviour. Parallel studies were undertaken on specimens aged under controlled laboratory conditions for specified periods, and samples weathered under a reasonable range of "ambient" surroundings commonly encountered in service. Further, the effects of ageing were assessed by undertaking observations of fibre and interface features using a scanning electron microscope (SEM). An attempt was made to relate any changes in mechanical behaviour to the microstructure.

The specific objectives of the research were:

- To choose suitable mix proportions and hence produce mortar of good workability and flow characteristics.
- To assess any changes in mechanical behaviour over several months of ageing.
- To develop a dedicated accelerated ageing facility for assessment of long-term performance of TC.
- To establish the linkage between the mechanical behaviour and the microstructure at a phenomenological level.

- To develop a prediction model of multiple cracking of TC based on the analysis of the mechanical behaviour.

The main findings of the research were that cyclic Hot/Cold (HC) conditions were the most damaging to plain fibres, and carbonation densifies the matrix and makes it brittle. The results further indicated that direct exposure to sunlight of bare fibres caused loss in strength and embrittlement. The damage was ascribed to ultraviolet (UV) radiation but this was not tested. However, by embedding the fibres in the matrix, these effects were substantially reduced. On TC itself, this research showed that the fibre/matrix bond strength improves with ageing, and the composite exhibits "pseudo-ductility" due to multiple cracking with minimal strain softening and remarkable toughness.

It was concluded that Textile Concrete is tolerant to a range of exposure regimes. To elaborate this finding, limited exposure of TC samples to typically encountered natural environments was undertaken with no adverse effects being observed on the tensile behaviour of the weathered composites. It was further deduced from analysis of the results of mechanical tests that the following were the dominant mechanisms operating at the microstructural level: matrix embrittleness, matrix microcracking, changes in fibre strength and stiffness, and increase in fibre/matrix bond strength with ageing. These mechanisms were not always complementary but were sometimes competing and contributed to the mechanical behaviour of TC.

This research was limited to a single mortar mix which was suitable for production of TC using hand lay-up techniques. Therefore the influence of mortar mix proportions on the mechanical properties was not investigated.

For wider acceptance of TC in the market place, there is need for standardising the mix design, its production process, and incorporation of an environmental factor in the design. Thus the prediction of the engineering performance, such as strength and toughness may be possible leading to design of "fit for purpose" Textile Concrete products.

Acknowledgement

In work on a developing subject such as this, one is inevitably dependent on the advice of experts in specific topics. I begin by registering my appreciation to my supervisors Prof. R.B. Tait and Prof. M.G. Alexander who had faith in me from the beginning of the programme. They provided guidance and bore the burden of making me understand the philosophy of Fibre Reinforced Cementitious Composites, design of experiments, techniques of mechanical testing, and research in general. I thank them for providing the much needed positive criticism, for providing relevant reading materials, and for bringing me back on track whenever I seemed to drift away from my objectives. In addition, the assistance of Mr. Don Hourahane regarding the sourcing of textile material, and for facilitating my field trip *eGoli* (land of gold), is highly appreciated.

I am indebted to my sponsors, Universities Science, Humanities, Engineering Partnership in Africa (USHEPiA) for financing the programme. Their enthusiasm in sorting out all my financial research needs and helping me settle in South Africa was great. I wish to register my gratitude to Leslie, Reiner Canning, Nan, Carol, Zubaida and Masego for creating a USHEPiA family for me in Cape Town. At the Department, I am greatly indebted to Mrs. Clare Bloomer for efficiently managing my research fund and going beyond the call of duty in coordinating my numerous trips in and out of Cape Town.

I acknowledge the assistance provided by the staff in the Mechanical Engineering workshop; Messrs Glen, Horst, Martin, Len and Peter for their valuable advice and assistance in fabrication of specimen moulds and grips for

use in mechanical tests. In particular, I acknowledge the assistance given to me by Mr. Hubert Tomlison, who together with Steve, and Willy, were always available whenever there was a need to modify the rig. Many thanks also go to Julian for his assistance with the electronics part of my experiments. I am grateful to Prof. Knutsen, Prof. Lang, Norma, Penny Parker-Ross Doreen and Nandipa for their assistance in the materials testing laboratory.

I acknowledge the assistance given by Ms Elly Yelverton for keeping me updated on the activities in the Department of Civil Engineeering, Messrs Noor Hassen, Kyle Stanish, Charles May, Dion Manuel, and all the technical staff in the concrete materials laboratory regarding casting and testing of the specimens.

My warmest gratitude goes to my better half and husband Col. Dr. Mũmenya and my sons Soiyana Wambũgũ and Yohana Kago a.k.a. Kahĩĩ, for allowing me time off to pursue my research away from home, and for the many times they have had to reassure me to have faith in myself and to keep going and never give up. The many prayers offered on my behalf by my parents Rev. John Kago and Grace Kibũi will forever be appreciated.

I am sincerely thankful to Dr. Samuel Kwofie, without whose help modelling would have remained a daunting task. You made me appreciate the linkage in material properties and structural behaviour. To my office-mates Odesh Rambocus and Leon von Zwiklitz for your help in photography and trouble-shooting the computer problems I had to deal with in the course of my thesis write-up.

To Dr. Karanja Kibicho for his help in setting up of the experiment, for proof-reading parts of the manuscripts, and for being a participant on this lonely journey, I thank him most sincerely. My appreciation goes to my friends Kanuthu and Wangechi for always being there for me and for constantly reminding me "the darkest part comes before dawn". I am greatly indebted to Leah Sikoyo, for being a good neighbour at All Africa House. My feelings at this juncture are best expressed by a Gĩkũyũ proverb that encourages sojourners to keep going and never give up: "Gũtirĩ ũtukũ utakĩa".

Contents

List of Tables

List of Figures

Notation

The following notation has been used in this thesis. These are the basic symbols and they are defined in Chapters where they first occur. Unless otherwise defined in the local area of the text, the definitions for the symbols apply throughout the whole text.

c	Composite
d_f	Fibre diameter
E_c	Elastic modulus for the intact composite material
E_f	Elastic modulus for the fibre
E_m	Elastic modulus for the matrix
f	Fibre
g	Gravitational force
K_{Ic}	Crack tip fracture toughness
l	Fibre length
l_c	Critical fibre length
l_e	Fibre embedded length
l_1	Shorter fibre segment embedded in matrix
l_2	Longer fibre segment embedded in matrix
l_{cu}	Critical fibre embedded length
l_f	Fibre length
m	Matrix
N	Number of fibres bridging a crack
P	Load
P_1	Effective load at the end of the longer fibre segment

	embedded in matrix
P_2	Effective load at the end of the shorter fibre segment embedded in matrix
P_{max}	Load at maximum maximum point
P_{peak}	Peak load at onset of debonding
r	Fibre radius
V_f	Fibre volume fraction
V_{fc}	Critical fibre volume fraction
V_m	Matrix volume fraction
x'	Crack spacing
δ	Crack opening displacement
δ_1	Crack opening displacement corresponding to load P_1
δ_2	Crack opening displacement corresponding to load P_2
δ_b	Fibre bridging stress
δ_s	Stress at "saturated" cracking state
$\delta*$	Opening displacement for an "opening only" crack when all bridging fibres have completed debonding
ϵ	Strain
ϵ_{pc}	Strain capacity
$\epsilon(x)$	Strain along the embedded fibre segment
$\epsilon_m(x)$	Axial strain in the composite at the time of attainment of the maximum load P_{max}
ϵ_{cu}	Ultimate strain in the composite
ϵ_{fc}	Matrix cracking strain
ϵ_s	Strain at crack saturation state
$\epsilon*$	Peak strain at saturation state for a representative volume element
λ_m	Surface fracture energy of the matrix
ν	Poisson's ratio of the composite material
ρ	Density
ρ_w	Density of water

σ	Stress
σ_b	Fibre bridging traction
σ_{fc}	Composite first cracking stress
σ_c	Composite crack bridging stress
σ_{fu}	Fibre tensile strength
σ_{fc}	Composite first cracking stress
σ_{mu}	Matrix tensile strength
σ_{peak}	Composite peak bridging stress
σ_s	Stress at crack saturation state
σ_{ss}	Steady state cracking stress of the composite
$\sigma*$	Peak strength, or bridging strength, of a representative volume element at saturation state
τ	Average interfacial bond strength
τ_s	Interfacial bond stress (alternative notation)
τ_i	Initial frictional fibre/matrix interfacial bond stress
$\tau(x)$	Shear stress at the fibre/matrix interface at distance "x" along the fibre embedded segment

Chapter 1

Introduction

1.1 Introduction

This Chapter is an introduction of the contents of the thesis which covers the following: a brief introduction to the technological advancements in the field of Fibre Reinforced Cementitious Composites (FRCC), the motivation of the study, objectives of the study, and the structure of the thesis.

Over the last century, there has been growing interest in the performance of fibres, and recently, of woven textiles in cementitious matrices. The main reason for such interest is the need for an increase in toughness and tensile properties of the composite.

Since the early 20^{th} century, asbestos fibres have been most successful as fibre reinforcement to cement pastes in thin element applications, mainly due to the excellent chemical bond existing between the fibres and the cement-based matrices (Hannant 1978). However, due to problems related to the supply of asbestos in the long term, and also because of possible health hazards associated with handling of the fibres (Takahashi, Case, Dufresne, Fraser, Higashi & Siemiatycki 1994), the search for suitable replacements for asbestos fibre products has been on the increase. The possibilities for substitutes for asbestos in cement-based products range from natural to synthetic fibres.

Within the last decade, a new class of Civil Engineering materials re-

ferred to as High Performance Fibre Reinforced Cementitious Composites (HPFRCC) has emerged in the Industry with Textile concrete (TC) and Engineered Cementitious Composites (ECC) being sub-classes of HPFRCC.

TC is essentially a multi-layered laminate produced by casting textile fabrics in cement paste, mortar, or fine grained concrete. The mesh fabrics are commonly produced from Polypropylene (PP) because PP offers a combination of very attractive properties, namely resistance to chemical attack in the highly alkaline cement medium, resistance to degradation under moist environments, high elongation at break with low specific gravity, and no major handling difficulties (Hibbert & Hannant 1982). Thus, in South Africa for example, PP textiles, locally referred to as CemForce, have been specially manufactured for application in cementitious matrices.

Due to a wide range of applicability, this new material has found many uses especially in thin element formats such as: architectural and industrial cladding, simulated rock features for gardens, waterproofing, permanent shuttering forms which create superior products when used in conjunction with steel reinforcing bars, non-pressure pipes and many more. Figs. 1.1 to 1.5 illustrate the diversity in applications of Textile Concrete.

Being a relatively new product, TC technology is still at its infancy with sparse information, particularly on its mechanical performance under different environments. However, there is growing interest in mechanical characterisation of TC and in the recent past, the flexural and direct tensile behaviour of the laminates have been characterised (Tait & Guddye 2002), (Mumenya, Tait & Alexander 2003), (Mumenya, Tait & Alexander 2006). An extension of the research in the area of Textile Reinforced Concrete (TRC) has focussed in modelling of the material properties (Kabele 2003*b*). However, the durability, or long term performance of this new material is still a major concern and there is need for the establishment of a reliable method for assessment of its long term behaviour.

Figure 1.1: Architectural finishes

Figure 1.2: Artificial rock cladding

Figure 1.3: Residential garden applications

Figure 1.4: Permanent shuttering forms

Figure 1.5: Water-proof membranes for water reservoirs

In essence, there are two aspects of mechanical behaviour of TC that are investigated in this thesis: the interfacial bond property characterisation, and the tensile behaviour. In conventional FRC, these two properties have been the subject of research in the recent past (Banholzer, Brameshuber & Jung 2005).

The current understanding of the fibre-matrix interfacial mechanics is based on the response of an embedded fibre to a pull-out force, which is commonly investigated using so-called single "fibre pull-out" tests. Although it is sometimes believed that the mechanism of single fibre pull-out from a cementitious matrix is different from the bulk fibre behaviour in the composite (Banthia & Trottier 1994), the test is, nevertheless, a suitable means of initially assessing the effectiveness of the fibre as a medium of stress transfer. In the fibre pull-out test, the slip between the fibres and the matrix is monitored and the response expressed as a function of the applied load. The load-displacement relationship is then used in characterisation of the fibre/matrix interfacial properties.

The fundamental difference between HPFRCC and the conventional Fibre Reinforced Cementitious Composites (FRCC) is the behaviour in tension. In FRCC, fracture localisation occurs immediately after formation of the first crack, whereas in HPFRCC, the process of fibre bridging causes a second and subsequent matrix cracks to develop elsewhere thus preventing localisation of the first crack. This process results in propagation of multiple cracks as the stress increases. This process is commonly referred to as macroscopic "pseudo- strain-hardening". In TC, this phenomenon is accompanied by high ductility, hence TC has presented a new range of thin element applications in the construction industry.

Research work on the topic of TC in the literature clearly shows that there is a gap in knowledge regarding standard guidelines on composite testing procedures (Naaman & Reinhardt 2006), long-term durability, service life performance, and property specifications. In this research study, a preliminary attempt is made to characterise mechanically the matrix and the

individual fibres as well as the composite itself. Secondly, the study is extended into investigations of the changes that occur to the mechanical behaviour after exposure to different environments but representative of a range of ambient conditions. A better understanding of these changes is gained by undertaking limited microscopic studies under a scanning electron microscope (SEM). If ageing and the durability of this new material could be understood and accounted for at the design level, the composite is a possible replacement for asbestos cement.

1.2 Objectives of Thesis

The first objective of the research was to initially choose suitable mix proportions in order to produce a mortar mix of good workability and flow properties. The mix consisted of ordinary Portland cement (OPC), a reasonable proportion of the mineral additive Ultra-fine Fly Ash (UFFA), and a fine aggregate. For production of TC laminates with strain hardening properties, and robust enough to withstand experimental handling, it was necessary to carefully choose the number of CemForce layers to be cast in the mortar. After several trials using bending tests, six layers of CemForce were chosen for this research study.

The second objective was to assess any variation in mechanical behaviour of the matrix and the composite over several months. This was achieved through characterisation of the uni-axial tensile behaviour of the composite but it was necessary to firstly develop an appropriate specimen geometry suitable for the test, and thereafter refine the specimen production technique. Tensile testing involved loading the specimens to rupture and thus characterisation of the whole range of the stress-strain (σ-ϵ) behaviour. From the tensile tests, the beneficial effects of CemForce in reinforcing the inherently brittle cementitious matrix (at the micro level) were demonstrated.

The third objective was to develop and run an extensive testing programme for the assessment of the durability of TC. Five different environmental regimes were studied, three of which involved accelerating the ageing

of specimens by cyclic hot/cold, wetting/drying and continuous carbonation regimes. Although freeze-thaw is important in northern climates, the regime was not considered critical in moderate and tropical climates and was therefore not investigated in the scope of this thesis. Limited exposure to natural environments in moderate and tropical climates was also undertaken. Durability was evaluated from a comparison in the mechanical behaviour of the weathered specimens and samples previously aged under controlled laboratory conditions for the same time periods. Any changes in the mechanical behaviour of TC after exposure to different environments were attributed to ageing and durability performance.

The fourth objective of this study concerned an attempt to link the mechanical behaviour with the microstructure. This was achieved through carrying out parallel studies involving examination of individual fibres and the fibre/matrix interfaces under a scanning electron microscope (SEM).

The fifth objective of this research study was to develop a model of mechanical behaviour of Textile Concrete and use it in prediction of the multiple cracking behaviour of TC. The predictive capability of the model was tested on experimental data of a tensile TC specimen and acceptable correlation between the data and theoretical values was observed.

1.3 Structure of Thesis

This thesis is presented in seven chapters as follows:

i. Introduction
ii. Background and literature review
iii. Theoretical framework
iv. Experimental techniques
v. Results and analysis of mechanical tests
vi. Discussion
vii. Conclusions and recommendations

A brief background to Fibre Reinforced Cementitious Composites, cement and concrete, and development of Textile Concrete technology are presented in Chapter 2, the emphasis being on the review of the published research on FRCC.

The theoretical framework of Fibre Reinforced Cementitious Composites (FRCC) is outlined in Chapter 3. This essentially covers a description of fibre/matrix bonding property and the quasi-ductile tensile behaviour of FRCC materials. The development of theoretical models of the fibre pull-out mechanism are also given (Wang, Li & Backer 1988), (Naaman, Namur, Alwan & Najm 1991*b*), (Alwan, Naaman & Guerrero 1999), (Lin & Li 1997). A brief introduction to Aveston Cooper and Kelly (ACK) model (Aveston, Cooper & Kelly 1971) for fibre reinforced composites is also presented as well as theoretical models that describe the tensile stress-strain behaviour of the so called Textile Reinforced Concrete (TRC).

A brief overview of preliminary characterisation of Textile Concrete is firstly given in Chapter 4, and secondly, the experimental programme and the methods used for data acquisition are described. The main highlights of the experimental programme are: choosing of suitable mix proportions, characterisation of constituent materials, characterisation of the matrix, and characterisation of the composite behaviour using fibre pull-out and composite tensile tests. The studies were carried out over a period of approximately 24 months under the following environments:

- Controlled laboratory conditions
- Accelerated ageing simulating hot/cold (HC), wetting/drying (WD), and carbonation (C_c)
- Limited exposure to natural environments

The temperature in the laboratory environment was controlled at approximately 21°C and the Relative Humidity was 53 percent. Different temperatures and Relative Humidities existed in the facilities used for accelerating the ageing of samples. As is to be expected, natural environmental conditions varied over the entire exposure period.

Analysis and discussions of the results of the mechanical tests on the matrix, fibres, and the composite are dealt with in Chapter 5. The discussion covers the mechanical behaviour of the matrix, fibres, fibre pull-out, and the composite itself, as a function of age and weathering.

From the analysis in Chapter 5, the physical and chemical processes that affect the mechanical behaviour of TC, due to exposure to different environments, are synthesised.

Chapter 6 is structured in two parts. The first part is an investigation of the mechanisms of ageing affecting the properties of the matrix, fibres, and the fibre/matrix interface, and linkage of the macro behaviour to the microstructure. The second part is an analytical framework that is used in development of a prediction model for multiple cracking of Textile Concrete. Conclusions and recommendations of the research are presented in Chapter 7.

Many analytical investigations on the bond between fibres and cementitious matrices have been undertaken but the studies have mainly been limited to mechanical characterisation under controlled laboratory conditions (Currie & Gardner 1989), (Naaman, Namur, Alwan & Najm 1991*a*), (Naaman et al. 1991*b*). It is believed that this thesis contributes to the body of knowledge by focusing on the durability aspects of Textile Concrete. In addition, the thesis attempts to address the difficulties inherent in direct tensile testing of thin cementitious materials. The possibility of testing thin TC laminates to fracture in direct tension is considered useful contribution to the understanding of mechanical behaviour of HPFRCC.

Microstructural investigations contributed to a better understanding of the mechanisms of weathering of TC. Although the study was limited to qualitative identification of different phases in the microstructure, it nevertheless made a useful contribution to the understanding of the mechanisms of weathering of TC.

1.4 Summary

In this Chapter, the background to new innovations in the field of fibre cements and concretes was given, the motivation for the research spelt out, and the gap in current knowledge in the field of Textile Concrete identified.

Five specific objectives for undertaking the research were stated, and a brief overview of the research approach contained in seven Chapters outlined. Finally, the research output was given in form of contribution to knowledge.

Chapter 2

Background and Literature Review

2.1 Introduction

In this Chapter, the technological advancements in cement-based materials are discussed. A major development within the cement and concrete industry, which is the focus of this research, is a class of materials commonly referred to as Fibre Reinforced Cementitious Composites (FRCC). Over the last three decades, these products have continued to draw increasing interest, motivated by the need for a substitute to hazardous asbestos fibre cement products, resulting in rapid growth in a variety of FRCC applications.

Among the developments highlighted in this Chapter is the increasing use of supplementary cementitious materials (SCMs) and chemical admixtures that modify the properties of cementitious products. The utilisation of these products as a partial replacement of ordinary portland cement (OPC) in concrete is well established and a wealth of information is reported in the literature.

The role of supplementary cementitious materials and chemical admixtures in modifying the properties of cementitious matrices is highlighted. A distinction is made between the effects of SCMs on the properties of conventional concrete and on FRCC, focussing more on the flow characteristics since these are the properties linked to workability of the mix in the fresh

state. Based on information obtained from this literature survey, a choice is then made of the supplementary cementitious material considered most suitable for the purposes of this research.

The advancements that have taken place in materials science and methods of production of Fibre Reinforced Cementitious Composites are reviewed. In particular, the underlying principles of the mechanics of fibre/matrix interfaces are described. This leads to a survey of literature on current advancements in mechanical characterisation of the new material, Textile Concrete (TC), which is the subject of this research. TC is a development of FRCC, and past works on ageing, long-term performance, and durability of FRCC are briefly reviewed. Finally, some of the industrial successes in fibre cement composites are mentioned.

2.2 Background: Composite Materials

The concept of combining two or more constituent materials to form a composite with new properties has been known since materials were first used. However, since the early 1960s, the understanding and development of the properties of composite materials have been the subject of intense interest as reported in treatises by Brautman and Krock (Broutman & Krock 1975) and also by Hannant (Hannant 1978). The treatises contain a wide representation of contributions on the subject of composite materials technology and its transfer to industrial and consumer applications.

The basis for development of composite materials is to achieve a combination of properties not possessed by the constituent materials acting alone. In situations where the constituent materials were incapable of satisfying particular performance requirements, composites were developed to meet this need (Broutman & Krock 1975). A classic example is plain concrete which is essentially a particulate composite material with cement as the basic binder constituent, modified with coarse and fine aggregates.

Hardened cement paste itself is brittle, has low tensile strength and poor fracture toughness. However, when combined with aggregates and used in

compression, it forms a hard and strong cementitious composite, and when produced using modern technology, compressive strengths of up to 100 MPa or more are easily achievable (Neville 2002).

Conventional concrete is ideal for compression members in structures, but for bending and tension members, it is, like cement paste, brittle, and prior to failure, exhibits a low tensile strength of typically between 1 and 4 MPa. This tensile strength is an order of magnitude lower than its potential compressive strength, thus imposing numerous design constraints.

In view of the low tensile strength of plain cement and concrete, the conventional approach has been to provide appropriate reinforcing with materials of adequate mechanical properties in regions subjected to tensile stresses. On a macro scale, steel in the form of bars or mesh has been employed as tensile reinforcement, and on the meso scale short fibre additions provide the required reinforcement for thin cementitious products. In these composites, the fibres interact with the cementitious matrix, resulting in an improvement in properties such as toughness, impact and moisture resistance, although handling and installation are sometimes compromised (Gilbert 2004).

The improvement in mechanical properties of cementitious products after fibre inclusions is attributed to the ability of the fibres to modify the failure mechanisms of the composite through interaction with cracks at the micro and macro levels. Due to these benefits, Fibre Reinforced Cementitious Composites (FRCC) are finding a wide range of potential applications, and therefore are receiving increased attention (Xu, Magnani, Mesturini & Hannant 1996), (Hegger, Schneider, Sherif, Molter & Voss 2004).

2.2.1 Fibre Reinforced Cementitious Composites

The use of fibres in their natural state for reinforcement to cementitious matrices has been known since ancient civilizations in which vegetable and animal fibres were added to clay blocks and lime mortars to obtain greater strengths, or to reduce shrinkage cracking during setting (Moropoulou, Bakolas & Anagnostopoulou 2005). This technology was common in early Egyptian

civilisation (Moropoulou et al. 2005).

During early civilisations, fibres were used in their natural state but the technology suffered major drawbacks owing to durability problems. The alternative to natural fibres for application in cementitious composites was mineral fibres which offered a solution to durability problems. In this regard, the commercial merit of asbestos fibres in thin sheet cementitious products became known during the mid-nineteenth century (Hein 2001) (Klos 1975).

Asbestos cement sheeting was undoubtedly the most successful development of fibre cement composites in the twentieth century, and was extensively used for roofing, cladding and pipe manufacture all over the world. The unique nature of this product owes much to the favourable dimensional and chemical stability of the fibres and strong interaction between the fibres and the cement particles. However, the various health problems associated with the handling, fabrication, and use of the fibres and its products, have led to the demise of the widespread use of asbestos fibres, and initiated wide ranging studies for alternative reinforcing elements for thin sheet applications (Swamy & Hussin 1989).

Within recent decades, great demand has developed in the search for a suitable substitute. This demand is accelerated by the rising awareness among workers, researchers and journalists, of the hazardous effects of asbestos fibres. Indeed, a lot of pressure has been put on various Government bodies to ban asbestos cement trading. In India for example, there is mounting pressure for the Government to place a ban on asbestos fibre trade (Browne, Varadarajulu, Lewis-Michla & Fitzgeralda 2005), (Subramanian & Madhavan 2005).

As the asbestos cement industry was grappling with the mounting pressure to have the use of asbestos fibres banned, other industries found ready opportunity and market for their new products. Within the cement composites industry, natural fibres in short strand form, for example, sisal and cellulose based fibres became possible substitutes for asbestos (Vittone 1986), (Agopyan, Savastano, John & Cincotto 2005). Despite these fibres being

widely available, especially in most developing countries, and therefore potentially convenient materials for brittle matrix reinforcement, they present limited long-term durability performance due to elevated permeability and lack of resistance to crack growth (Swift & Smith 1978), (Savastano, Warden & Coutts 2003), (Agopyan et al. 2005).

The possibility of using discrete ductile fibres such as steel, or mineral fibres like glass, carbon, or boron, to reinforce brittle matrices has been the subject of extensive research (Gopalaratnam & Shah 1987*b*), (Wang, Li & Backer 1990), (Bentur & Mindess 1990), (Banthia & Trottier 1994) (Gilbert 2004). However, there have been major concerns about degradation of glass fibres and placement of particulate steel fibres in the highly alkaline cement environment. The high cost of carbon and boron fibres militates against their more widespread use. Therefore, these fibres do not offer an ideal solution to asbestos fibres replacement in the cement industry, particularly from a toughness and placement viewpoint.

2.2.2 Developments in Fibre Reinforced Cementitious Composites

In an effort to overcome the mixing and fabrication difficulties associated with reinforcing cementitious matrices with synthetic fibres, research has taken several forms ranging from the use of short discrete fibres, to fibrillated and continuous forms (Hannant, Zonsveld & Hughes 1978). At the same time, the search for alternative production techniques for FRCC has been on-going.

Since polypropylene (PP) fibres are readily available and have a relatively low cost, high extensibility and adequate strength, the fibres in short fibrillated films and monofilaments have in the past found various commercial applications. For example, a lightweight cement and coal fly ash composite reinforced with waste PP fibres from a carpet manufacturing plant had by 1983 been developed for architectural applications (McGovern 2001). The product was then known as Syndecrete.

Syndecrete was an alternative to limited or non-renewable natural materi-

als, and found many applications such as kitchen counter tops, sinks, bathtub surrounds, tile flooring, and furniture items. Along similar lines, the incorporation of polypropylene fibre mats proved to be a viable and economical reinforcement in precast low density cementitious applications (Hannant & Hughes 1986). In these applications, the presence of fibres, and addition of micro filler, modifies the microstructure and improves tensile strength of the composite.

In the recent past, specially formulated types of High Performance Polyvinyl Alcohol Engineered Cementitious Composites (PVA-ECC) for structural applications have been developed (Li & Stang 1997), (Li & Mobasher 1998), (Wang & Li 2003). By tailoring the fibre, matrix, and interface microstructures and micromechanical properties, the pseudo strain-hardening behaviour in tension is satisfied with a minimum amount of fibres. In Engineered Cementitious Composites (ECC), the fibres are oil coated to achieve controlled pull-out and high toughness. While the technique is unique, and indeed pseudo strain-hardening behaviour is satisfied, tailoring the interface in order to attain strain-hardening with a minimum amount of fibres is faced with processing and cost constraints. This is in contrast to using polypropylene textiles where the pseudo strain-hardening condition is easily satisfied at a relatively lower cost.

Research at Columbia University was recently undertaken to identify an appropriate type of fibre mesh for thin sheet cement-based products (Mu, Meyer & Shimanovich 2002). Two types of fibre meshes were compared: Alkali Resistant (AR)glass and polypropylene. In terms of flexural performance, AR-glass fibre mesh was found to be much more efficient as reinforcement than polypropylene fibre mesh, primarily because of its stronger and stiffer yarns. However, it was also about 10 times as expensive by mass or 30 times by volume. AR-glass fibres were also found to undergo a loss in strength and ductility and subsequently embrittlement after exposure to humid environments over long periods.

The high cost of AR-glass fibre mesh and the potential ageing problem

provide incentives to improve the performance of polypropylene fibre mesh, for example, by enhancing its bond properties.

The use of thin FRCC continues to grow rapidly in a variety of construction applications. In a recent symposium organised by the American Concrete Institute (ACI), current state-of-the-art and recent advances in material science,manufacturing methods, and practical applications of thin reinforced cement-based products and construction systems were explored by different authors.

In one of the reports of the ACI symposium, developments in glass fibre reinforced concrete (GFRC) over a thirty year period were reported (Gilbert 2004). In the report, different production methods are related to industrial applications. The report underscores the importance of protection of fibres from calcium hydroxide ($Ca(OH_2)$) as key to addressing durability problems in GFRC.

By describing material properties at macro, meso and micro levels (Hegger, Schneider, Sherif, Molter & Voss 2004), and by applying the properties in appropriate models to simulate mechanical behaviour, a better understanding of the performance of FRCC is gained. The study by Hegger *et al.* (Hegger, Schneider, Sherif, Molter & Voss 2004) illustrates that the load-bearing behaviour of TRC depends on the combined effect of the interaction between filaments (fine fibres) and the matrix at the micro level, and bonding between a roving (fibre bundle) and the matrix.

RILEM Committee TC 201-TRC that deals with Thin Fibre Reinforced Cementitious Products has compiled contributions of research in Textile Reinforced Concrete (TRC) in which theory, applications, bond characteristics, production technologies, material properties and bonding behaviour are investigated.

There are possibilities of using textiles in repair and rehabilitation of reinforced concrete structures as shown in a study by Bruckner *et al.*(Bruckner, Ortlepp & Curbach 2006). The study investigated the additional strengthening that was observed when textiles are bonded to the tension face of a

concrete beam. In a different study (Banholzer, Brockmann & Brameshuber 2006), the matrix mechanical and fracture properties were reported to make a significant contribution to the final failure of a composite.

Theoretical investigations in load-displacement behaviour of damaged reinforced concrete elements rehabilitated with textile meshes (TRC) have made use of mechanical tests results as the input parameters in simulations of the composite behaviour (Hegger, Will, Bruckermann & Voss 2006). These parameters are: textile and rovings orientation, fibre cross section, and ultimate strength of the fibres. Based on the simulations, a method for design of TRC is suggested.

A collaborative research project at RWTH Aachen University in Germany involved studies on the load carrying and failure mechanisms of TRC at micro, meso, and macro levels (Konrad, Chudoba, Butenweg & Brukermann 2003). Fibre pull-out behaviour of TRC was conceptualised as being a function of bond distribution across yarn at the micro level, which was characterised by the initial slope of fibre pull-out curves.

The results by Konrand *et al.* and also by Hegger *et al.* (Hegger, Sherif, Brukermann & Konrad 2004) illustrate that micro-mechanical models contribute significantly to the understanding of the macro behaviour of TRC. The experimental and theoretical investigations were carried out to determine and study the mechanisms of fibre/matrix interaction manifested in fibre/matrix bonding, fibre debonding, fibre damage and rupture, and matrix cracking. From the work by Hegger *et al.*, (Hegger, Sherif, Brukermann & Konrad 2004) the application of AR-glass Textile Reinforced Concrete as exterior cladding panels in a pilot project was demonstrated. Although the thin walled panels were an efficient and economical alternative for conventional reinforced concrete or natural stone facades, the long-term durability was still considered a major concern.

The RILEM committee on High Performance Fibre Reinforced Cementitious Composites (HPFRCC) has proposed guidelines on characterisation of the tensile response of strain-hardening of Fibre Reinforced Cementitious

Composites (FRCC) (Naaman & Reinhardt 2006). The study focusses on the practical aspects of the performance of strain hardening composites. Three properties were considered as key to characterisation of the strain-hardening of FRCC. These properties were: tensile strength of composite after cracking, σ_{pc}, tensile strain capacity of the composite, ϵ_{pc}, and elastic modulus E_c. Recommendations were made by Naaman and Reinhardt (Naaman & Reinhardt 2006), which included: setting limits of maximum tensile stress and strain capacity, and setting the minimum modulus of elasticity. Variations in test results were attributed to size effect and a standard specimen size for tensile testing was proposed (Naaman & Reinhardt 2006).

In order to advance the widespread use of strain-hardening FRCC particularly in large scale structural applications, the test standards and procedures still need to be addressed. In addition, a comprehensive analysis would be needed to ascertain how different types of FRCC influence the performance of structural members. Theory of mechanical behaviour of FRCC is dealt with in Chapter 3.

The future of FRCC depends largely on the ability of these materials to compete cost effectively with similar products made using other materials such as metals and plastics. Since polypropylene fibres are more cost-effective in comparison with other fibres such as carbon, AR-glass and PVA, it is appropriate to examine PP fibres in more detail, which is dealt with in section 2.3.

2.2.3 Summary: Composite Materials

The relationships between conventional Fibre Reinforced Cementitious Composites (FRCC) and the newly developed cementitious composites described in the previous sections is illustrated schematically in Fig. 2.1

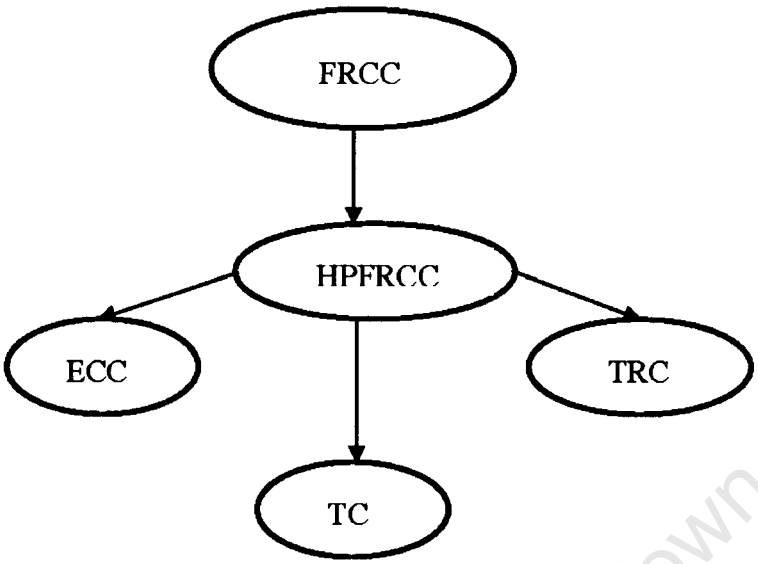

Figure 2.1: Main classifications of Fibre Reinforced Cementitious Composites

The main findings reviewed in the previous sections are:

- In the recent past, FRCC has received increasing attention due to the ability of fibres to modify failure mechanism of a brittle matrix through interaction with cracks at micro and macro levels.
- Rapid developments in FRCC were highlighted, which are motivated by the need for a substitute for asbestos fibres in cementitious composites.
- Some of the ways of improving the performance of synthetic fibres in cementitious matrices were briefly described as: modifications to fibres (in ECC), and by using fibres in textile formats (in TRC and TC).

2.3 Background: Polypropylene Fibres

Polypropylene (PP) is a thermosetting plastic obtained by polymerisation of propene ($CH_3CH{=}CH_2$) to form a linear polymer in which the structural units are connected one to another in linear sequence. PP has the following molecular formula: -CH-CH_3-CH_2- which has strong covalent bonds between carbon and hydrogen atoms.

PP materials grew out of the the discovery by Natta of "Ziegler-type" catalysts capable of producing high molecular weight PP with linear structures (Moore 1996). The main driving force in the PP industry has been the ability to achieve the polymerisation process as a result of improvements in the catalysts. Depending on the degree of regularity of the -CH_3 groups, PP is classified according to molecular structure as: isostatic, syndiotactic or atactic, the major production being in isostatic PP (iPP) which has a linear monomer structure.

The regularity of iPP allows it to display substantial crystallinity although the degree of stereoregularity (and consequent crystallinity) among conventional PPs varies considerably (Moore 1996), (Azapagic, Emsley & Hamerton 2003), (Campell 2000). These variations are usually due to the effectiveness of the polymerisation catalyst, but the production process also can have some effect. PP is manufactured either in molded (or nonoriented) forms, or as intentionally oriented formats such as thin films and fibres.

Depending on the end-use, fibre manufacture essentially involves processing of the PP resin into: staple, bulk continuous filaments, melt-blown, spunbonded fibres and a variety of other applications. An important stage in this process is stabilisation against weathering. The following are the typical end-use properties that define the major characteristics of PP (Moore 1996):

- Maximum temperature at which PP can be put to practical use
- Modulus of elasticity
- Tensile strength
- Impact strength
- Hardness.

The melting point of PP is approximately 169^{o}C and it is fairly resistant to chemical agents such as acid, alkalis, and salts.

Like all polymers, the mechanical state of polypropylene varies according to how close the temperature is to its glass transition temperature, T_g, above which deformation may occur by relative sliding between chain molecules.

Indeed, an increase in temperature of the order of 10°C near T_g results in reduction in the modulus of elasticity by several orders of magnitude (Dhir, Jones, McCarthy, Zheng, Chittirattnakorn & Scorey 2002). The mechanical state ranges from brittle-elastic at low temperatures, through plastic to viscoelastic or leathery, to rubbery and finally to viscous at high temperatures. Each mechanical state covers a certain range of normalised temperature T/T_g (in Kelvin). The glass translation temperature of polypropylene is -16°C (257°K) (Campell 2000) and therefore T/T_g at room temperature is approximately 1.1 in Kelvin terms.

Fig. 2.2 shows the way in which Young's modulus E for a linear polymer changes with temperature for a fixed loading time (From (Ashby & Jones 1986) p. 218). The dynamic mechanical properties of polymers are described

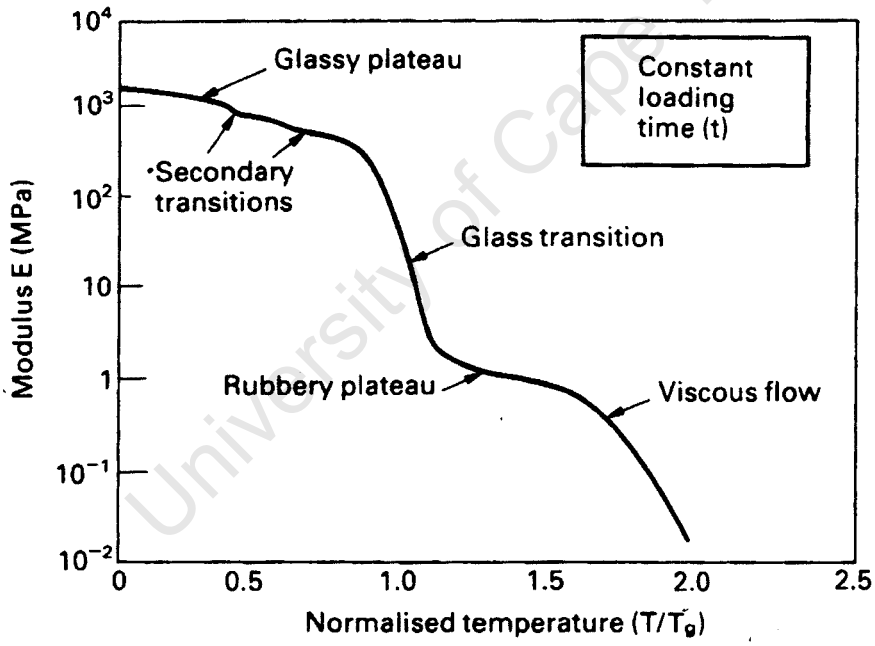

Figure 2.2: Schematic of variation of Young's Modulus E for linear polymer changes with temperature

in terms of "loss modulus", which measures the rheological response of a polymer within a temperature range. Loss modulus is determined according to ASTM standard (ASTM D4065-93 1993). For polypropylene itself, the variation of loss modulus with temperature (for PP having various amounts

of β crystalline phase) is illustrated by Fig. 2.3 (Labour, Gauthier, Seguela, Vigier, Bomal & Orange 2001). The figure (in which the vertical scale refers to the lower curve whereas the other curves are arbitrarily shifted upwards) illustrates a sharp change in loss modulus within the vicinity of the glass translation temperature of approximately -16°C.

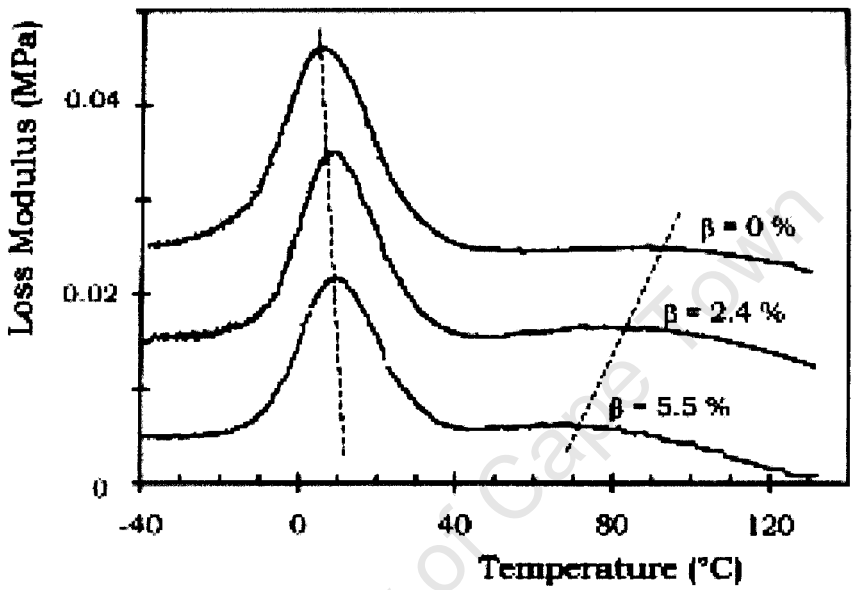

Figure 2.3: Loss modulus versus temperature of polypropylene

In tensile deformation of a plastic, it elongates to some degree, depending on the conditions. With PP, elongations of several hundred percent are normal at room temperature and slow extension rates, and much of the deformation is irreversible (Moore 1996). As the temperature is lowered (or the extension rate is increased), the glass transition temperature is approached, and the molecular chains are incapable of accommodating the deformation and fail in a brittle manner. In that case, there is very little extension of PP since the deformation is elastic in nature. In brittle failure, the energy is about an order of magnitude less than that absorbed in ductile failure (Moore 1996).

A polymer in use interacts with the environment and degrades (or ages) over time. Degradation is any process by which the original polymer struc-

ture is changed and failure results from that physical or chemical change. Degradation is differentiated from ultimate failure phenomena such as tensile failure or abrasive wear. It is also differentiated from failures which result from changes in properties due to increased temperature which in effect alter the ultimate properties. Degradation results in a change in the molecular structure, usually molecular weight or composition.

All polymers are susceptible to various degradation processes depending on their composition and the environment in which they are used. There may be imposition of energy in the form of heat, or by mechanical action (including ultrasonic or sonic energy), radiation such as gamma rays, X-rays, visible light, ultraviolet light, infrared radiation, or electrical in the form of dielectric effects. There may also be chemical effects such as non-abrasive wear, oxidation, hydrolysis, "yellowing", chemical attack by solvents and detergents (Wiliams 1975) (Brydson 1975), (Azapagic et al. 2003). Often, more than one agent of degradation may be active under given conditions such as during weathering or exposure to corrosive environments. The mechanisms of chemical degradation which bring about any of the above changes are: loss of portions of the polymer molecule, crosslinking between molecular chains, scission of the molecular chains, or changes in side chains. Depending on the temperature, the degree of cross-linkage affects the modulus of elasticity of polymers as illustrated in Fig. 2.4 (from p. 227, (Ashby & Jones 1986)). The figure shows that stiffness and strength are increased by causing some crosslinking (also referred to as vulcanisation) to occur. It is also illustrated that high temperatures lead to failure.

2.3.1 Mechanisms of Degradation in PP

Ageing (or degradation) in PP is any process by which the original polymer structure is changed. Therefore, the following mechanisms result in degradation:

- Volatilisation or leaching of stabilisers
- Rotation of segments of molecular chains

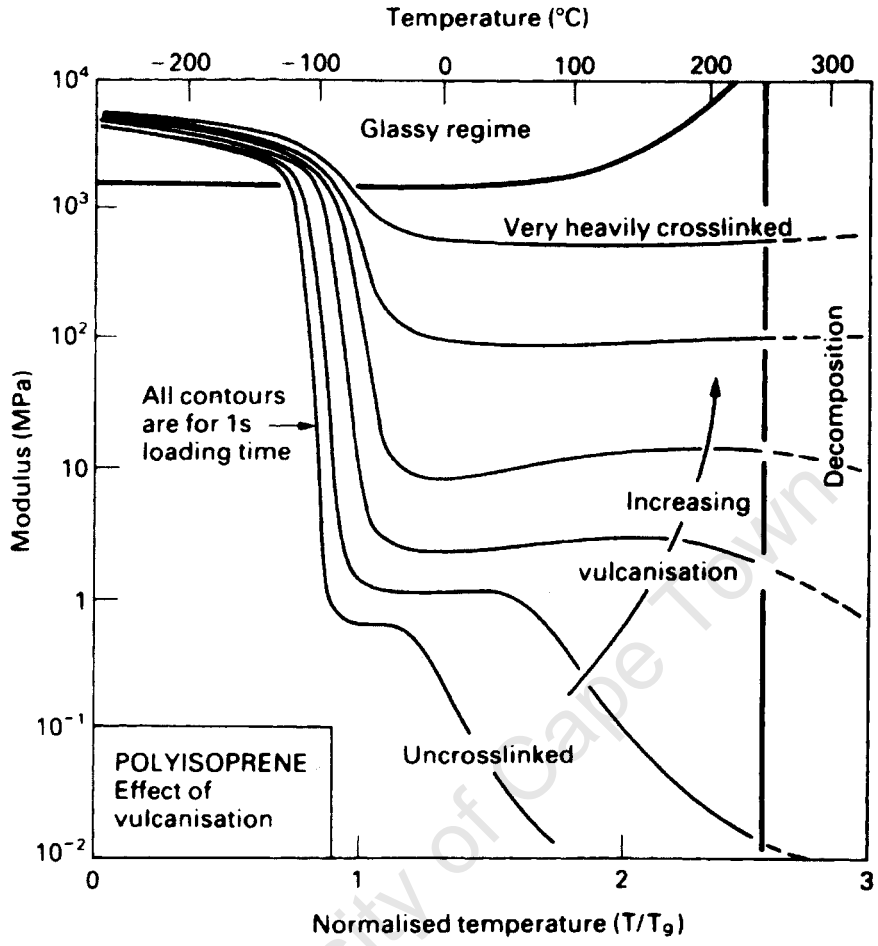

Figure 2.4: Schematic of the effect of degree of cross-linking on the elastic modulus E of a polymer

- Changes in bonding nature of the basic polymer structure (-CH-CH_3-CH_2-)
- Addition of different ions to the basic polymer structure
- Modifications in cross-linking

The agents of degradation are elevated temperature, oxygen from the environment, hydroxide ions (OH^-), gases from the atmosphere (such as carbon dioxide (CO_2), and sunlight (i.e. UV).

When considering a simple polymer, the glass transition temperature (T_g) often governs the maximum temperature at which a polymer may be

used. At temperatures beyond T_g, the polymer experiences rotation of segments of the molecular chains and the degree of cross-linking is substantially reduced. At macroscopic scale, rotation of segments of the molecular chains accounts for softening of the polymer. T_g for PP is -16°C so it is used substantially above its T_g.

Linear polymers are usually cross-linked with sufficient number of side chains between the macromolecules to form three-dimensional networks that impart special properties to the primary linear polymer such as reduction in solubility and improvement in strength. Cross-linkages in PP are easily destroyed after exposure to warm moist environments (Mills 1986).

To partially neutralise the intermolecular forces and thus prevent the polymer molecules from slipping past each other when the material is stressed, stabilisers are commonly added. However, changes in temperature and environment can induce volatilisation or leaching of the stabilisers leading to chemical disintegration, which is a change in the basic composition (or molecular weight) and structure of the polymer.

Chemical disintegration of the polymer structure, referred to as depolymerisation, is the destruction of hydrogen bonds or chemical cross-links between polymer chains (Azapagic et al. 2003). This leads to loss of strength.

When most polymeric materials are exposed to elevated temperatures in aerated conditions, the basic molecular structure is destabilised due to formation of an oxide. Therefore, the polymer loses the initial properties and embrittles. Although there is still some dispute about the details of the embrittlement mechanism in oxidised plastics, the most obvious changes include reduction in the elongation at break in a tensile test (Mills 1986).

When solid polymers are stored under hot damp conditions, OH^- groups from water react with the polymer molecule leading to random chain scission and reduction in the average molecular mass (Mills 1986). This mechanism, which is referred to as hydrolysis, causes a modest drop in molecular mass. At the macro level, hydrolysis reduces the performance of the polymer to a level that brittle failure occurs in a tensile test.

If there is a thin layer of brittle material deposited on the surface of a relatively tougher material, for example the formation of a brittle outer layer on PP due to strong surface absorption of the ultraviolet part of the sun's rays, the tensile failure strain of the outer surface layer will be lower than that of the substrate so that it will fail first. The final failure depends on the toughness of the substrate. If the substrate layer is tough, the cracks will stop, but if it has a low resistance to the fast propagation of cracks, the cracks will continue and brittle failure results (Mills 1986).

PP is considered fairly resistant to gaseous degradation at atmospheric pressures. However, at pressures in excess of 5 atmospheres, the polymer is susceptible to CO_2 ingress and chemical changes occur in the molecular structure (Mills 1986). The main change in the mechanical properties that is attributed to carbonation at high pressures is embrittlement.

Prolonged exposure of PP to light and heat in an environment of high humidity modifies cross-linking in the molecular structure and causes "yellowing" or loss of glaze. When cross-linking is increased in a process whereby the broken bonds reform between adjacent molecules, the polymer undergoes hardening and eventual embrittlement (Azapagic et al. 2003).

When plastics are used outdoors they are exposed to solar radiation and the polymer molecule absorbs the most energetic photons at the short end of the spectrum thereby raising the energy level. PP has a strong absorption capacity of wavelengths of 370 nanometres (Mills 1986). If the energy level of the excited state is high enough, it can transfer energy to a bond dissociation reaction. The whole process of photon absorption and the subsequent bond breakage is referred to as photodecomposition.

2.3.2 Effects of Cyclic Heating and Cooling on Polypropylene

The progress of ageing of PP strongly depends on the difference between ageing temperature (T) and glass transition temperature (T_g). Thermal effects are evidence of the changes in the elastic modulus that occur within

a relatively narrow temperature range in the vicinity of 35 °C (308 °K) ($\frac{T}{T_g}$ of approximately 1.2) (Campell 2000), (Ashby & Jones 1986). Similarly, the tensile strength of PP is known to decrease as the temperature increases, and similarly, toughness is reported to be lowest at temperatures around $\frac{T}{T_g}$ of approximately 1.2 (Alcock, Cabrera, Barkoula, Reynolds, Govaert & Peijs 2007). Fig. 2.5 illustrates the changes in the mechanical properties of PP with ageing as reported in the literature.

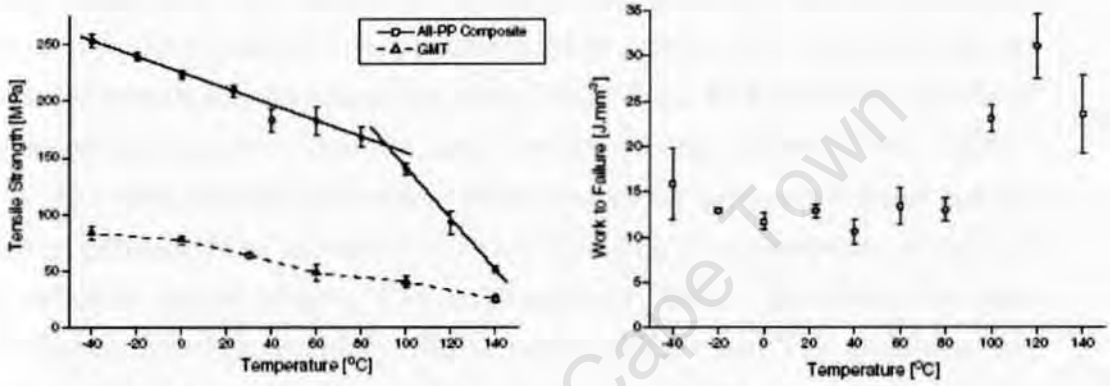

(a) Effect on tensile strength (b) Effect on toughness

Figure 2.5: Effect of temperature on mechanical properties of PP (from Alcock *et al.*2007)

2.3.3 Polypropylene-Reinforced Cementitious Products

Towards the latter half of the twentieth century when new methods of physical and chemical analysis were developing and the principles that govern the properties of natural polymers were discovered, a new industry of man-made organic materials was created. Among these new products, polypropylene (PP), polyethylene and nylon fibres with potential for application in the cement products industry were innovated.

PP was a popular choice for the fibre mainly because it is inert to the alkalinity of cement, and is suitable for textile manufacture. However, with regard to bonding with cementitious matrices, the performance of synthetic fibres did not compare well with asbestos fibres. There were concerns with poor

interfacial bonding for polymeric fibres, particularly polypropylene, which was improved by using fibrillated formats of the fibre rather than discrete forms (Hannant et al. 1978). In this context, fibrillated fibres are regarded as continuous open networks created by micro-slits in PP tapes thus creating an expanded surface area for effective interaction and bonding with the cementitious matrix.

The concerns with poor fibre/mtrix interface bonding were aggravated by the resistance by manufacturers to change composite production techniques from the conventionally established Hatschek process that was originally developed specifically for asbestos cement production. This inhibited the development of alternative fibres for use in cementitious matrices (Vittone 1986).

The chemical and mechanical properties of the alternative fibres are entirely different from asbestos, and their bonding characteristics are also of a different nature (Akers, Tait & Hourahane 2003). Therefore, the conventional Hatschek composite production technique would be unsuitable for most of the alternative fibre types. Moreover, mixing steel, glass or polymeric fibres, particularly in short strand form, in a conventional Hatschek plant would be faced with the common difficulty of workability, mixing, and placement. Achieving high fibre volume fractions (V_f) (in excess of 3 percent) would be problematic mainly due to clumping and the hydrophobic nature (resistance to wetting) of synthetic fibres and it would be difficult to attain effective reinforcement, load transfer, required mechanical strength and toughness property performance without causing severe fibre bundling and clumping.

2.3.4 Reinforcing Action of Polypropylene Fibres

The reinforcing action of PP fibres in cementitious matrices is well documented and this is illustrated by long term studies by Hannant (Hannant 1998) and other researchers (Galloway, Williams & Raithby 1981). However, the reinforcing action of cementitious matrices with polypropylene fibres has not been as successful as asbestos fibres mainly due to difficulties associated

with interface bonding, and problems in working with the material in short strand form.

Short polypropylene fibres have fairly low strength and modulus, and when placed in cementitious matrices have low interfacial bond strength but have high toughness. These fibres therefore pull out of the concrete matrix at relatively low stresses (Gray 1972). Moreover, when these fibres are used as reinforcement to concrete in the short strand form, there is a lack of control over fibre dispersion as well as location and orientation within the matrix. This is because the typical batch plant storage and weighing hoppers, as well as discharge systems employed in concrete mixing, are unable to handle such fibre inclusions. Consequently, the difficulties in the use of short polypropylene fibres as concrete reinforcement have led to the search for other long-term solutions.

Polypropylene fibres are intrinsically hydrophobic, and whilst this property confers the advantages of not affecting the water:cement ratio particularly when short, distinct fibres are employed in a cement matrix, the resulting lack of adequate physico-chemical bond in the hardened state, combined with three dimensional orientations, do not contribute to the best performance characteristics in thin section applications. Continuous fibre forms are therefore particularly attractive in such sections, from bond and reinforcing considerations. Therefore extensive research has been carried out in which fibrillated open networks are incorporated in cement-based matrices, and the engineering properties and durability effects assessed (Gardner & Currie 1983), (Gardner, Currie & Green 1983).

Although the strength and modulus of PP are not very high, as the modulus is in the vicinity of 1 GPa, careful design through appropriate placement and high fibre volume fraction (V_f) would lead to strength and stiffness in the composite sufficient to meet specific requirements, while at the same time achieving high toughness.

In general, the properties of concrete reinforced with fibres depend not only on the fibre type, but also on fibre volume fraction V_f, a parame-

ter affecting the strength of the fibre-matrix bond (Gray 1972). A balance between V_f and concrete workability is key to achieving the desired performance. However,high volumes of fibre in the composite lower the workability of plastic concrete (Owens 2002).

Loss of workability could be compensated for by increasing water, which increases the water: cement ratio (w:c) if cement content is constant, but this is not recommended since it lowers the strength and durability of the composite (Neville 1971). One way of overcoming the difficulties associated with placing PP fibres in cement-based mixes is using fibres in fibrillated or woven fabric or textile forms rather than in short discrete form.

The possibility of using woven polypropylene mesh fabrics for thin cement sheet reinforcement commenced in the early 1980's in independent studies at the Universities of Sheffield and Ulster in the United Kingdom whereby open networks of fibrillated polypropylene films proved successful in meeting the performance demands of Fibre Reinforced Cementitious Composites (FRCC) (Hannant 1980), (Vittone 1986).

The early research (Vittone 1986) initially appeared to indicate that open networks of polypropylene films gave better performance in FRCC than woven meshes. However, subsequent work demonstrated that proper use of the meshes would not only produce excellent flexural properties, but also a wide range of products, and product shapes could be successfully manufactured (Swamy & Hussin 1986),(Swamy & Falih 1985). The main advantage of woven fabrics is convenience in their handling, and relative ease in placement and orientation either manually or in factory productions. In addition, by careful use of woven meshes the difficulty encountered in attempting to choose the fibre volume fraction (V_f) and workability of the mix during composite production are sufficiently addressed.

When a load is applied to a polymeric fibre embedded in a cement matrix, the fibre undergoes radial contractions due to Poisson's effect. The effects were reviewed by Wang *et. al* (Wang, Li & Backer 1988) based on perfect fibre alignment and smooth fibre surfaces. In theory, Poisson's effects would

cause unstable debonding of concrete reinforced with polypropylene, and in fibre pull-out tests, unstable load drop would be expected. However, in practice, fibres have slight misalignments and the fibre surfaces have asperities, which offset the Poisson's effect significantly. Indeed, multiple cracking of Fibre Reinforced Cementitious Composites (FRCC) has been observed in direct tensile tests (Mumenya et al. 2006) indicating that radial contractions did not cause significant effects in fibre pull-out behaviour. In addition, no unstable load drop has been observed in fibre pullout tests of polypropylene fibres (Wang, Li & Backer 1988). Therefore, radial contractions due to Poisson's effects in polypropylene fibres embedded in cementitious composites are considered insignificant.

In the search for a possible replacement of asbestos fibres cement, and in an attempt to deal with the difficulties associated with placement of fibres with high V_f and fibre orientation, a new technology has emerged within the last decade in the thin element cement-based industry, namely Textile Concrete (TC) technology. In this new technology, woven textiles are specially made for application in cement-based matrices. This has created great enthusiasm among researchers, engineers and contractors (Aspiras & Manalo 1995), (Callec 2003).

2.3.5 Summary: Polypropylene Fibres

The essential findings in section 2.3 were:

- The glass transition temperature T_g of polymers is related to mechanical properties. T_g of PP being approximately -16^{o}C means that significant changes occur in the molecular structure of the polymer at ambient temperatures.
- Polymers easily deteriorate in hot and damp conditions, elevated temperatures, and when exposed to ultraviolet (UV) irradiation.
- PP is resistant to gaseous degradation at atmospheric pressures, but above 5 atmospheres, the polymer is susceptible to carbonation. PP

is inert to alkaline environments, which makes it a suitable fibre reinforcement for cementitious matrices.

- The reinforcing action of PP is improved by use of fibres in fibrillated form, continuous fibre formats, or as textiles.
- Textile Concrete (TC) technology is described as a new development in Fibre Reinforced Cementitious Composites (FRCC).

2.4 Background: Cement-Based Products

In its most basic form, plain concrete comprises portland cement, water, fine and coarse aggregates. Concrete has a long history that can be traced back to ancient civilisations. Indeed, evidence of its use in the form of gypsum mortar in construction of the great pyramids of Egypt has been documented. In a study on the elemental composition of samples obtained from a historical site in Egypt (Demortier 2004), it is suggested that the ancient Egyptian pyramids were constructed using materials similar to concrete as opposed to the use of hewn blocks. By using physico-chemical analysis, the elemental composition of the samples was studied from which evidence of the presence of limestone aggregates was demonstrated (Demortier 2004). In addition, the study showed that the blocks used in the ancient constructions were held together with a binder containing sodium carbonate (Na_2CO_3), alumino-silicates, and water. The composition of binders used in ancient constructions were comparable to the compounds in the raw materials used for the manufacture of portland cement which are rich in lime (CaO) and silica (SiO_2) (Stutzman 2004).

A form of concrete probably was known in the pre-Roman times. The use of pozzolanic mortars and plasters in ancient Greek and later in Roman buildings is reported in a study by Moropoulou *et al.* (Moropoulou et al. 2005). The study gives a background of the use of concrete in the ancient structures of the Mediterranean basin, and reports the results of thermal analysis on four hundred samples. The results of the study indicated that the ancient Greek and Roman mortars and concrete were of high quality probably due to good

workmanship and careful selection of raw materials for use in mixing, bedding or moulding, compaction, and maintenance (Moropoulou et al. 2005). The studies on ancient mortar and concrete (Moropoulou et al. 2005) contribute to the understanding of the physico-chemical and mechanical characteristics of the composites used in the past. This knowledge could be useful in defining specifications for restoration mortars, which would preferably be similar in properties to the original composites employed in the ancient structures.

The basic ingredient in all concretes is a binder, portland cement being a specific case whose production has shown an uninterupted and steady growth trend as reported by Szabo et al. (Szabo, Hidalgo, Ciscar & Soria 2006). The study gives an overview of the global cement production and consumption for 1997. By using a prediction model, the future trends in cement production are analysed. The model is based on cement production processes namely: population, consumption by volume, international trade, carbon emissions among others. An increasing trend in world cement production is predicted from 1550 metric tons in 1997 to 2800 metric tons in 2030, illustrating that a high demand for cement-based products is expected in the future.

2.4.1 Cement

Concrete owes its essential binding property to the hydraulic action of cement. Conventionally, cement is used either as the sole binder in concrete, or is blended with other hydraulic, pozzolanic, or non-pozzolanic materials. The development of cement evolved from natural binders to the manufactured form commonly known as portland cement. Natural binders are essentially a mixture of ash or clay with lime, which harden when in contact with moisture to produce reaction products that are cementitious in nature.

2.4.1.1 Cement Chemistry

Portland cement is produced by fusion of raw materials which are rich in lime and silica, typically shale or clay, and limestone. The five principal components present in the raw materials are oxides of calcium (CaO), magnesium

(MgO), aluminium (Al_2O_3), iron (Fe_2O_3), and silicon (SiO_2).

The raw materials are ground and heated to a temperature of approximately 1450°C where the oxides mutually react, and on cooling form a clinker that is composed of the following compounds (Taylor 1997*a*), (Richardson & Cabrera 2000):

- Tricalcium silicate ($3CaO.SiO_2$), notated C_3S
- Dicalcium silicate ($2CaO.SiO_2$), notated C_2S
- Tricalcium aluminate ($3CaO.Al_2O_3$), notated C_3A
- Tetracalcium aluminoferrite ($4CaO.Al_2O_3.Fe_2O_3.$), notated C_4AF
- Magnesium oxide (MgO)
- Free calcium oxide CaO

The microstructure of a clinker showing particles of the constituent minerals and voids is shown in Fig. 2.6 (Stutzman 2004).

Figure 2.6: SEM backscattered electron image of a coarse clinker: from Stutzman and Clifton (2004)

Portland cement is produced by grinding clinker with a limited amount of calcium sulphate and other minor constituents as specified by various

standards (EN197-4 2004). Calcium sulphate controls the rate of set and strength development. By varying the chemical and mineralogical composition, portland cement is produced with formulations designed to meet market demands.

Conventional portland cement is categorized according to its composition as follows: general purpose cement, blended cements, blast furnace cement and pozzolanic cement, which are designated CEM I, II, III and IV respectively (EN197-4 2004). Portland cement continues to be the major binding material in concrete, with a world-wide annual production in the vicinity of 1 billion tons (Dhir, McCarthy, Zhou & Tittle 2004).

Over the years, portland cement has essentially been used in the same state but in the recent past, significant technological advancements have been made particularly in the area of supplementary cementitious materials and chemical admixtures. These materials are added to cement mixtures in order to modify the rheology and improve the early age strength and durability of concrete, among other benefits (Dhir et al. 2004).

The commercial production of the manufactured form of cement known as portland cement did not take place until after 1824 when Joseph Aspdin of Leeds registered the first patent for its manufacture. The chemical composition of cement could then be controlled and the properties could be pre-determined. The properties of this artificial form of cement have gradually been improved over the years to the quality of portland cement that has found a wide application today (Hein 2001), (McGovern 2001).

To achieve sufficiently high strength levels at early ages and thus maintain fast construction schedules, increases have been made in the fineness and C_3S content of portland cement (Metha & Burrows 2001). However, this may impact negatively on durability since the high strength although beneficial also increases risk of concrete cracking (Burrows 2007).

2.4.1.2 Hydration of Cement

Hydration of cement is mainly characterised by the two calcium silicate constituents (C_3S and C_2S). When cement is mixed with water, an exothermic reaction takes place and an alkaline solution (pH $\sim$ 13) is produced by the dissolution of calcium, sodium and potassium hydroxides. The high pH-value in the pore solution is a favourable condition for the hydration reaction. There are two chemical reactions in cement hydration: (a) addition of water molecules (H_2O) and (b) hydrolysis involving splitting of a bond in a water molecule and releasing hydrogen cations (H^+) and hydroxide anions (OH^-).

Soon after addition of water to cement, calcium and sulphate ions react with tricalcium aluminate to form short, hexagonal needle-like crystals (ettringite) at the surfaces of clinker particles. The other hydration products are calcium silicate hydrates (C-S-H) which usually contain small amounts of ions of aluminium, iron, magnesium, and other ions. The hydration products formed soon after water is added are too fine to completely cover the clinker particles. Consequently the mobility of the cement particles in relation to one another is only slightly affected, and therefore the consistency of the cement paste undergoes only slight stiffening (Scrivener, Cabiron & Letourneux 1999). Cement hydration takes place in different stages as follows:

Stage 1: Initial C_3A hydration generating heat and possibly early stiffening. This stage lasts for a few minutes.

Stage 2: C_3A hydration products cover cement grains and limit access of water and slow reactions. This is a dormant period which lasts for a few hours.

Stage 3: Calcium becomes supersaturated in solution and shells around cement grains break open. Silicate reactions start, causing heat, setting and initial strength gain. During this period, C-S-H continues forming on the clinker surfaces and the microstructure densifies. These reactions start after approximately one to three hours and continue for approximately three hours.

Stage 4: Hydration products start to fill space and surround cement grains, again slowing reactions. The reactions continue up to 24 hours after mixing. Stage 5: This is a long term slow hydration and densification which continues for years.

After the dormant period, an intense hydration of clinker phases takes place. During this period the basic microstructure of cement paste is formed, consisting of needle-shaped (and platy) C-S-H particles, platy calcium hydroxide and ettringite crystals growing in longitudinal shape. The microstructure also contains unhydrated cement particles, and voids or pores.

As hydration progresses, crystals continue to grow, bridging the gap between unhydrated cement particles. The hydrated particles bond firmly to the un-reacted cement causing hardening of cement paste. Hydration causes the density of the microstructure to increase and pores get filled with hydration products. The filling of pores causes strength gain and the cement forms a hardened paste (HCP) (Richardson & Cabrera 2000), (Scrivener et al. 1999), (Stutzman 2004).

C-S-H contain less calcium oxide than the calcium silicates in cement clinker. Calcium hydroxide is formed during the hydration of portland cement, which is available for reaction with other cementitious materials such as ground granulated blast furnace slag and pozzolans such as fly ash and silica fume (Addis & Owens 2001).

Pozzolans are materials rich in reactive silica and sometimes alumina, and react with lime (CaO) in the presence of moisture to produce cementitious compounds. Since calcium hydroxide (hydrated lime) is produced during cement hydration, pozzolans are often combined with portland cement in which the pozzolanic reaction is driven by the cement's normal reactions with water (Stutzman 2004).

2.4.1.3 Microstructure of Hardened Cement Paste

Cement paste in a plastic state is a network of particles of cement in water which after setting has the following microstructure:

- Poorly crystallised hydrates of the various compounds, referred collectively as gel
- Voids in the gel referred to as gel pores
- CH ($CaOH_2$) crystals
- Unhydrated cement particles
- Residue of water-filled spaces referred to as capillary pores
- Some minor components

The microstructure of hardened cement paste continues to change as it undergoes (initially) setting, followed by hardening and drying. In the presence of water, cement continues to hydrate over a long period leading to densification of the microstructure, which is caused by the formation of CH crystals and other hydration products of different physical and chemical structures (Salicimen, Shameem, Barry, Ibrahim & Abbasi 2003).

The microstructure of a 100-day old sample of cement paste prepared with water:cement (w:c) ratio of 0.30 and cured at room temperature is shown in Fig. 2.7 (Diamond 2004).

The microstructure in Fig. 2.7 shows a residual cement grain with a hydration rim of C-S-H products (labeled A), a partially hydrated C_2S particle (labeled B), and a fully hydrated grain with no visible cement core (labeled C).

2.4.1.4 Microstructure of Hardened Concrete

Concrete is a composite material produced by mixing cement with fine aggregate (sand), coarse aggregate (gravel or crushed stone), water, and often small amounts of admixtures to control setting time and plasticity. Stiffening, setting and hardening are caused by accumulation of hydration products of varying rigidity which fill the interstitial spaces originally filled with water.

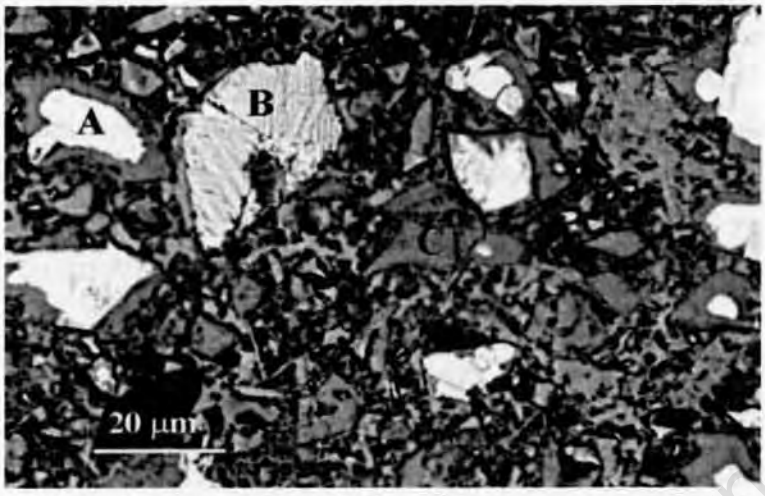

Figure 2.7: Microstructure of a 100-day old cement paste (w:c 0.30), cured at room temperature (Diamond 2004)

Stiffening, setting and hardening therefore depend on the size of the interstitial spaces and on the water:cement ratio. Hardened concrete has a fine network of pores and capillaries which forms moisture and vapour diffusion paths.

Fig. 2.8 shows the microstructure of concrete with hardened cement paste, aggregate particles, and porosity close to the aggregate surfaces (Scrivener et al. 1999). The degree of cross-linking in the molecular structure (poly-

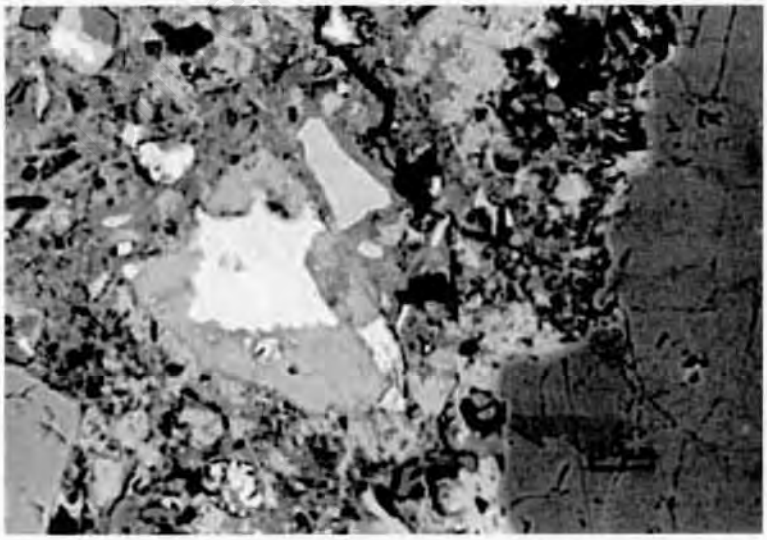

Figure 2.8: Micrograph of plain concrete (Scrivener et al. 1999)

merization) of silicates in cement paste progressively increases with time, a process that is accelerated by increase in temperature. Hydration of cement at high temperatures is known to coarsen the pore structure, and to increase the density of C-S-H in the microstructure (Neville 1971).

2.4.2 Summary: Portland Cement

A summary of the findings on portland cement that was dealt with in section are:

- Basic cement chemistry comprises, a series of oxides, with the main constituent compounds of portland cement being tricalcium silicate C_3S, dicalcium silicate C_2S, tricalcium aluminate C_3A, tetracalcium aluminoferrite C_4AF, magnesium oxide (MgO), sulphates (SO_3), and free calcium oxide CaO.
- Cement hydration is the reaction in which water is chemically combined with anhydrous phases in the grains of cement to form hydrated compounds. The hydration products are calcium silicate hydrates (C-S-H), calcium hydroxide ($Ca(OH)_2$), and ettringite.
- As hydration progresses, the microstructure of hardened cement paste changes as hydration products form around the cement particles. The paste transforms from a fluid state, when the particles remain separate, to a fixed form after the layer of hydration has bridged the particles.
- Increased hydration results in an increase in the degree of polymerisation and high curing temperatures are associated with densification of C-S-H around unhydrated cement grains as well as coarsening the pore structure.

2.4.3 Advances in Cement-Based Materials

Due to high concrete demand and changing needs, the construction industry has taken considerable strides forward over the last two to three decades. Advancements in new techniques of concrete production have led to the development of High Strength Concrete (HSC) which is part of the general

class of concrete products known as High Performance Concrete (HPC) as illustrated schematically in Fig. 2.9. At the same time, alternatives to conventional concrete to meet specific needs have been the subject of research in the recent past. Fig. 2.9 illustrates the main classifications of cement-based products.The following notation is used in Fig. 2.9:

OC: Ordinary concrete
SCC: Self Compacting Concrete
HPC: High Performance Concrete
HSC: High Strength Concrete
FRCC: Fibre Reinforced Cementitious Composites
HPFRCC: High Performance Fibre Reinforced Cementitious Composites
ECC: Engineered Cementitious Composites
TRC: Textile Reinforced Concrete
TC: Textile Concrete

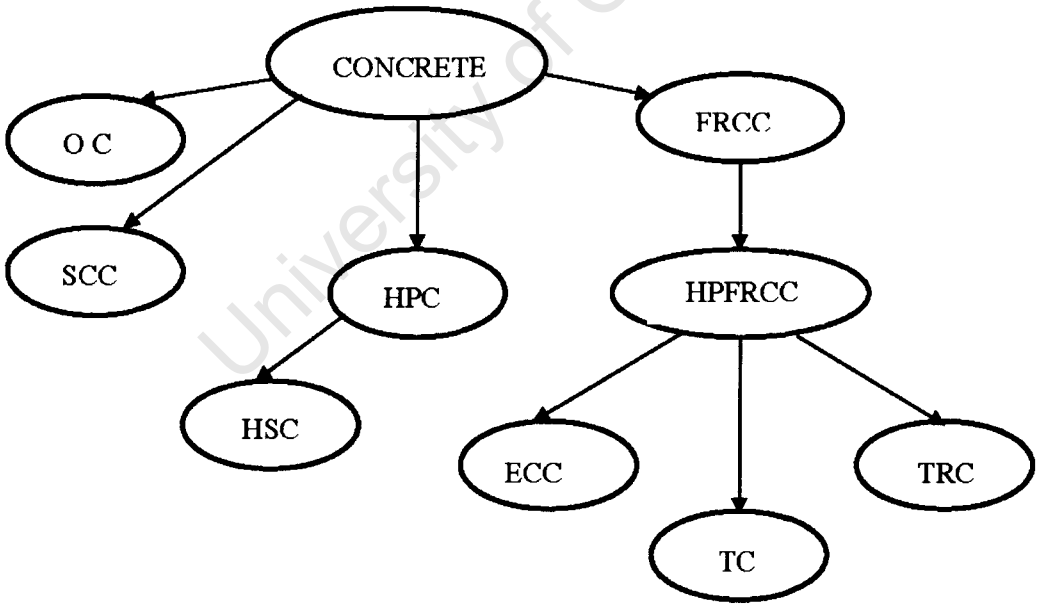

Figure 2.9: Main classifications of cement-based products

A group of cementitious composites that has been progressing rapidly and has attracted considerable interest within the last three decades is Fibre

Reinforced Cementitious Composites (FRCC). However, FRCC is not an entirely new concept as natural fibres have been employed as reinforcement to brittle materials since ancient times and indeed, their use traces back to the early Egyptian fibre composites technology (Broutman & Krock 1975). These early civilizations employed natural fibres for brittle matrix reinforcement, with the advantages of their availability, renewability, and low cost.

Fibrous materials were commonly used to obtain greater strengths or to avoid cracks during setting (Moropoulou et al. 2005). However, the use of natural fibres as reinforcement to brittle cementitious matrices is often faced with difficulties associated with long-term fibre shrinkage and deleterious effects of the strongly alkaline cement environment on the fibres, which impacts on the long term performance of the composite. This need has motivated the search for alternative fibres which would be more suitable for reinforcing cementitious matrices.

The Fibre Reinforced Cementitious Composites (FRCC) industry has made major strides in recent years, due on the one hand, to technological developments in the choice of the matrix properties, fibre volume fraction (V_f), and the interfacial properties (Miguel & Amparo 1997). New innovations in the composite production process have also contributed to a better understanding of the fundamental mechanisms controlling the mechanical behaviour of FRCC (Konrad et al. 2003), (Kabele 2003*b*).

By an appropriate choice of the properties of the constituent materials and the interfaces, the following properties are achieved: quasi-strain hardening behaviour, improved strength, toughness, energy absorption capacity, stiffness, durability, and corrosion resistance. These properties characterise a good engineering material. For FRCC to meet the performance demands listed here, it is usual to modify the binder properties by the addition of supplementary cementitious materials and chemical admixtures at its production stage (Dhir et al. 2002).

2.4.4 Supplementary Cementitious Materials and Admixtures in Cement-Based Products

Supplementary cementitious materials (SCMs) are finely divided latent hydraulic or pozzolanic materials that exhibit cementitious properties when added to normal concrete mixtures. The beneficial role of SCMs, either as additions or as partial replacements for portland cement or the fine aggregate in cementitious products, is well documented (Addis & Owens 2001), (Sahmaran & Yaman 2005), (Park, Noh & Park 2005). These additions can be used to achieve desired performance. Therefore, where available, supplementary cementitious materials are becoming widely accepted as routine ingredients in concrete mixtures.

In FRCC production, SCMs are beneficial in improving workability and flow properties, which often become compromised by fibre inclusion. Most SCMs are by-products of the power generation or metal smelting industries, and among them, Fly Ash (FA), Condensed Silica Fume (CSF), and Ground Granulated Blast Furnace Slag (GGBFS) are most common. In the recent past, a new product known as Ground Granulated Corex Slag (GGCS) has become available in the cement industry of the Western Cape Province of South Africa. GGCS is similar to GGBFS but has more ultra-fine particles than conventional blast-furnace slag. It also has higher proportions of calcium, magnesium, and aluminium oxides and therefore, possesses a higher hydraulic activity than GGBFS.

Elsewhere, rice husk ash, which is a by-product of agro-based industries, with pozzolanic properties has been shown to have potential for application in cementitious products (Nehdi, Duquette & Damatty 2003), (Ajiwe, Okeke & Akigwe 2000). In the South African cement industry a relatively recent entrant is Ultra Fine Fly Ash (UFFA), commercially referred to as "Super-Pozz". Due to the above benefits the use of alternative binders to partially replace ordinary portland cement or the fine aggregates has also become common practice in FRCC production. The properties of UFFA are dealt with in the section that follows.

2.4.4.1 Ultra-fine Fly Ash in Cementitious Products

The early age strength of concrete has assumed considerable significance in the modern construction industry due to the need for striking forms and transferring loads in a short time. The strength is achieved in various ways and among them, the use of Ultra-fine Fly Ash (UFFA) has been accepted in recent years as one of the effective techniques in producing high early-strength concrete (Baoju, Youjun, Shiqiong & Jian 2001).

Studies carried out recently by Isaia *et al.* (Isaia, Gastaldini & Moraes 2003) have addressed the issue of physical and pozzolanic action of mineral additions in cement-based materials. Although the studies have not been directly focussed on the use of UFFA, it is clear that the presence of conventional Fly Ash (FA) in cementitious materials has beneficial effects particularly on the compressive strength as the material ages. It has also been shown that substitution of cement by 15 percent FA causes an increase in the compressive strength of concrete mixes by over 100 percent between 28 days and 180 days (Pala, Ozbay, Oztas & Yuce 2005). Similar effects would be expected in UFFA mixes as well. Indeed, UFFA is credited with highly reactive silicate activity. Therefore, as a partial replacement, it finds wide application in high performance concrete products such as grouts, repair mortars, and sprayed concretes.

The main feature of UFFA that renders it highly pozzolanic is a unique particle size distribution and spherical shape. The mean particle diameter of UFFA typically ranges between 3.9 and 5.0 μm with over 90 percent of the material having a particle diameter of less than 11 μm. Whilst silica fume is finer, it is predominantly single sized compared to UFFA, which by contrast typically has a variable particle size distribution modes as shown in Fig.2.10. UFFA particles are spherical and act like ball bearings within the concrete microstructure. Therefore, the water requirement for a given workability is reduced substantially leading to a less permeable material (Kayali 2004).

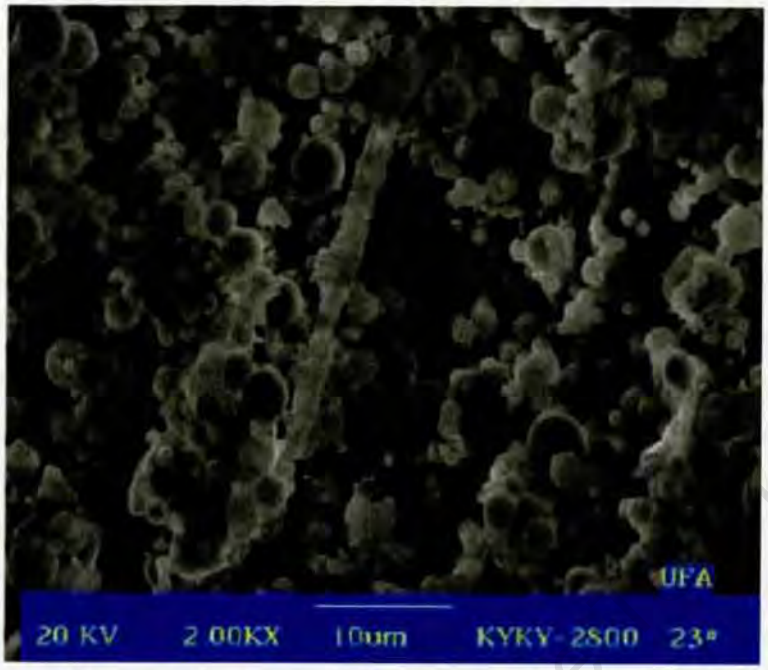

Figure 2.10: Micrograph showing variable particle distribution of UFFA (from World Wide Web 2007)

2.4.4.2 Chemical Admixtures

Admixtures are manufactured chemicals, which are added to concrete in minor proportions (of less than 1 percent by mass of cement) before or during mixing. They impart special properties to conventional fresh or hardened concrete mixes such as; control of setting time (achieved by addition of gypsum), improved workability, strength enhancement, and durability. Due to these advantages, admixtures are commonly added to cementitious mixes in order to overcome difficult construction situations such as hot or cold weather placements, pumping requirements, early strength requirements, or very low water:cement ratio specifications.

The most widely used chemical admixtures for concrete are water reducers (plasticisers), air entraining agents, retarders, and accelerators. An admixture in common use, both as a water reducing agent and a retarder, is lignosulfonate, which is a by-product of wood processing industries. In the unpurified form, lignosulfonates contain substantial proportions of sugars

and other salts which contribute to the retarding property (Dransfield 2003). When lignin in wood pulp is processed to remove sugars and other materials, the product is used for manufacture of admixtures referred to as Modified lignosulfonates (MLS).

High range water reducers are chemical admixtures that reduce the quantity of mixing water required to produce concrete of a given consistency by more than 12 percent (ASTM C494 2005). High range water reducing admixtures are commonly called superplasticizers whose use has become common practice in high quality concrete production (ASTM C494 2005). Indeed, the standard has been modified to include this high-range class of water-reducing admixtures.

Superplasticizers are linear polymers containing sulfonic acid groups attached to a polymer backbone at regular intervals. Most of the commercial formulations belong to one of the following families: Sulfonated melamine-formaldehyde condensates (SMF); Sulfonated naphthalene-formaldehyde condensates (SNF) and Polycarboxylate derivatives. It has been reported that these admixtures exhibit very good dispersing effects in fresh concrete, and can reduce water demand of concrete by up to 25 percent while still maintaining the flow characteristics (Pei, Wang, Hu & Xu 2000).

Superplasticizers were originally developed in Japan and Germany in the early 1960's and later introduced in the United States of America in the mid-1970's. The literature abounds with the beneficial effects of superplastizers in modifying the rheological properties of cementitious materials (Hannant 1998), (Bouzoubaa, Zhang & Malhotra 1998) (Grabiec 1999).

The use of superplasticizers and viscosity modifying admixtures has also led to the development of self-compacting concrete (SCC) for special applications, such as heavily reinforced structures and in placements where adequate consolidation by vibration is not readily achievable. The use of superplasticizers has also contributed to technological advancements resulting in high performance concrete (HPC) with characteristic compressive strengths double or even triple what has been achieved in the past (Wee, Matsunaga &

Sakai 1995).

SMF-based superplasticizer has been successfully employed in the production of Fibre Reinforced Cementitious Composites without causing major workability problems (Hannant 1998). However, a commercially available polycaboxylate was selected for this work to improve flow.

2.4.5 Summary: Advances in Cement-Based Materials

- Technological advancements in concrete production have contributed to a better understanding of behaviour of Fibre Reinforced Cementitious Composites (FRCC).
- In order to meet performance demands in FRCC such as quasi-strain hardening, improved strength, and toughness, properties of binders are modified by addition of supplementary cementitious materials (SCMs) such as fly ash (FA), condensed silica fume (CSF), ground granulated blast furnace slag (GGBFS), and ground graduated corex slag (GGCS).
- The benefits of ultra fine fly ash (UFFA) as a supplementary cementitious material are attributed to spherical particles which act like ball bearings within the concrete microstructure leading to a substantial reduction in water requirement for a given workability, which results in reduction of permeability.
- Chemical admixtures impart special properties to conventional fresh mixes or hardened concrete such as; workability, strength enhancement, and durability.
- Superplasticisers are high range water reducing admixtures which are added in concrete for viscosity modification, which has led to development of self-compacting concrete (SCC) for special applications. Superplasticisers have also been successfully employed in production of FRCC.

2.5 Ageing and Degradation of Concrete

Degradation in concrete refers to reduction in quality and essential properties over time. Normally, concrete undergoes degradation with age but the minimum required quality is not expected to be reached before the end of the design service life. The nature of degradation of concrete depends on: (i) internal factors such as; permeability, binder type, binder content, and water:binder ratio, and (ii) physical or chemical factors associated with the environmental exposure. Physical attack is due to mechanisms of abrasion, erosion, cavitation, or expansive reaction such as freeze-thaw. On the other hand, chemical attack is driven by dissolved gases and liquids, which cause sulphate attack, alkali-silica reaction, and carbonation (Rendell, Jauberthie & Grantham 2002). Chemical degradation depends on the nature and concentration of aggressive fluids and increases with increasing temperature and humidity (Addis & Owens 2001).

This thesis is mainly concerned with degradation related to the moisture state of FRCC, the role of temperature in the degradation process, the mechanical effects of cyclic wetting and drying, and degradation associated with carbonation; therefore, these are dealt with in the sections that follow.

2.5.1 Effects of Moisture and Temperature

The microstructure of concrete is characterised by capillary pores, voids, and discontinuities at the macro level, and minute gel pores at the micro level. These features provide paths for gases and liquids to penetrate the microstructure. The rate of movement of gases and ions through the pore structure is influenced by the amount of moisture in the pores (Addis & Owens 2001). The rate of ingress of fluids into concrete increases with increasing temperature.

Moisture may dissolve cement hydration (for example CH) products which if leached out of the concrete lead to efflorescence and eventual destruction of calcium silicate hydrate (C-S-H), causing loss of concrete strength.

Similarly, when acids react with products of hydration as well as unhydrated cement, corrosion of the concrete matrix ensues.

Cyclic action of temperature and moisture that is common in some tropical environments has been attributed as the course of leaching of concrete and subsequent propagation of microcracks (Savastano et al. 2003). The physical effects of thermal changes are volume movements which induce stresses in the microstructure leading to increase in microcracking in concrete. Gases and fluids are absorbed and retained within the microcracks where they cause physical and chemical expansive reactions.

2.5.2 Effects of Carbonation

Atmospheric carbon dioxide (CO_2) combines with water in the pores and capillaries of cement-based products to form carbonic acid, which in turn reacts with $Ca(OH)_2$ and hydrated calcium silicate to form $CaCO_3$ and water. Carbonation reactions are described by Eqs. 2.1 to 2.3 (Rendell et al. 2002). The common carbonation reaction is described by Eq. 2.2, and a more severe form of carbonation (resulting in the formation of a silica gel) is described by Eq. 2.3.

$$CO_2 + H_2O \rightarrow H_2CO_3 \tag{2.1}$$

$$H_2CO_3 + Ca(OH)_2 \rightarrow CaCO_3 + 2H_2O \tag{2.2}$$

$$H_2CO_3 + CaO.SiO_2.H_2O \rightarrow CaCO_3 + SiO_2 + 2H_2O \tag{2.3}$$

The ingress of CO_2 into a cementitious matrix of medium humidity is associated with reduction in pH and increase in the tendency of hydration products ($Ca(OH)_2$ and C-S-H) to dissolve. The product of carbonation

($CaCO_3$) is subsequently transported to more porous zones where it is deposited (Bentur & Akers 1989). $CaCO_3$ occupies a greater volume than the replaced $Ca(OH)_2$) and therefore carbonation causes a volume change and reduction in the average pore size in the microstructure. The production of $CaCO_3$ results in reduction in pH of concrete from 12 to about 8 (Rendell et al. 2002), which leads to depassivation of reinforcing steel.

When concrete carbonates, $CaCO_3$ crystals are deposited in the voids thereby increasing the density of cement paste (Neville 1971). The increase in density causes an increase in surface hardness and strength, reduced surface permeability and moisture movement. The rate of carbonation depends on concrete quality, water:cement ratio and compaction. Optimum carbonation rate of concrete occurs at relative humidities of between 50 and 70 percent (Neville 2002). Therefore, carbonation rate is lower for concrete that is continuously exposed to high humidity, or alternatively very low humidity.

With regard to Fibre Reinforced Cementitious Composites, the particular concern is that whereas carbonation is accompanied by reduction in porosity of the matrix, chemical changes occur in fibres after exposure to CO_2-rich environments. For example, carbonation has been found to cause a breakdown of molecular chains of cellulose fibres, which negatively affects the long-term reinforcing potential of the fibres (Akers & Studinka 1989).

2.5.3 Swelling and Shrinkage of Concrete

At early age, concrete undergoes moisture loss which is commonly accompanied by volume change. Shrinkage in cementitious materials is a volume change that is dependent on temperature and environmental conditions (Addis & Owens 2001). When concrete is restrained, shrinkage causes tensile stresses to be induced leading to cracking.

During cyclic wetting/drying of cementitious materials, capillary forces are created which cause swelling and shrinkage. Swelling occurs during a wetting cycle whereas shrinkage occurs when the capillary forces are created in the microstructure due to the effects of drying. The changes in relative

humidity induce dimensional changes in C-S-H which introduce local high stress regions in the microstructure leading to localised creep (Addis & Owens 2001).

The movement of water in and out of hydrated particles affects the particle spacing. During a drying cycle, water is lost from the paste, first from the larger pores such as capillaries and then from the smaller gel pores. Water inside the pores is in a state of tension which is normally balanced by compressive stresses in the surrounding gel, causing a reduction in particle spacing. Reduction in particle spacing with time leads to a decrease in total energy of the system and new bonds are formed between hydrate layers. This mechanism results in shrinkage (Addis & Owens 2001). On the other hand, wetting creates a free-water layer within the microstructure, which hinders adsorption resulting in disjoining pressure or swelling.

Carbonation causes reduction in volume referred to as carbonation shrinkage. This form of shrinkage in concrete is optimum at intermediate humidities (between 50 and 70 percent) when there is sufficient water in the pores within the cement paste for CO_2 to form carbonic acid. The mechanism of carbonation shrinkage involves changes in the basic structures of CH as well as C-S-H. Cement paste undergoes temporary increase in compressibility resulting from dissolution of CH from regions under compressive stresses created by capillary tension in the liquid (Neville 1971). While this mechanism may account for the individual contribution of CH to shrinkage, a dimensional change in cement paste due to the removal of calcium ions (decalcification) is largely responsible for carbonation shrinkage (Chen, Thomas & Jennings 2006).

Carbonation shrinkage was recently investigated and interpreted as a special case of a more general decalcification shrinkage (Chen et al. 2006). Decalcification occurs in cement pastes due to processes of leaching by soft and acid waters, and carbonation. Below Ca/Si of approximately 1.2, an increase in polymerisation of silicate molecules in C-S-H occurs (Chen et al. 2006). This finding is consistent with an earlier study that was carried out on carbonation shrinkage in autoclave aerated concrete (AAC) (Matsushita,

Aono & Shibata 2004).

Studies by Matshushita *et al.* were undertaken on AAC at carbonation levels ranging from 25 to 65 percent. It was found that the structure of tobermorite, which is the principal binding mineral in AAC, changed due to dissolving of calcium ions from calcium oxide layers causing the structure of C-S-H to undergo reorganisation by polymerising to a silica gel structure. These microstructural changes in C-S-H largely account for carbonation shrinkage in concrete.

2.5.4 Summary: Ageing and Degradation of Concrete

- Degradation of concrete is caused by physical and chemical processes at macro and micro level, which are driven by either internal factors or exposure conditions.
- Moisture provides the medium for gases to dissolve, and cracks, capillaries, and pores form the paths for the dissolved gases and fluids to diffuse into the microstructure and react with hydration products.
- High temperatures accelerate chemical reactions such as sulphate attack, alkali-silica reaction, chloride ions diffusion, and carbonation.
- Cyclic wetting and drying leads to shrinkage and swelling which result in cracking.
- $CaCO_3$ which is produced after carbonation reaction occupies a greater volume than the replaced $Ca(OH)_2$ which causes a reduction in the pore size, hence densification of the matrix.
- Carbonation causes changes of the C-S-H structure after decalcification resulting in carbonation shrinkage.

2.6 Benefits of Fibres in Performance of FRCC

The mechanical theory of reinforcing action of fibres in cementitious matrices is dealt with in Chapter 3. The beneficial effects of fibres in cementitious matrices are that tensile cracking of the composite is controlled and delayed

so that unstable and uncontrolled tensile crack growth is transformed into slow controlled crack growth. Therefore, fibres modify post-cracking behaviour of the composite to give increased strain capacity and enhanced energy absorption (Swamy 1980). The fibres' performance in controlling cracking and maintaining toughness of FRCC is dependent on the fibre volume fraction V_f. The relationship between composite stress-strain behaviour and V_f is illustrated schematically in Fig. 2.11, which is according to the following classification by Perrie and Butler (Perrie & Butler 1994):

- If the fibre volume content is below a critical value V_{fc}, the composite will fail suddenly by fibre breakage after first matrix crack (A).
- If V_{fc} is exceeded but the bond strength and aspect ratio are such that the stress in the composite is not sustained when the matrix cracks, the composite will not undergo multiple cracking. Failure will be by fibre pull-out in a gradual manner with a falling stress tail, a behaviour referred to as strain softening (B).
- If the fibre content exceeds V_{fc}, fibre strength is low, and the fibre/matrix bond is strong, a plastic deformation after first crack will occur, indicating the ability of the composite to continue deforming without either losing or increasing in load. The composite will fail by fibre damage followed by rupture (C).
- If the fibre content, strength and bond are all sufficient, then the load in the composite is transferred onto bridging fibres and a rising stress-strain curve results. The composite will exhibit fibre stretching between cracks prior to failure (D).

For a given fibre volume, the typical tensile stress-stress behaviour of a composite changes according to the matrix microstructure, fibre type, and environmental conditions, factors which affect the mechanisms of ageing in FRCC. The benefits of fibres in the behaviour of FRCC are dealt with in the sections that follow.

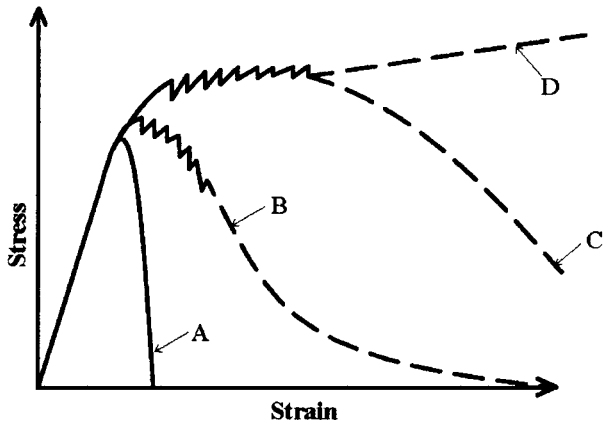

Figure 2.11: Idealised stress-strain curves for FRCC

2.6.1 Role of Fibres in Weathered FRCC

In wet/dry environments where there is adequate hydration, cement hydration products develop around embedded fibre surfaces. For cellulose fibres which are naturally hollow, the hydration particles cause embrittlement to the hollow fibres. If the products migrate to the fibre lumen and fill the pores, they cause the fibres firstly to be brittle and secondly the fibres become petrified (Bentur & Akers 1989). Brittle hollow fibres are essentially weak and they break prematurely leading to loss in composite strength and toughness (behaviour type C).

Petrification of cellulose fibres is commonly found in carbonated composites, which develop higher strength, stiffness, and dimensional stability than un-aged composites (Bentur & Akers 1989). Dimensional stability means that there is less tendency for the embedded fibres to shrink away from the matrix following carbonation shrinkage. The changes in fibre properties together with a denser matrix after carbonation accounts for increase in strength and reduction in toughness in carbonated composites (Bentur & Akers 1989), (Akers & Studinka 1989).

Cyclic action of temperature and moisture increases porosity (leading to leaching), and propagation of microcracks which weaken the matrix at the vicinity of the fibres (Savastano, Warden & Coutts 2005). When the matrix is weak, but the fibres retain satisfactory bonding with a matrix, the

composite toughness is improved because the microstructure allows greater energy dissipation through microcracking (in the vicinity of fibre surfaces), as well as enhancing the mechanism of fibre pull-out.

2.6.2 Role of PP Fibres in Weathered FRCC

Polypropylene (PP) fibres do not easily absorb water from a wet environment nor give it up to a drier one (they are hydrophobic), hence the fibres do not undergo swelling and shrinkage like concrete does during wet/dry cycling.

In Fibre Reinforced Cementitious Composites (FRCC), PP fibre surfaces provide additional sites for deposition of cement hydration products, which are not easily removed in concrete during swelling and shrinkage. Deposition of hydration products on the fibres contributes to an increase in fibre/matrix bonding with age (Hannant 1978).

The beneficial effects of PP fibres in cementitious matrices is that they control cracking and alter the post-cracking behaviour of the composites in the short-term. In the long-term, the composite performance is evaluated from mechanical tests on samples aged under different environments.

Durability studies were undertaken using fibrillated films to enable easy penetration of cement mortar and promote bond with the cement paste (Hannant 1998). The studies involved evaluation of the durability of the polypropylene fibers subjected to natural weathering, storage in laboratory air, and storage under water for periods of up to 18 years. For samples stored under water, a reduction of about 19 percent in polypropylene film strength after 18 years was reported, which was considered a satisfactory strength retention. Long-term toughness was also reported in the study (Hannant 1998).

Evaluation of fibre/matrix bond strength was undertaken from crack spacing which showed that the bond strength remained constant at about 0.4 MPa regardless of time, or exposure conditions (Hannant 1998). This implied that the bond strength depended on the intermolecular shear strengths of the aligned polymer chains, which were time stable and did not depend on the matrix microstructure.

2.6.3 Summary:Benefits of Fibres in Performance of FRCC

- The main benefits of fibres in FRCC is increase in toughness. Densification of the matrix around the fibres contributes to lowering of the composite toughness by reducing the flexibility and deformation capacity of the fibres. Depending on the fibre type, and environmental exposure, matrix densification can be accompanied by reduction, or increase in composite strength.
- The prevailing behaviour in aged cellulose fibre cement composites is loss of toughness, due to changes in fibre properties and matrix microstructure at the fibre/matrix interface.
- Extended surfaces of PP fibres that are used in cementitious matrices are additional sites for deposition of hydration products, which reduces adverse effects of swelling and shrinkage in the matrix.
- Bond strength between polypropylene and cement was relatively unaffected by exposure condition, and long-term toughness over many years is documented.

2.7 Textile Concrete Technology

In the past, South Africa has adopted the use of fibres in cementitious products and applications, driven by the need for cost-effective and innovative solutions to unique problems associated with mining. Therefore, fibre cement applications in South Africa were developed largely for the mining industry. Over the last 10 years, Textile Concrete (TC) technology has been employed in some of these applications (Taylor, Mostert & Hourahane 1997).

Polypropylene (PP) has been in use as plain fibres for more than 50 years and as non-woven textiles in concrete for approximately 30 years. Therefore, the behaviour of PP fibres is well understood making a PP a commonly chosen polymer for reinforcement of cementitious matrices.

2.7.1 Textile

During the last decade or so, textiles have been customised for application in cementitious mixes (Kenai, Refai & Brooks 1995), (Konrad et al. 2003). The development of the textiles owes much to the work of Hannant and co-workers (Hannant et al. 1978), (Hannant & Zonsveld 1978) in which continuous open fibrillated polypropylene films were employed as alternatives to asbestos fibres in thin sheet products. The developments were aimed at producing quasi-ductile cement-based composites capable of developing closely spaced cracks at failure (Hibbert & Hannant 1982), without the deleterious health aspects associated with asbestos.

In South Africa particularly, the key development in the textile production process was a specially developed fibre consisting of a polymeric fibre as the core over which an outer fluffy layer is spun to form a sheath. To prevent separation of the outer fluffy layer from the inner core, it is intermittently ultrasonically welded (referred to as bonded fibre in Fig. 2.12) to the core at approximately 6 mm centres to form a "hybrid fibre". The two fibre formats are illustrated in Fig. 2.12. The inner core surrounded by an outer fluffy layer is shown in Fig. 2.13. The ultrasonic welding of PP fibres illustrated in Fig. 2.12 was developed by Textile Concrete Consultants in South Africa (World Wide Web 2006*d*).

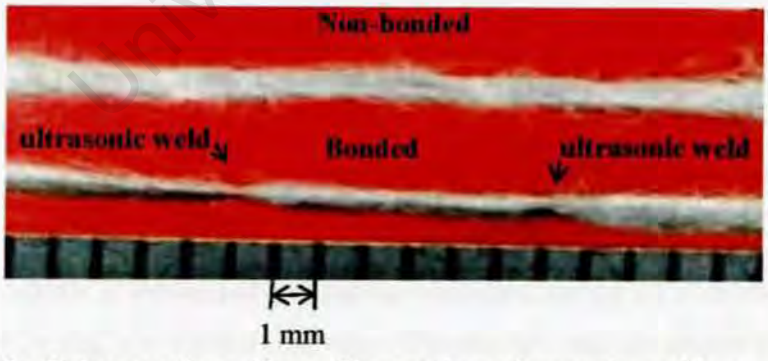

Figure 2.12: Polypropylene fibres illustrating ultrasonic welds on a bonded fibre (courtesy of Textile Concrete Consultants, 2006)

The "hybrid fibre" is a unique feature of the yarn since it provides the

Figure 2.13: Non-bonded fibre showing central core (on the left stripped by a fingernail) and the outer fluffy layer on the right

basis for achieving not only sufficient strength, but controlled mechanical bond to the cementitious matrix and reists fibre pullout behaviour, simulating asbestos fibre bonding with cement (Tait & Guddye 2002). However, the "hybrid fibre" characterisation is on-going as part of this research. The "hybrid fibres" are then woven into a fine or coarse matrix cloth, further providing localised strength, or they are ultrasonically bonded to water-proof membranes to provide the desired properties. A typical PP textile, commercially referred to as CemForce, showing an extended fibrous interface area is depicted by Fig.2.14.

Fig.2.14 shows the main fibre in the weft direction with the outer fluffy layer and warp fibres threaded in between. Non-bonded refers to main fibres with a fluffy layer that has not been ultrasonically welded to the central core (illustrated earlier in Fig. 2.13). The quoted nominal strength of the textile material is 20 kN per metre width, has a mass of 125 g/m^2 and compresses during hand lay-up technique to a thickness of between one and two millimetres.

2.7.2 Textile Concrete Production

Textile concrete is essentially a thin structured composite produced from woven textile and a cementitious mix. The textile can be placed in the mix in the appropriate location and orientation for optimum performance. The woven textile is impregnated with cement paste, mortar or a fine concrete mix, applied by dip coating, spraying or block brushing the textile with

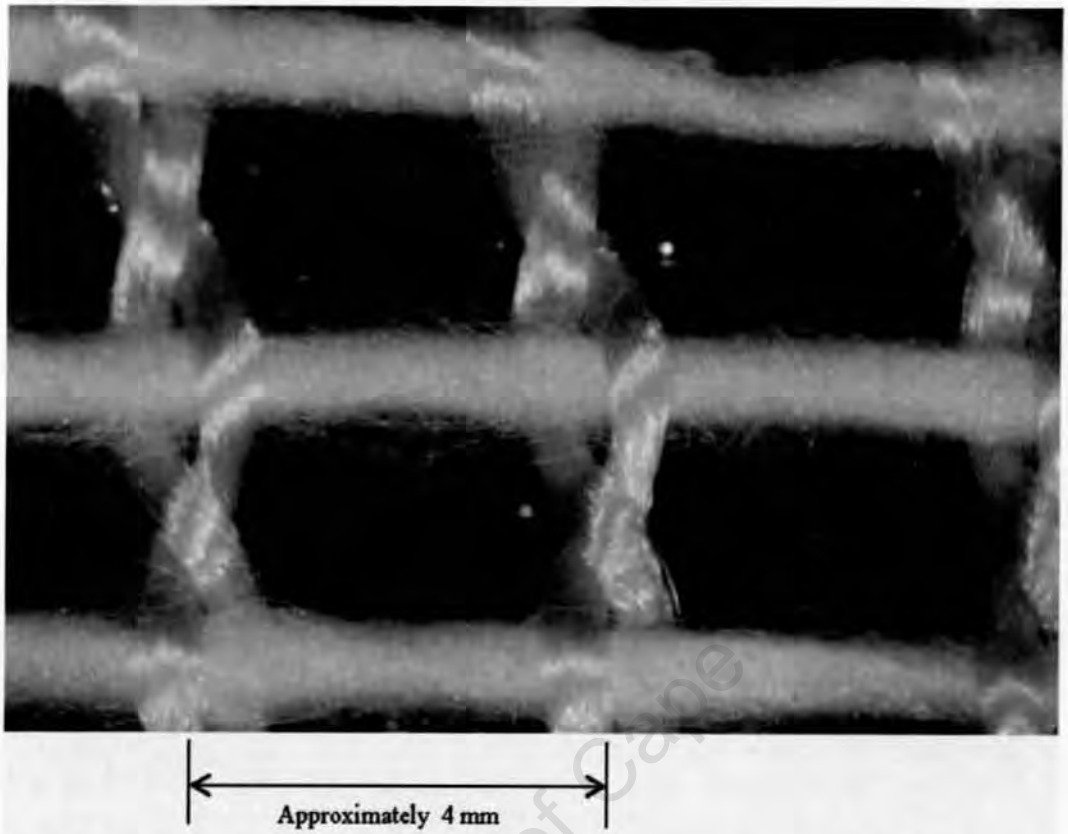

Figure 2.14: 8 X magnification of CemForce showing non-bonded fibres in the weft direction

the wet matrix. The mix can also be worked manually using "hand lay-up" techniques, or through a mechanised process for industrial productions. This technique is not faced with the kind of handling problems encountered when discrete fibres are used in bulk mixes, as is the case with conventional Fibre Reinforced Cementitious Composites. To increase the homogeneity and reduce water and void content, the mix is mechanically pressed into the textile.

The Textile Concrete production process is perhaps best illustrated in a pictorial manner. Layers of CemForce prior to casting are depicted in Fig.2.15, and they are seen across a section of the composite in Fig.2.16. At the casting stage, blotting papers were used on the top and bottom to soak up water (Taylor et al. 1997).

During the fibre/matrix interaction, the fibrous system acts as a filter, allowing water to exude, which in the original case (Taylor et al. 1997) was absorbed using blotting paper. This method was not employed in the present study, since the fines and water were retained were retaining in the interstices of the fibres with which the cementitious matrix can interact and mechanically bond in the hardened state. At the same time, the fibre/matrix interaction initiates crystal formation and growth during the hydration process of cement (Currie & Gardner 1989), (Bentur & Akers 1989). As the cementitious matrix flows around the fine fibrils, it creates a bond and sets into a homogeneous, tough and strong material with a "concrete-like" weatherproof surface. The fibres are firmly embedded in the matrix and are therefore sufficiently protected from adverse weathering effects.

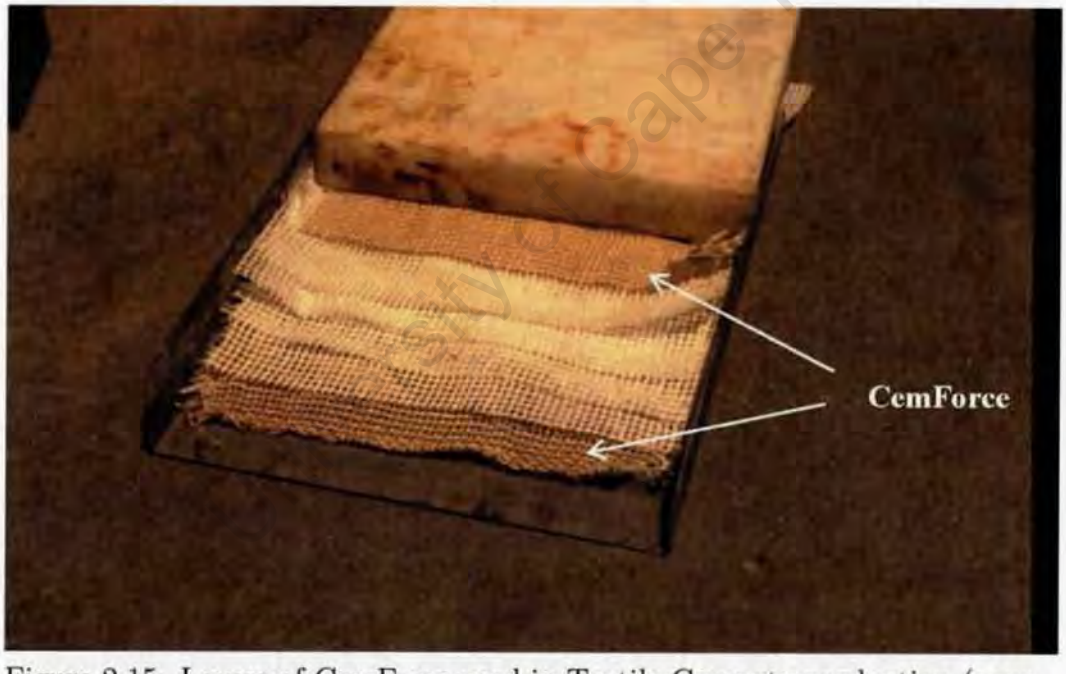

Figure 2.15: Layers of CemForce used in Textile Concrete production (courtesy of Taylor *et al.* 1997 and Textile Concrete Consultants 2006)

Textile Concrete composites with V_f in excess of 10 percent are possible. This V_f is much higher than volume fraction of fibres ordinarily incorporated in short fibre reinforced concrete (typically less than 3 percent).

In most applications, TC is in the form of laminates of textile layers

Figure 2.16: Cross-sectional view of Textile Concrete (courtesy of Taylor *et al.* 1997 and Textile Concrete Consultants 2006)

cast in mortar or cement paste. For example, textile concrete laminates with nominal thickness of 8 mm have been produced with PP textile fibre contents of between 6.25 to 12.5 kg/m^3 using hand lay-up techniques. This is against typically 1 kg/m^3 of loose fibre that could conventionally be wet mixed into the matrix (Mumenya et al. 2003). In related work, a similar TC production technique was employed and light-weight elements with remarkable strain hardening properties were produced, and preliminary characterisation of the mechanical properties of these elements was undertaken by the author (Mumenya et al. 2006).

Textile Concrete exhibits high toughness and minimal corrosion susceptibility, is user friendly and tolerant to bending and impact loads. The textile material can be ultrasonically welded to waterproof membranes. As a result, the new material (after casting in cementitious matrices) has found diverse applications, even though its development is still in the early stages. The applications include architectural features such as cladding of buildings, artificial rock features for gardens, permanent shuttering for concrete members (which eliminates surface blemishes), ecological habitats for fish, and waterproof members for reservoirs and ditches.

2.7.3 Advances in Textile Concrete Technology

Despite being a relatively new concept, Textile Concrete technology is gradually gaining acceptance, not only in South Africa, but also in other parts of the world, notably, the United States of America, New Zealand, and Europe.

In Germany, a special research project based at the Technical University of Aachen is dealing with different levels and scales of textile/matrix interaction (Hegger, Sherif, Brukermann & Konrad 2004). For example, a multi-level approach to visualisation of textile concrete structures was recently proposed (Konrad et al. 2003) leading to the development of a consistent material model. Using this approach, a better understanding of damage and failure mechanisms of TC is gained.

At a micro level, the loading mechanism is visualised as the interaction of firstly, the individual fibrils, and then of a matrix-fibrils system. The assembly of fibrils, spanning around the central core, together with their interaction with the matrix represents a structure at the meso level. At meso and micro levels, the physical and mechanical properties of the fibre and matrix as well as the nature of the interfacial bond influence the composite material properties.

Other mechanisms playing a key role in loading and failure mechanics of TC are the cracking mode and the fibre end slippage. These mechanisms have been modeled by unifying the micro-mechanics and fracture mechanics effects with the fibre/matrix bond properties (Wang, Li & Backer 1988).

The fracture mechanics-based factors that adequately describe the mechanics of fibre/matrix interface are: the flaw size, crack initiation, crack alignment, crack tip and fibre bridging toughness. These fracture mechanics-based parameters have been numerically related to material properties by various researchers (Kanda, Lin & Li 2000*a*), (Kabele 2003*b*).

At the macro level, the material structure is visualized as composed of the woven textile interacting with the bulk matrix structure. At this level, failure is characterised by multiple cracking, which is normally modeled by the relationships between the bridging stress (σ) that is provided by the

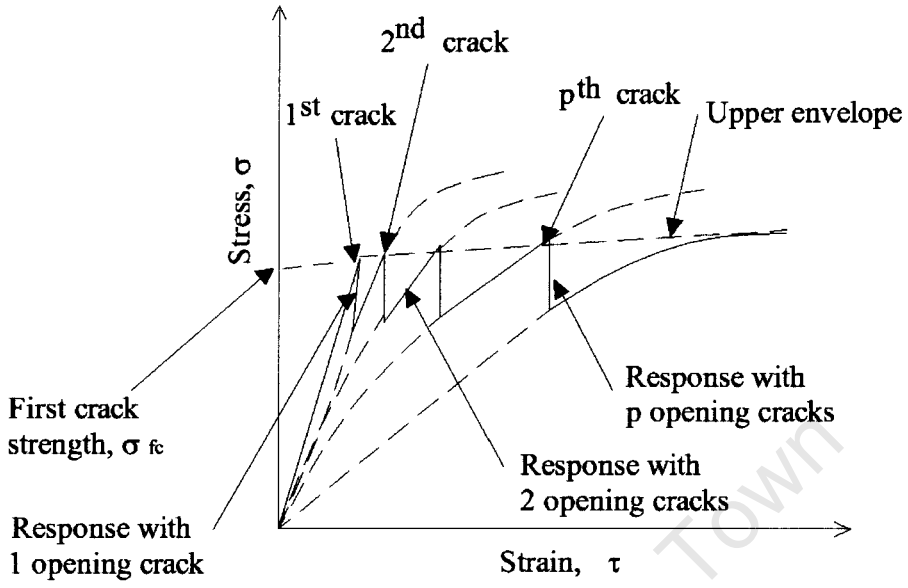

Figure 2.17: Multiple cracking in HPFRCC

reinforcing fibres, and the extent of crack opening displacement (d) (Kabele 2003*b*).

2.7.4 Mechanism of Multiple Cracking

Fibre reinforced cementitious composites that exhibit multiple cracking and strain hardening, as illustrated schematically by Fig. 2.17, have traditionally been referred to as the High Performance Fibre Reinforced Cement Composites (HPFRCC) (Jasper, Bush & Henrick 1989). During the multiple cracking and strain hardening stage, a large amount of energy is absorbed by the material, hence the high energy absorption capacity or toughness (stresses of the order of 3 MPa) of HPFRCC materials.

A micro-mechanics-based approach to the analysis of the mechanical behaviour of High Performance Fibre Reinforced Cementitious Composites (HPFRCC) has advanced the understanding of matrix micro-cracking. Cracking in HPFRCC is influenced by: slippage at the fibre end, the counteracting actions of frictional slip resistance at the fibre-matrix interface, fibre bridg-

ing traction σ_b, and crack opening displacement (COD) (Lin & Li 1997). COD and σ_b are conventional fracture mechanics-based concepts which are essentially competing mechanisms in that the tendency of cracks to open is counteracted by the stresses in the fibres bridging the cracks. In the past, these mechanisms have been modelled in order to characterise the mechanical behaviour of Engineered Cementitious Composites (ECC), which include: mechanics of crack initiation, debonding, decaying fibre/matrix interfacial frictional stresses (Li, Wang & Backer 1991*b*), (Kabele 2003*b*).

It is recognised that a suitable cementitious composite for bending and impact loading applications should have sufficient tensile strength and stiffness, as well as high toughness. In addition, the composite should exhibit strain hardening after the first crack rather than strain softening (described earlier in section 2.6), as commonly found in low fibre volume and strong fibre cementitious composites (Wang & Li 2003).

Strain softening in FRCC was recently addressed in polyvinyl alcohol (PVA) fibre-cement composites by locally lubricating the fibres to reduce the fibre/matrix interfacial bond (Wang & Li 2003). These products are referred to as Engineered Cementitious Composites (ECC). Using such an approach it has been possible to achieve strain hardening characteristics and adequate strengths (≈4 MPa) in the composites (see Fig. 2.18), and "ductile" strain (≈4%), for single fibre pullout tests.

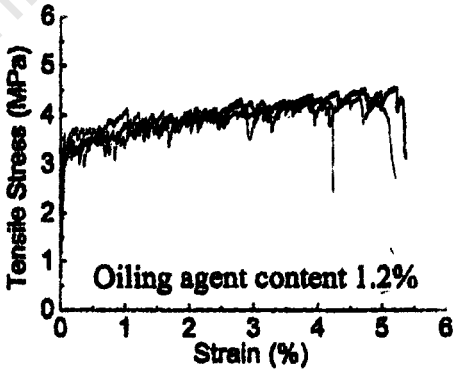

Figure 2.18: Tensile stress-strain curve of composites from (Wang & Li 2003)

Similar high toughness results have been achieved by Tait and Guddye

for single fibres (Tait & Guddye 2002), as well as Taylor *et al.* (Taylor et al. 1997) for laminated composites, using PP fibres. The work by Taylor *et al.* illustrates that by increasing the number of textile layers in the laminate, the flexural strength is progressively improved as shown in Fig. 2.19.

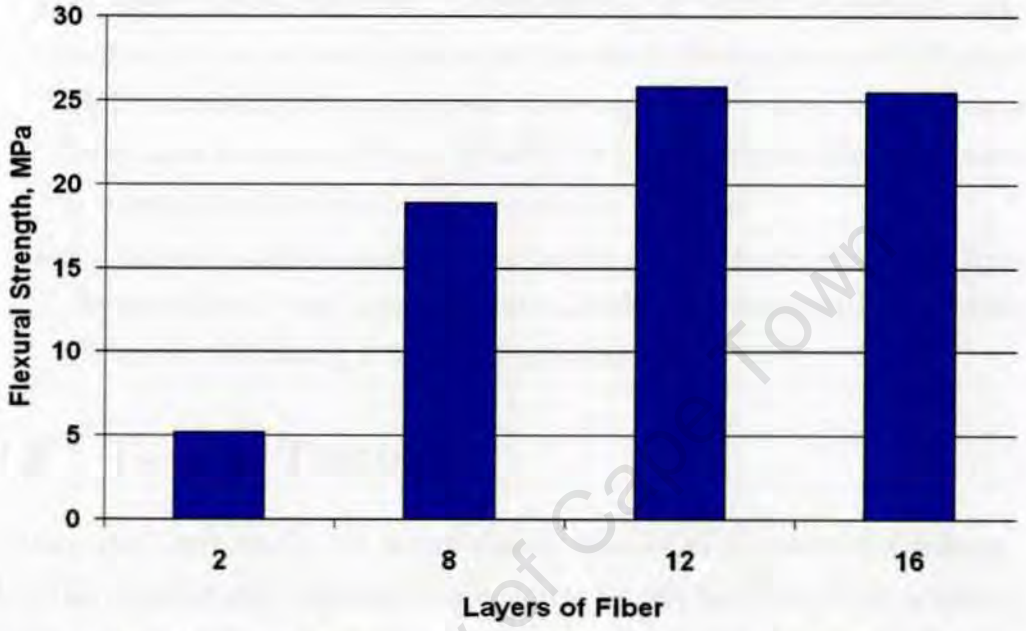

Figure 2.19: Results of Flexural tests on polypropylene textile-cement composites from (Taylor *et al.* 1997)

The mechanical behaviour of HPFRCC is well documented and models describing the behaviour have been developed based on work originally carried out in the early 1970's (Aveston et al. 1971). Later on, mathematical models that described the mechanism of fibre pull-out were developed using either the so called "one-sided" or "two-sided" fibre pull-out approaches (Currie & Gardner 1989). The input parameters in these models are determined from experiments and have been useful tools particularly for studying the fibre/matrix interfacial property and fibre pull-out mechanics (Wang, Backer & Li 1988). The models and theory are dealt with more comprehensively in Chapter 3.

2.7.5 Summary: Textile Concrete Technology

- The developments in PP fibres for use in cementitious matrices is attributed to the work by Hannant (Hannant 1978) on fibrillated PP films as alternative to asbestos fibres.
- In South Africa, the key to development in textile production techniques for use in cementitious matrices is the development of a "hybrid fibre" consisting of a polymeric fibre tape as the core, over which a fluffy layer is spun to form a sheath. To prevent separation, the sheath is intermittently ultrasonically welded to the core.
- Specialised textiles commercially known as CemForce are woven from "hybrid fibres" and tapes and are suitable for production of Textile Concrete (TC) using a hand lay-up technique.

2.8 Tensile Testing

Among the early works on direct tensile testing of cementitious composites, the stress-strain response of a concrete tensile specimen was predicted (Maage 1978). The prediction was based on an approach whereby constituent material properties at micro level were smeared into the uni-axial tensile behaviour of the specimen at the macro level.

More recently, a general broad overview on the subject of uni-axial tensile testing of cement-based products was given by Swaddiwudhipong et al. (Swaddiwudhipong, Lu & Wee 2003). The study investigated the tensile strain capacity of concrete (a brittle specimen) from direct tensile tests. A description of the testing technique is given which includes: fabrication of special moulds which are durable and easily demountable, modifications to conventional gripping systems so that load eccentricity and non-uniformity of stress and strain are sufficiently addressed, and the design of a self-centering joint connecting the testing machine with the specimen in order to eliminate bending moments during the test, hence ensure purely axial loading. The results (Swaddiwudhipong et al. 2003) showed that strain values up to ap-

proximately 70 percent could be monitored, and most of the samples (100 out of 117) failed in the middle section as desired.

Elsewhere, a concise summary of the critical elements in the tensile test set-up for determination of fracture parameters of concrete has been compiled (Van Mier & Van Vliet 2002). Specific problems of the uni-axial tensile test are discussed, which include: analysis of closed-loop testing, and the specimen shape in relation to the prevention of premature failure. The importance of using an appropriate gripping system is discussed, which was also addressed by Swaddiwudhipong et al. (Swaddiwudhipong et al. 2003). The studies show that uniaxial tensile test is a fundamental test to determine the fracture properties of a material.

The work going on in different research laboratories in the area of direct tensile testing of the so called Ductile Fibre Reinforced Cementitious Composites (DFRCC) was recently coordinated by RILEM technical commitee TC 182 HFC and the tensile characteristics of these materials evaluated in a round robin test. In one of the studies on evaluation of tensile characteristics of DFRCC (Kanakubo, Shimizu, Katagiri, Kanda, Fukuyama & Rokugo 2005), uni-axial tensile tests were performed on polyvinyl-alcohol Engineered Cementitious Composite (PVA-ECC) using specimens of four different shapes. Using "dog-bone" shaped specimens, tensile stresses and strains of 4.10 MPa and 1.89 percent respectively were reported. The study illustrates the benefits of tensile tests as a means of evaluating other tests such as bending tests. The value is demonstrated from the results of the study by Kanakubo *et al.* in which values of the ultimate tensile stress and strain which were calculated using a proposed bending moment-based model showed good agreement with tensile test results. From the evaluation, a standard for the test was proposed (Kanakubo et al. 2005).

Part of the round robin tests by RILEM involved characterisation of the tensile mechanical properties of High Performance Fibre Reinforced Cementitious Composites (HPFRCC) as reported by Yang and Fischer (Yang & Fischer 2005). The micromechanical behaviour of PVA-ECC samples,

which had been cured for different time periods (14 days, 28 days, and 9 months) was investigated using uni-axial tensile tests, and the behaviour characterised by stress-crack opening displacement (COD). The tensile test results were utilised in a model that simulated the micromechanical properties of PVA-ECC composites, namely, interface bond characteristics, matrix flaw size, and fibre bridging behaviour. The particular contribution of the study (Yang & Fischer 2005) was in creating a better understanding of the effects of micromechanical properties to the stress-strain behaviour of PVA-ECC composites such as: fibre bridging stress-crack opening relationship of the composite, and the distribution of the matrix flaw size.

Despite many trials of experimental tensile testing and published results, there is no comprehensive agreed upon a tensile test standard for FRCC. Therefore, there is need for a standard test method for characterisation of the strain hardening response of Fibre Reinforced Cement Composites(FRCC). Naaman and Reinhardt (Naaman & Reinhardt 2006) proposed a performance-based classification of HPFRCC using two points on a tensile stress-strain curve: (a) stress and strain at the first crack (σ_1,ϵ_1) and (b) stress and strain at the peak point (σ_2,ϵ_2) as shown in Fig. 2.20.

It was further proposed by Naaman and Reinhardt (Naaman & Reinhardt 2006) that the following information would be required for design: strength classification, minimum strain capacity at peak stress, minimum modulus (at 90 percent confidence level for experimental data), specimen size, and limit of the post-cracking strength. It is illustrated from the literature that uni-axial tensile testing is considered the basis for understanding different aspects of mechanical behaviour of FRCC. These aspects range from theoretical simulations to practical aspects such as design of structural elements.

From the fore-going, it is illustrated that despite the complex nature of tensile testing of cementitious materials, the possibility of standardising the test is within reach. Indeed, uni-axial tensile tests were recently carried out on thin Textile Concrete specimens and the behaviour characterised by the author (Mumenya et al. 2006). Of concern however, is the aging performance

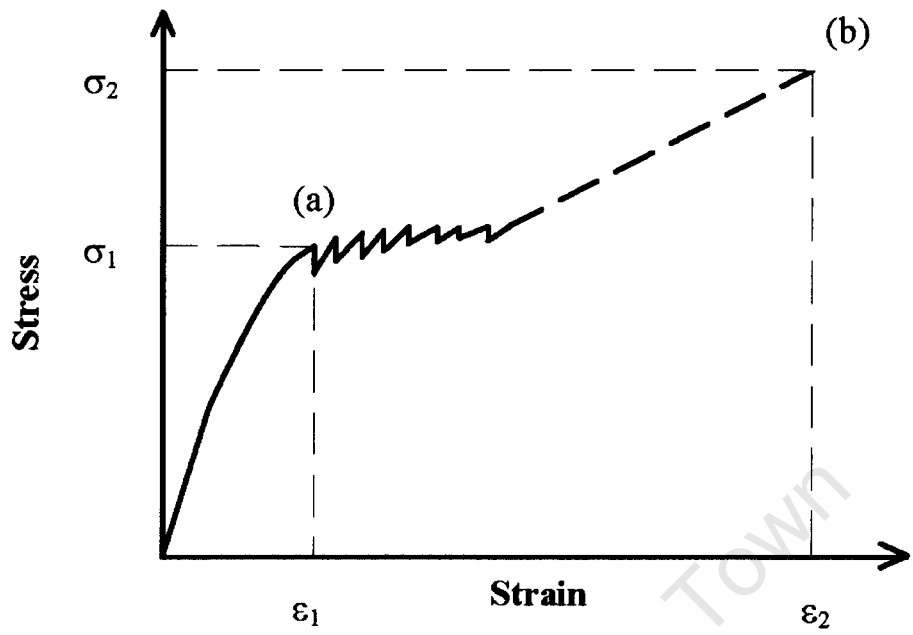

Figure 2.20: Information on tensile stress-strain of FRCC needed for design

of TC and how this behaviour changes with time and environmental factors. The aspects of the ageing phenomenon in cementitious materials in general are briefly dealt with in section 2.9.

2.8.1 Summary: Tensile Testing

- Preliminary mechanical characterisation of TC has been undertaken by the author, and it is shown that TC exhibits strain hardening in flexure, and is capable of achieving high toughness.
- Research developments in Textile Reinforced Concrete (TRC) have taken new dimensions such as: theoretical modeling of the tensile stress-strain behaviour, efforts towards standardisation of tensile test and performance classification for design of FRCC.

2.9 Ageing of Fibre Reinforced Cementitious Composites

When cementitious composites are exposed to different environments, the microstructure is modified due to the physical and chemical processes of ageing. These changes affect the mechanical properties of the material as shown by studies on cellulose fibre cement composites (Akers & Studinka 1989).

Akers and Studinka (Akers & Studinka 1989) evaluated the mechanical, physical, and chemical properties of composite samples after exposure to a CO_2-rich environment, and after natural exposure for five years. Matrix densification and gain in strength were reported, which was attributed to carbonation. Samples exposed to natural environments underwent a general increase in flexural strength and E-modulus, which were also attributed to carbonation of the matrix. An increase in fibre/matrix interface bond, and chemical changes in the fibre were also reported.

In the study by Akers and Studinka (Akers & Studinka 1989), ageing in the cellulose fibres was in the form of breakdown in the molecular chains (causing embrittlement) which was attributed to a decrease in the degree of polymerisation. The studies showed that the increase that was observed in fibre/matrix bonding after carbonation compensated for fibre embrittlement, hence the increase in flexural strength and E modulus. However, in the long-term, carbonation had a negative effect in the reinforcing potential of cellulose fibres due a reduction in composite toughness.

Among the important properties of FRCC are curing, and environmental exposure such as relative humidity and temperature, which influence the micro-mechanical interactions in cementitious materials. Studies were carried out (Tait & Akers 1989) on the mechanism of strength development and composite failure in freshly prepared synthetic and cellulose fibre cement materials as well as composites subjected to natural weathering. The study found that failure occurred due to interactions of microcracking, stress

redistribution, fibre debonding, fibre pull-out, and fibre failure.

Ageing of FRCC is dependent on the fibre properties which may be modified by exposure conditions. For example, when glass reinforced cement (GRC) is exposed in hot and humid climates over a long time period, the alkalinity of pore water in the matrix embrittles the composite (Bergstrom & Gram 1984). On the other hand, the reinforcing action of polypropylene fibres is not affected by alkalinity of cement-based matrices (Hannant 1998).

Micromechanical interactions in HPFRCC have been measured from crack growth studies by Yang and Fischer (Yang & Fischer 2005). The study utilised a notched specimen which was loaded in uniaxial tension and the behaviour characterised by the stress-crack opening displacement (stress-COD) relationship. It was found that the characteristics of interfacial bonding between fibre and matrix play a significant role in the shape of the stress-COD curve. In addition, the fibre properties influenced the bond characteristics (frictional or chemical bond). The study (Yang & Fischer 2005) also showed the post-cracking deformation mode to be characterised by fibre bridging, which was influenced by the interfacial bond together with fibre orientation and length.

A direct relationship between coefficient of thermal expansion (α) and humidity has been reported (Bazant 1979). For young cement pastes, α is maximum at a relative humidity of approximately 70 percent, but as the cement hydrates and the material ages, the coefficient of thermal expansion drops to approximately 50 percent (Neville 2002). On the other hand, the modulus of elasticity of cementitious materials (E) is not affected so much by the state of temperature as by the variations thereof (Bazant 1979). Cyclic temperatures induce volume changes in the composite which result in microcracking and reduction in stiffness. It is also shown that microcracking progresses faster under cyclic thermal changes than under constant temperatures (Bazant 1979).

Modifications of material properties is manifested in changes in mechanical behaviour. For instance, carbonation exposure together with tempera-

ture and humidity variations has in the past been shown to lead to matrix densification and cellulose fibre embrittlement which affect the mechanical properties of Fibre Reinforced Cementitious Composites (FRCC) (Akers & Studinka 1989). Similar effects have been observed on synthetic and cellulose fibre cement composite materials aged by natural weathering (Tait & Akers 1989). Ageing causes an increase in fibre bond which increases the propensity for fibre failure as opposed to fibre pull-out. Therefore, the long-term performance of the composite is dependent on the ageing characteristics.

As it is not feasible to wait several years for ageing to occur naturally, an approach for assessing the long-term performance of FRCC has been to accelerate the environmental degrading agents in laboratory-controlled tests and then subject the degraded materials to mechanical tests.

An accelerated ageing protocol, developed by Akers and Studinka (Akers & Studinka 1989), and later adopted by Kim and co-workers (Kim, Wu, Lin, Li, deLhoneux & Akers 1999), was particularly interesting. In that work, which essentially involved durability studies on cellulose cement composites, the combined effects of wetting/drying, and carbon dioxide exposure were shown to quite accurately simulate the effects of long-term natural weathering of cellulose composites.

Environmental degrading agents are essentially synergetic and a better insight into their individual effects would be gained by separating the different exposure regimes rather than using a combined universal test. In any case, incorporating all the environmental factors would be difficult to devise and would be faced with major operational constraints as illustrated in the literature (Kim et al. 1999), (Hannant 1998).

Ageing of Fibre Reinforced Cementitious Composites (FRCC) involves chemical and physical changes in the matrix, fibres, and the fibre/matrix interface. Changes in the matrix phase affect the nature of bonding due to accumulation of hydration particles in the fibre vicinity. In a study by Bentur and co-workers on the development of bonding of polypropylene fibres on a cementitious matrix (Bentur, Mindess & Vondran 1989), it was shown that

there is an increase in interfacial adhesion as the composite ages. It was suggested that the increase was due to the development of intimate contact between the fibres and the dense matrix, that is, development of hydration products around fibres.

2.9.1 Synergetic Effect of Hot/Cold, Wet/Dry, and Carbonation

Volume changes in FRCC are influenced by temperature cycling, which leads to cracking. The cracks commonly develop along aggregate surfaces, reflecting the differences in coefficient of linear expansion between cement paste and aggregates (Rendell et al. 2002).

The combined effect of high temperature and moist conditions is that microcracking can develop rapidly thereby providing further sites for cement hydration products in a process of self healing. In addition, concrete with excessive permeability (due to microcracking) provides secondary paths for ingress of CO_2 other than a diffusion process.

In environments where concrete is exposed to cyclic wetting and drying, CH, a soluble product of hydration, precipitates in the voids within the microstructure (Taylor 1997*a*). Wet/dry environment combined with with CO_2 exposure induces carbonation shrinkage which contributes to crazing of exposed concrete (Neville 1971).

2.9.2 Accelerated Ageing Versus Natural Weathering

In the past, accelerated ageing tests have been used for prediction of natural ageing of glass fibre concrete samples in two different natural environments: tropical climate in Nigeria and Swedish climates (Bergstrom & Gram 1984). In the study, laboratory samples were conditioned for periods varying between seven days and two years in water at a temperature of $+50^{o}$C. The ages of the laboratory samples were correlated with natural ages in tropical and Swedish environments. In this context, the ratio of the time taken in a natural climate (t_n) to result in similar ageing effects in a sample weath-

ered in the laboratory for a time t_a, is referred to as the factor of correlation ($\frac{t_n}{t_a}$). In the study by Bergstrom and Gram (Bergstrom & Gram 1984), the average factors of correlation were 14 and 215 for tropical and Swedish environments respectively. Using these age correlation factors, it was shown that it was possible to make a prediction of the long-term performance of Fibre Reinforced cementitious composites.

Establishing correlations of accelerated ageing with natural exposure requires some limited time-based data from behaviour in exposure sites. This means that different environments will have different correlation factors. Studies on accelerated ageing and natural exposure (Akers & Studinka 1989) illustrated the potential of time-based data in prediction of durability of cellulose fibre cement composites. The natural exposure carried out in the research provided a set of time-based data for carbonation exposure only. To be able to correlate accelerated tests with natural environments, more data needs to be taken for other exposure regimes such as: hot/cold, wet/dry, ultra/violet irradiation, and freeze/thaw.

2.9.3 Summary: Ageing of Fibre Reinforced Cementitious Composites

- The mechanical behaviour of FRCC varies with fibre type, matrix microstructure, and the physical and chemical conditions at the fibre/matrix interface.
- Ageing of FRCC involves chemical and physical changes in the matrix, fibres, and fibre/matrix interface, factors which are a function of the environmental exposure conditions.
- Carbonation exposure leads to matrix densification and embrittlement of cellulose fibres. This results in brittle composites with increased flexural strength but reduced toughness.
- Polypropylene fibres have demonstrated stability in cementitious matrices after long-term exposure to a natural environment.

- Environmental degrading agents are synergetic with the main effect being volume changes which leads to increase in matrix cracking.
- Accelerated ageing tests are useful for evaluation of long-term durability but there is need for establishing correlations between the tests and natural ages for different environments.

2.10 Industrial Successes of Fibre Cement Composites

Asbestos and steel fibres have being used in concrete since the end of the 19^{th} century. Asbestos fibres enabled thin rigid sheeting to be made whereas steel fibre concrete was used to fabricate machine bases and frames. By 1965, the harmful effects of asbestos fibres were known and pressure groups in the United States of America and other parts of the world sought a ban on asbestos trading. This motivated the search for alternative fibres for cementitious applications.

Polypropylene fibres (in form of "cut tape") were first used to reinforce concrete in the 1960s. Between 1965 to 1975 many changes took place in the fibre cement and concrete industry. For example, in the United States of America, Fibre Reinforced Shotcrete was developed at Battelle Institute by adopting a technology that was developed for production of slurry infiltrated steel fibre concrete (SIFCON). Shotcrete found many applications in safes, vault doors, explosion proof chambers, and bullet proof buildings in security areas. Shotcrete was also used in heavy duty floor panels.

In the 1970's Hannant of Surrey University in the United Kingdom developed an alternative product to asbestos fibre cement for use mainly as roof sheeting. The product, then known as Netcem, was a fibrillated polypropylene mesh that created an open mesh suitable for use with cementitious mixes. Surrey University sold Netcem to Montecatinni of Italy, where it was marketed as Retiflex. This product was used in Europe, New Zealand and South Africa, where the major application was in mine drain channels (World Wide

Web 2006*d*).

In the late 1990s, "cut tape" PP fibres as well as steel fibres for use in cement matrices were produced in South Africa. The production of PP fibres was undertaken on traditional textile looms. Experiments by Textile Concrete Consultants (World Wide Web 2006*d*) led to innovation in production of woven PP textiles. After refining, this technology was patented in 2001. The PP fibres have been used in many cement-based applications such as architectural cladding, permanent forms, amphorae, and many more.

James Hardie Industries Ltd. was first listed on the Australian Stock Exchange in 1951. The industry specialises in fibre cement products such as lightweight pipes which are beneficial during transportation and installation. James Hardie autoclave technology was developed in Australia in 1981 and successfully introduced in many parts of the world especially in the USA where its use has spread widely. This technology has particularly contributed to standardisation of low pressure fibre cement pipes. James Hardie Industries Ltd restructured and relocated to Netherlands in 2001 from where it continues to advance the fibre cement industry (Coutts 2005).

In Switzerland, air cured technology was developed and used for manufacture of micro concrete roofing (MCR) and fibre concrete roofing (FCR). This technology has been on the market since 1983 and has found wide application in developing countries such as India (World Wide Web 2007).

Evolution of cellular fibre concrete for reinforced precasts in South Africa is documented by Taylor *et al.* (Taylor et al. 1997). The development is traced back to 1987 when a fire destroyed Kinross Mine in South Africa killing 180 mine workers. Since the fire was propagated by polyurethane foam which had been used for insulation, the search for alternative insulation material ensued. In an effort to provide an alternative material, Grinaker-Duraset introduced cellular fibre concrete (CFC) technology which was employed in manufacture of drainage channels in the mining industry. Since its introduction, CFC technology has been successfully employed in other applications such as building blocks.

The success of CFC mixes in the mining industry has stimulated development of other applications, including lightweight blocks and panels for use in housing construction. Research by Textile Concrete Consultants (World Wide Web 2006*d*) led to development of CemForce, which is a polypropylene textile formulated for use in cementitious matrices which is used for Textile Concrete (TC) production. Mechanical evaluation of the effect of environmental exposure on this new product is the focus of this research.

2.11 Summary

This Chapter dealt with the background to conventional concrete and Fibre Reinforced Cementitious Composites (FRCC). From a historical perspective, it has been illustrated how technological advancements in cement and concrete, conventional construction materials, have changed since ancient civilizations. Similarly, technological advancements that have taken place in the area of FRCC since the mid-nineteenth century were outlined.

The role of supplementary cementitious materials (SCMs) and chemical admixtures in modifying the properties of cementitious mixes and in the production of High Performance Cementitious (HPC) products, was elaborated on. It was illustrated from the literature that with the advent of high range water reducing agents, performance demands of cementitious materials have been achieved without consuming additional cementitious materials.

The performance of FRCC is mainly dependent on the fibre/matrix interfacial properties, in particular the fibre/matrix bonding nature and fibre pullout properties which are discussed in Chapter 3. It was pointed out that the motivation for FRCC research is the need for a suitable replacement for asbestos cement particularly for thin element applications.

Among the preferred substitutes for asbestos fibres, polymeric fibres have been the most popular due to their cost effectiveness, availability, and stability in the highly alkaline cement environment. However the alternative fibres have serious limitations especially when applied in short discrete forms. This has led to rapid growth in the use of fibrillated polypropylene fibres in cement-

based applications, and recently to a new innovation: Textile Concrete (TC) technology.

For a better understanding of the mechanical properties of FRCC and indeed of TC, the fibre pull-out and composite tensile behaviour were identified as the two aspects of mechanical properties that are particularly key. The mechanics of the behaviour is governed by the process of load transfer across the fibre/matrix interface, visualized at micro and macro levels of the material structure. From the work reviewed in this Chapter, it was illustrated that mechanical characterisation of TC is on-going and the literature on the material is not complete. Despite being a relatively new product, it has found many thin element applications. Of concern however, is the long-term performance and durability of this new composite.

The effect of time, age, and environmental factors on the mechanical properties of Textile Concrete is the main focus of this research. To gain a better understanding of these effects, firstly it was necessary to identify the degradation processes that are likely to lead to ageing of cementitious materials. These are; variation of temperature and moisture condition, and carbonation exposure. The need to accelerate these effects under laboratory controlled conditions was highlighted. The mechanical behaviour of FRCC in general including TC is reviewed within a theoretical framework described in Chapter 3.

Chapter 3

Theoretical Framework

3.1 Introduction

The literature reviewed in Chapter 2 dealt with the mechanical behaviour of Fibre Reinforced Cementitious Composites (FRCC), and general background of cement and concrete. A key factor in characterising fibre composites bonding is based on single fibre pull-out and tensile behaviour of the composite. A commonly used approach in characterisation of the single fibre pull-out behaviour has been by use of load-displacement (P-δ) curves whereas for the tensile tests, stress-strain (σ-ϵ) curves are utilised. Theoretical and mathematical models describing these two aspects of mechanical properties of FRCC are the focus of this Chapter.

The mechanisms interacting at three loading stages during the fibre pull-out process are described. The micro-mechanical models on interfacial debonding and fibre pull-out in FRCC are reviewed from the literature. The load-displacement behaviour is used to describe the over-all fibre pull-out behaviour.

The fibre/matrix interface bonding and debonding properties are firstly dealt with. Fibre debonding prior to attainment of the peak load is described using stress-based and energy-based debonding models. Secondly, the overall load-displacement behaviour characterising the fibre pull-out test is described using models from the literature. The models are referred to by the name

of the first cited author followed by a brief discussion. The discussion covers the general aspects of the bonding action of the fibres that are commonly employed in cementitious composites with more emphasis on polypropylene (PP) fibres.

The theory governing uni-axial tensile behaviour of Fibre Reinforced Cementitious Composites is reviewed based on the micro-mechanical properties of the fibre/matrix interface. The theory is in form of mathematical models, starting with the theory by Aveston, Cooper and Kelly (ACK) (Aveston et al. 1971), which was originally developed to describe an idealized stress-strain behaviour of polymer-based composites and later adapted for conventional FRCC.

The limitations of ACK theory are illustrated showing that the post-peak strain-hardening behaviour, and multiple cracking exhibited by High Performance Fibre Reinforced Cementitious Composites (HPFRCC), was not adequately accounted for. In this Chapter, the way this shortcoming is addressed is illustrated from different mathematical models which have been developed in the recent past in order to account for the "pseudo-ductile" behaviour exhibited in HPFRCC and in particular, in Textile Concrete. Finally, the mechanisms of ageing and damage in FRCC due to different environmental degradation agents are briefly outlined.

3.2 Overview

The mechanical behaviour of fibre reinforced cementitious materials is influenced to a large extent by the fibre-matrix interfacial properties. This is demonstrated from the work by Bentur and Mindess (Bentur & Mindess 1990) which mainly focussed on the micro-structure of polypropylene (PP) fibres-cementitious systems. The study indicated that bonding strength is influenced more by the mechanical anchoring of fibres into the cementitious matrix, than by interfacial adhesion. This view was supported later in independent studies by Li (Li 1992) in which the strength of the fibre/matrix bond was linked to the fibre bridging stress across the matrix crack, which

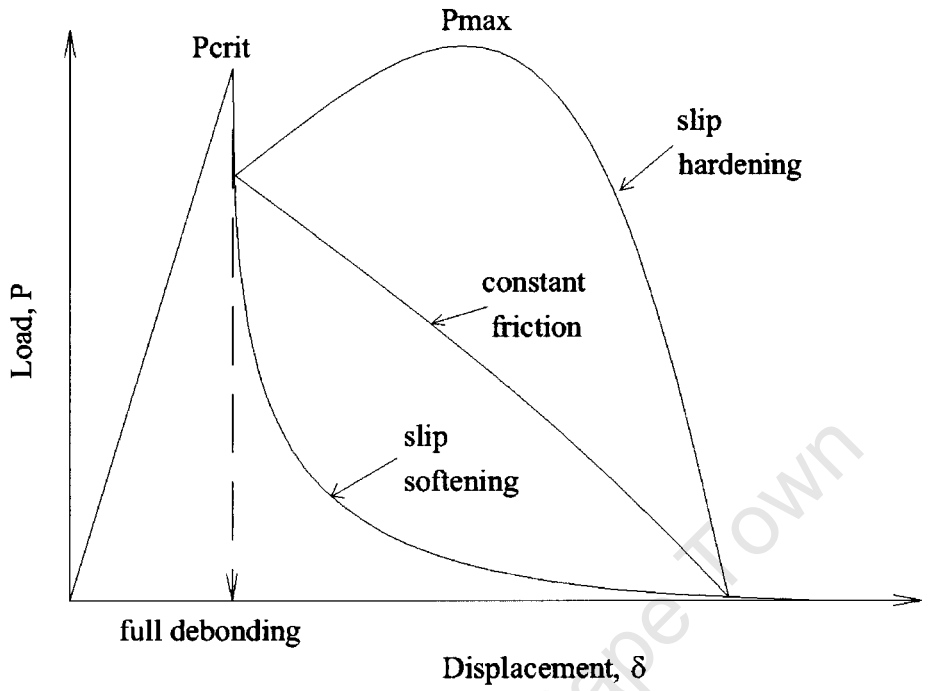

Figure 3.1: Effect of bonding nature on mechanical behaviour

partly accounted for strain-hardening observed in HPFRCC.

The influence of interfacial bond properties and their effects on the load-displacement (P-δ) behaviour of FRCC is illustrated schematically in Fig. 3.1. The fibre/matrix interactions at micro level are described by the bond strength, interfacial shear stress, and critical energy release rate, the key parameters that characterise the load transfer mechanics across the interfacial zone. The work required to separate a fibre from the matrix is dependent on the energy required to propagate a steady crack growth at the interface, characterised by the critical energy release rate, which is a material property (Kelly 1995).

When a tensile load is applied to a composite, the load is transferred from the matrix to the fibres, and shear stresses are set up at the fibre/matrix interface. The tensile load increases until the critical load P_{crit} when the matrix cracking strength is attained. The shape of the load-displacement behaviour after P_{crit} is governed by the fibre volume fraction (V_f), fibre/matrix

bond strength, and the elastic moduli of the fibre (E_f) and the matrix (E_m). For composites with fibre volume fraction beyond a critical value (V_{fc}), the load will be carried entirely by the fibres before final failure occurs. The load-displacement behaviour of different composites is therefore described as follows (Perrie & Butler 1994):

- Slip softening characterises composites with low V_f and $E_f < E_m$.
- Constant friction characterises composites with low V_f and $E_f > E_m$.
- Slip hardening characterises composites with high V_f and $E_f > E_m$.

3.3 Fibre Pull-Out Behaviour

In a typical fibre pull-out test, the load-displacement curve is used in characterising the fibre pull-out behaviour and the curve is described by four regions corresponding to the following stages in behaviour:

i. Initial linear pre-peak slope corresponding to an intact fibre/matrix interface in which the shear stresses are elastic in nature.

ii. A second slope, also preceding the peak load, which corresponds to an interface undergoing microcracking, which might influence initiation of debonding. Load drops are due to matrix cracks and opening up before the fibre takes load. During this partial debonding stage, the load is still increasing (the rate depending on E modulus for the fibre) indicating a mobilisation of interfacial friction with associated damage (Bentur & Mindess 1990). This second stage prevails until the fibre completely debonds from the matrix and the peak load (P_{max}) is attained.

iii. The third slope corresponding to the region beyond P_{max}. This stage is characterised by a change in gradient from positive to negative. At this post-peak stage, the fibre is fully debonded and thus progressively pulls out of the matrix. At this stage of the load-displacement curve, the stresses within the interfacial microstructure are frictional in nature and this causes the cracks to propagate in an unstable manner.

The magnitude of this negative gradient depends on the nature of the microstructure.

iv. As loading progresses, fibre slippage and pull-out take place thus causing substantial damage to the microstructure. Therefore, cracking at the interfacial zone stabilizes. This region, which is the final stage on the load-displacement curve, is therefore characterised by a negative slope that is asymptotic to the horizontal.

Before the fibre fully debonds from the matrix, the load-displacement relationship remains independent of the interfacial bond properties. However after full debonding, the behaviour is mainly governed by the material properties illustrated by Fig.3.2.

During the last loading stage, and depending on the fibre type, the loading mechanism involves progressive fibre pull-out, fibre rupture, or a mechanism between these two extremes. In situations where the embedded fibre length is greater than twice the critical length l_c defined later by Eq.3.2, the failure mechanism is characterised by fibre rupture.

If the embedded fibre length is less than twice the critical length ($2l_c$), the fibres are pulled out with maximum amount of work without failing. As the loading progresses, the fibre is rigidly displaced from the matrix and the pull-out resistance is fully supplied by decaying interfacial stresses between the fibre and the matrix up to failure. Polypropylene fibres undergo necking before pull-out occurs. The different mechanisms of the loading process are represented schematically in the idealised P-δ curve of a typical fibre pullout response in Fig.3.2.

3.3.1 Mechanisms of Fibre Pull-out

A common method of fibre-matrix interfacial properties characterisation is through fibre pull-out tests. In the tests, the fibre bridging-crack opening phenomenon is simulated during the fracture process. The typical output of the test is the load-displacement curve which provides the following information: the elastic bond strength, the characteristics of fibre debonding and

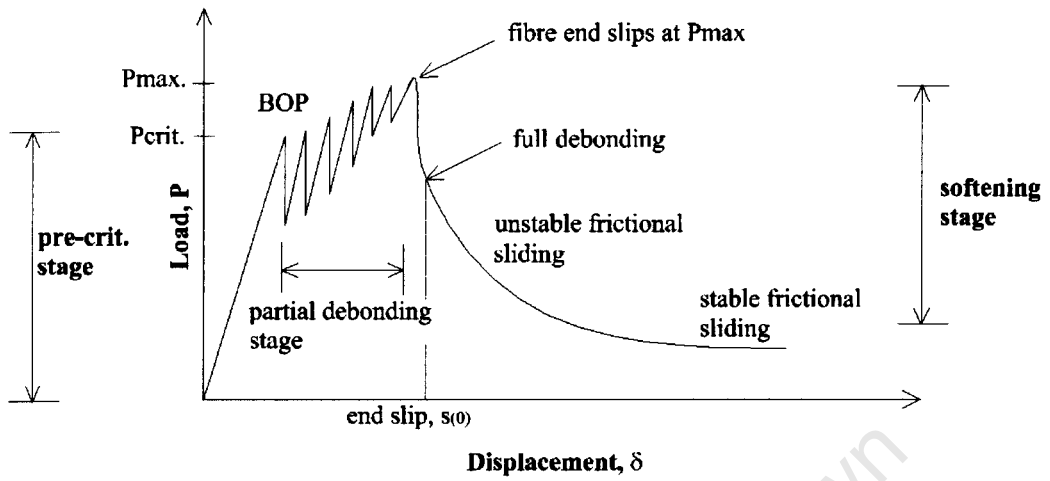

Figure 3.2: Stages in fibre pull-out on idealised load-displacement curve

fibre end slippage, the maximum pullout load, residual frictional bond, and fibre rupture load. Fig.3.3 shows a schematic diagram of the key parameters describing a typical fibre pull-out test.

At the early loading stages, particularly regarding polypropylene fibres in cementitious matrices, a frictional bond is developed. With additional loading, the interfacial shear stresses reach the critical shear strength and additional energy is supplied to the material at the interface. At this stage, the debonding criteria are met and therefore the debond zone advances and the fibre undergoes frictional sliding at a constant shear stress, τ_i. The debonding point is identified by a "kink" on the load-displacement (P-δ) curve, which corresponds to the critical load P_{cri}.

The post-peak P-δ relationship that was shown earlier in Fig. 3.2 as the partial debonding region is nonlinear due to progression of debonding with increasing load. Complete debonding is achieved after attainment of the maximum load P_{max} (Gopalaratnam & Shah 1987*a*).

The bond strength for carbon and steel cementitious composites has been modeled using an average bond shear stress τ. It is estimated from equilibrium considerations and is related to P_{max} and the material properties

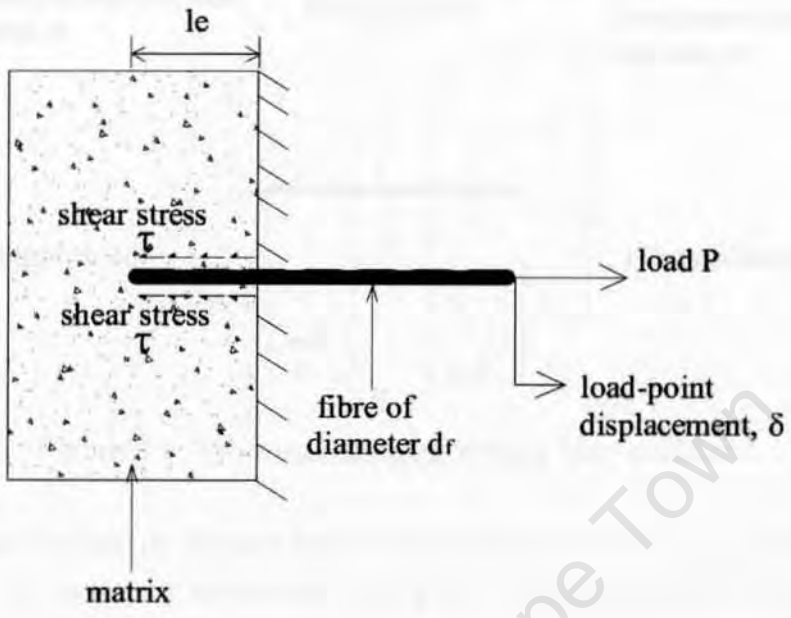

Figure 3.3: Parameters describing fibre pull-out test set-up

according to Eq. 3.1 (Currie & Gardner 1989).

$$\tau = \frac{P_{max}}{\pi d_f l_e} \tag{3.1}$$

where d_f and l_e are the fibre diameter and embedded fibre length respectively. A similar relationship exists for other fibre-cementitious matrix systems. Equation 3.1 is based on the assumption that prior to attainment of P_{max}, the interfacial bond strength is constant along the fibre length, and is frictional in nature. It is also assumed that the fibre fully debonds and pulls out without rupture. For specimens to be more susceptible to fibre pull-out as opposed to fibre failure, the fibre embedded length should not exceed twice the critical fibre length l_c, which is related to the fibre strength σ_f^u and the average bond strength τ according to Equation 3.2 (Katz, Li & Kazmer 1995).

$$l_c = \frac{d_f \sigma_f^u}{4\tau} \tag{3.2}$$

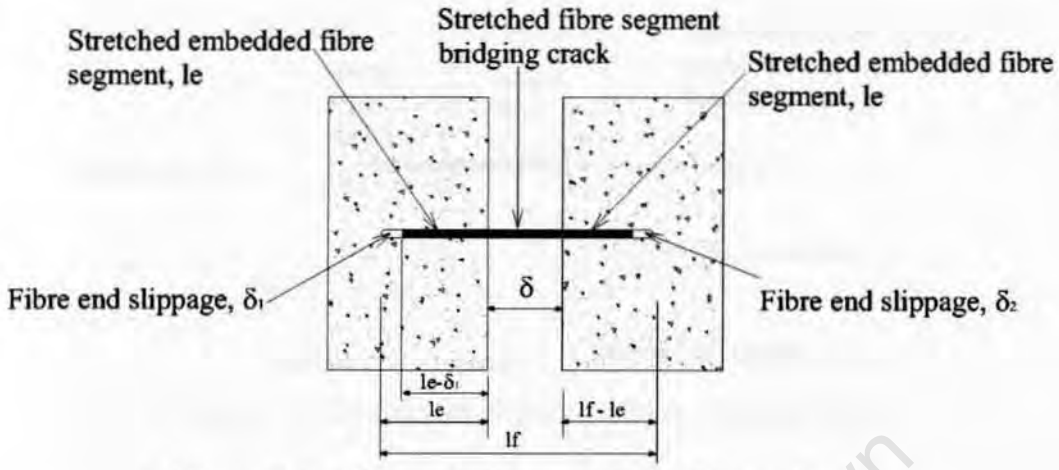

Figure 3.4: Fibre end slippage during fibre pull-out

As fibre debonding progresses beyond the maximum load P_{max}, mechanical anchoring of fibres into the matrix takes place. This mechanism is dependent on the fibre type and surface geometry. Fibre pull-out is then characterized by a residual frictional bond stress τ_i, which varies with the slippage distance (δ_1 and δ_2) between the fibre and the matrix. Residual frictional bond stress τ_i is a material property and could be of constant, slip softening, or slip hardening nature. For polypropylene fibres, a slip-hardening type of bond is developed when the fibres are embedded in cement-based matrices. The slip-hardening bond stress is a function of the fibre end slippage distances s_1 and s_2 illustrated in Fig. 3.4 (Li, Wang & Backer 1991*a*), (Zhandarov & Mader 2005).

3.3.1.1 Wang Model of Fibre Pull-Out Problem

The fibre pullout mechanism has been modeled from the initial stages of load application to the strain softening stage at failure (Wang, Li & Backer 1988). The model was based on a fibre with its two ends embedded into a cementitious matrix thus simulating fibre bridging a crack plane. The embedded lengths of the fibre were l_1 and l_2 as schematically illustrated in Fig.3.5.

When a tensile load is applied, the fibre is subjected to loads P_1 and P_2 at

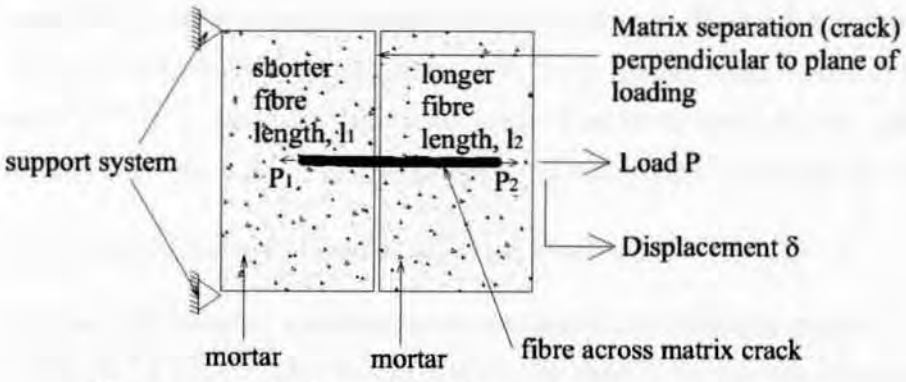

Figure 3.5: Double sided fibre pullout configuration

its ends causing displacements δ_1 and δ_2 respectively. From the configuration in Fig. 3.5, the prediction of the pull-out response is made. This involves firstly, the computation of the shorter fibre P_1-δ_1 relationship from which the maximum load, P_{max} is determined. On the P_1-δ_1 curve, P_{max} is identified by a sudden reduction in the load. Unlike the shorter fibre response to loading, the P_2-δ_2 response for the longer fibre segment is composed of two loading stages; the initial loading stage followed by the unloading part. The P-δ responses for the two fibre segments are combined based on compatibility and equilibrium considerations, which are represented by Eqs. 3.3 and 3.4 respectively.

$$P = P_1 = P_2 \tag{3.3}$$

$$\delta = \delta_1 + \delta_2 \tag{3.4}$$

3.3.1.2 Naaman Model of Fibre Pull-Out Problem

The fibre pull-out load of smooth short aligned fibres embedded in a cementitious matrix has been related to a dimension at the micro level (fibre end slip δ_1 or δ_2) in a model developed by Naaman et al. (Naaman et al. 1991*b*), which was later adopted by Alwan and co-workers (Alwan et al. 1999). The model differed from the Wang model in that the mathematical formulations

were necessarily more comprehensive mainly because the pull-out problem took into account the fibre end slippage δ_1 or δ_2 rather than the total displacement of the system δ. Naaman model has been used in the past to describe the pull-out load P in the pre-critical and partial debonding stages.

3.3.1.3 Lin Model of Fibre Pull-Out Problem

A micro-mechanics based load-displacement model has been proposed by Lin and Li (Lin & Li 1997). The model relates the load P to the displacement δ instead of the fibre end slip s in Naaman model (Naaman et al. 1991*b*). Up to the time of complete debonding, the fibre end slip is usually small, therefore, the load at the maximum load P_{max} is an estimate of the interfacial bond stress τ_s. δ corresponds to the displacement at which the entire embedded fibre segment debonds from the matrix. The slope of the pull-out curve after P_{max} is described using an empirical parameter characterising the damage processes at the fibre/matrix interface and accounting for slip hardening on the interface shear stress.

3.4 Models of Tensile Behaviour

Different approaches have been adopted for theoretical treatment of tensile loading and the mechanisms of failure in conventional Fibre Reinforced Cementitious Composites. Theoretical models describing the properties of the fibre, matrix, and the interface in relation to the composite strength have been suggested. These models are typically based on the cracking phenomenon and are categorised in the literature as: continuum composite models, interface micromechanics models, and fracture mechanics models (Gopalaratnam & Shah 1987*b*).

The mechanics of the tensile behaviour of "pseudo-strain hardening" materials reinforced with textiles is not well established. However, the area has attracted the attention of researchers in recent years because of the numerous potential applications of these materials especially as thin elements (Hegger, Sherif, Brukermann & Konrad 2004).

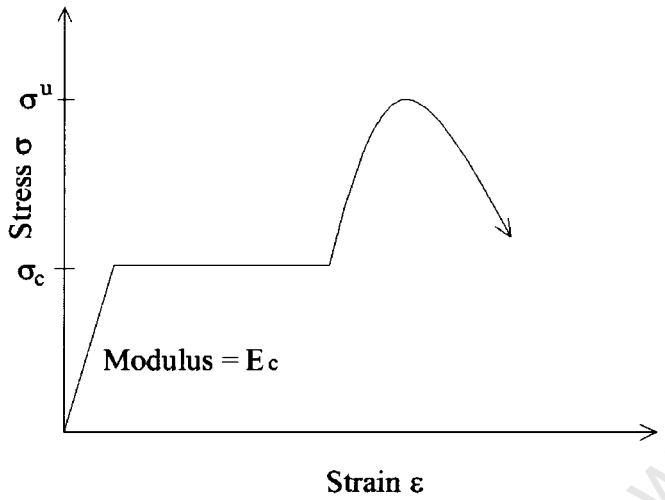

Figure 3.6: ACK model of idealized tensile stress-strain relationship

3.4.1 Aveston, Cooper, and Kelly (ACK) Model

The basic theory, which represents the tensile behaviour of FRCC was developed by Aveston, Cooper, and Kelly and is commonly referred to as the ACK model (Aveston et al. 1971). The model applies an energy balance approach to predict the degree of multiple cracking in the composites, and a frictional bond is assumed to exist in a system of cementitious matrix reinforced with continuous aligned polymer fibres. In addition, ACK theory idealises the tensile behaviour with the stress-strain ($\sigma - \epsilon$) curve which is schematically illustrated in Fig.3.6. The input parameters in ACK model are derived from the law of mixtures for composite materials, concepts of fracture mechanics, and the mechanisms of multiple cracking.

Prior to attainment of the cracking strength (σ_c) when the first matrix crack is formed, the Young's modulus of elasticity of the composite (E_c) is determined from the simple law of mixtures which is described by Eq.3.5 as follows:

$$E_c = E_m V_m + E_f V_f \tag{3.5}$$

where V_m and V_f are fibre volume fractions of the matrix and the fibre respectively. At this loading stage, the tensile behaviour is described by the

following linear elastic stress-strain relationship:

$$\sigma = E_c \epsilon \tag{3.6}$$

The relationship between the critical fibre volume fraction (V_{fc}) for aligned and fully bonded fibres of strength (σ_{fu}) in a weak brittle matrix of direct tensile strength (σ_{fu}) is approximated from Eq. 3.7:

$$V_{fc} \approx \frac{\sigma_{mu}}{\sigma_{fu}} \tag{3.7}$$

By assuming a constant frictional shear stress distribution at the interface, the ACK model gives a prediction of the matrix fracture strain resulting due to the presence of fibres by:

$$\sigma_{mu} = \left[\frac{12\tau\lambda_m E_f V_f^2}{E_c E_m^2 \tau V_m} \right]^{1/3} \tag{3.8}$$

where E and V represent Young's modulus and the volume fraction respectively; subscripts m, f, and c represent the matrix, fibre, and composite respectively, and τ is the interfacial shear strength. The surface fracture energy of the matrix is described by Eq. 3.9.

$$\lambda_m = 0.5 \frac{(K_{Ic})^2}{E_m} \tag{3.9}$$

A major limitation of the ACK theory is that it is applicable to composites whereby the matrix and fibre are characterised by a linear elastic failure behaviour. This condition is not always obeyed in FRCC. Moreover, the law of mixtures does not fully address the strain hardening response exhibited by a large group of FRCC including Textile Concrete. These materials are characterised by non-uniform matrix failure strains beyond the elastic region and cracks are formed progressively rather than the steady cracking assumed in the ACK model. Essentially, these materials exhibit the so called "pseudo-strain hardening" behaviour.

Failure in "pseudo-strain hardening" materials is further complicated by the instantaneous load reduction as each crack is formed. In addition, the

ACK model is based on the assumption that the matrix has a single valued cracking stress over the multiple cracking region, as shown in Fig. 3.6, which does not account for the strain-hardening behaviour in High Performance Fibre Reinforced Cementitious Composites (HPFRCC).

Recently, formulations of multiple cracking in FRCC were proposed, providing solutions to steady-state matrix cracking problems. The formulations applied the principles of fracture mechanics, energy theories, and various fibre-matrix interfacial properties (Kabele 2003*a*), (Kanda et al. 2000*a*).

3.4.2 Aveston Model of Crack Quantification

The principles behind quantification of crack spacing and crack widths for the simplified case where the bond between the fibres and the matrix is purely frictional and the matrix has a well defined single valued breaking stress was developed by Aveston *et al.* (Aveston et al. 1971) and has been comprehensively reviewed by Hannant (Hannant 1978). It is assumed in developing the theory that after the matrix has cracked there is a linear transfer of stress from the fibres bridging the crack back into the matrix.

For long fibres with frictional bond, the crack spacing (x') is calculated from a simple balance of the load ($\sigma_{mu}V_m$) needed to break unit area of matrix and the load carried by N fibres of radius r across the same area after cracking. This load is transferred over a distance x' by the limiting maximum shear stress (τ). The relationship is represented as follows:

$$N = V_f/\pi r^2, \quad 2\pi r N \tau x' = \sigma_{mu} V_m, \quad or \quad x' = \frac{V_m}{V_f}.\frac{\sigma_{mu} r}{2\tau} \tag{3.10}$$

The theory is modified to predict the properties of cement reinforced with short fibres.

3.4.3 Kabele Model of Multiple Cracking

Studies by Bentur and Mindess (Bentur & Mindess 1990) on the interfacial property characterisation of polypropylene fibre cementitious matrix composites suggested that prior to fibre rupture, increasing the interfacial bond

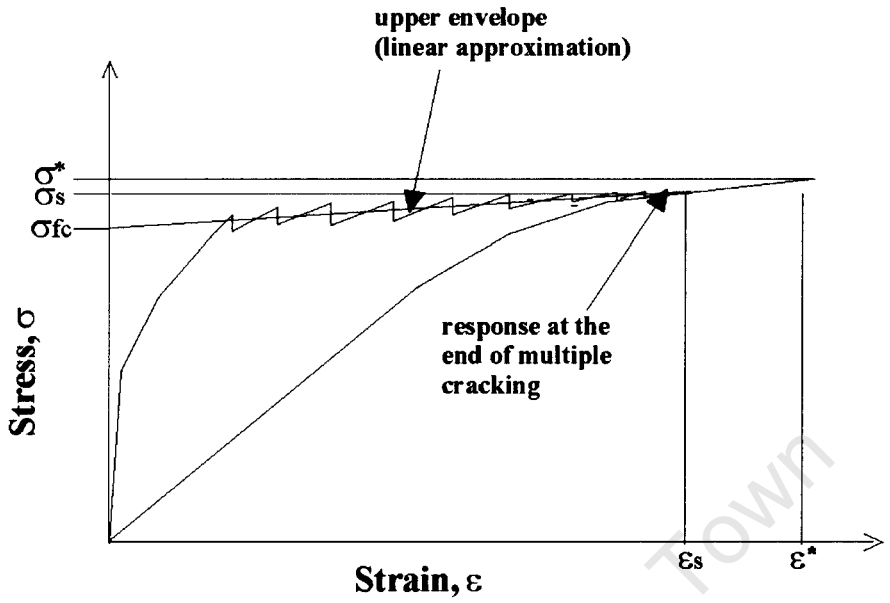

Figure 3.7: Approximation of composite behaviour during multiple cracking

accounted for an increase in the composite strength and toughness, a theory supported later by Li et al. (Li et al. 1991*b*). Based on such a premise, and also taking into account the progressive multiple cracking characterising HPFRCC, constitutive models of the tensile behaviour have been developed (Kabele 2003*a*),(Kanda, Lin & Li 2000*b*).

After the composite achieves the first cracking stress σ_{fc}, it enters the so called "pre-saturated" region when multiple cracking progresses, and the stress-strain curve is approximated by a linear function defined by the points; $(\sigma_{fc}/E_c, \epsilon)$ and $(\epsilon_s, \sigma s)$ in Fig. 3.7. A linear approximation of the upper envelope indicated in Fig. 3.7 has been suggested (Kabele 2003*a*).

3.4.4 Lin Model of Multiple Cracking

Mathematical models of the load-displacement relationship of Fibre Reinforced Cementitious Composites are based on a clear understanding of the micro-mechanics of crack initiation, debonding, and the decaying interfacial frictional stresses. These are conventional fracture mechanics concepts which serve in advancing the understanding of matrix crack opening and sliding dis-

placement relationships (Lin & Li 1997).

Matrix cracking is influenced significantly by the fibre end slippage, which induces a frictional slip resistance at the fibre-matrix interface. At the same time, the frictional slip resistance contributes to the fibre bridging action. These different mechanisms are related by a fibre bridging stress, σ_b versus the crack opening displacement, δ relationship (σ_b-δ), which characterizes the mechanical behaviour of the composite (Lin & Li 1997).

The σ_b-δ relationship is one of the most crucial links between the properties of fibre and the matrix, the interface, as well as the overall composite behaviour. This relationship defines the ultimate stress and strain in the tensile test, and also gives the energy consumption due to the fibre bridging action. The strength, ductility and fracture toughness of the composite also depend on the energy consumption during loading.

For the model by Lin and Li (Lin & Li 1997) to be applicable to FRCC, the crack length and opening displacement need to be accurately measured. However, even in modern materials research laboratories, there is currently no straightforward experimental procedure suitable for such measurements, and hence determine the bond stress versus slip relationship of a fiber-matrix system and the corresponding stress distribution at the interface (Lin & Li 1997).

Despite the difficulties associated with measurement of crack lengths and opening displacements, there is growing recognition among researchers that for a better understanding of the composite's overall behavior and performance, these interfacial properties need consideration. Therefore analytical and numerical models have been developed aimed at yielding the bond stress versus slip relationships (τ-δ), most of which are based on different types of single and multi-fiber pull-out tests (Lin & Li 1997). This aspect of mechanical characterisation is outside the scope of the current research and therefore the related models will not be explored further.

3.4.5 Integration of Theories into This Thesis

The theories described in this Chapter provide a better insight into the micro-mechanical behaviour of the composite material based on the following properties:

i. Modulus of elasticity of the matrix E_m and fibres E_f
ii. Fibre-matrix interfacial bond stress τ
iii. Embedded length of fibre in the matrix l_e
iv. Relationship between the interfacial bond stress, τ and the fibre end slippage, δ

Exposure to natural weathering processes, or accelerated ageing in the laboratory, results in modifications to these basic material properties. The theories therefore form the basis for setting up of an experimental programme aimed at inducing changes to the material properties described in the models. For example, by exposure of TC to cyclic hot/cold, wetting/drying, and carbonation environments, the stiffness of the matrix, E_m and the fibres, E_f may be modified accordingly, and from the theories presented here, it is apparent that the mechanical behaviour would then vary in a similar manner. Similarly, modifications in the fibre/matrix interfacial properties will be investigated from changes in bond strength τ resulting from exposure to these different environments.

3.5 Summary

The governing theories of conventional Fibre Reinforced Cementitious Composites (FRCC) were briefly reviewed from a micro-mechanics and fracture mechanics perspectives. Theories of fibre/matrix bonding and debonding were firstly described and secondly, it was highlighted that the main property characterising the balance of shear stresses at the fibre/matrix interfacial zone is the bond property τ, which is essentially the shear stress at the fibre/matrix interface. It was also shown from the literature how the usage of

the peak load P_{max}, and the interface bond τ varied according to different theories.

Many experimental techniques have been proposed for determination of the fibre/matrix bond property. Among them, the fibre pull-out test is the most popular mainly due to its simplicity in terms of the test set-up. It has been illustrated in this Chapter that there are four clearly distinct mechanisms in the classical fibre pull-out test which describe different loading stages illustrated by the load-displacement curve. These mechanisms are related to the bonding character of the system τ and vary with the loading stage.

The fibre/matrix bond changes from being predominantly elastic at the pre-peak stage, to frictional at complete fibre pull-out and failure stage. From the theories described in this Chapter, the contribution of individual fibres and the matrix in the composite action, and the interaction of the fibres with the matrix at the interface zone, have been shown to play a key role in the overall fibre pull-out behaviour.

The theory governing the tensile behaviour of conventional FRCC composite materials is based on the principles of the theory described by the classic ACK model. The theory was described and its main limitation of not adequately addressing the "pseudo-strain hardening" behaviour unique to Textile Concrete (TC), highlighted.

More recent theories on "pseudo strain-hardening" behaviour of Fibre Reinforced Cementitious Composites (FRCC) were reviewed. Finally integration of the theory into the thesis was briefly described.

Chapter 4

Experimental Techniques

4.1 Introduction

This Chapter describes the experimental work carried out in this research and the methods used for data collection. The Chapter is divided into two main parts. The first part gives a brief description of the preliminary investigations that were carried out in order to select appropriate matrix materials and the number of textile layers, based on trial tests, that would provide specimens to be most representative of Textile Concrete (TC).

The second part of this chapter describes the experimental process of characterisation of TC and the weathering techniques employed.

The initial stage of characterisation involved determination of the physical and chemical properties of the binders: cement and the mineral additive Ultra-Fine Fly Ash (UFFA), which was employed to enhance the workability of mortar. The analysis of the binders: cement and UFFA was carried out at the Pretoria Portland Cement (PPC) laboratories in Cape Town and the results are presented in this Chapter. The experimental work forming the second part of this Chapter involved a series of experiments categorised as follows:

i. Determination of suitable mortar mix proportions
ii. Characterisation of the flow characteristics and cube crushing strength of mortar

iii. Determination of density and tensile strength of polypropylene (PP) fibres

iv. Solution of suitable TC specimen geometry and sample preparation techniques

v. Mechanical tests on mortar, fibres and the composite

vi. Development of the accelerated weathering facility

vii. Quantification of cracks developed on TC specimens after tensile testing

To be able to link the information from mechanical tests with the microstructure, images of fractured TC surfaces were observed in a scanning electron microscope (SEM) and analysed physically thereafter. The SEM technique is described in more detail in this Chapter, along-with the results obtained from the studies.

4.2 Characterisation of Textile Concrete

In the past, studies on the durability of Fibre Reinforced Cementitious Composites (FRCC) have focussed more on mechanical, and to a lesser extent on the chemical aspects (Hannant 1998) (Salicimen et al. 2003). A chemical approach concerns an investigation into the processes involving rearrangement in the material structure, whereas a mechanistic approach deals with the effects of a physical nature including application of forces and weathering. In this thesis, a mechanistic approach was adopted as it was believed that it would lead to a better understanding of the fibre/interface bonding, which for PP fibres in cement-based matrices, is more of a mechanical than chemical nature.

Fibre pull-out tests were employed as the means of quantifying the fibre/matrix bonding property of TC, whereas for the macro composite behaviour, tensile testing was employed for investigating the mechanical properties and multiple cracking behaviour (Wang, Li & Backer 1988).

The mechanical properties of Fibre Reinforced Cementitious Composites (FRCC) are complex due to fibre/matrix interactions at different levels.

Therefore, it would be inaccurate to use a single parameter to fully describe the mechanical properties of the material, but rather a combination of different factors to describe the behaviour is more appropriate. As it was not possible to investigate all the material parameters within the scope of this research, the main properties influencing the mechanical behaviour were firstly identified and then investigated experimentally. The physical properties of the fibres plays a key role in the fibre/matrix interface bonding properties. Indeed, this was of special interest in this work and was part of preliminary investigations carried out in the recent past (Tait & Guddye 2002).

The PP fibres used for production of the textile material known as "CemForce" had a unique surface in form of an outer "fluffy" sheath of PP fibres illustrated earlier by Figs. 2.14 in Chapter 2. In one form of CemForce, the fluffy layer is held more firmly to the central core by further intermittently bonding it using ultrasonic welding to the central core forming a "hybrid fibre". This feature is unique and enhances the mechanical bonding of PP to the cementitious matrix. In this research, the bonded format of CemForce was employed in preliminary investigations and in individual fibre characterisation. However, for production of large volumes of the composite specimens required for the research, nonbonded (i.e. non ultrasonically welded) CemForce was employed, because it was more readily available in large quantities.

Preliminary studies were carried out in order firstly, to perfect the hand lay-up method as the laminate production technique. The process underwent several trials before the technique was refined sufficiently for specimen production. The number of CemForce layers that was most suitable for specimens for use in this experimental work needed to be established. After several trials involving three-point bending tests on thin laminates, a six-layered TC composite was found to be suitable for the work because it could easily be produced using hand lay-up techniques, and the specimens thus produced were robust enough to withstand the experimental handling. Indeed, six layers of textiles have been employed in production of thin cementitious specimens and found to produce specimens with consistent results (Kenai &

Brooks 1993).

Thin TC laminates of nominal thickness of 10 mm were produced and tested in three-point bending, which showed that for the composite reinforced with the "ultrasonically welded" fibres, higher fibre/matrix bonding was achievable and was manifested in bending forces that were higher than in the non-bonded type as shown in Appendix A (Mumenya et al. 2003).

4.2.1 Textile Material Development

Textiles specially specified for use in cement-based products are manufactured in conventional mills with the yarns being specified in D'Tex or d'tex terms. The definition is such that one d'tex of yarn implies 10 kilometres weigh 3 grammes (or D'tex definition refers to the fibre weight in grammes per kilometer). During the last decade, the textiles have been customised for application in cementitious mixes. However, because PP is a hydrophobic polymer, hydraulic matrices do not readily adhere to its surfaces, but by spinning fibres as a sheath around a fibrillated PP core yarn, and where necessary by bonding the fibres to the core, this problem has been overcome. A factory where the technology is employed is Standerton Mills, a local traditional textile manufacturing factory in South Africa where the textile for this research project was sourced.

The key development in the textile production process was to use a fibrillated form of polymeric fibre as the core. The core usually consists of two strands of fibrillated PP fibres of 110 D'Tex each. To this core, an outer fluffy layer composed of fine 3 d'tex PP filaments has been spun to form a sheath as illustrated in Fig. 2.12 in chapter 2. The spinning process arranges the fine fibrils helically as well as extending them lengthwise along the core. The sheath is further secured onto the core by providing overlaps of approximately 40 mm. To prevent separation of the outer fluffy layer from the inner core, it is intermittently ultrasonically welded to the core at approximately 6 mm centres to form a "hybrid fibre". Figs. 2.12 and 2.13 show the ultasonically welded, and non-welded fibres.

4.2.2 Physical Properties of the Fibres

A description of the textile material employed in this research was given earlier in section 2.7 in Chapter 2. By use of micrographs, it was illustrated that the PP fibres used in weaving of the textile were essentially an ensemble of fine fibrils spun round a cental core to form a yarn. The commercially quoted density of 0.91 g/cm^3 for the fibrillated polypropylene fibres needed to be verified experimentally. Therefore, an experiment was devised to determine the density of the yarn as described in Appendix A. The method was essentially a displacement technique in which the volume of a known mass of yarn was determined by firstly casting it in silicone of a known density, and subsequently determining the volume of silicone, from which the fibre density was computed. A more detailed description of the experimental technique is given in section A.2 in Appendix A.

The density of the yarn (ρ_f) was approximately 0.94 g/cm^3, which was slightly higher than the quoted density of 0.91 g/cm^3 for conventional PP fibres. The discrepancy could have been due to trapped dust particles in the interstices of the fibres, which increased the fibre mass.

Table 4.1: Physical properties of fibre

Property	Fibre type			
	Non-bonded		Bonded	
	Value	Standard deviation	Value	Standard deviation
Mass per metre length	0.286 g	0.005 g	0.349 g	0.007 g
Cross-sectional area	0.303 mm^2	0.005 mm^2	0.370 mm^2	0.007 mm^2
Mass of woven textile	125 g/m^2		125 g/m^2	

The average cross-section area of the fibres was computed directly from ρ_f and the mass per metre length of fibre was determined. The cross sectional areas for nonbonded and bonded fibres were 0.303 mm^2 and 0.370 mm^2 respectively. The slight increase in mass per metre length of the bonded fibres was attributed to closer packing of the fluff to the central core after ultrasonic welding. The physical properties of the fibres are summarized in

Table 4.1. While these values appear significantly different, this is due to closer packing of the fluff to the central core after ultrasonic welding, and is a real effect.

4.2.3 Mechanical Properties of the Fibres

The mechanical properties of fibres are conventionally described by the Young's modulus of elasticity E_f, and the ultimate tensile stress σ_{fu}. The Poisson's ratio ν of fibres is also commonly specified but it was not considered critical in this research. σ_{fu} was obtained from tensile tests performed on individual fibres form which E_f was computed. To determine the tensile properties of the fibres, the gripping system was firstly standardised.

A suitable gripping system was designed with special features to hold the fibre in position and at the same time be compatible with the standard fixtures of ZWICK Universal Testing Machine (UTM). A grip was devised as shown in Fig. 4.1. A fibre specimen from the polypropylene textile was carefully removed. The fibre was wrapped three times round the bracing device on the grip and was held in position by tightening the screws on the metal strip. The grip was attached to the load cell of the UTM through coupled pinned connections. The main features of the upper grip with the fibre in position are shown in Fig. 4.1.

The fibre was wrapped three times round a 12 mm diameter dowel pin which was inserted through a circular mounting piece (Figs. 4.1. Both fibre ends were then taken back to the upper fibre grip so that the test was effectively double-fibre tensile test and for evaluation purposes the load was halved 4.2). The mounting piece which closely fitted the standard fixtures of the UTM was fixed to the fixed crosshead using rigid pinned connections in order to eliminate parts movement during the test. The lower fibre grip is shown in Fig.4.2.

The grip to grip separation was measured to the nearest mm and the force set to zero. The UTM was programmed for a ramp rate of 10 mm per minute and a maximum displacement of 100 mm. The crosshead position

Figure 4.1: Customized upper fibre grip

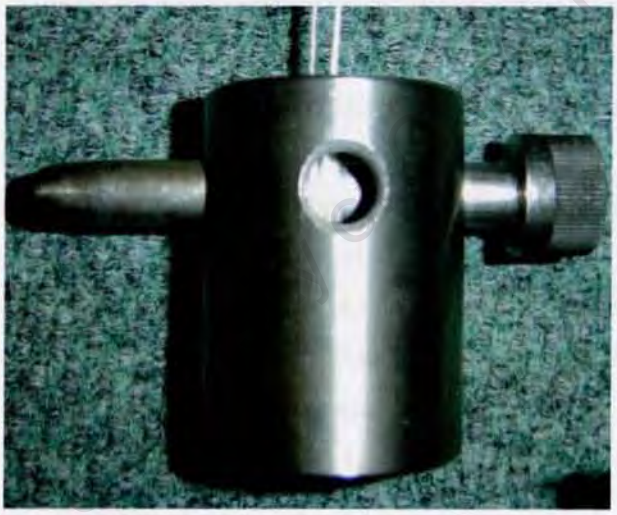

Figure 4.2: Lower fibre grip

was adjusted to remove slack in the fibre, the force was set to zero once more before the test was started to eliminate pre-load effects. The friction developed within the wrapped sections of the fibre and the gripping device was sufficient to prevent fibre slippage. Failure was characterized by rupture typically near the middle of the fibre, and the load-displacement traces were readily captured using a computer interface to the UTM. Where failure occurred in the grips (which was rare), the results were ignored. The test was repeated on a minimum of ten fibres and repeatable results were obtained as

shown in Fig. 5.6(a) in Chapter 5. The test was repeated on bonded fibres for comparison purposes as well as on weathered fibres that had experienced various regimes of environments.

4.2.4 Selection of the Binders

The role of mineral additives and chemical admixtures in cementitious matrices has been elaborated earlier in the text. In the field of Fibre Reinforced Cementitious Composites (FRCC), which is the main focus of this work, the common difficulty associated with the presence of fibres is the resulting reduction in workability caused by an increase in the internal resistance to flow especially at high fibre volume contents (V_f).

By incorporation of an appropriate supplementary cementitious material (SCM) or superplasticizer, this difficulty is adequately addressed. However, the choice of the SCM needs to be made carefully to ensure that it suits the research purposes. Firstly, the mortar mix should be designed to be workable and to have minimum segregation and secondly, the mortar should, on the one hand, possess an early age strength in order to withstand the experimentation process, and on the other hand, be permeable enough to gasses and moisture during durability studies. In this particular case the mix comprised of a fine grained dune sand with maximum nominal size of 600 μ, fineness modulus (FM) of 1.8, aggregate:cement ratio of 1.1, and water:cement ratio of 0.5.

Preliminary trials were undertaken on the suitable mix proportions using a fine graded dune sand with a maximum nominal size of 600 μm and a fineness modulus of 1.8. The aggregate/cement ratio was 1.1 and the water/cement ratio was 0.5. The preliminary studies showed that although the incorporation of 1 percent of the superplasticizer, "Sikament-NN" in the mix produced a workable mortar, the early age strength was much lower than in mortars with mineral additives. Therefore, the mineral additive option was explored further.

Despite major advancements in the role of supplementary cementitious

materials and chemical admixtures in High Performance Concrete (HPC), optimization and production of engineered pozzolanic products intended for use in specific portland cement-based formulations is not well established. In addition, there are no clear guidelines on selection of the most appropriate type of additive for Fibre Reinforced Cementitious Composites, therefore, an elimination approach was adopted in this research, based on the flow characteristics of the mix and the early age strength development.

Due to the availability of Condensed Silica Fume CSF, Ground Granulated Blast Furnace Slag (GGBFS), and Ultra-fine Fly Ash (UFFA), these were the only additives that were considered. UFFA was preferred to the other mineral additives due to its unique particulate nature.

Particles of Ultra Fine Fly Ash effectively fill the void spaces between the fine aggregates in cementitious mixes and create a "fine filler effect" in that the spherical shape of UFFA minimises the particle's surface to volume ratio, resulting in low fluid demands (Ferraris, Obla & Hill 2001). Mortar of good workability is therefore produced, at the same time, a high early age strength is achieved. This feature is particularly beneficial in this study where the mortar needed to be self compacting and of high consistency in order to sufficiently impregnate the fibre surfaces and thus develop good fibre/marix bonding.

The performance of CSF is equally satisfactory and indeed, higher matrix densification is achieved in CSF mixes. Although this is considered advantageous, for the purposes of this research dense matrices are undesirable due to associated difficulties of gas and moisture permeability during durability studies. On the other hand, UFFA facilitates the production of cohesive mortar mixes with reduced bleeding and segregation, at the same time, the matrix density is not excessive. Therefore, UFFA was preferred to other mineral additives in this research.

4.2.5 Characterisation of the Binders

Ordinary portland cement (OPC) designated CEM1 (EN 197-1 2000) is readily available and is commonly employed in ordinary concrete works in South Africa. Therefore, OPC type CEM1 42.5 was chosen for use in this research. Five bags of cement were used in the research and were obtained from the PPC cement factory in Cape Town. In order to minimise experimental scatter due to variations in cement composition, the cement used for this work was produced in a single batch that was obtained consecutively from the same production run. The bags of cement were labeled and protected from moisture until required for mixing.

Approximately one kilogramme of cement was sampled from each of the five bags, it was thoroughly blended and sent to the Pretoria Portland Cement (PPC) laboratories in Cape Town for physical characterisation and oxide analysis. The oxide analysis was carried out using x-ray diffraction techniques. One kilogramme sample of the mineral additive Ultra-Fine Fly Ash (UFFA) was also sent for similar analysis. The physical properties and oxide analysis of the powders are shown in Table 4.2.

4.2.6 Fine Aggregate

The most widely used sands in Cape Town area of South Africa are alluvial pit sand that is locally referred to as "Klipheuwel", and a finer grained dune sand. These two types of sand are commonly used in civil engineering works and were therefore the sands that were considered for this research. The actual choice was based on a balance between the mortar properties in the wet and dry states.

Table 4.2: Characterisation of the binders

	Quantity	
Property	CEM1 42.5	Ultra-fine Fly Ash
Specific gravity	3.12	2.25
Particle size and fineness	Blaine fineness: 395 m^2/kg	Surface area: 13000 cm^2/g Malvern Mastersizer: Top cut, 90% passing: 11μm Top cut, 99% passing: 25μm
Particle shape	Spherical	Spherical
Colour	Light grey	Light grey
Setting time	Initial: 145 min. Final: 275 min.	N/A N/A
Compressive strength	1 day:17.2 MPa 3 days: 27.3 MPa 7 days: 32.1 MPa 28 days: 38.8 MPa	N/A N/A N/A N/A
Calcium oxide (CaO)	64.4%	5.3%
Silicon oxide (SiO_2)	20.5%	50.4%
Aluminium oxide (Al_2O_3)	4.2%	34.1%
Ferric oxide (Fe_2O_3)	3.13%	3.41%
Silicon trioxide (SO_3) Silicon dioxide (SO_2)	2.41%	 50.4%
Magnesium oxide (MgO)	0.9%	1.5%
Manganese trioxide (Mn_2O_3)	0.05%	
Titanium trioxide ($Ti0_3$)	0.29%	1.80%
Phosphorous oxide (P_2O_5)	0.12%	0.80%
Chlorine (Cl) content	0.01%	0.01%
Potassium oxide (K_2O)	0.55%	0.67%
Sodium oxide (Na_2O)	0.11%	0.20%
Loss on ignition (LOI) at 1500°C	3.01%	1.37%

Mortar consistency was a major consideration since hand lay-up techniques were to be employed for production of composite specimens. Therefore, preliminary trials were run to determine the workability of the mortar. The results indicated that the performance of the coarser grained sand did not compare well with the finer dune sand because "Klipheuwel" sand produced less workable mortar in comparison with dune sand. In addition, the penetration of mortar into the textile material during the composite casting process was more easily achievable with the finer sand than the coarser variety. The finer grained sand was therefore the more preferred sand and was adopted for the study.

To further enhance the performance of dune sand, the nominal maximum grain size was limited to 600 μm, the same upper limit to grain size of sands

employed in previous studies (Kenai, Brooks & Dalton 1987), (Kenai 1994), (Akers et al. 2003).

Sand was characterized by density, grading and fineness modulus (FM) in the dry state. The density of the sand was 2.60 g/cm^3. The particle size distribution of dune sand was determined in accordance with ASTM standard test method (ASTM C136-01 1993). The results of sieve analysis were used in determination of the fineness modulus.

Table 4.3: Sieve analysis for dune sand

Sieve size, μm	Cumulative % passing	Cumulative % retained
600	100	0
300	27.17	72.83
150	1.83	98.17
75	0	100
Pan	0	100
Fineness Modulus (FM) = 1.71		

Materials retained on sieves coarser than 600 μm were discarded and the finer fraction weighed according to the sizes. The analysis was performed on three samples taken from different batches and the average grading computed. The sieve analysis involved determination of the the average proportions of sand retained on each sieve as shown in Table 4.3.

The cumulative percentage of materials retained on sieves of aperture sizes 150 μm and coarser was computed. The value thus obtained, divided by 100, described the FM of the sand (Neville 2002). FM was found to be 1.71 which indicated a fine sand (Fulton & Crawfold 1982). While this sand grade would not be ideal for conventional concrete, it was satisfactory because it could be easily worked into textile material used in this research study.

The grading of the sand was described by using a graph of the sieve analysis plotted with the cumulative percentage retained on each sieve on the vertical axis, and the sieve sizes (on a logarithmic scale) on the horizontal axis. The grading of dune sand is shown in Fig.4.3. Sand was stored in a moist-proof environment in which it maintained a dry environmental

condition prior to mortar production.

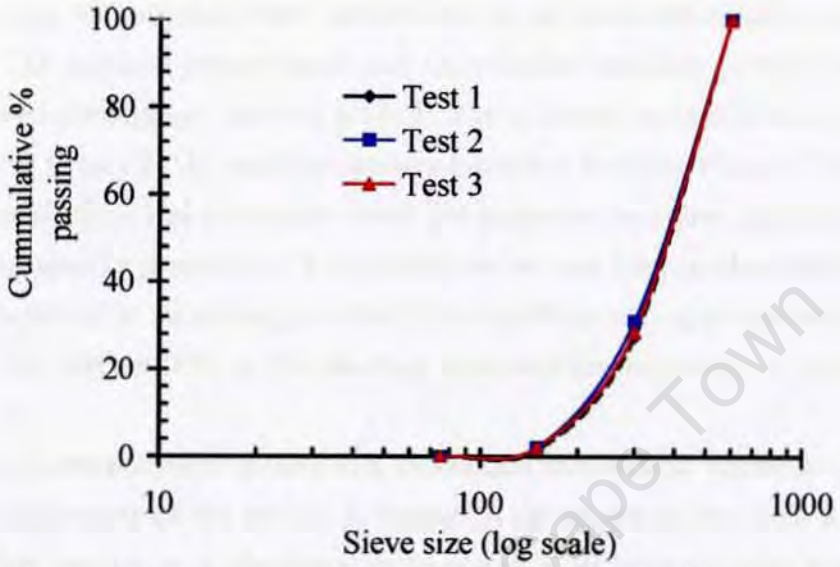

Figure 4.3: Average particle size distribution for Dune sand

4.2.7 Mortar Preparation

The aim was that the mortar density and porosity were representative of Textile Concrete applications in service. At the same time, the mix needed to be cohesive and of a consistency that was suitable for working into six layers of the textile. In order to minimise variations in specimens' densities within a single batch of mortar, a maximum period of 30 minutes between mixing of materials and casting of specimens was found to be practical and therefore a mix with a slight delay in setting was used (which is within the allowable setting time of 90 minutes (ASTM C94/C94M-00e2 2000)). To meet these demands, the mortar mix proportions were optimised.

The binder composed of a mixture of thoroughly blended cement and Ultra-Fine Fly Ash (UFFA) and was used in various water:binder (w:b) ratios. The mixes were varied by using water:cement ratios of between 0.3 and 0.6. For maximum benefits from the addition of UFA, it was recommended

by the manufacturers that a minimum dosage of 10 percent and a maximum of 30 percent mass replacement of CEM1 42.5 be added to the mix. The sand content was similarly varied to yield mortar of different consistencies.

Mixing of materials was carried out in an environmentally controlled room. The ambient temperature and the relative humidity in the room were monitored throughout the test period. The temperature variations were between 20° C and 24° C, and the relative humidity between 65 and 75 percent. These environmental conditions were not expected to cause significant variations in mortar properties. The mixing water was kept in the control room for 24 hours prior to mixing to allow it to equilibrate to approximately 19°C, which was within 2°C of the average temperature recorded in the mixing room.

The materials were mixed in a motorized mechanical mixer in order to ensure uniformity of the mixes. A Hobart A120 model mixer, with a stirring hook that moved in a planetary motion and a 10 litre capacity bowl, was used in mixing of materials. By choice of gears on the mixer, the hook could run at speeds of 1.20, 1.25 and 2.27 revolutions per second about the bowl axis, and 2.7, 2.8 and 5.0 revolutions per second about the hook axis. The speed of the mixer was determined from the time taken for the bowl or the hook axes to make 100 revolutions. The revolution times are recorded in Tables A.1 and A.2 in Appendix A. The mixing time was arrived at after several trials, and a time of two minutes with an average mixer speed of 2.7 revolutions per second about the hook axis was adopted. To reduce the loss of the fine powders out of the mixing bowl, water was added first, followed by the powders while sand was added last.

Although there are standard guidelines for mix design of mortar for use in Fibre Reinforced Cementitious Composites, the same can not be said for use in FRCC. The proportions appropriate for this research were determined from trial tests in which nine batches were employed. The weight of all materials per batch was limited by the capacity of the mixer. Therefore, a maximum of 0.750 of a kilogramme of the binder was used for each batch, and the sand

content was varied between 0.690 kg and 0.870 kg, and the water:binder (w:b) ratio between 0.45 and 0.54. In two of the mixes, 0.1 percent of the chemical admixture "Sikament NN", referred to earlier in section 2.4.4.2, was added to the mix instead of UFFA. By combining different mix proportions, nine types of mortar mixes shown in Table 4.4 were produced.

Highly plastic mixes were aimed for and therefore several trials on mortar consistency were undertaken. A dosage of 10 percent of UFFA was developed from trials. Similarly, trials were undertaken in order to determine the appropriate mixing time for each batch of materials. The mortar was examined for signs of excessive bleeding and segregation after standing undisturbed for approximately 15 minutes in the mixing bowl. Bleeding was not a problem in this mix. The plasticity and consistency of the mixes to be used with textile concrete specimens was also evaluated by means of flow tests (ASTM C1362 1997).

It was found necessary as a part of choosing a suitable mix to test the properties of hardened mortar (ASTM C 109/C 109M-05 2005). Therefore, 50 mm cubes were cast and after setting, they were water cured at 21°C. The cubes were used in the determination of the early age strength of the hardened mortar, which was done after three, seven, and 28 days of water curing (for cube crushing strength procedure see section 4.2.8). The trials indicated that a mixing time of 120 seconds was optimum for production of mortar without excessive bleeding. Therefore, the materials were mixed for 120 seconds for each mix type given in Table 4.4.

Table 4.4: Mortar mix specifications

Mix type	Sand , kg (s)	Cement (c), kg (b)	UFFA (u), kg (b)	Water, ml (w)	Sand/binder ratio (s/b)	Water/binder ratio (w:b)	u/c%
1	0.750	0.690	0	375	1.09	0.54	0
2	0.675	0.750	0.075	375	0.82	0.45	10
3	0.690	0.750	0	375	0.92	0.50	0
4	0.750	0.675	0.075	375	1.0	0.50	10
5	0.870	0.600	0.150	375	1.16	0.50	20
6	0.750	0.750	0	375	1.0	0.50	0
7	0.870	0.675	0.075	375	1.0	0.50	10
8	0.750	0.750	0.75 ml Admixture	375	1.0	0.50	0.1% admixture /cement
9	0.870	0.750	0.75 ml Admixture	375	1.0	0.50	0.1% admixture /cement

The trial tests showed that the mixes with water:binder ratio of 0.5 produced mortar of good consistency and strength of more than 10 MPa after three days. The tests also showed that despite mixes with the chemical admixture comparing well with UFFA mixes in terms of workability and consistency, the early age strengths of UFA mixes were much higher. For example, after 7 days, mix type 4 had an average cube crushing strength of 10 MPa compared with 5 MPa for mixes with the chemical admixture, and therefore the use of the chemical admixtures was not pursued further.

Preliminary trials showed that mix Types 1 to 5 were of good consistency and workability, but of these mixes, the actual choice for use in the research was based not solely on workability and high early strength, but on the setting time as well. This criterion ensured that the consistency of the mortar was such that it facilitated enough time for the specimens to be cast, which was found to be a two hour period between mixing of materials and casting of the specimens. To characterise the setting times, flow tests were carried out on the five mixes as described in the section which follows.

4.2.7.1 Flow Test

The value of the flow test lies in assessing the cohesiveness of very high workability or flowing cementitious mixes, and is an indication of the consistency of the mix and its susceptibility to segregation (Neville 2002). The higher the flow, the lower the viscosity of the cement paste component of the mix. Ordinarily, low viscosity is undesirable because of easy downward movement of the aggregates within the mortar leading to segregation. Therefore, for conventional cementitious materials, low flow mixes are usually targeted. However, despite the advantages of low flow mixes, a high flow is normally considered where the specimen production techniques require the mix to be highly workable. A simple means of assessing the cohesiveness of mortar was employed by measuring the spread of a freshly mixed pile of the mortar on a table subjected to jolting.

The mortar flow test was in accordance with ASTM standard (ASTM

C1437-01 2001). The specification closely follows the South African standard (SABS Method 1245 1994) for determination of consistency of fresh concrete, which measures mortar response to a specific condition, that is, the spread of fresh mortar after compaction on a so-called "flow table", but does not necessarily measure the basic mix property such as rheology or shearing resistance.

The main advantage of the flow test over other workability tests was its simplicity. Another advantage of the test, which was particularly relevant in this research, was that the treatment of mortar during the test was comparable and closely related to the manner in which mortar was to be placed during casting of the specimens. Therefore the "flow table" technique was adopted and fresh mortar flow was characterised accordingly. Fig. 4.4 illustrates the "flow table" technique for determination of mortar flow properties.

Figure 4.4: Measurement of flow properties on a flow table

The test equipment had three components; a "flow table", a brass mould, and a tamper made of hard rubber with a nominal cross-section of 22 mm x 11 mm, and a length of 125 mm. The table had a 250 mm diameter circular smooth stainless steel top capable of vertical movements within the tolerances specified in ASTM C230 (ASTM C230 1990). The brass mould was in the shape of the frustum of a cone which had a nominal height of 70 mm. The cone had a lower nominal diameter of 100 mm and its upper diameter was 80 mm.

4.2.7.2 Flow Characteristics

Preliminary trials involved mixing of materials for 30 seconds after which flow was measured. The procedure for the flow test was in accordance with the standard method for determination of the flow of hydraulic cement (ASTM C1362 1997).

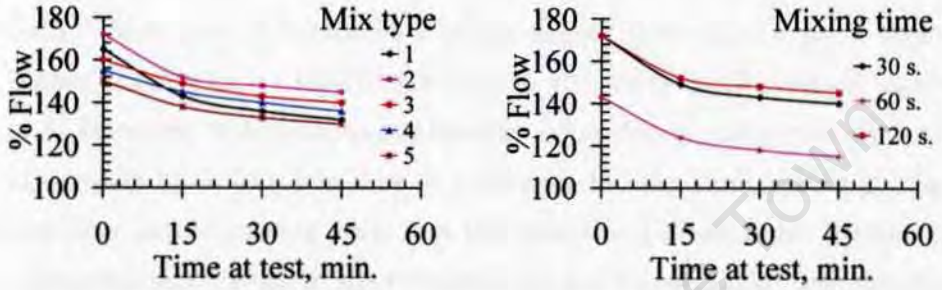

(a) Rate of flow loss (b) Mix type 2

Figure 4.5: Flow loss for 120 seconds mixing time

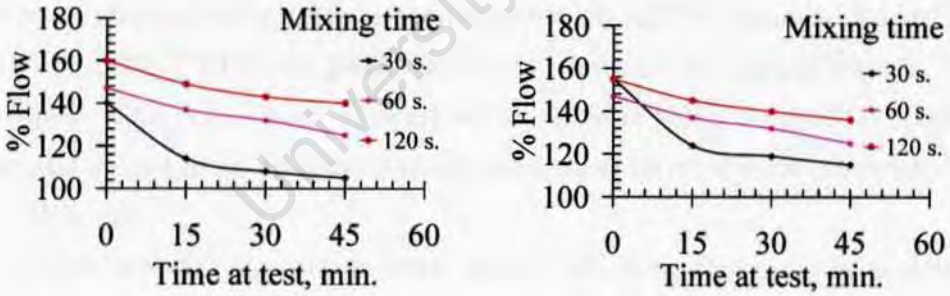

(a) Mix type 3 (b) Mix type 4

Figure 4.6: Flow loss for mixes with the highest consistency: 120 seconds mixing time

To assess the sensitivity of flow to the mixing time, different mixes were studied by means of the ASTM "flow" table (ASTM C1362 1997) at three mixing times of 15, 30, and 45 minutes as shown in the flow characteristics in Fig. 4.5(a). The results of the flow tests are shown in Table A.3 in Appendix

A. Figs. 4.5 and 4.6 are typical graphs representing the flow characteristics of different types of mortar investigated. It was clear from these curves that a mixing time of 120 seconds was suitable as it yielded mortars of flow greater than 130 percent in the all the mixes, even after standing for approximately 45 minutes. Mix type 2 exhibited the highest flow which was attributed to low cement:binder ratio (w:b) of 0.45. However, such a low w:b is not representative of mortar mixes in common use and w:b of 0.5 would be more realistic. Mix type 3 exhibited slightly higher flow than type 4 especially at higher mixing times which was due to the lower sand content in mortar type 3. However, this mix had a harsher consistency compared with type 4 as illustrated by a very low flow at a shorter mixing time, although the mix gained flow as the mixing time was increased to 120 seconds. To determine the optimum mix for use in the research, further investigation was undertaken on the hardened mortar strength as described in the section that follows.

4.2.8 Characterisation of Hardened Mortar

Within 30 minutes from the time of mixing of materials, cubes were cast into 50 mm cubical steel moulds in accordance with ASTM standard for concrete (ASTM C192/C192M-00 2000). 30 cubes were cast for testing after 3, 7 and 28 days. The cubes were covered with a plastic sheet to prevent moisture loss and stored in an environmentally controlled room of approximately 24°C for 24 hours.

After setting, the cubes were struck off from the moulds and water cured for 28 days to allow hydration of cement and strength development to progress under optimum conditions. The curing water was maintained at a temperature of approximately 21°C. Three cubes were weighed and tested after three days of curing, and similarly, after 7 and 28 days. The cube crushing test was carried out in accordance with ASTM standard specifications (ASTM C 109/C 109M-05 2005) with the exception that the cubes were tested in a dry state rather than the wet state recommended in the Standard. This was a necessary condition in the current research because a

part of ageing under investigation was the effects of wetting/drying cycles on samples under a controlled environment, therefore wetting samples prior to mechanical testing would vary the ageing cycle time, and the extent of this variation was not easily quantifiable.

4.2.8.1 The Cube Test

The cube crushing test procedure was in accordance with ASTM Standard (ASTM C 109/C 109M-05 2005). The early age cube crushing strength for different mortar types cured under different conditions were compared and the results are given in Table A.4 in Appendix A.

The nine mortar mixes has a water/cement ratio of 0.5. From the results of the cube crushing tests, mix type 2 exhibited the highest strength of 38.4 MPa after 28 days of curing. This was however only marginally higher than the corresponding strength of mix type 3 (38.0 MPa). The high strength exhibited by these two mixes could be attributed to the lower sand:binder ratios of 0.82 and 0.92 in mix type 2 and 3 respectively. The presence of a mineral additive in mix type 2 also enhanced its 28 days strength. On the other hand, mix type 4 had an average density of 2.20 g/cm^3 and the average cube crushing strength was 38.20 MPa after 28 days. The strength:density ratio for mix type 4 (17.27) was slightly lower than for mix type 2 (19.70) with average density and strength of 2.00 g/cm^3 and 38.40 MPa respectively. The disadvantage of low strength of mortar type 4 was compensated for by better flow characteristics of the mix relative to type 2.

When the flow properties and workability were evaluated against the cube crushing strength and the performance of mortar types 2, 3 and 4, type 4 was found to be more preferable to types 2 and 3 because it exhibited satisfactory workability and minimal bleeding, and therefore mix type 4 was chosen in this research. To assess the compressive strength of the matrix component in the composite, porosity tests were carried out on plain mortar and trial composites subsequently produced.

4.2.8.2 Porosity

After the cubes were water cured for 28 days, 10 mm thick specimens were sliced from three cubes. Porosity of the specimens was determined in accordance with ASTM standard (ASTM C642-97 1997), utilising the Principal of Archimedes which relates the weight of a suspended body to the upthrust as illustrated by Eq. 4.1.

$$\text{Upthrust} = \text{Volume of solid} \times \text{Density of water} \times \text{g} \tag{4.1}$$

where with g is the acceleration due to gravity.

The slices were vacuum saturated for five hours which was carried out in Calcium hydroxide ($Ca(OH)_2$) solution in order to avoid leaching the specimens, which were thereafter submerged in water and the mass of each specimen taken, M_{sat}. The specimens were then oven dried for three hours at 105°C and the dry mass also taken, $M_{ovendry}$. The specimens were left standing for 18 hours to relax any residual stresses induced during the drying process. After relaxing, each specimen was suspended on a thin string below a weighing scale and submerged in water and in this position, the suspended mass, M_{sus} was taken. Porosity was thus determined on eight specimens chosen at random. From the different masses of each specimen, the upthrust on the specimen was then determined. Eqs. A.1 to A.9 in Appendix A illustrate how the porosity was computed from the masses taken, and Table 4.5 gives the porosities of eight representative mortar specimens.

Table 4.5: Porosity of mortar

Specimen	$Mass_{sat}$, g	$Mass_{ovendry}$, g	$Mass_{sub}$, g	Porosity
1	21.59	19.93	10.90	0.16
2	21.04	19.01	10.90	0.20
3	19.92	17.89	10.30	0.21
4	18.32	16.73	9.20	0.17
5	17.43	15.96	8.60	0.17
6	23.79	21.57	11.50	0.18
7	17.90	16.12	9.00	0.20
8	20.68	18.90	10.30	0.17

Mean porosity: 0.18 ± 0.02

Table 4.6: Porosity of the matrix component of the composite

Specimen	$Mass_{sat}$, g	$Mass_{ovendry}$, g	$Mass_{sub}$, g	Porosity	Volume, ml
1	51.43	46.51	28.10	0.21	22.0
2	60.25	54.50	33.66	0.22	29.5
3	52.61	47.46	28.86	0.22	23.0
4	52.99	47.90	29.06	0.21	24.5
5	48.92	44.00	26.77	0.22	23.5
6	46.47	42.12	25.67	0.21	22.0

Mean porosity: 0.21 ± 0.005

Similarly, specimens were cut from the trial textile concrete specimens and their porosities determined. Table 4.6 gives the porosities of the matrix component of six representative specimens.

The porosity of the matrix component of the trial composite was approximately 17 percent higher than plain mortar, which was regarded as a minor increase considering the presence of fibres in the specimen. From the porosity test, it was concluded that hand lay-up could reliably be employed as the composite production technique. This information was necessary before development of an appropriate specimen geometry for tensile testing, and the gripping system described later in subsection 4.4.1 could be designed. Thereafter, the production of Textile Concrete (TC) specimens was initiated but it is in order, firstly to discuss the fibre pull-out specimens.

Ordinary Portland cement (OPC) CEM I 42.5 (ASTM C150-07 2007) was used in production of the mix type 4, with proportions shown in Table 4.4, which was then used for production of all specimens used in this research. The mixing of the materials was as described earlier in section 4.2.7.

4.3 Fibre Pull-out Specimen

The following are the criteria for fibre pullout specimens:

- The loading on the fibre to remain unaffected by the grip system (Currie & Gardner 1989).

- Different lengths and orientations of fibres to be embedded in the matrix
- The specimen geometry to allow for variation of matrix mix proportions.
- The method should be repeatable.
- The whole fibre should be encapsulated in the matrix.
- Be able to measure both the interfacial bonding strength and friction.

A "one-sided" model of fibre pull-out specimen is a popular approach to studying the fibre/matrix property mainly due to its simplicity. However, a "two-sided" configuration comprising of a fibre embedded in the shape of "figure eight" , or the more commonly used term, "dog-bone" specimen, is the preferred geometrical model due to its robustness.

The specimen in "figure eight" geometry comprising of a symmetrical mortar briquette, with a fibre at the middle crossing a matrix crack, simulates the fibre bridging action encountered during the composite's fracture process. This specimen model was originally developed by Maage (Maage 1978) and later adopted by Wang and co-workers in studies involving brittle fibres of microscopic diameters (Wang, Backer & Li 1988). A similar geometry was later used by Currie and Gardner (Currie & Gardner 1989) but the test was faced with fibre brittleness and alignment problems and was therefore, modified and later used successfully to provide more comprehensive information on the fibre/matrix interfacial properties (Katz et al. 1995).

By using fibres of a much higher diameter than in the test by Wang *et al.* (Wang, Backer & Li 1988), fibre orientation was more accurate and better control of the matrix surrounding the fibre was possible. The "two-sided" (or "figure eight" shape) geometry was adopted in this thesis not only because of its simplicity during preparation and testing, but because it met the criteria specified above. Fig.4.7 is schematic illustration of the "figure eight" geometry of the briquette used for fibre pullout studies.

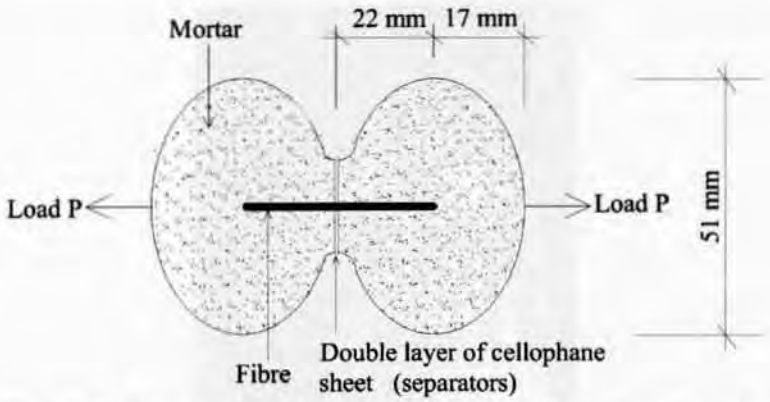

Figure 4.7: Geometry of "figure eight" pullout test specimen

4.3.1 Fibre Pull-out Specimen Moulds

The specimen moulds needed to be fabricated in a manner that facilitated easy casting and striking of the specimens after setting, and also that they were rigid enough and resistant to repeated wetting as well as being sufficiently wear resistant. Therefore, the moulds were fabricated from 110 x 85 x 8 mm thick rectangular pieces of a Polyvinyl Chloride (PVC) sheet in briquettes shaped in a "figure of eight".

The moulds were split longitudinally to facilitate easy striking after setting of the mortar. The bottom parts of the moulds were rectangular pieces of hardboard which could be clipped onto the bottom of the two PVC mould pieces, thus providing a smooth hard bottom surface for the specimen, at the same time holding the mould firmly in place during specimen production as shown in Fig. 4.8.

60 such moulds were machined for fibre pull-out specimens in order to facilitate production of 15 specimens, for a given weathering condition, in each a single batch.

4.3.2 Specimen Production

The embedded fibre length (l_e) was estimated from the relationship between the fibre diameter and interface bond strength (τ) given by Eq. 4.2 (Currie

Figure 4.8: Assembled mould for the pull-out specimen

& Gardner 1989).

$$\tau = \frac{P_{max}}{\pi d_f l_e} \tag{4.2}$$

By substituting the quoted theoretical value of fibre/matrix bond τ of 0.4 MPa, and a cross-sectional area of 0.303 mm^3, an embedded fibre length of 22 mm was arrived at. Therefore, fibre pieces of theoretical desired length of 44 mm ($2l_c$) each were cut at random from non-bonded fibres for the pull-out tests.

Mortar mix "Type 4" was employed for the production of all specimens. The fibre pull-out specimen was prepared by filling the mortar halfway up the mould and then evenly spreading it using a steel trowel. A piece of stiff acetate sheet approximately 0.2 mm thick and including 2 mm hole was located across the narrowest section at the middle of the mould to act as a

debonding (or separation) sheet and separate it into two identical sections, thus creating in the hardened specimen, an effective crack plane. The fibre was thereafter carefully threaded through this debonding sheet at mid-height so that it was positioned horizontally on the fresh mortar. The layer of mortar together with the acetate sheet provided support for the fibre to remain in place at the middle of the mould. The mould was then filled up with mortar, at the same time gently shaking it sufficiently to infiltrate the fibre surfaces. The top mortar surface was troweled flush with the edge of the mould thus giving the specimens a uniform thickness of approximately eight millimetres.

15 specimens were cast for each batch, which were thereafter covered with an impervious sheet for moisture control and kept under controlled environment with temperature of approximately 23^o C for 24 hours to set. After setting the specimens were water cured at approximately 21^oC for 28 days. Different batches of specimens were cast in an environmentally controlled room for different exposure environments. All samples were cast in the same environmentally controlled room in order to minimise variability across batches.

4.4 Uniaxial Tensile Specimen

The reinforcing action of fibres in cementitious matrices is most beneficial in the tensile mode. Indirect methods such as splitting tensile tests, and bending tests have conventionally been employed to determine the tensile properties of cementitious materials (Neville 2002). These tests are ordinarily simple to perform. However, there is no straight-forward correlation between the tensile stress-strain ($\sigma - \epsilon$) characteristics and the corresponding deflection behaviour and this is a major limitation on the use of these indirect methods.

Since the precise position of the neutral axis is indeterminate during the bending test, uni-axial tensile testing (UTT) was chosen as it provides more rational and reliable information on the tensile mechanical behaviour of cementitious materials (Keer & Hannant 1986). In addition, UTT enables objective distinction between the material parameters; tensile strength and

fracture energy, or toughness, thanks to the nominally uniform tensile stress distribution, unlike in bending or other indirect tensile tests. By using a self-centering specimen gripping device for the tensile test, the effects of bending induced by misalignment were minimised.

In this research, the geometry of the tensile specimen and the gripping system were customised to be adaptable to the standard fixtures of the testing machine. Since the specimens were intended for use in durability tests, it was important that they were thin enough to be permeable to gases and moisture during the tests. However, the thickness of the specimens was limited by the practical situation, considering that hand lay-up production techniques were to be employed for their production.

Preliminary trials, referred to earlier in section 4.2, indicated that six layers of CemForce could easily be worked into thin mortar layers, and with sufficient pressure application, specimens with a nominal thickness of 8 millimetres could easily be produced for tensile tests. Trials indicated that 8 millimetre thick specimens were robust and capable of withstanding excessive manual handling without being damaged during the experimentation process. The moulds used in casting of the specimens similarly had to withstand repeated wetting and laboratory curing conditions. When all these factors were taken into account, a thickness of 8 millimetre thickness was adopted for all specimens for this research.

4.4.1 Specimen Geometry for Tensile Testing

The specimen geometry for tensile tests was a major consideration based on the need for the facilitation of easy production of the laminates. Firstly, the gripping areas were based on the lateral pressure likely to be exerted on the edges of the specimen by the grips during the test as shown in Fig. tensilegrip. Parallel tests on mortar cubes indicated that for specimens previously water cured for 28 days, the compressive stress which could be withstood by the specimens without local crushing was 35 MPa. This information was useful in designing the gripping sections of the specimens.

The laminate geometry formed the basis for design of detachable grips which were compatible with the standard fixtures of ZWICK Universal Testing Machine (UTM). The grips were in the shape of truncated 'V' as shown in Fig. 4.9 and were machined from a 10 mm thick aluminium plate. Each grip weighed 335 gm and closely fitted the specimen gripping areas without slipping. The two grips formed a dedicated specimen holding system that

Figure 4.9: Aluminium grip for the tensile specimen

was adaptable to the stationary and moving crossheads of the UTM. In an attempt to refine the design of the grips, trial tensile tests were carried out by loading the specimens to failure.

As part of the experimentation process, two sizes of specimens were employed; a shorter one with a gauge length of 25 mm and the other 125 mm, and both were of the same width of 50 mm. The overall lengths of these specimens were 200 mm and 300 mm respectively. The gripping area was smoothly rounded into the gauge sections with 100 mm radii. The widest section at the gripping area was therefore, 90 mm, reducing to 50 mm over a length of 50 mm. The two specimen geometries are shown in Fig. 4.10

The two types of specimens were identical at the gripping areas and closely fitted into the aluminium grips as shown in Fig. 4.11.

4.4.2 Tensile Specimen Mould

Part of the consideration in the tensile specimen production process was suitable moulds which facilitated convenient casting of the Textile Concrete laminates. The moulds were designed such that the specimen could be held

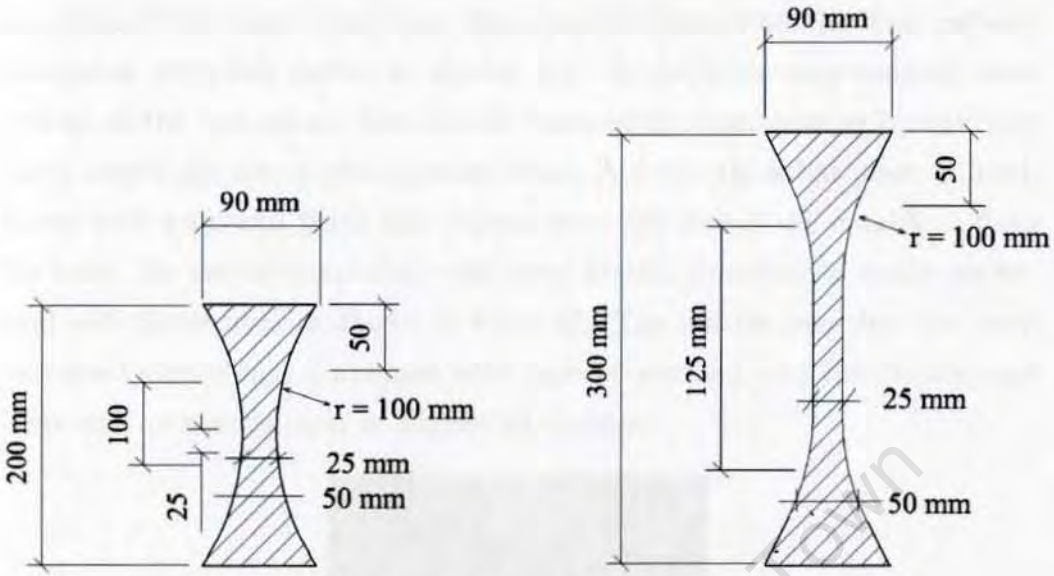

Figure 4.10: Specimen geometries

Figure 4.11: Tensile specimen gripping system

in place during casting and throughout the curing period. The design also facilitated easy removal of the specimens without incurring damage to the specimens. A suitable material for such a mould was a rigid plastic such as polyvinyl chloride (PVC). The moulds were fabricated from a plain 8

mm thick PVC sheet, which was the same thickness with the fibre pull-out specimens described earlier in section 4.3. To facilitate easy removal after setting of the specimens, the moulds were made demountable by splitting them lengthwise across two opposite sides. A 5 mm thick flat piece of hardboard with a smooth finish was clipped onto one side of the moulds to form the base. By use of metal clips, the three mould pieces could easily assembled and demounted as shown in Fig.4.12. The mortar used for this work had good consistency combined with ease of working into the textile, and there was no porous layer or significant leakage.

Figure 4.12: Assembled mould for the tensile specimen

4.4.3 Tensile Specimen Casting Technique

For each of the two specimens with geometries shown in Fig. 4.10, ten trial samples were cast employing the hand lay-up technique. The first step in the production involved evenly placing a thin layer of mortar at the bottom

of the assembled mould. A piece of textile mesh was cut in the shape of the specimen, and with the weft threads running in the longer axial direction, was placed on top of the the mortar layer. In this terminology weft refers to the main fibre with an outer fluffy layer and warp refers to cross fibres threaded in between (Fig. 2.14). Pressure was applied to the fabric forcing some of the mortar to exude out of the mesh apertures while avoiding contact of the textile piece with the base of the mould. This ensured that the textile material remained embedded within the matrix, which simulated protection of polypropylene textile from effects of ultra-violet radiation.

The next layer of mortar was spread onto the piece of textile material inside the mould and again worked by hand into the mesh for full impregnation. The hand lay-up process was repeated until six layers of textile pieces were embedded in mortar. The final layer of mortar filled the mould to the top and the surface was finished smooth with a steel trowel. Immediately after casting, the Textile Concrete laminates were covered with an impervious sheet and allowed to set for 24 hours in a laboratory environment. A cross-section of a specimen is shown in Fig. 4.13 illustrating textile layers evenly spaced through the thickness.

Figure 4.13: Cross-section of Specimen showing fibres location in the matrix

After setting, the specimens were water cured at a temperature of 23°C for 28 days. The moulds were stripped after the specimens had cured in order to minimize damage. After curing, specimens were conditioned in a control room at a temperature of approximately 21±1°C and relative humidity of

53±2 percent for a minimum of one month in order to equilibrate and dry the surface moisture. Control specimens remained in the laboratory under controlled conditions comprising of temperature of approximately 21±2°C and relative humidity of 53±2 percent. Thus control samples were differentiated from weathered samples. The other batches of cured samples were weathered under the same environmental conditions with the cubes, fibres, and pull-out specimens. The environmental regimes in which the samples were weathered are described in the following section.

4.5 Environmental Regimes

Different batches of specimens were aged in the following environments:

i. 100 hot/cold cycles: Maximum temperature was 50±1°C, minimum temperature was 23±1°C, RH was 20±2 percent, temperature was raised from 23±1°C to 50±1°C in 30 minutes and cooling time was 45 minutes.
ii. 100 Wetting/Drying cycles: Maximum temperature was 35±1°C, minimum temperature was 23±1°C, RH varied between 52 percent and 100 percent over a 24 hour period.
iii. Continuous carbonation exposure for 6 months at a temperature. of approximately 30±1°C and relative humidity varied between 50 and 70 percent.
iv. Natural exposure in a moderate climate for 11 months.
v. Natural exposure in a tropical climate for 11 months.
vi. Natural exposure in a tropical climate for 16 months.
vii. Control samples at 21±1°C and 53±5 percent Relative Humidity for periods ranging from 28 days to 20 months.

The accelerated ageing protocol that was adopted in this research involved subjecting samples to different exposure regimes in order to simulate the following environments separately: so called "hot/cold", "Wetting/Drying", and continuous carbonation exposures. The integrated hot/cold and Wetting/Drying facility formed a semi-automated environmental facility. The

main features of the system were an assembly of trays made from grade 316 stainless steel together-with a heating unit, water supply and drainage systems.

The unique feature in the hot/cold environmental facility was a set of three 500 Watt halogen bulbs that heated the samples while for the Wetting/Drying component of the facility, the main feature was a specially designed vacuum chamber capable of withstanding negative pressures of approximately 10 millimetres of mercury (-97 to -100 kPa). The effects of light on the tests were not investigated in this research but this aspect of accelerated ageing is recommended for future studies. The integrated environmental facility showing the assembly of hot/cold and Wetting/Drying chambers, heating and water supply systems is shown in Fig. 4.14.

Figure 4.14: Integrated environmental facility

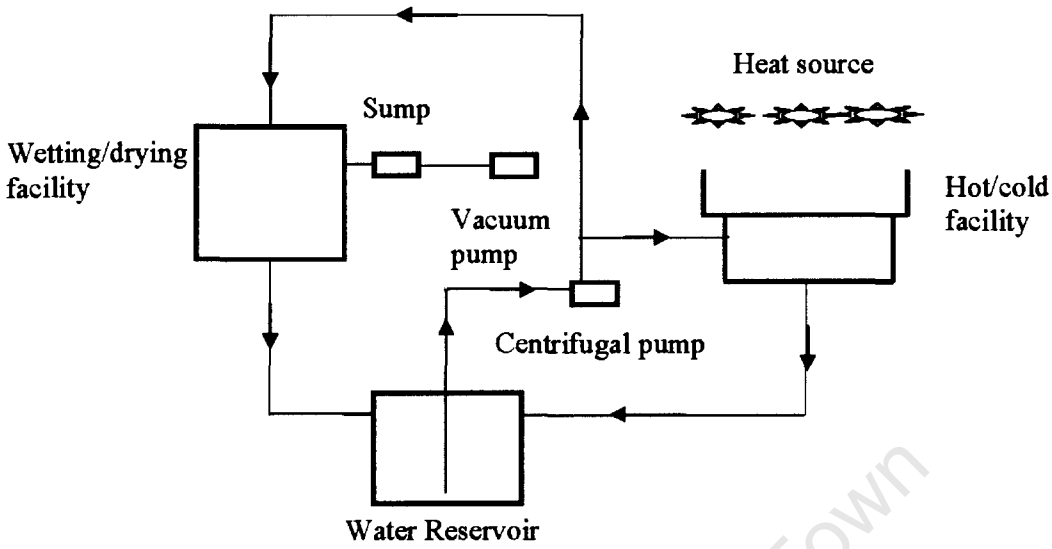

Figure 4.15: Block diagram of the integrated facility showing direction of water flow

A system of a timer and relays controlled the hot/cold cycles by synchronizing the change-over between the heating and cooling regimes. The system was adaptable to the Wetting/Drying system as illustrated by the block diagram in Fig. 4.15.

Carbonation exposure was carried out separately from the hot/cold and Wetting/Drying facility in a dedicated research-based incubator. The weathering processes of each of these three ageing facilities is discussed further in the sections that follow.

4.5.1 The Hot/Cold Facility

The hot/cold facility is shown in Figs. 4.14 and illustrated in the block diagram in Fig. 4.15. The main features of the hot/cold system was a 650 x 650 x 100 mm tray capable of holding five mortar cubes, ten fibre pull-out and five tensile samples in a single batch. The tray formed the top covering lid to a smaller tray with a size of 600 x 600 x 300 mm, thus providing a 25 mm overhang over the lower tray. Samples were held on the smaller upper tray. The heating source for the system was 500 Watt halogen light bulbs positioned directly above the top tray.

Preliminary trials were carried out to select the suitable number of bulbs required for effective heating of the system, and to determine their position above the specimens. By use of thermocouples attached to the surfaces of the specimens, the temperature was monitored over a 1 hour period on the top surfaces of specimens. The number of bulbs and their position above the top tray were varied until average temperatures of 50°C and 23 °C in the heating and cooling modes respectively were achieved. This temperature range was chosen since it was what was commonly experienced in local environments.

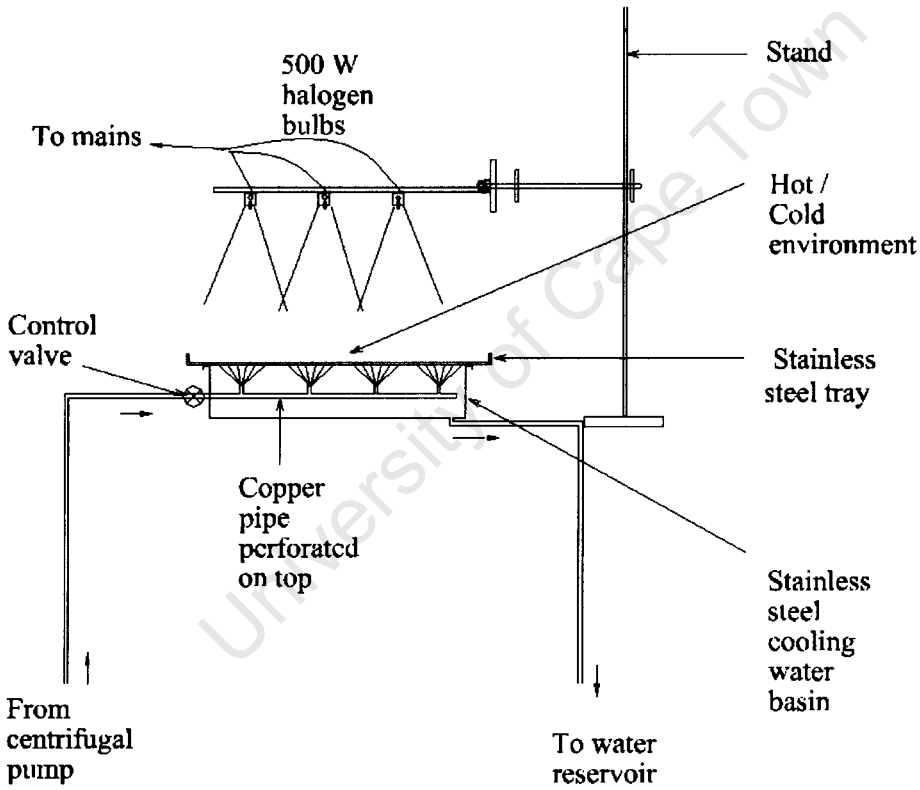

Figure 4.16: Schematic of hot/cold components of environmental facility

With three bulbs positioned at 100 mm above the trays, the environmental temperature could be raised from 23°C to 50°C in approximately 30 minutes and then reduced to 23°C in approximately 45 minutes, thus the hot/cold cycle time was 75 minutes.

A 15 mm diameter copper pipe with 1 mm wide perforations at 25 mm

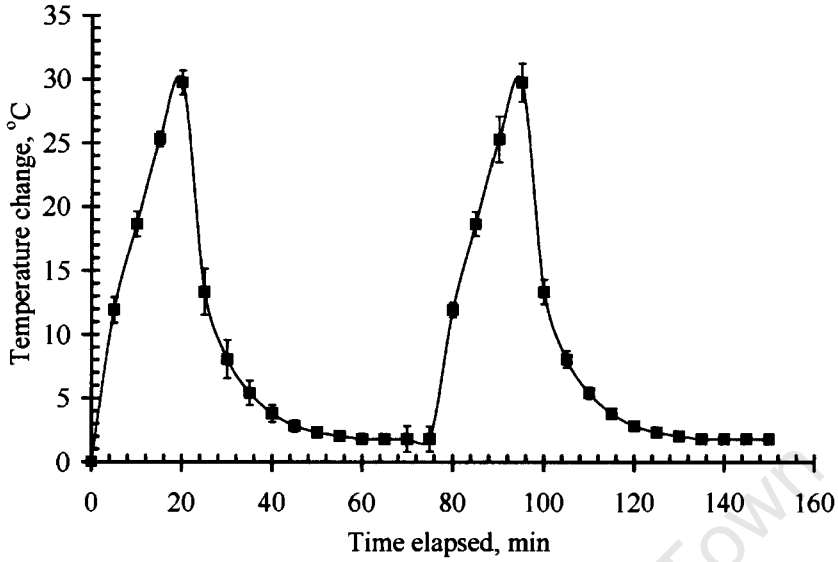

Figure 4.17: Two hot/cold cycles in semi-automated facility

spacing along its top surface traversed the lower tray at a height of 100 mm. By use of a 0.5 HP (0.373 kW) centrifugal pump, cold water was pumped through the perforated pipe from a 10 m^3 capacity ground water reservoir. As the water flowed through the pipe under pressure, a fine mist of cold water was sprayed to the undersurface of the top tray thus cooling the system. Excess water was drained through a 15 mm diameter opening at the bottom of the lower tray and drained back into the ground water reservoir.

The heating cycle was characterised using temperatures measured at the top and bottom surfaces of four specimens which were placed at the middle of the tray. By use of thermocouples, the temperatures were taken at five minute intervals over a 75 minute period and measurements were repeated six times and the average temperature computed. Fig. 4.17 shows the characteristic hot/cold cycle in the semi-automated facility. All the specimens were weathered by exposure to eight hot/cold cycles over a 10 hour period. At the end of this period, a nominal increase of 2°C in the water temperature was noticed but the effect was not cumulative since the system was stopped for the following 14 hours to cool off completely and for the water in the reservoir to equilibrate to approximately 21±1°C. 100 hot/cold cycles

were run continuously over a two week period after which the specimens were sealed and kept in the control room at 23±1°C and 51±5 percent relative humidity until required for mechanical testing.

4.5.2 Wetting/Drying Facility

The Wetting/Drying chamber facilitated wetting of specimens and draining of excess water. By use of an electrically heated Incoloy tape that was wound round a coiled copper tubing inside the chamber, the inside temperature of the chamber was controlled between 23 ±1°C and 35 ±1°C. Preliminary wetting and drying studies were carried out to determine the effectiveness of a typical Wetting/Drying cycle, the procedure is given in section A.7 in Appendix A.

The preliminary studies showed that the specimens could be sufficiently wetted after 15 minutes of submersion in water and subsequently vacuum dried to an equilibrium moisture content after approximately 5 hours. This indicated a significant difference in the hot/cold and Wetting/Drying cycle times. Therefore, a fully automated integrated environmental system that had been originally envisaged could not be made fully self-actuating but rather, the ageing cycles were run independently in a "semi- automated" state.

The Wetting/Drying environmental system consisted of a 600 x 600 x 600 mm stainless steel chamber capable of holding and effectively weathering five mortar cubes, ten fibre pull-out and five tensile samples in a single batch, at the same time withstanding a vacuum in the vicinity of 10 millimetres of mercury. Any vacuum-induced damage on the samples was not quantified and indeed, this is acknowledged as one of the research limitations. Future work to create a better understanding of the nature of vacuum-induced damage in accelerated ageing tests is suggested.

The chamber was braced with two non-corroding metal frames at the top and mid-height. A stainless steel angle plate was welded long the top edges of the chamber to form a 25 mm wide flange which facilitated a close fitting

coupling between the chamber and a removable lid. The lid was a square piece of 650 x 650 x 20 mm thick "Perspex" plate.

The Wetting/Drying chamber was evacuated using a 0.75 HP (0.563kW) pump through a 15 mm diameter opening at 540 mm height on one face of the chamber. The system was connected to the vacuum pump by a 15 mm diameter rubber tubing. To protect the vacuum pump from damage from the exhaust moisture, the exhaust air was passed through a dessicator containing one kilogramme of silica gel crystals to dehydrate the exhaust air.

The water supply for the Wetting/Drying facility, which was integrated with the supply to the hot/cold system, consisted of a 0.5 HP (0.373 kW) centrifugal pump through a 15 mm copper inlet pipe connection to the chamber. As a means of regulating the temperature of water flowing into the chamber a section of approximately 2.5 metres of the inlet pipe was formed into a coil that passed through an urn filled with water at controlled temperature of approximately 60^{o}C.

The water supply pipe-work was connected to one side of the chamber at a height of approximately 480 mm through a 15 mm copper pipe and was extended inside the chamber to transverse the width. Inside the chamber, the lower surface of the pipe had 1 mm diameter perforations at 25 mm spacing that extended over a 0.5 m length. The perforated copper pipe was extended downwards, then bent horizontally into an "m" shaped pipe-work system of a total length of approximately 6 m at the middle of the chamber. The pipe was supported horizontally on the non-corrosive metal frame. The pipe-work system of the semi-automated Wetting/Drying facility is illustrated schematically in Fig.4.18. During the wetting cycle, the inside temperature of the chamber was approximately 35^{o}C while the relative humidity was at a maximum value of approximately 99 percent.

In order to control the environmental temperature inside the chamber an Incoloy heating element was taped on the non-perforated section of the copper piping. The element was powered from the mains supply and maintained the average temperature of 39^{o}C during the drying period. To prevent

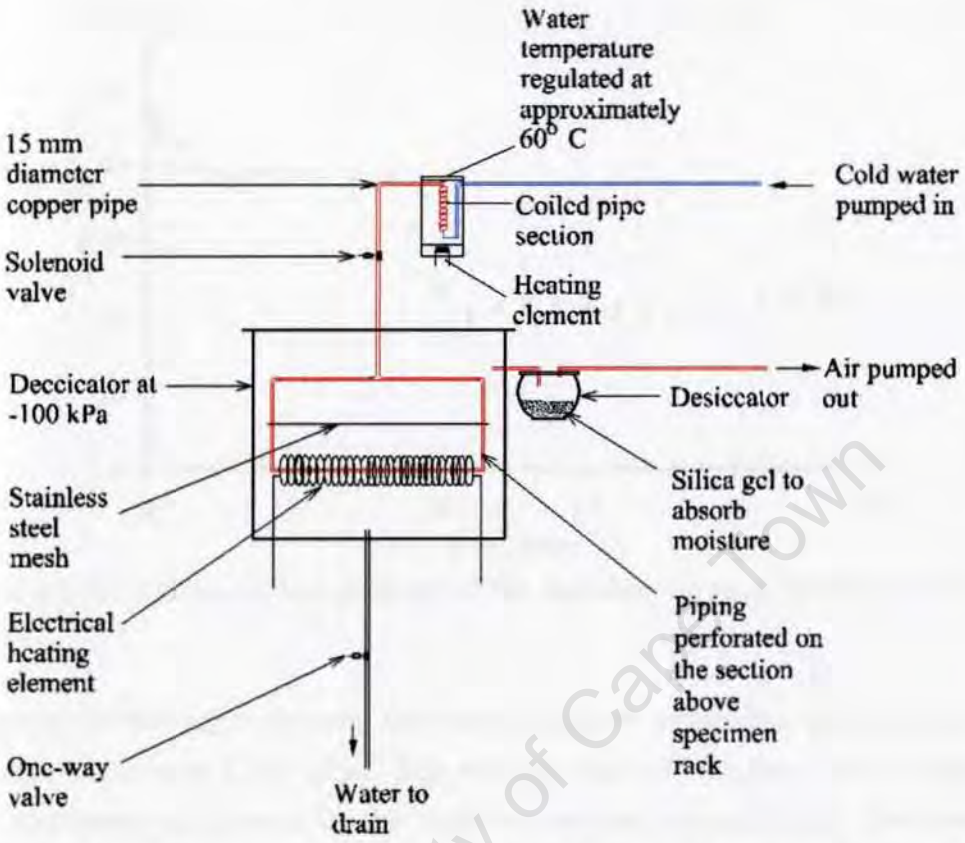

Figure 4.18: Schematic of semi-automated Wetting/Drying environmental chamber

localized drying on the specimens, a stainless steel rack was positioned at approximately 40 mm above the heating element to support the specimens. Excess water was drained out of the chamber through a 20 mm diameter non-return valve at the bottom of the chamber as illustrated in Fig. 4.18. All pipe connections were made airtight by customized washers.

Wetting of the samples was carried out by spraying pre-heated water for 30 minutes with the chamber open. The system was left open and allowed to drain freely for one hour after which the humidity reduced from the saturated condition to approximately 65 ± 2^{o}C percent. The chamber was thereafter sealed by use of mechanical clamps.

A vacuum was drawn in the chamber, and the pressure level was measured on a dial gauge attachment to the top of the dessicator. Within 20

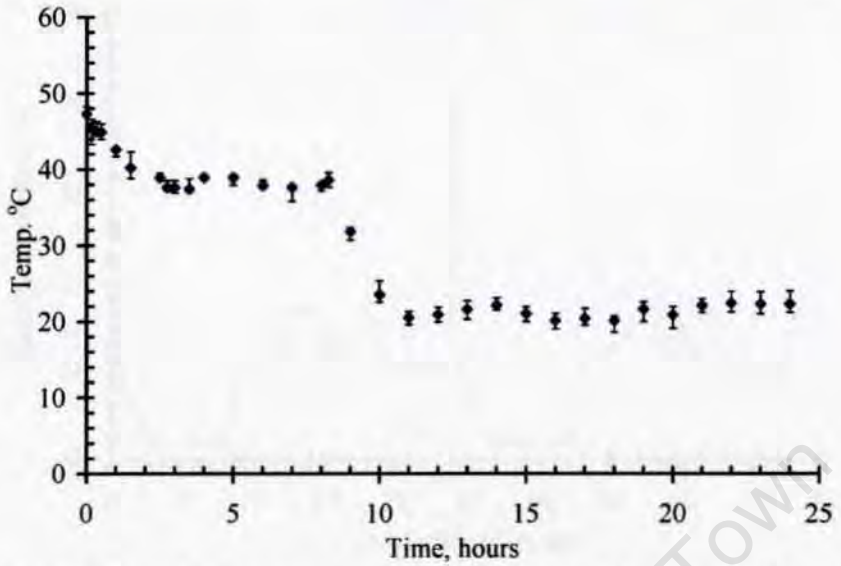

Figure 4.19: The inside temperature of the chamber during a Wetting/Drying cycle

minutes of drawing a vacuum, the inside pressure reduced to approximately 10 mm of mercury (-100 kPa). The vacuum was held for five hours to allow the specimens to dry and for the moisture content to equilibrate. The inside temperature and Relative Humidity (RH) of the chamber were monitored during the wetting and drying cycles. Figs. 4.19 and 4.20 show the average temperature and RH respectively during a typical Wetting/Drying cycle. Drying of specimens was assessed on ten specimens firstly over a three hour period, and subsequently after five hours of vacuum drying. Table 4.7 shows the drying characteristics of the Wetting/Drying weathering facility.

Table 4.7 together-with the 24 hour drying characteristic curves shown in Fig.4.21 show that one Wetting/Drying cycle in the semi-automated facility took approximately 5 hours to get to a constant mass. This was lower than air drying time of approximately 17 hours (obtained from preliminary trials) for comparable range of moisture loss.

In addition to exposing fibres to a Wetting/Drying environment, samples were exposed to a continuous wetting environment in water with pH of 7 and temperature of 22± 1°C for three months. The fibres are referred to here as

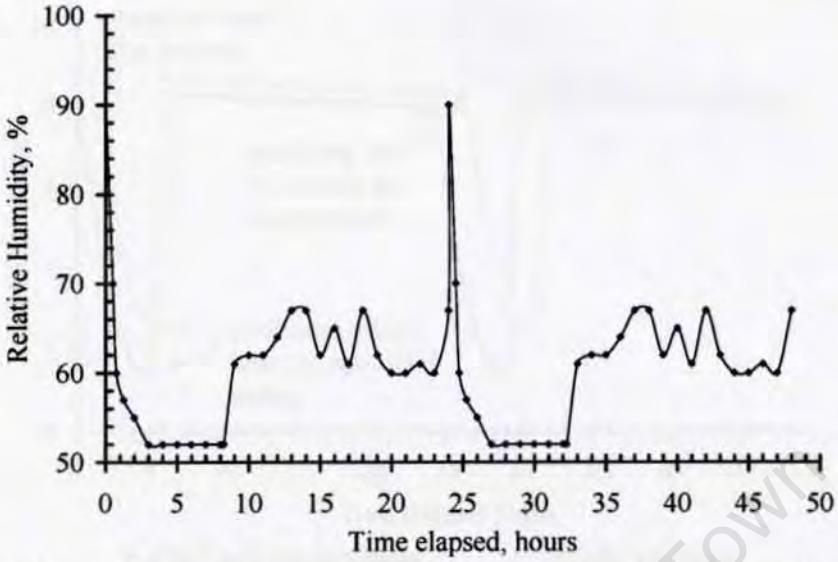

Figure 4.20: Relative humidity inside the chamber during two Wetting/Drying cycles

"soaked" samples.

Table 4.7: Drying characteristics of the weathering facility

Specimen	% Moisture content of semi-saturated specimen	% Moisture content (MC) of matrix after drying specimen for:					
		% MC after 3 hours	5 hours				Average loss after 5 hours (%)
			test 1		test 2		
			% MC	% Loss	% MC	% Loss	
1	8.13	4.74	2.59	68	2.61	68	68
2	8.91	5.51	2.14	76	3.41	62	69
3	8.55	4.37	2.40	72	2.48	71	72
4	8.82	4.74	2.31	74	3.40	61	68
5	9.04	2.67	2.49	72	2.25	75	73
6	7.07	2.28	1.90	73	2.22	69	71
7	7.56	2.60	2.42	68	1.73	77	73
8	8.41	1.34	1.52	82	0.74	91	87
9	8.60	2.74	0.25	97	0.75	91	94
10	8.77	1.67	1.20	86	0.31	96	77

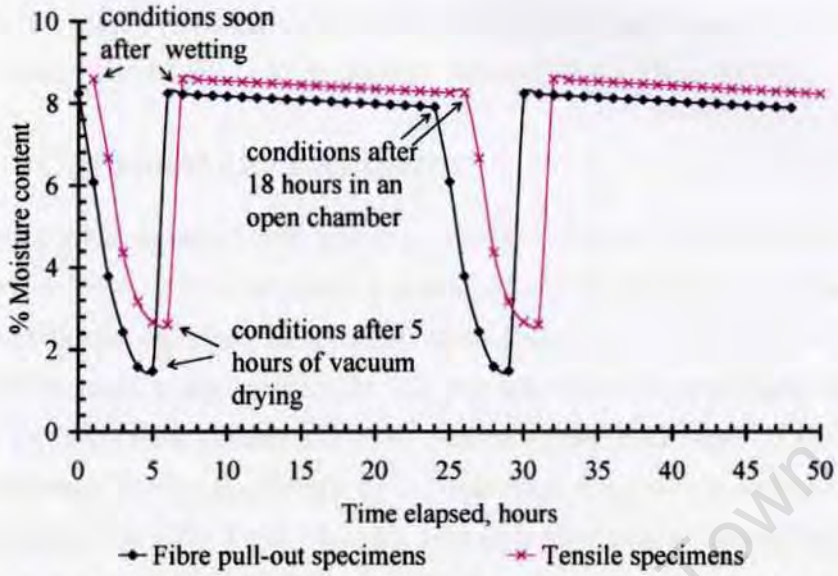

Figure 4.21: Specimen moisture content during two Wetting/Drying cycles

Fig. 4.21 provides a graphical representation of a mass based typical Wetting/Drying cycle over a 24 hour period. Specimens were exposed to 100 Wetting/Drying cycles over a 115 days period.

As the weathering process progressed, specimens were taken from time to time and examined first visually, and also under an optical microscope for any damage likely to be induced by weathering. However, there were no visible signs of weathering on the specimen surfaces at the end of 100 Wetting/Drying cycles. After weathering, the specimens were sealed and kept under laboratory environment of approximately 20±3°C and relative humidity of 53±2 percent until required for mechanical testing.

4.5.3 Exposure to Natural Environments

After 28 days of water curing, ten samples were taken for weathering in a moderate climate (NM) in Cape Town, South Africa, and ten were exposed to a tropical climate (NT) in Nairobi, Kenya. This was necessary in order to get comparative data for the naturally exposed samples, despite the exposure period being limited to a maximum period of 16 months. The average annual temperatures and Relative Humidity of the two natural climates are shown

in Table 4.8 for South African Weather Service and the Kenya Meteorological Department (World Wide Web 2006*a*), (World Wide Web 2006*b*).

4.5.4 Carbonation Exposure

Accelerating the aging of cementitious composites in a carbon dioxide (CO_2) rich environment simulates natural ageing as shown in studies on durability of cement-based cellulose fibre composites (Kim et al. 1999). The natural carbonation level is approximately 0.2 percent which is considered not high enough to cause a significant effect to cement-based materials. Therefore, to effectively weather the specimens by carbonation, the process was accelerated by increasing the CO_2 level. In this research this was achieved by using a commercially available LEEC model of research incubator, which was set for automatic CO_2 and temperature control.

The CO_2 system in the chamber was factory calibrated and the "Zero" or "Baseline" set for high humidity incubation at 30°C. Initially, the CO_2 concentration was controlled to a pre-set level of 1 percent and carbonation depth in a sacrificial specimen monitored over a three month period as described later in section 4.5.4.1. However, CO_2 level of 1 percent was not effective in carbonating the samples. Therefore the level was increased to 10 percent for the subsequent six month period.

The optimum carbonation rate in cementitious materials occurs at RH of between 50 and 70 percent (Papadakis, Vayenas & Fardis 1991). Therefore, the humidity inside the chamber was monitored from time to time and was manually controlled by using distilled water to increase the RH, or placing silica gel crystals inside the chamber to desiccate the environment in the chamber to the required level. An average RH of 65 percent was measured during the ageing period. The specimens were loosely arranged on a stainless steel rack inside the chamber, and the samples were continuously carbonated for six months. During this period, carbonation depth was periodically monitored. Figure 4.22 shows the carbonation chamber with samples arranged on racks and silica gel crystals at the bottom of the chamber.

Figure 4.22: Samples inside the carbonation chamber and silica gel crystals at the bottom of the chamber

4.5.4.1 Determination of Carbonation Depth

The conventional standard methods of determination of carbonation depth of cementitious materials rely on physical procedures such as: chemical analysis, X-ray diffraction techniques, infra-red spectroscopy, and thermo-gravimetric analysis. One of the problems associated with these physical procedures is that they are complex and the operator is faced with the need to acquire special skills. Therefore, in this research the phenolphthalein test, which is a much simpler method, was used to monitor the extent of carbonation penetration into the specimens. The phenolphthalein test is an indicator of the pH of the pore solution, the colour being pink above pH of 9.0 (Papadakis et al. 1991) and clear otherwise. The procedure involved treating a freshly broken specimen surface with a solution of phenolphthalein in dilute alcohol. The presence of free calcium hydroxide ($Ca(OH_2)$) was indicated by a deep pink colouration but in regions with at least 50 percent carbonation the indicator remained colourless (Chang 2005).

Using the phenolphthalein test, carbonation depth was monitored and after 6 months, a depth of approximately 10 mm was evident as illustrated

in a broken section of a mortar cube in Fig. 4.23(a). Since polypropylene does not carbonate at atmospheric pressure (Mills 1986), the pink colouration showing on the fibres after phenolphthalein test in Fig. 4.23(b) indicates contaminated of the fibres with cementitious particles before exposure. After six months in CO_2-rich environment, the particles had carbonated sufficiently. Fig. 4.24(a) illustrates typical treated surfaces of the composite before complete carbonation and Fig.4.24(b) shows that carbonation penetrated across the depth of the specimens after 6 months of ageing.

(a) Sacrificial cube (b) Fibres contaminated with cementitious particles

Figure 4.23: Determination of the extent of carbonation

(a) Partial carbonation (b) Full carbonation

Figure 4.24: Monitoring of carbonation depth in fibre pull-out specimens

In order to test the extent of carbonation in naturally weathered samples, remnants of samples weathered in a moderate climate (NM-weathered) and in a tropical climate (NT-weathered) fibre pull-out specimens were fractured and the carbonation depth determined as illustrated in Figs. 4.25 and 4.26.

In the two sets of samples, CO_2 had not penetrated the samples to the fibre/matrix interfacial zone.

Figure 4.25: Carbonation depth in NM-weathering specimen

After weathering, the specimens were carefully sealed to protect them from damage and then kept in the control room until mechanical testing. Before the test, specimens were visually inspected for signs of damage in the form of cracks, which were quantified in a procedure described later in section 4.7.

As has been illustrated from the foregoing, the ageing regimes varied from one environmental condition to the other. Therefore, the age at which the specimens were tested varied according to the exposure regime. From the carbonation depths, the rate in a moderate environment was found to be higher than in a tropical environment. An overview of the ageing regimes and testing procedure are dealt with in the next section.

Figure 4.26: Carbonation depth in NT-weathering specimens

Table 4.8: Mean environmental conditions of NM and NT environments

	Cape Town (NM)				Nairobi (NT)					
	Mean temperature, °C				Mean temperature, °C			Mean RH, %		Sunshine, average hours
Month	Highest	Daily Maximum	Average Minimum	Lowest	Maximum	Minimum	Average	9.00 AM	3.00 PM	per day
January	39	26	16	7	26.8	13.1	13.7	79	45	8.9
February	38	27	16	6	28.0	13.4	14.6	74	37	9.5
March	41	25	14	5	27.4	14.4	13.0	82	43	8.7
April	39	23	12	2	24.6	14.3	10.3	86	53	7.0
May	34	20	9	1	24.1	14.2	9.9	85	55	5.7
June	30	18	8	-1	23.1	12.6	10.5	85	59	5.8
July	29	18	7	-1	22.3	11.5	10.8	83	53	4.4
August	32	18	8	0	22.7	11.8	10.9	85	53	4.2
September	33	19	9	0	25.3	12.2	13.1	82	50	5.9
October	37	21	11	1	26.2	13.7	12.5	80	47	7.0
November	40	24	13	4	23.6	14.4	9.2	36	57	7.0
December	35	25	15	6	25.1	13.6	11.6	83	5	7.9
Yearly average	41	22	11	-1	24.9	13.3	11.6	78	46	6.8

Early age tests on specimens water-cured for three, seven and 28 days were undertaken within approximately 15 minutes of removal from the curing water bath. These specimens were therefore tested wet. However, after water curing for 28 days, specimens to be tested at later ages were removed from the water bath and conditioned in a dry state under laboratory conditions in which the temperature and RH were 20±3°C and 53±2% respectively. The samples were kept under these controlled conditions for the periods specified in Fig. 5.3 prior to testing. These specimens were therefore effectively tested "dry".

4.6 Mechanical Testing

The ageing and testing programme for the samples studied in this research is outlined in Table 4.9.

Table 4.9: Specimen ageing regimes

Weathering condition	Exposure period	Age at time of test, months		
		Cubes	Fibre pull-out samples	Composite
100 hot/cold cycles	2 weeks	8	5	11
100 Wetting/Drying cycles	3 months	10	8	14
Carbonation	6 months	12	12	16
Moderate	11 months	12	12	12
Temperate	11 months	20	12	12
Temperate	9 months	N/A	16	N/A

4.6.1 Fibre Pullout Testing Procedure

The fibre pullout test rig was designed to be adaptable to the standard fixtures of 100 kN capacity ZWICK Universal Testing Machine (UTM) but with special 10 kN load cells. The boundary conditions of the frame were a fixed lower section and a self-centering fixture which was connected to the load cell but the actual grip connection to the specimen was facilitated through

paired connections with pins in order to minimise any bending component, which would shift the neutral axis of the sample from the middle during the test, leading to erroneous results. The main features of the rig were two "C" shaped aluminium grips, each weighing approximately 465 grammes. The fibre pull-out test rig is schematically shown in Fig. 4.27.

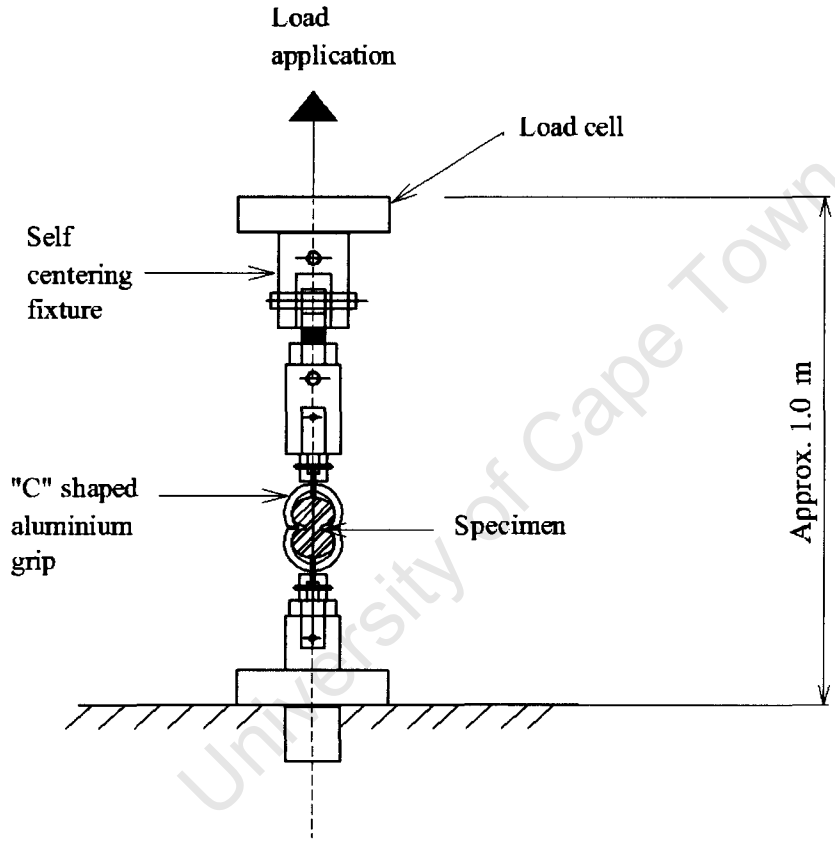

Figure 4.27: Schematic of fibre pull-out test rig

The specimen was centrally mounted between the two grips and aligned in the rig as shown in Fig. 4.28. Preliminary trials were carried out to determine the critical embedded fibre length (l_e) that would cause failure by pull-out as opposed to breaking. A length of 22 mm into each side of the sample was found satisfactory. The preliminary tests also served as a check to the performance of the aluminium grips. The tests were carried out on specimens cured for different time periods as shown by representative

Figure 4.28: Fibre pull-out specimen before test

load-displacement curves in Fig. 4.29. .

During the test, there were no stress concentration problems since there were no visible signs of damage on the specimens surfaces in contact with the grips, nor slippage of the grips, showing that the "figure eight" geometry was suitable for fibre pull-out specimens. Therefore, this specimen geometry was adopted for fibre pull-out testing.

The specimens were quite brittle and were therefore handled carefully before mounting the specimens onto the test frame. The specimens were given a slight twist to ensure that only the fibre was to be tested at the crack planes and not the tensile strength of the matrix. The UTM was then programmed for a ramp rate of 10 mm per minute, a maximum load of 80 percent of the load cell capacity, and to capture the entire fibre pull-out behaviour, the maximum displacement was set at 25 mm. The pre-load was set at 0.4 N, the weight of half the specimen and the top grip that would still be connected to the load cell after the fibre had completely pulled out of the specimen.

Fibre pull-out behaviour was characterized by one-sided fibre pull-out. The load-displacement traces were readily captured and saved in a spread

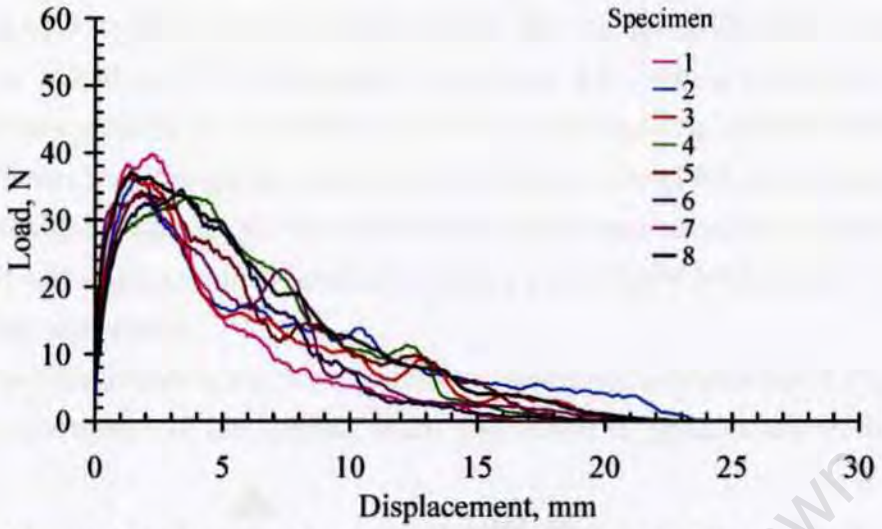

Figure 4.29: Typical load-displacement traces for fibre pull-out

sheet. All control specimens were tested dry (as conditioned under controlled laboratory environment with a relative humidity of approximately 51 percent) for periods between 5 weeks and 16 months.

4.6.2 Composite Tensile Testing Procedure

For most engineering materials, uniaxial tensile testing (UTT) offers one of the most straightforward tools for mechanical characterisation and the testing procedures for different materials have been standardised. However, the direct tensile test for cementitious materials has been given little attention in the literature, despite being of considerable theoretical and practical value. This is because tensile testing is one of the most problematic mechanical tests for cementitious materials and in particular for thin specimens. Moreover, it is generally regarded as too demanding with respect to laboratory equipment sophistication and staff expertise. However, direct tensile tests as opposed to bending provide more direct information about the mechanics of load transmission at the micro-level, and the damage induced on the material during loading.

Among the key conditions in Uniaxial Tensile Testing (UTT) of cement-based composites is that the testing machine should be sufficiently stiff, and

should have a close-looped control system. By using the ZWICK Universal Testing Machine (UTM) described in section 4.6.1, these conditions were sufficiently addressed. In addition, the test train and grip system needed to be sufficiently self aligning and free of bending, so use of rotational and fixed ends at the boundaries above and below the specimen respectively (and both pinned self aligning units) facilitated such a pure tensile loading (free of any bending component).

The tensile testing rig, with a mounted specimen is illustrated in Fig.4.30. The performance of the loading train was tested in preliminary trials on a

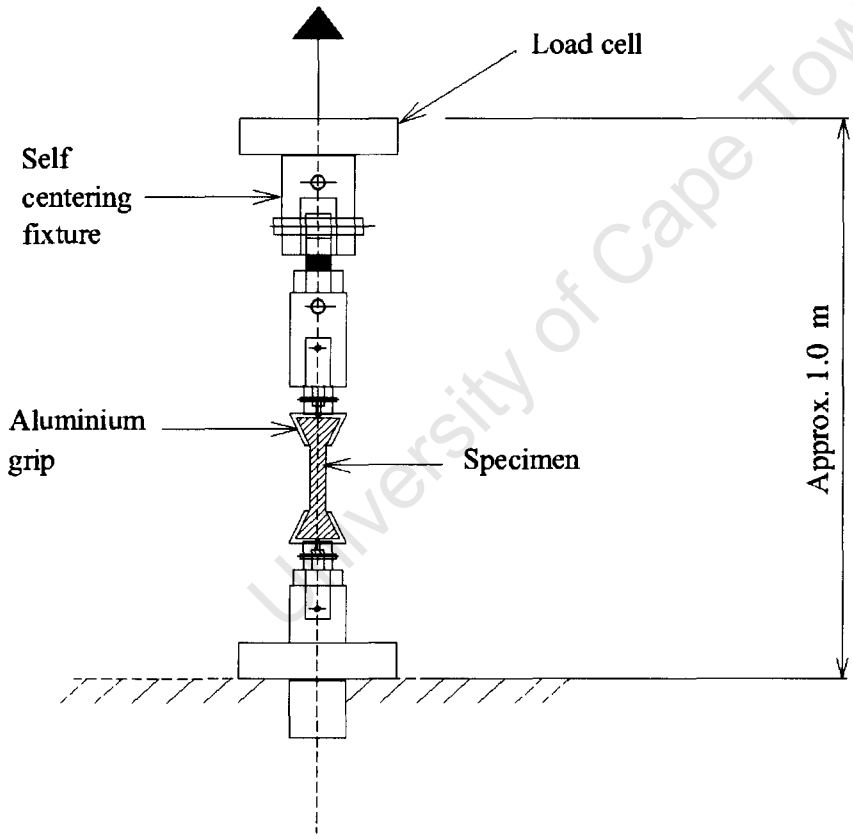

Figure 4.30: Schematic of tensile test rig

14 day old specimen. Loads were measured using a 10 kN load cell with an accuracy of 0.5 percent and the crosshead travel was used to measure displacements. The specimen was loaded in tension at the rate of 10 mm

per minute under displacement control of the crosshead separation. Up to loads of approximately 1950 N, there were no visible signs of cracking in the widened gripping areas and cracking ONLY occurred in the gauge areas.

Displacements were measured using the crosshead travel of the UTM. The load-displacement (P-δ) plots were readily captured on an interfaced computer output device and results automatically saved. Fig.4.31 shows typical traces for one year old samples.

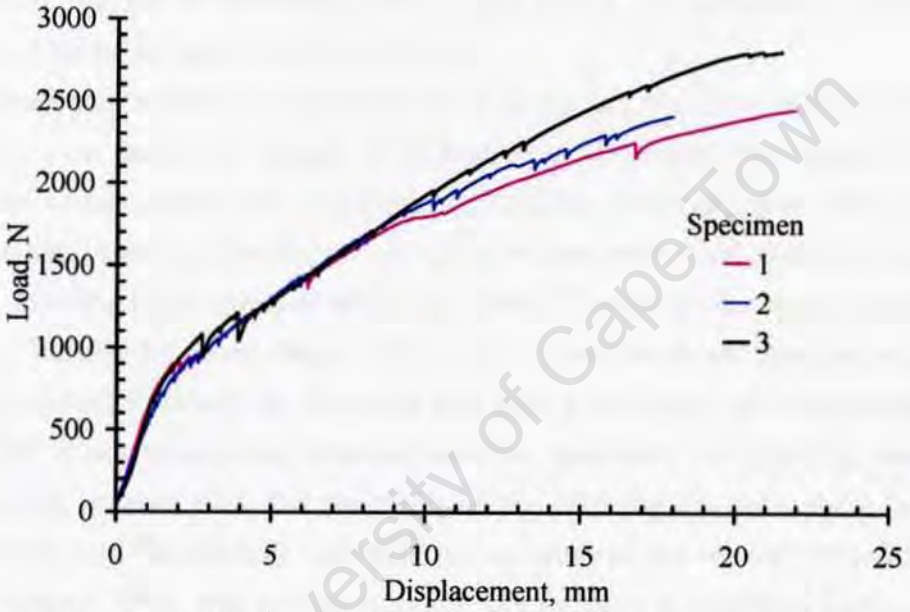

Figure 4.31: Load-displacement behaviour of 1 year old control specimens

To be able to present the load-displacement data in stress-strain format and hence estimate the modulus of elasticity, E_m of the matrix, an extensometer with a maximum gauge length of 40 mm and travel of 20 mm was employed for extension measurements.

4.6.2.1 Specimen Adaptation for Tensile Testing

Tensile testing was preceded by several trial runs on different TC samples in short as well as long formats. The trial tests indicated that when the loads were in the vicinity of 1950 N the gauge areas of the specimens were extensively microcracked (permeated by several fine cracks) . As loading in-

creased beyond 1950 N, multiple cracking (several macro cracks) propagated into the widened gripping areas, which caused the embedded fibres to pull out of the matrix, causing serious alignment problems in some specimens. As the test progressed, these effects lead to crushing of the gripping areas of the specimens. The test could therefore not be progressed to failure. To contain the crack propagation within the gauge areas and hence overcome the gripping difficulties, the widened gripping sections of the specimens were modified in order to withstand the crushing forces. In the process, testing of the specimens to failure was facilitated.

Specimen modification involved firstly stripping of mortar within the grip regions to a maximum length of 50 mm from the edges thus exposing the textiles at the same time avoiding pre-cracking the specimens. By use of the original casting moulds, the gripping regions were then re-cast in epoxy resin ensuring full impregnation of the fibres. The specimens were thereafter left to harden for three days. The edges of the hardened specimens were sand-papered to closely fit the grips and were then ready for tensile testing.

The epoxy-remoulding process used for specimen modification was an aggressive process with the potential of pre-cracking the inherently brittle specimens and thus reduce the expected accuracy of the tensile tests. Therefore, diligent effort was put to minimise the damage to practical levels after which representative samples were tested to failure.

The testing machine was programmed for a ramp rate of 10 mm per minute. In order to capture the whole range of the stress-strain curve, failure recognition was set at 100 percent drop from the maximum load. The gauge length of the extensometer was adjusted to 25 mm for the short specimens and increased to 40 mm for the longer ones.

The extensometer essentially comprised two clip-gauges that made physical knife-edge contact with the specimen in an attempt to avoid problems associated with the machine compliance. Fig. 4.32 shows the clip-gauges of the extensometer and a sample in place, and Fig. 4.33 shows the load-displacement behaviour for long specimens at low strain levels before the

gauge areas were modified. Extensions in Fig. 4.33 were measured using the extensometer. By modifying the gripping areas, a strong fibre/epoxy-matrix

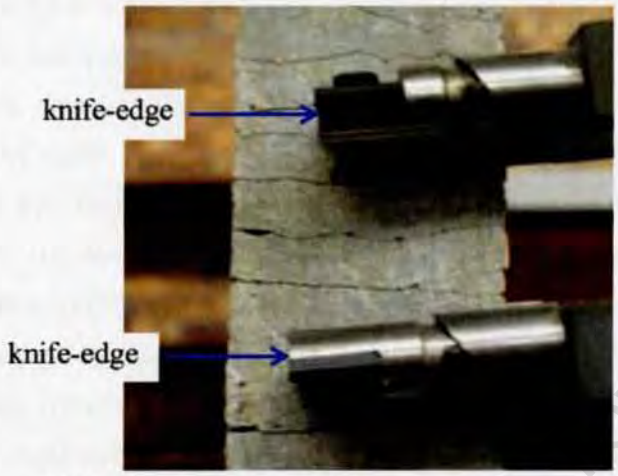

Figure 4.32: Extensometer clip-gauges on a specimen

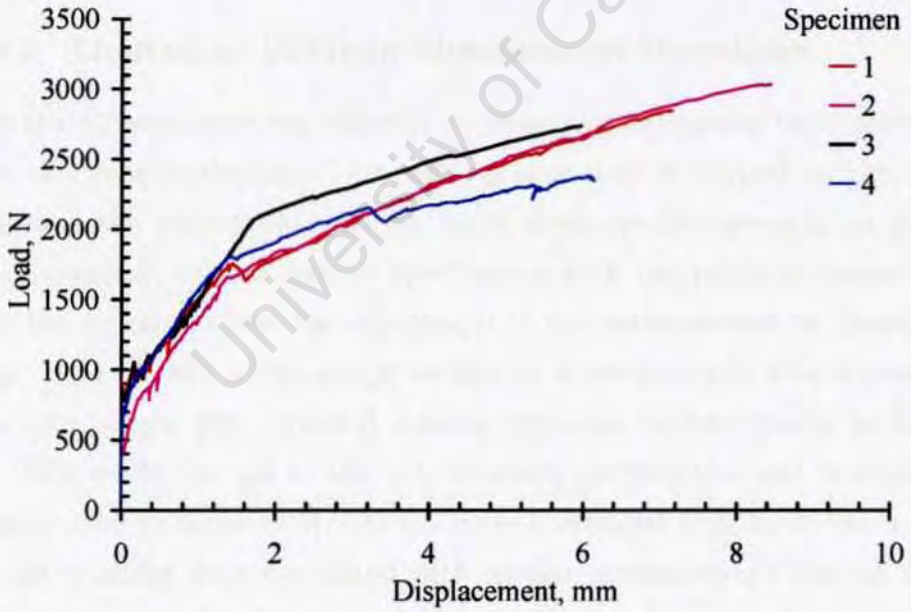

Figure 4.33: Load-displacement of tensile specimens measured using an extensometer (before modifications on specimens' gripping edges)

bond was developed thus eliminating fibre pull-out effects during the test. In addition, the associated gripping difficulties were substantially reduced.

The load-displacement curves were characterised by an initial linear part as the specimens underwent micro-cracking. This state progressed until development of macro-cracks, which was marked by a reduction in the slopes of the curves. As loading progressed, further reduction in the slopes and perturbations of the stress-strain curves were observed. This occurred at loads in the vicinity of 1000 N (stresses between 3 MPa and 5 MPa) as shown in Fig. 4.33. A key feature of the load-displacement (σ-ϵ) curves, which is characteristic to the so-called High Performance Fibre Reinforced Cementitious Composites (HPFRCCC) was a characteristic strain hardening and multiple cracking (propagation of several cracks), which lead to the achievement of very high strains in excess of 20 percent. The specimen modification technique of strengthening the gripping areas was therefore adopted and all specimens were modified accordingly. It was then possible to capture the whole range of the σ-ϵ behaviour up to fibre rupture at failure.

4.6.2.2 Limitations in Strain Measurement Techniques

While the extensometer was effective in measuring extensions up to the early stages of strain hardening, the rough surfaces that developed on the specimens, and the subsequent opening up of these cracks especially as failure was approached, caused serious interference with the physical contact between the specimens and the clip-gauges of the extensometer as illustrated in Fig. 4.34. When a clip-gauge wedges in a macro-crack, free movement of the clip gauges gets impeded making extension measurements problematic. This made the use of the extensometer problematic and therefore it was only used to measure strains on three specimens from each batch, and then the readings were correlated with similar measurements also on three samples using the cross-head travel of the testing machine. Due to equipment constraints, these measurements were taken on two independent test runs.

For all the tests, the machine was set for a pre-load of 40 N which effectively took up the slack due to machine compliance particularly during the initial stages of the test. Due to equipment constraints, it was not possible to

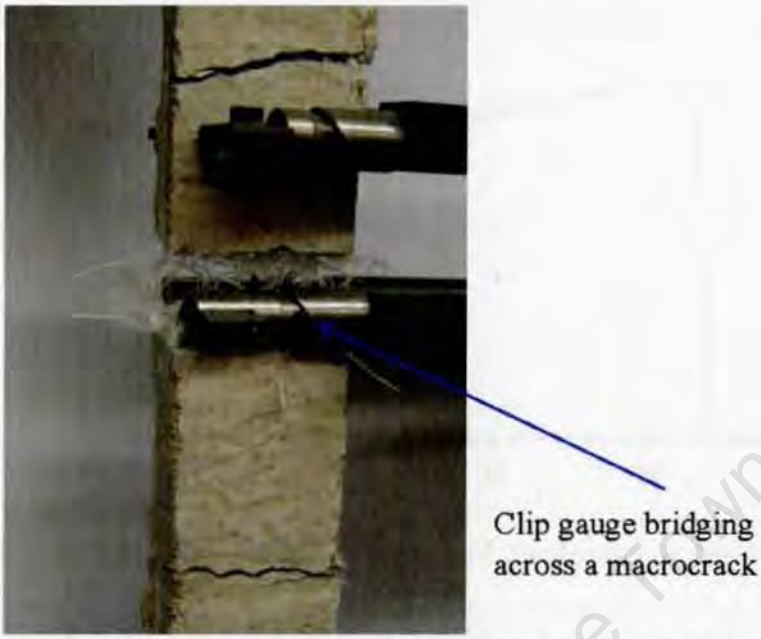

Figure 4.34: Problem encountered with the use of extensometer

evaluate the correlation between the two displacement measuring techniques on the same specimens simultaneously, therefore the average of three samples was taken for each method.

By using an extensometer, any microcracking that occurred outside the contact points of the clip-gauges was not recorded as opposed to the crosshead which picked displacement over entire gauge sections of the specimens. Therefore for the same stress level and before macrocracking, a higher displacement was recorded using the cross-head than the extensometer. However, after the specimens had sufficiently cracked, the discrepancy between the two displacement methods was not significant and this is illustrated in Fig. 4.35 (for samples aged for one year under controlled conditions).

The main discrepancy between the results obtained using the extensometer, and cross-head travel was during the initial elastic stage which was attributed to the much shorter gauge length that was measured using the extensometer, in comparison with a much longer length measured by the cross-head travel of the machine. Nevertheless, this discrepancy was within practical limits considering that the main aim of tensile testing was to capture

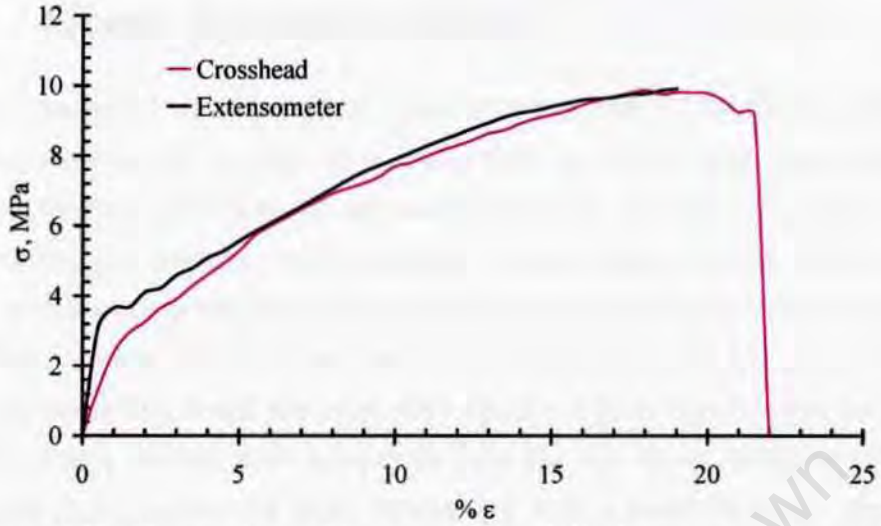

Figure 4.35: Comparison of two methods of displacement measurement

the entire strain-hardening and multiple cracking behaviour of the specimens as well as the final failure modes. In addition, the toughness of the material could only be assessed precisely using the entire stress-strain curve of the specimen from the unloaded stage to complete failure. However, these characteristics were masked when the extensometer was employed, which justified the use of cross-head travel of the UTM as a viable displacement measurement method.

In order to compare the tensile behaviour of laboratory-produced Textile Concrete (TC) samples with applications in the South African Industry, specimens were prepared from a disused TC board for tensile testing. However, unlike the laboratory-produced specimens, the Industrial specimens were four-layered CemForce laminates as opposed to six-layered laboratory-produced specimens. The board had undergone natural weathering for 24 months, thus providing an additional natural exposure regime to the moderate and tropical environments. Rectangular specimens of size 100 x 25 x 6 mm were cut from the board and the ends were cast in epoxy to form gripping areas similar to the laboratory-produced samples. The Industry specimens were appropriately labeled and subsequently tested in tension to failure.

4.7 Crack Quantification

The mechanical behaviour of the specimens was defined by the cracking behaviour after tensile testing. The cracks that developed after tensile loading were quantified according to age and weathering history. For each batch of samples, the average crack spacing, average crack density and average crack width were measured on five representative specimens. The crack density was a measure of the amount of cracking within the gauge sections of the specimens and crack spacings were obtained from direct linear measurements. Crack widths were measured with the aid of an attached (Vickers hardness type) scale on a light microscope with a resolution of 1 μm. For each specimen, crack widths were measured at five locations that were chosen at random over the gauge sections of representative samples.

4.8 Scanning Electron Microscopy:Overview

Microstructural studies involved firstly observing the specimens at 50 times magnification in order to have a general view of the microstructure, and subsequently progressively increasing the magnification up to a maximum of 200 times to get detailed features of the fibre/matrix interface. Fine fibrils of diameters ranging from approximately 15 to 20 μm were visible.

Due to the inhomogeneous nature of the internal structure of the textile material that consisted of fibrils spun over a fibrillated tape, an accurate description of the mechanical behaviour observed at the macro level was a non-trivial task. One way that the load-carrying capacity and the failure process of the so-called "Textile Reinforced Concrete" (TRC) has been addressed in the past is by conducting investigations at the micro-, meso- and macro-levels (Hegger, Sherif, Brukermann & Konrad 2004).

The macro-level investigations are comprised of mechanical testing while at the micro-level, investigations cover the factors that influence the interaction of single fibrils with the cementitious matrix. This multi-level approach is adopted in this thesis in an effort to gain an understanding as to why Tex-

tile Concrete (TC) responds to loading in the manner observed during the experiments. Towards this end, microscopic studies were undertaken, firstly on individual fibres, and then on the fracture surfaces of the composite.

The nature of the interface between a fibrillated polypropylene fibre and hardened cementitious matrix has in the past been observed in optical and scanning electron microscopes in which the fibre/matrix interaction at the micro level was found to be characterised by interfacial adhesion and mechanical anchoring effects (Bentur et al. 1989). The mechanical anchoring of the fibres to the matrix that was also observed on aged composite was attributed to a combination of mechanisms at the microstructural level involving interlocking of the fibres with the matrix. An increase in the interfacial bond that is associated with ageing was accredited to increase in hydration products of cement that progressively become attached to the fibres (Banholzer et al. 2005).

In studies carried out by Banholzer (Banholzer et al. 2005), microstructural changes in FRCC, which were associated with ageing, were attributed to an increase in adhesional and frictional interfacial bond strength, interface stiffness and toughness. In TC that is under this research study, the interaction of a two-dimensional textile mesh that is cast in a cementitious matrix is expected to further enhance the fibre/matrix bonding properties due to additional mechanical anchoring caused by the extended fibrous area of the fine fibrils. The cross fibres (warp) did not have a fluffy outer layer and therefore the contribution to bonding of warp fibres was not considered to be significant. The role of the cross fibres was to hold the main fibres in position.

4.8.1 Scanning Electron Microscopy Technique

Microstructural studies involved firstly observing the specimens at 50 times magnification in order to have a general view of the microstructure, and then progressively increasing the magnification up to a maximum of 2000 times in order to get detailed features of the fibre/matrix interfacial microstructure.

Fine fibrils of diameters ranging from approximately 15 to 20 μm were visible, which was an indication of the extent of variability of the fibril diameter.

Fibres were selected at random from CemForce fabric and cut to sizes of approximately 10 mm suitable for studies in the SEM. The basis for a suitable TC sample for microscopic studies was that the state of the fibre/matrix surface remained undisturbed in order to be a good representation of the effects of ageing and weathering. The surfaces of the composite samples were not sufficiently conductive and charging of the surfaces occurred within the SEM. The accumulation of surface charges on specimens in the SEM appeared as a bright surface and also caused image distortion. It was therefore not possible to carry out meaningful studies with samples of the tensile composites due to the charging problems, hence fibre pull-out specimens were chosen for studies on the composite.

4.8.1.1 Specimen Preparation

The specimens were firstly notched on one of their surfaces in the direction of fibre orientation as illustrated in Fig. 4.36, and then fractured by application of a nominal bending force. This technique was employed in order to expose the fibre/matrix interface, with the fibres still intact and bonded to the matrix, at the same time minimising damage to the surface under investigation. Samples were then reduced, by sawing off the edges which were not under investigation (but not the fibre/matrix interface), to practical sizes of approximately 10 x 5 x 5 mm in order to fit into the specimen chamber of the SEM.

Soon after fracturing the surfaces, the specimens were glued onto mounting stubs using carbon/glue mixture in order to provide a conductive medium and thus reduce the charging problem. The surfaces were thereafter sputter coated with a thin layer of palladium gold to facilitate electron imaging which was carried out in high vacuum conditions (of 10^{-7} millimetre of mercury) of the SEM. The specimens were mounted in a chamber which could hold up to eight specimens at a time.

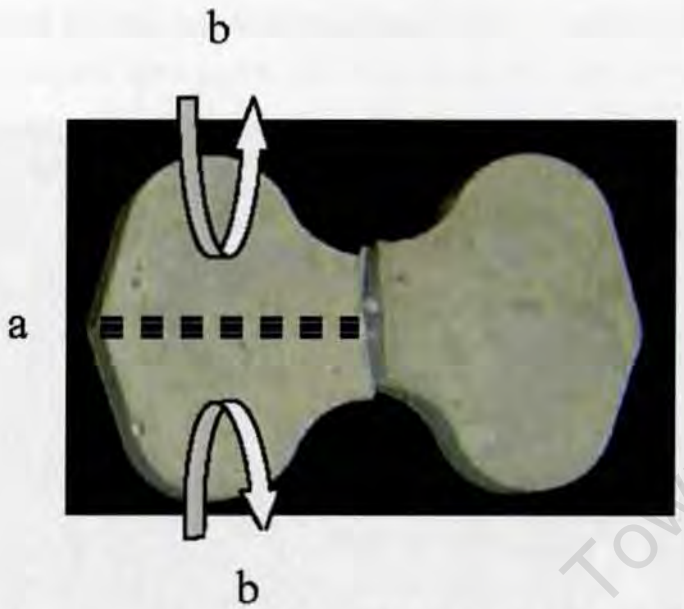

Figure 4.36: Sample preparation for SEM illustrating (a) position of notch on top surface and (b) direction of bending force application

4.8.1.2 Imaging of the Specimens

In the SEM, an incident beam of electrons from a tungsten source was focussed and scanned over the specimens. The electron gun operated over an accelerating voltage of 20.00 keV and the specimen was maintained at earth potential. From electron signals that were detected from emission of secondary electrons, topographic images of the specimen surfaces were obtained. By varying the magnification between 50 and 2000 times, images of control and weathered samples were obtained. Micrographs of representative samples and the interpretation of these images in relation to mechanical behaviour are discussed more fully in Chapter 6.

4.8.2 Microstructure of the Fibre

Fig. 4.37 shows a typical SEM image of fibre samples magnified 50 times. The fluffy fibrils spun round the main core forming a uniform outer sheath are clearly visible. This feature distinguishes this type of polypropylene yarn from conventional fibrillated PP fibres. The outer fluffy layer, which is spe-

cially formulated for cementitious matrices, forms an extended surface for the matrix to interact with and bond. A close-up of a fibre further illustrat-

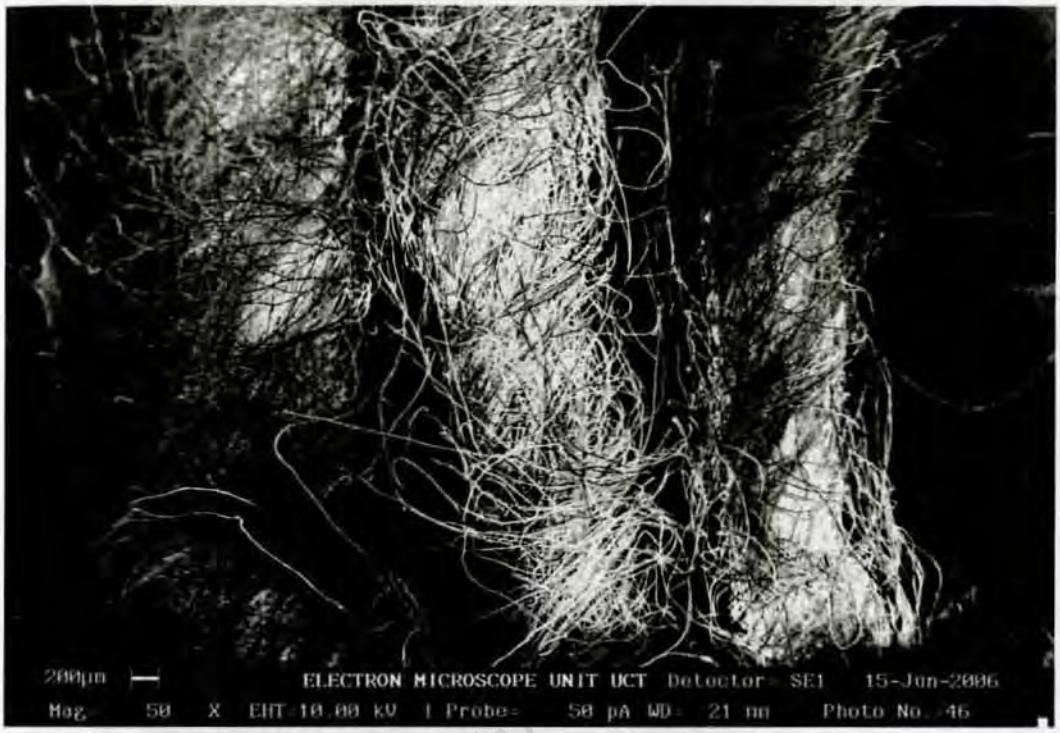

Figure 4.37: 50 X magnification of SEM of three fibre specimens

ing the role of the fine fibrils in the bonding action is shown in Fig. 4.38. In this image, which was taken on a fibre still embedded inside the matrix, exemplifies the interaction between fine matrix particles and the fibrils. Fig. 4.38 illustrates that mortar particles were still strongly bonded to the fine fibrils after the specimen was fractured.

4.8.3 Microstructure of the Composite

The microstructural studies were of necessity carried out on specimens with the fibre still firmly embedded in the matrix as illustrated by Fig. 4.38. Therefore, actual debonding and damage on the fibre/matrix interfacial zone due to fibre pull-out were not quantifiable from the micrographs. However, there was evidence of mortar densification and good bonding particularly as the specimens aged.

Figure 4.38: 101 X magnification showing fibrils spun on the central core

The microstructure of the interface varied with ageing, from porous to fully dense, according to the weathering conditions. For specimens weathered under controlled laboratory conditions for 16 months, mechanical keying of the fine fibrils into the matrix was easily visible at magnifications of 600 times and above, indicating good bonding. In a number of specimens which were investigated, the fibre/matrix separation, or debonding at the interface, was clearly evident but the matrix at the interface still appeared relatively dense. In specimens weathered in a tropical climate for approximately 16 months, the interface consisted of fine whisker-like crystals forming an interpenetrating mat in the voids between partially hydrated cement grains. Micrographs

of representative samples were used for illustration.

Studies were undertaken on control and weathered samples at different ages. A typical fibre/matrix interface surface is shown in Fig. 4.39 shows a fractured surface with a fibre embedded in the matrix and Fig. 4.40 strong fibre/matrix bonding.

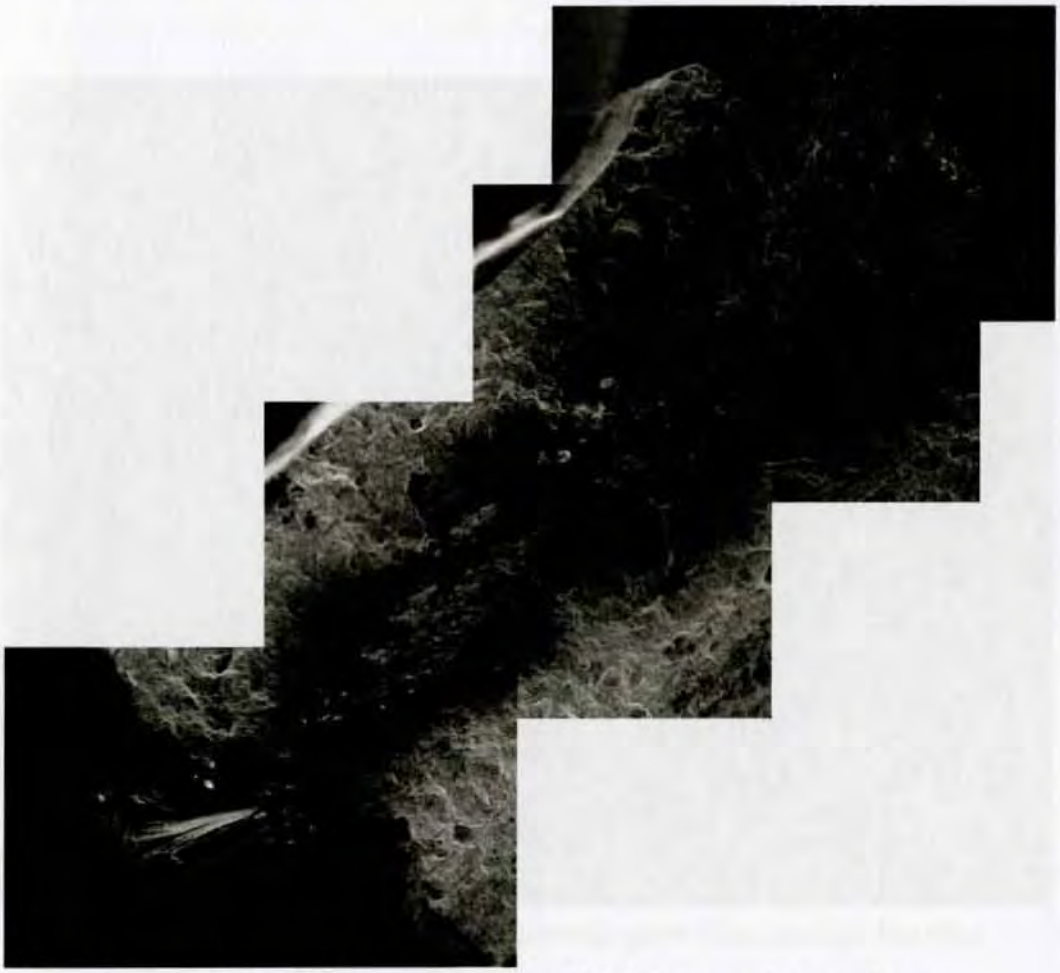

Figure 4.39: 52 X magnification of SEM composite specimen

Figure 4.40: 50 X magnification showing good fibre/matrix bonding

4.9 Summary

This Chapter essentially described the experimental programme and the methods used for characterisation of Textile Concrete, which included firstly the analysis of constituent materials, selection of materials and testing techniques within practical limits, that is, choice of the mix proportions, mortar flow characterisation, and cube crushing strength. Subsequently, the methods used for specimen preparation and production for mechanical testing were described.

The sample preparation process was described, which involved: casting techniques, curing conditions, and labeling system. In addition, the ageing conditions were described which were: controlled laboratory environment, accelerated ageing conditions, natural climates.

In this Chapter, a description of the experimental set-up was given involving the development of a semi-automated environmental system capable of simulating the different exposure conditions. The techniques employed in the design, fabrication and calibration of the dedicated accelerated ageing facility were elaborated.

The techniques used in mechanical testing to characterise the fibre/matrix interfacial property, and uni-axial tensile behaviour were dealt with. The investigations carried out on Textile Concrete samples after weathering and mechanical testing were described. These post-testing investigations were essentially crack quantification in terms of crack density, crack spacing and crack widths.

The limitations of the experimentation was underlined. In particular, the need for appropriate adaptations of the customised specimen gripping system to the fixtures of the locally available testing machine was reiterated in the Chapter. The difficulties associated with tensile testing pointed out and the way they were addressed was described.

The crack quantification technique was limited in scope in that it was not possible, using this method alone, to fully gain an understanding of the link between the mechanical properties of TC and the microstructure. Therefore,

the study was extended to microscopic examination of the specimen surfaces in a scanning electron microscope (SEM). The technique was described in this Chapter.

A schematic illustration of the programme showing the scope of work, the specimen types and ageing regimes is shown in Fig.4.41. The results of the mechanical tests and microstructural studies are dealt with in the next Chapter.

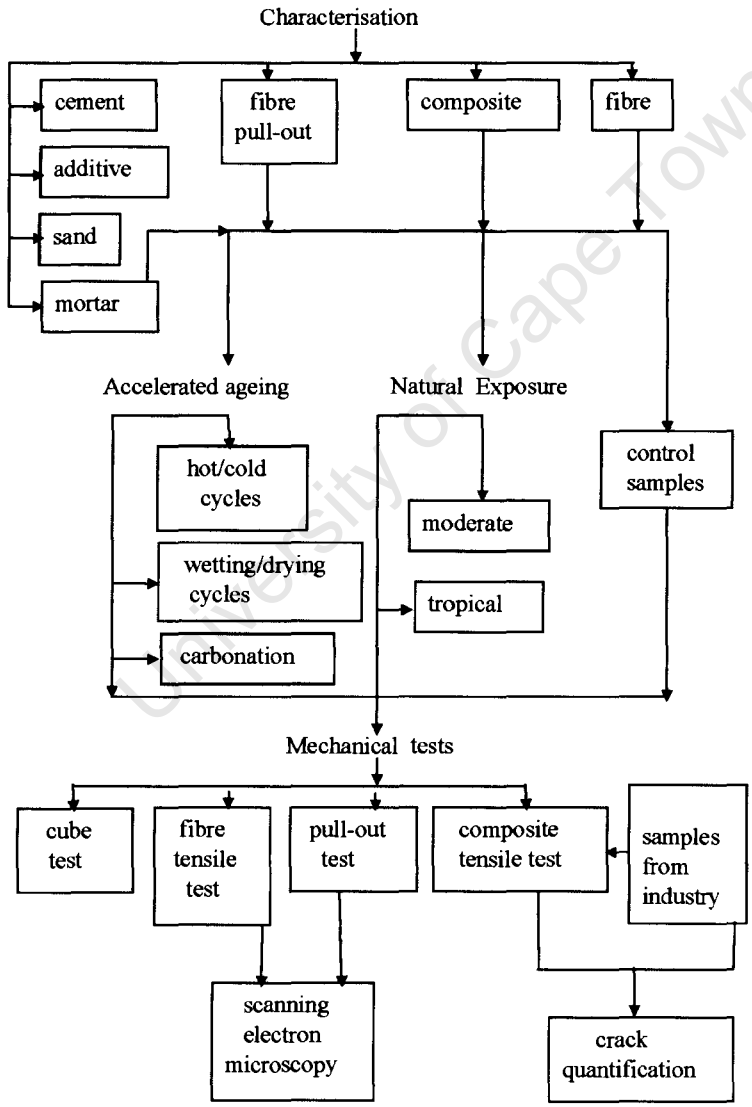

Figure 4.41: Experimental programme

Chapter 5

Analysis of Results of the Mechanical Tests

5.1 Introduction

In this Chapter, the results of the mechanical tests are discussed together-with uncertainties and errors in the physical and mechanical measurements. Results include cube crushing tests on plain mortar; tensile tests performed on single fibres; pull-out and tensile tests on the composite, all as a function of environmental exposure. The following are the objectives for each of the four major sets of tests discussed in this Chapter:

- Determination of density of the matrix and cube crushing strength of mortar specimens.
- From individual fibre tests, determination of the tensile strength and the stiffness of the fibres after exposure to different environments.
- Characterisation of the fibre pull-out behaviour and determination of the mechanisms at each of the following four stages on the curves: pre-peak stage, peak point, debonding stage, and final fibre pull-out stage.
- Evaluation of the interfacial bond and its variation with ageing and environmental exposure conditions.
- Characterisation of the tensile stress-strain behaviour of Textile Concrete (TC) and attempt to identification of the underlying mechanisms that contribute to the observed behaviour.

- Endeavor to building up of links and relationships between the findings in the four sets of tests, hence developing a model of the mechanical behaviour of Textile Concrete.
- Use of cracking patterns on TC specimens as a means of substantiating the "model" of mechanical behaviour of Textile Concrete.

At the end of the Chapter, the constituent mechanisms are combined into a "matrix" of observed behaviour across the four sets of tests.

The compressive strength of mortar is obtained from the cube crushing strength whereas for the individual fibres, the modulus of elasticity E_f is obtained from the results of fibre tensile tests. Similarly, for the fibre pull-out tests, an average curve is computed from the test results to characterise the load-displacement (P-δ) behaviour. Representative gradients along the average curve vary as illustrated in Fig. 5.1 (see section 5.5.5.5 for definitions of the slopes).

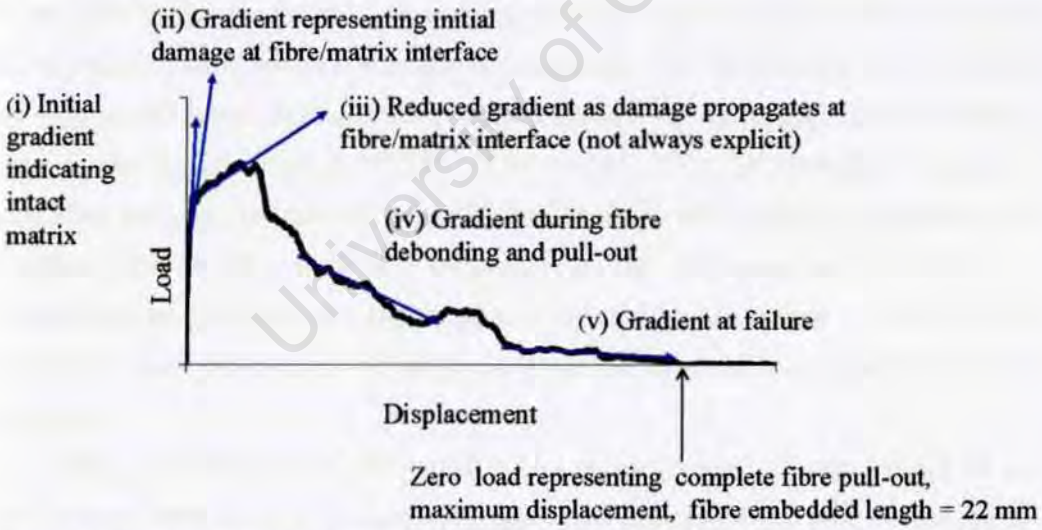

Figure 5.1: Definition of gradients along a fibre pull-out load-displacement curve

The results of the composite tensile tests are presented as stress-strain ($\sigma - \epsilon$) curves as illustrated for a typical curve in Fig. 5.2. The main features of the curve are: an initial linear part for low loading; micro-cracking stage; strain hardening region, and final failure.

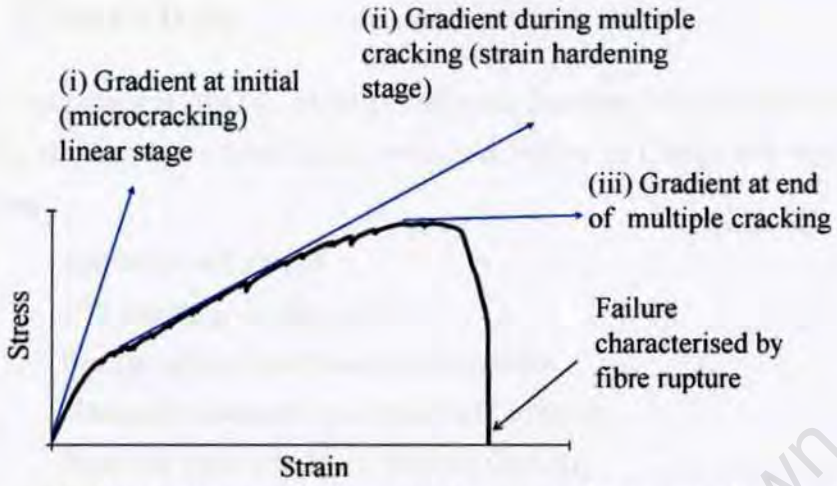

Figure 5.2: Typical tensile stress-strain curve of a composite specimen

The conventional statistics of representing the experimental data as an average value ($\overline{x}$) with uncertainties stated as standard deviations ($\pm\ \sigma$) will apply to all the results, assuming Gaussian behaviour (Taylor 1997*b*). An exception to the convention of stating one standard deviation will be in the fibre pull-out test results whereby the average P-δ curves will be bounded by upper and lower boundaries at two standard deviations ($\pm 2\ \sigma$) on either side of the mean (Taylor 1997*b*). The use of $\pm 2\ \sigma$ to represent the average fibre pull-out behaviour is justifiable because fibre pull-out behaviour is characterised by high scatter, particularly at the post-peak stage when fibre debonding and pull-out are taking place. By setting boundary curves at $\pm 2\ \sigma$ from the mean, 95 percent of the data at all the loading stages are effectively enclosed.

After presentation of the results, the consequences of uncertainities in the various measurements taken during experimental work will be outlined, and subsequently, further analysis of the results will be undertaken in order to establish any changes in behaviour that can be accredited to ageing and environmental conditions. Finally, interpretation of the research findings will be carried out in an attempt to create new understanding.

5.2 Overview

The labeling system used to identify different batches of specimens is consistent with the exposure conditions described earlier in Chapter 4 and defined as follows:

HC	100 hot/cold cycles
WD	100 wetting/drying cycles
C_c	Six months of carbonation exposure
NM	Natural exposure in a moderate climate
NT	Natural exposure in a tropical climate

Textile Concrete specimens, hereafter referred to as TC, were produced under controlled laboratory conditions. In all these laboratory-produced samples, mortar designated "Type 4" with a water/binder ratio of 0.5 and sand/binder ratio of 1.0 was employed. The tensile behaviour of the laboratory-produced samples was compared with specimens cut from a four-layer board, also made of TC, produced under conditions in Industry that were different from the laboratory-controlled environment. The TC board had previously undergone natural weathering for approximately 24 months in a factory yard in Johannesburg. The samples were cut into 50 mm long by 25 mm wide samples, the gripping edges were cast in epoxy-resin for adaptation to tensile testing and then labeled "I" for identification.

Damage to all specimens before and after testing was visually examined and the crack patterns quantified. The crack widths were measured using an optical microscope which had a resolution (using the Vickers eyepiece system) of 1 μm. This aspect of TC forms a major part of discussions in this Chapter.

The crack quantification method, which involved measurements of non-uniform crack widths and spacings, was limited in that characterisation of the physical condition of the damaged specimens using this method is essentially subjective and therefore not conclusive. This was because the total strain was measured on loaded specimens whereas crack widths were measured after loading when cracks had closed slightly. The information is nevertheless

useful for comparison purposes. By carrying out limited microscopic studies in a scanning electron microscope (SEM), it was possible to obtain supplementary information about the behaviour of TC with ageing. The SEM technique was dealt with in the previous Chapter.

In this Chapter, the results of the mechanical tests are discused and variations existing between the behaviour of control and weathered samples are assessed. The interpretation of these results and investigation into the link between mechanical behaviour and the microstructure of TC are also dealt with. Further discussions of the microstructure and an assessment of the effects of ageing on the performance of TC are dealt with in Chapter 6.

5.3 Results of Mortar Cube Tests

The objectives for mortar cube tests were:

- Determination of the effects of different environments on the physical and mechanical properties of the matrix, that is: density and cube crushing strength.
- Investigation of the variation of cube crushing strength with time.
- Identification of the effects of ageing and degradation on the matrix.

Results of the average crushing strength for cubes made from the same mix but exposed to different ageing environments are shown in Table 5.1. 42 cubes of size of 50 mm were cast for the tests and three were tested after curing for three days. The test was conducted after seven and 28 days of water curing. The average of these three tests was calculated in accordance to the standard requirements of cube crushing tests of cementitious materials (ASTM C 109/C 109M-05 2005). The results are shown in Table 5.1.

Table 5.1: Average cube crushing strength

Exposure condition		No. of tests	Density, g/cm^3 ($\pm 1\sigma$)	Strength, MPa ($\pm 1\sigma$)	Coefficient of variation, %		% Change due to weathering	
					density	strength	density	strength
3 Days	Control	3	2.060±0.020	10.8 ±1.1	1.0	9.8	N/A	N/A
7 Days	Control	3	2.090±0.020	20.8 ±2.0	1.0	9.6	N/A	N/A
28 Days	Control	3	2.060±0.023	35.2 ±2.9	1.1	8.2	N/A	N/A
8 Months	Control	3	2.000±0.040	36.9 ±1.4	2.0	3.8		
HC	Weathered	3	1.936±0.023	30.8±2.9	1.2	9.4	-3.2	-16.5
10 months	Control	3	2.080±0.023	44.4±2.8	1.1	6.3		
WD	Weathered	3	2.136±0.101	64.8±3.9	4.7	6.0	+2.7	+45.9
12 months	Control	3	2.064±0.023	48.0±4.3	1.1	9.0		
C_c	Weathered	5	2.072±0.023	64.4±4.5	1.1	7.0	+0.39	+34.2
12 months	Control	3	2.093±0.023	49.6±4.4	1.1	8.9		
NM	Weathered	3	2.147±0.083	56.8 ±7.9	3.9	13.9	+2.6	+14.5
20 months	Control	3	2.040±0.070	62.1±7.6	3.4	12.3		
NT	Weathered	4	2.050±0.030	66.0±6.4	1.5	9.7	+0.49	+6.3

Note: All control samples were water-cured for 28 days at 23°C; thereafter at 20°C and 53 % RH

"Weathered" refers to exposure in the stated environment

Variability in the results was indicated by the standard deviation (σ) of the average crushing strength as shown in Figs. 5.3 to 5.5 for control and weathered samples respectively. Three tests may seem rather low in number (from statistical analysis perspective) but the use of three cubes is the accepted conventional practice, which is documented in South African Standards (SANS 5863 (SABS SM 863 1994) 2006).

Figs. 5.3 and 5.4 show the variations in the average cube crushing strengths for control specimens with different ageing histories. The cubes were exposed to the five ageing regimes described earlier and these had previously been water-cured for 28 days as described in section 4.2.7 in Chapter 4.

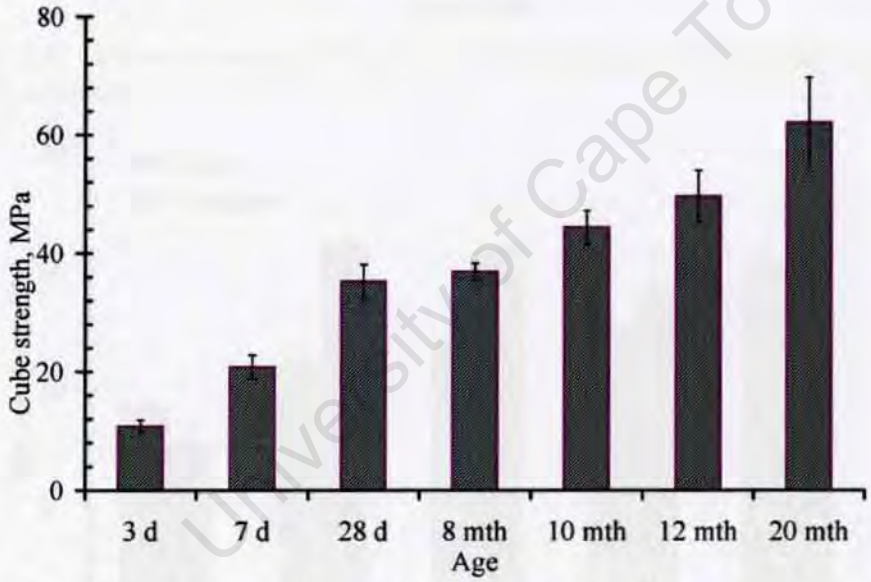

Figure 5.3: Variation of cube crushing strength with ageing for "control" specimens (vertical lines represent $\pm 1\ \sigma$)

5.3.1 Cube Crushing Strength of Control Samples

The cube crushing strengths shown in Figs. 5.3 and 5.4 refer to "control" specimens. The error bars shown in Figs. 5.3 and 5.4 are one standard deviation ($\pm\sigma$) on either side of the mean and represent the variability in results. Variability in early age strength for control samples was lower than at later ages partly due to dependence of mortar cube strength on the moisture condition of a specimen, which in turn was age-related. As the moisture level

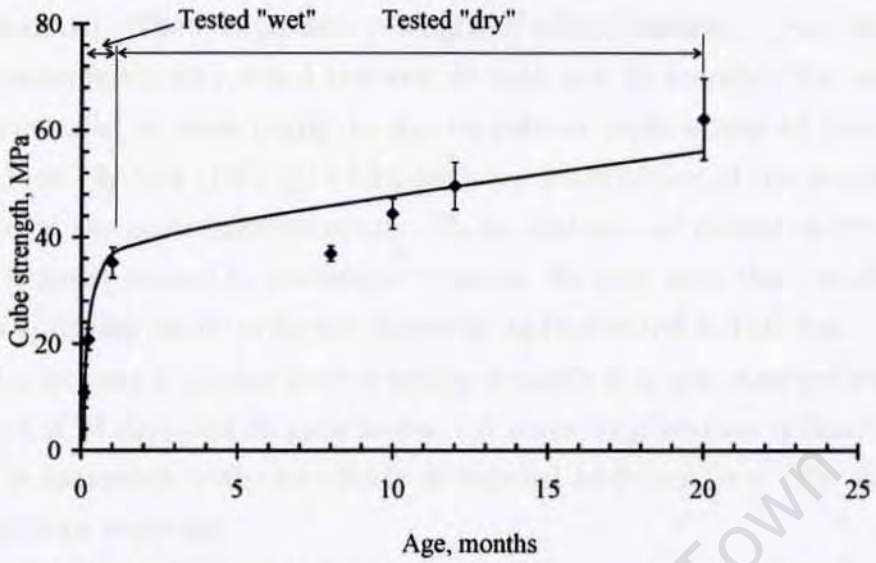

Figure 5.4: Increasing trend of cube crushing strength with ageing for "control" specimens

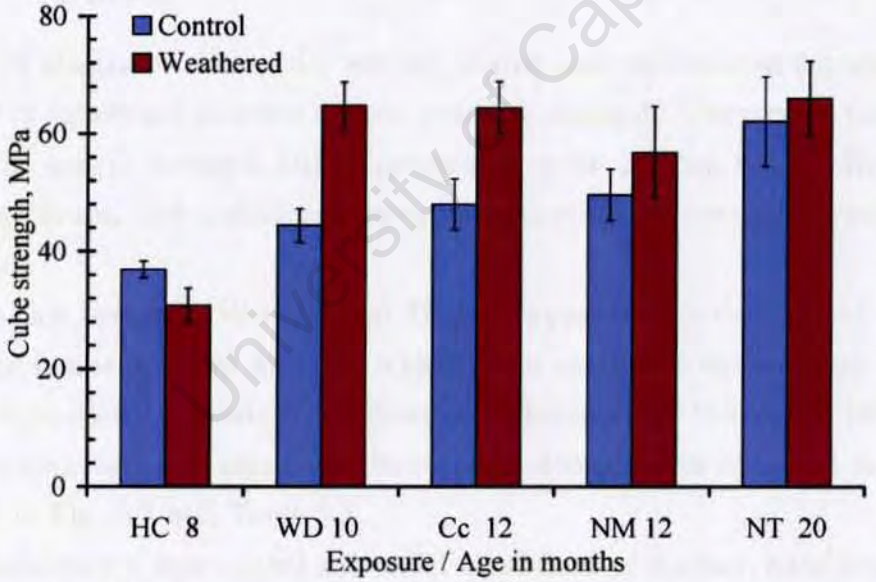

Figure 5.5: Effect of weathering environment on cube crushing strength

decreased (which may not have been at a uniform rate in all the samples), the cube strength progressively increased but there was more variation in the results.

A general increase in the cube crushing strength as the specimens aged

was observed. The compressive strength of control mortar cubes increased by approximately 88 percent between 28 days and 20 months. The increase was attributed at least partly to the 10 percent replacement of cement by Ultra-Fine Fly Ash (UFFA), which leads to densification of the mortar and changes in the paste microstructure. These changes are related to reduction in the porosity caused by pozzolanic reaction. At later ages, the contributory effects of drying result in higher strengths as illustrated in Fig. 5.4.

The increase in mortar cube crushing strength that was observed between the ages of 28 days and 20 months was not surprising because ordinarily this trend is consistent with the effects of mineral additions (e.g. Fly Ash) to cementitious materials.

5.3.2 Cube Crushing Strength of Weathered Mortar Cubes

Fig. 5.5 illustrates that cyclic wetting/drying and carbonation exposure resulted in significant increase in cube crushing strength. Conversely, the variation in matrix strength after exposure to cyclic heating and cooling was not significant, and a similar observation was made for naturally weathered samples.

In this research, Wetting and Drying exposure was carried out at an average temperature of 37 ± 2^{o}C, which was a conducive environment to cement hydration and matrix densification. Therefore, at the end of 100 wetting/drying cycles, a significant increase in strength was observed as illustrated in Fig. 5.5 and Table 5.1.

Carbonation was carried out under conditions of medium humidity with an average RH being 65 percent. The exposure was for a continuous period of six months and at the end of this period, the entire depth of samples had been CO_2-penetrated. Control samples were similarly conditioned under dry conditions with RH of approximately 51 percent but conversely, the control samples were not fully carbonated at the end of the exposure period. Therefore, the increase in cube crushing strength after carbonation exposure

was attributed to carbonation rather than drying. This was because despite control samples being conditioned under a less humid environment, and hence they were at a drier state than the carbonated samples, the cube crushing strength of carbonated samples was approximately 35 percent higher than for control samples (Fig. 5.5).

5.3.3 Summary of the Results of Mortar Cube Tests

The following is summary of the results of mortar cube tests:

- Cement hydration is age-dependent and it is well known that this leads to reduction in porosity of the microstructure, densification of the matrix, and increase in strength.
- The basic mechanism attributed to UFFA in the mix is pozzolanic reaction which enhances early as well as long-term strength development (Lewis, Sear, Wainwright & Ryle 2003).
- At later ages, the effects of drying of the microstructure, which is more pronounced after approximately eight months, contributes more to the strength than normal increase due to hydration.
- A Wetting/Drying environment was a favourable condition which led to good cement hydration and significant increase in strength.
- In a CO_2-rich environment, the underlying mechanism was interpreted as deposition of carbonate species in the pores within the microstructure thereby increasing the strength of cement paste, hence the marked improvement in the matrix strength (Neville 2002).

5.4 Results of Fibre Tensile Tests

The objectives of single fibre tensile tests were:

- To characterise the tensile strength and stiffness of non-bonded and ultrasonically bonded polypropylene (PP) fibres
- To determine the effects of different environments on the tensile properties of the fibres

- To gain insight into the mechanisms of weathering and deterioration in PP fibres

The results of the control tensile tests carried out on non-bonded and bonded fibre formats are shown in Fig. 5.6. The moduli of elasticity of the fibres (E_f) were calculated over the linear part of the Load-strain curves, with the cross-sectional area of 0.303 mm^2 based on the experimentally determined density of 0.94 g/cm^3 (see section A.2 in Appendix A). E_f for the control fibres was found to be 1077 MPa for the non-bonded fibres with a standard deviation of ±110.9 MPa, and for the bonded fibres the corresponding values were 1213 MPa and ±81.8 MPa respectively (the number of fibres tested for different environments ranged from 6 to 11).

5.4.1 Effect of Ultrasonic Welding

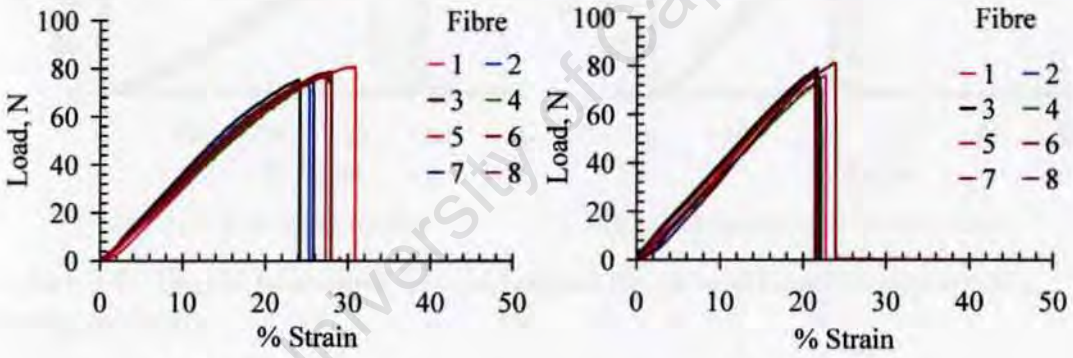

(a) Non-bonded (b) Bonded

Figure 5.6: Tensile behaviour of control fibres

The results of tests carried out on non-bonded and bonded fibres are shown in Fig. 5.6. The results illustrate that by ultrasonic bonding (welding) of the fine fibrils onto the central polypropylene (PP) core to form a "hybrid" fibre, the stiffness of the fibres improved by approximately 13 percent but the strength at failure was not affected significantly. Table 5.2 shows the average failure stress and strain of each fibre.

Although the fine fibrils on a non-bonded fibres were not ultrasonically welded to the central tape, they nevertheless interacted mechanically with

the cental PP tape and contributed to non-linearity near the peak. This is manifested in Figs. 5.6(a) and 5.6(b). The contribution of the fibrils to the tensile behaviour was also evident during the test (as shown in Fig. A.13 in Appendix A). By ultrasonically welding the fine fibrils to the cental core, the flexibility of the fine fibrils were significantly minimised accounting for the lack of ductility near failure for bonded fibres.

Non-bonded fibres were more readily available than the bonded format. Therefore, only non-bonded fibres were utilised for experimentation, which involved firstly exposure to different environments and subsequently tensile testing.

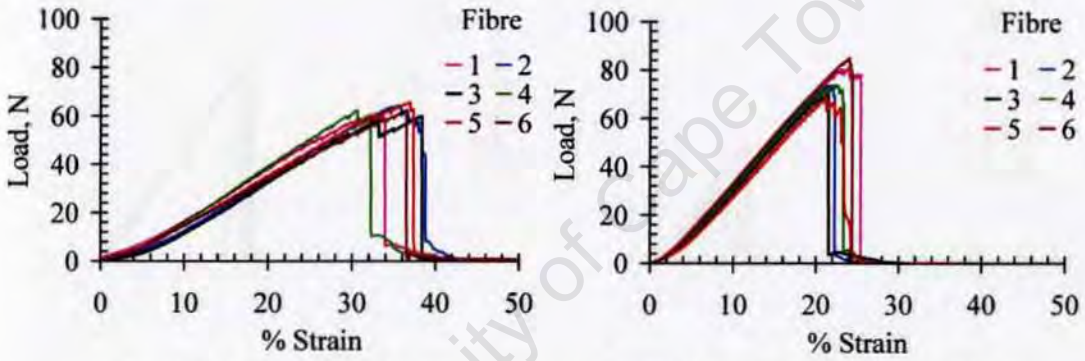

(a) 100 hot/cold cycles (b) 100 wetting/drying cycles

Figure 5.7: Tensile behaviour of non-bonded fibres weathered in accelerated ageing facility

The results of the soaked fibres referred to earlier as "soaked" samples in section 4.5.2 were an additional source of information that was useful for the analysis. The results of the tensile tests are dealt with in the sections that follow.

5.4.2 Effect of Ageing Conditions on Fibre Tensile Behaviour

The results of tests carried out on non-bonded fibres previously weathered under different environments, are shown in Figs. 5.7 to 5.9.

In a manner consistent with the effects of a hot/cold environment to the

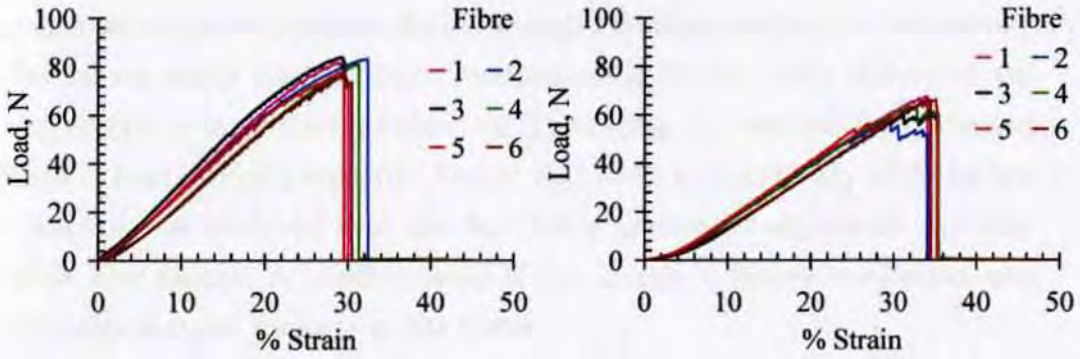

(a) Soaked fibres (b) Carbonating environment

Figure 5.8: Tensile behaviour of non-bonded fibres weathered under different environments

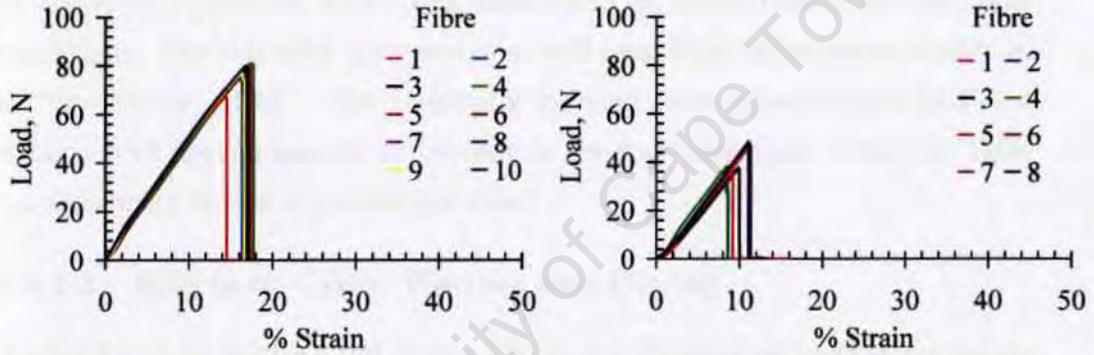

(a)Exposure to moderate climate (NM) (b) Exposure to tropical climate (NT)

Figure 5.9: Tensile behaviour of non-bonded fibres weathered under natural environments

mortar cubes, this regime was the most damaging to the fibres as illustrated in Fig. 5.7(a). After exposure, the fibres lose strength as well as stiffness.

5.4.2.1 Effects of Cyclic Heating and Cooling

The results of fibre tensile tests are summarised in Table 5.2. The average failure load of HC fibres was 60.8±3.8 N and the average strain was 36.1±2.9 percent.

At peak conditions, failure occurs by initial necking of the central core that is manifested as a minor form of ductility. Subsequently, brittle fracture of the central core occurs as shown in Fig. 5.7(a). Below approximately 10 N

as ultimate rupture is approached, a change in failure mechanism is observed. The failure mode changes from predominantly brittle, after failure of the central core, to more ductile behaviour illustrating the contribution of the fine fibrils in load carrying capacity. At low load levels in the vicinity of the failure strains, it was observed that the fine fibrils underwent significant ductility before final failure. A possible cause of the change in failure mechanism was thermally induced damage in the fibres.

Being a thermo-plastic polymer, PP is heat sensitive and although its melting temperature is in the range of 169 ^{o}C, cyclic heating to a temperature of 50^{o}C and subsequent cooling to approximately 23^{o}C has softening effects on the fibre properties, which was manifested by limited ductility near peak conditions. The ductility that was observed near final failure was attributed to "fine fibrils' effect". The thermally induced fibre softening resulted in a reduction of approximately 47 percent in the modulus E_f as shown in Table 5.2 indicating this is a permanent effect.

5.4.2.2 Effects of Cyclic Wetting and Drying

Ageing by cyclic wetting and drying (WD) at a slighted elevated temperature of 35^{o}C did not affect the failure load of non-bonded fibres significantly. However, minor ductility of the fine fibrils occurred near final rupture, which was clearly observed during the test, again demonstrating the influence of the fine fibrils in load bearing capacity of the weathered fibres. The observed behaviour varied from control fibres indicating a form of bonding of the fine fibrils to the central core after the weathering process. There was an increase in the fibre stiffness and reduction in toughness indicating that the fibres underwent some minor hardening as a result of this type of weathering.

Table 5.2: Characteristics of average load-strain parameters for the fibres

Fibre type	Exposure condition	No. of tests	Average peak load$\pm\sigma$, N	Average failure strain$\pm\sigma$, %	Coefficient of variation		Modulus of elasticity E_f, MPa	Area under the curve, J/m
					Load	Strain		
Non-bonded	Control	7	77.3±1.9	26.7±2.1	2.5	7.9	1077	10.32
Bonded	Control	8	77.0±2.0	22.0±0.9	2.6	4.1	1213	8.47
Non-bonded	100 Hot/Cold cycles at 23°C≤t≤50°C	6	60.8±3.8	36.1±2.9	6.3	8.0	566	10.97
Non-bonded	100 Wetting/Drying cycles at ~ 35°C	6	73.4±6.8	22.4±1.1	9.3	4.9	1123	8.22
Non-bonded	Wet fibres	6	80.4±3.1	30.2±1.3	3.9	4.3	878	12.18
Non-bonded	Carbonation at 30°C and ~55% RH	7	62.1±4.8	33.3±1.7	7.7	5.1	612	10.34
Non-bonded	Natural moderate (NM)	11	76.5±4.1	16.5±0.9	5.4	5.5	1678	6.31
Non-bonded	Natural tropical (NT)	8	40.0±6.2	9.6±1.4	15.5	14.6	1292	1.92

The results presented in this Table are interpreted in section 5.4.3

Results are reported to an accuracy of approximately 15 percent

PP fibres are known to be hydrophobic and hence drying, rather than wetting, was considered as having modified the fine fibrils-central core bonding nature. Since drying was undertaken by exposure for five hours to vacuum conditions after-which the environmental chamber was left open for approximately 18 hours under dry conditions, a modification of the fibre nature by the mechanism of hydrolysis was to be expected. It was also observed that the fibres had undergone "yellowing" after exposure to 100 wetting/drying cycles.

To validate the assumption that it was not the wetting regime but rather the drying condition that caused a change in the microstructure, non-bonded fibres which had been soaked in a cold water bath for a period of 3 months were tested as well. The behaviour was comparable to control samples in that the "near-rupture" ductility was not observed as shown in i.e. Fig. 5.8(a).

5.4.2.3 Effects of Carbonation Exposure

The stiffness of fibres exposed to a carbonation environment was reduced by approximately 43 percent after weathering, and a brittle failure was exhibited as shown in Table 5.2 and Fig. 5.8(b) respectively. It was understood that polypropylene does not carbonate under atmospheric pressure, as was the case inside the carbonation chamber (Mills 1986). However, the fibres were already contaminated with cementitious particles before carbonation exposure, which accounted for the pink colouration after the phenolphthalein test. After exposure the particles on the fibres were carbonated sufficiently as shown in Fig. 4.23(b).

However, the effect of exposure to the fibres was contamination with calcium carbonate ($CaCO_3$) particles from other concrete specimens in the chamber after the prolonged exposure in a CO_2-rich environment. The particles attached to the fine fibrils are clearly evident in micrographs in Fig. 6.5 in Chapter 6.

The reduction in fibre stiffness after carbonation was similar to thermally induced fibre softening after hot/cold exposure that was described earlier

in section 5.4.2.1 and necking of the central core is manifested by minor ductility at the peak conditions. Final rupture in carbonated samples was brittle rather than the ductile failure that characterised the tensile behaviour of HC weathered fibres. These contrasting failure modes are shown in Figs. 5.7 (a) and 5.8(b).

The tensile behaviour of carbonated fibres is interesting. The carbonation regime included significant thermal effects up to 30±1°C which could have led to softening and reduction in stiffness. In addition, the other weathering mechanism in the CO_2-rich environment was possibly the carbonation of the particles contaminating the PP fibres, which are seen in the micrograph in Fig. 6.5 in Chapter 6. At the end the exposure, the carbonated particles were more firmly attached to the softened fibre surfaces, and it is believed that this created stress concentration points leading to a lower peak stress. This mechanism contributed to the brittle failure observed in the failure mode while the bulk fibre behaviour was dominated by the thermo-related effects. Despite continuous exposure to a temperature of 30±1°C, localised scorching of the fibres was not evident from visual observation.

5.4.2.4 Effects of Exposure to Natural Environments

While accelerated ageing environments simulated controlled exposure conditions, the natural environment samples were exposed to direct sunlight and other conditions such as rain, dust and environmental moisture, and no protection from environmental degradation agents was provided.

Information about the natural climates was extracted from World Wide Web pages for South African Weather Service and the Kenya Meteorological Department (World Wide Web 2006*a*), (World Wide Web 2006*b*), which was shown earlier in Table 4.8. From the information about the natural climates, it was clear that Ultra-violet (UV) irradiation of PP fibres was significant considering that the fibres were continuously exposed for approximately 12 months.

The deterioration of PP fibres as a result of UV irradiation has been

studied in the past by Segre *et al.* (Segre, Tonella & Joekes 1998). The deterioration was attributed to irreversible changes in composition and structure of polymer molecules. Therefore, in this study, UV effects were presumed to have played a role in the tensile behaviour of PP fibres.

After the fibres were weathered by exposure to natural moderate (NM) and tropical (NT) climates, an increase in stiffness and a reduction in the failure strain characterised the tensile behaviour of the weathered fibres as shown in Table 5.2 and Figs. 5.9(a) and 5.9(b).

Fibres weathered in the two natural environments manifested remarkable differences in strength and toughness as illustrated by Fig. 5.9. While there was a significant loss in strength and toughness for NT weathered samples, the main change that was attributed to weathering in NM climate was minor reduction in failure strain and toughness, resulting in a behaviour similar to that observed in bonded fibres in Fig. 5.6 (b). The fine-fibrils' effects were not observed on the tensile load-strain curves of NM-weathered fibres implying that embrittlement was more pronounced in the fine fibrils than in the main tape.

This behaviour of NM-weathered fibres was not surprising considering that although the inner tape and the fine fibrils were made of polypropylene, they had different specifications (World Wide Web 2006*c*). While the inner tape was fibrillated PP specified as 110 D'Tex (grammes of fibre per kilometre of yarn), the outer fluffy layers were specified as 3 d'tex (10 kilometres of one d'tex of yarn weighs 3 grammes) (see section 2.7 in Chapter 2). Since the outer fluffy layers were made of a much finer PP and hence, had a higher surface volume ratio than the central core, it was deduced that the effects of UV irradiation were more severe in these layers than the core fibre. An increase in stiffness and a brittle tensile failure at a reduced strain characterised the tensile behaviour of NM-weathered fibres.

Severe fibre damage in NT-exposed fibres was accredited to considerable amount of sunshine in Nairobi where the specimens were weathered, as shown earlier in Table 4.8 in Chapter 4. A higher rate of UV irradia-

tion in a tropical climate than in a moderate environment was considered a major deterioration factor (Segre et al. 1998). It was further deduced from the loss in failure strength that in addition to embrittlement of the outer fluffy layer, the inner PP tapes had also undergone significant damage after continuous exposure for approximately 12 months. Contamination of fibres could also have contributed to further embrittlement and weakening of the NT-weathered fibres.

From the results of tensile tests on naturally-exposed fibres, it was inferred that the UV radiation rate was lower in Cape Town than in Nairobi. It was further assumed that UV rate accounts for the differences in the tensile performance of NM and NT fibres that is illustrated by Figs 5.9(a) and 5.9(b) respectively. This assumption was however not validated in this research, since other causes (such as acid rain, pollutants etc.) could have contributed to the behaviour, but further investigations in this regard are suggested.

5.4.3 Interpretation of Results in Table 5.2

The key parameters in the behaviour of the fibre tensile tests are summarised in Table 5.2. Stiffer fibres (WD and naturally weathered) have relatively lower toughness (areas under the curves), which is related to the influence of the fine fibrils in the load-bearing capacity and fibre flexibility. Thermally softened fibres (HC and carbonated) are less stiff than the control fibres but the toughness is higher.

Since carbonation was carried out at atmospheric pressure, no chemical reaction involving CO_2 took place. The main effect of carbonation was thermally-induced fibre softening considering that the temperature in the carbonation chamber was 30°C. Under these conditions, the physical nature of the fibres was modified in that the surfaces of fine fibrils were covered by particles as shown in Fig. 6.5 in Chapter 6. Despite the presence of this outer layer, the carbonated fibres were characterised by thermally-induced ductile failure.

The average curves characterising the typical tensile load-strain (P-ϵ) behaviour are shown in Fig. 5.10. The results indicate a close correlation between the environmental temperature, fibre strength and stiffness. For example, fibres aged in HC and carbonated environments have similar trends of lower stiffness but relatively higher toughness. Figs. 5.10 and 5.11 also illustrate that with the exception of NT-weathered fibres, the failure strains are related to stiffness. Stiffer fibres exhibited relatively lower failure strains. Conversely, the more flexible fibres failed at higher strains.

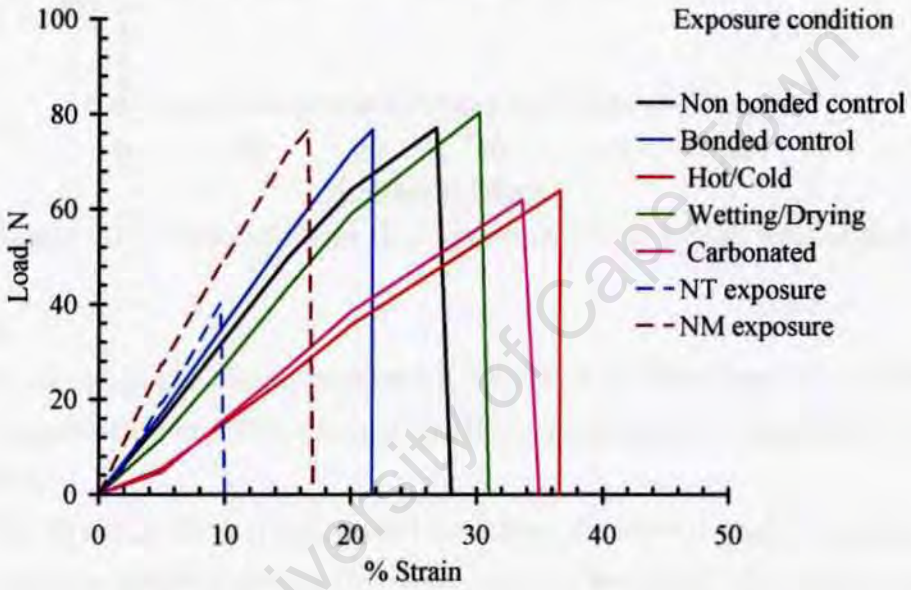

Figure 5.10: Average tensile stress-strain curves for non-bonded fibres

The loss in fibre strength arises from two different causes: thermally induced softening, which was manifested in fibres that were exposed to hot/cold and carbonated environments; or embrittlement, exemplified by NT-weathered fibres respectively. These effects are illustrated in Fig. 5.12.

The loss in fibre strength and stiffness that was observed after cyclic heating and cooling and similarly after carbonation exposure was an indication that the damage mechanisms in these two regimes were of a similar nature. Although the temperatures were much lower than the melting temperature of PP (approximately 165^{o}C), cyclic changes in temperature by 27^{o}C (50$\rightarrow$23^{o}C) over a short time span of 75 minutes was damaging to the

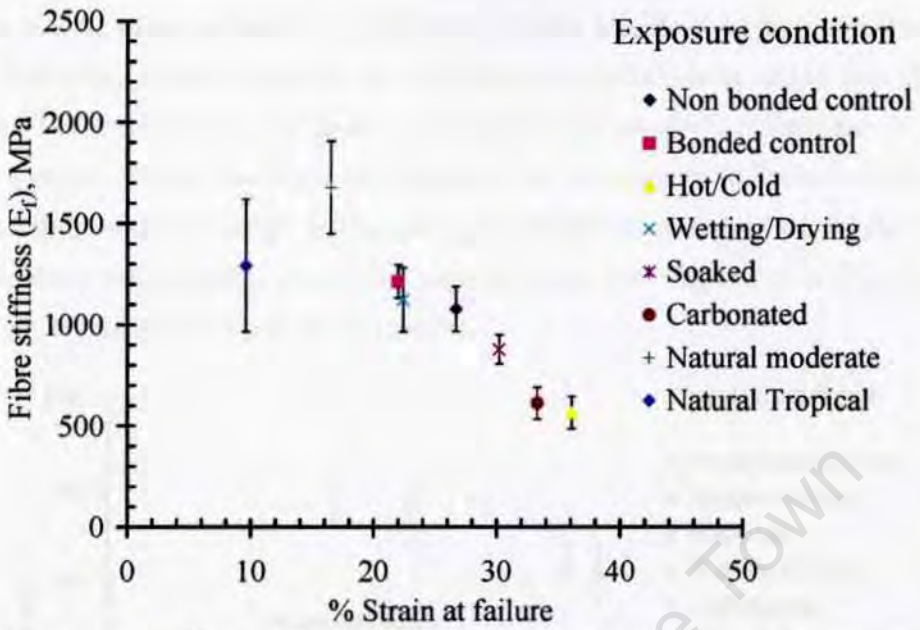

Figure 5.11: Fibre stiffness (E_f) versus strain at failure relationship

fibres.

Similarly, a six month continuous exposure of PP fibres in a chamber at a temperature of 30°C softened the fibres and caused a significant loss in strength.

The Wetting/Drying regime did not affect the fibre strength significantly but since the temperatures in this environment were slightly elevated at 35°C, the dominant mechanisms in this environment was therefore hydrolysis and "yellowing", which were manifested in a slight loss in ductility.

Natural environments exposed the fibres to a combination of physical and chemical processes such as oxidation, hydrolysis, carbonation, and UV radiation. As these processes are not always contributory but could also have competing effects, the results of tensile tests indicated that UV irradiation effects may well have dominated the ageing mechanisms particularly in a tropical climate, whereas in a moderate climate, the effects of UV irradiation were not as distinctive.

Weathering in a moderate climate for a limited period of approximately 12 months did not cause a major loss in fibre strength. Rather, a higher fibre

stiffness was observed and a significant reduction in failure strain. Although this behaviour could be partly attributed to embrittlement of the fine fibrils due to UV irradiation, the basic mechanism that caused an increase in stiffness was not clearly understood. However, an increase in stiffness meant that either there was a change in the material property or reduction in the fibre dimensions (shrinkage). As these aspects were not validated in this study, further investigations would be needed.

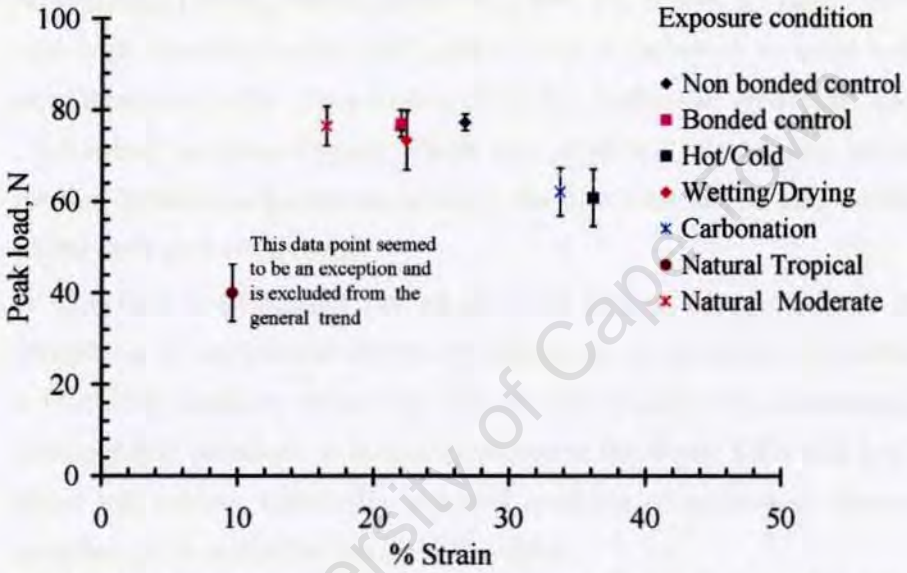

Figure 5.12: Peak load versus strain at failure for fibres exposed to different environments

Fig. 5.12 illustrates an increasing trend in the failure strains as the peak load decreases. The figure also shows close similarity between HC and carbonated samples suggesting that the effects of carbonation exposure were thermally related rather than a chemical changes in the PP microstructure.

5.4.4 Summary of Results of Fibre Tensile Tests

The effects of exposure of fibres to different environments and the associated mechanisms of degradation are summarised as follows:

- The fibres softened substantially after exposure to a hot/cold environment ascribed to thermally-induced rotation of segments of molecular chains.
- A Wetting/Drying environment exposed PP fibres to light, warmth, and high humidity with OH^- ions. This is believed to have induced modifications in the cross links within the molecular structure, causing "yellowing" or loss of glaze which was observed. As broken bonds reformed between adjacent molecules, the fibres hardened and eventually underwent embrittlement.
- A CO_2-rich environment (at an elevated temperature) resulted in the formation of occasional lumps of carbonate species on the surface of a relatively tougher substrate. Since carbonation was undertaken at atmospheric pressure, a chemical reaction involving CO_2 did not take place but rather, thermally induced rotation of molecular chains was manifested in a ductile tensile behaviour.
- In natural environments, a strong absorption of the ultraviolet part of the sun's rays may have resulted in formation of a thin brittle layer on the fibre surfaces. The tensile failure strain of a fibre depended on the relative failure strains of the brittle outer layer and the substrate. The results indicated that the effect of UV irradiation in Nairobi (a moderate altitude in the tropics) was more severe than in a moderate climate.

Table 5.3: Environmental effects on tensile behaviour of fibres

Influencing factor	Exposure condition				
	Hot/Cold (HC)	Wetting/Drying (WD)	Carbonated (C_c	Moderate (NM)	Tropical (NT)
Temperature	50°C-23°C	45°C-38°C for 5 hours 23°C for 18 hours	30°C	22°C-11°C	25°C-13°C
Relative Humidity	Dry	90%-55%	65%	70-80% (average monthly)	78%-46%
Access to oxygen	Open	Open for 18 hours Evacuated for 5 hours	10% CO_2	Open	Open
Exposure to light	Halogen light	Limited	Dark		7 sunshine hours (average per day)
Mechanism(s)	Softening	Oxidation/hydrolysis, yellowing, hardening	Softening, encrustation with carbonate layer	Low rate UV damage minor embrittlement	High rate UV damage major embrittlement loss of strength
*Changes in mechanical properties					
Failure load	Decrease	No change	Decrease	No change	Decrease
Stiffness, E_f	Decrease	Increase	Decrease	Increase	Increase
Toughness	Minor increase	Decrease	Minor increase	Decrease	Decrease

*Changes are shown in Table 5.2

5.5 Results of Fibre Pull-out Tests

The experimental data obtained from the fibre pull-out tests was processed into load-displacement (P-d) curves as shown by representative traces in Fig.5.13. The characteristic features of the curves were:

- An initial linear stage (A)
- A second pre-peak stage with a reduced gradient (B)
- A third reducing slope (C) leading to the peak point
- Post-peak stage (with a negative gradient) (D)
- A fourth stage with a lower negative gradient (E)
- A fifth stage at which the curve is tends to be horizontal (F)
- Failure point (G)

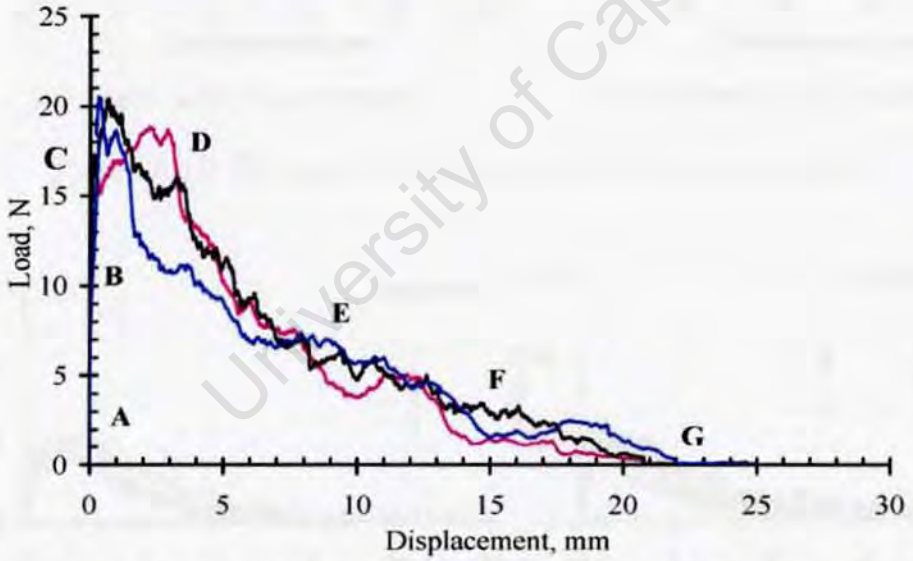

Figure 5.13: Representative traces of the results of fibre pull-out tests

For each ageing condition, an average curve representing the typical load-deflection behaviour was obtained using loads at displacement intervals of 1 mm. At each displacement point, average loads (P_{ave}) and standard deviations (σ) were then computed. Upper (U) and lower (L) boundaries to the

average curve were computed from P_{ave} at $\pm 2\sigma_{ave}$ from the mean. The average curve (ave) and the two boundary curves U and L represented 95 percent of the test results.

Representative results of the fibre pull-out of specimens aged under controlled laboratory conditions are shown in Fig. 5.14. The results illustrate the early age fibre pull-out performance. At this early age, change in behaviour was not substantial.

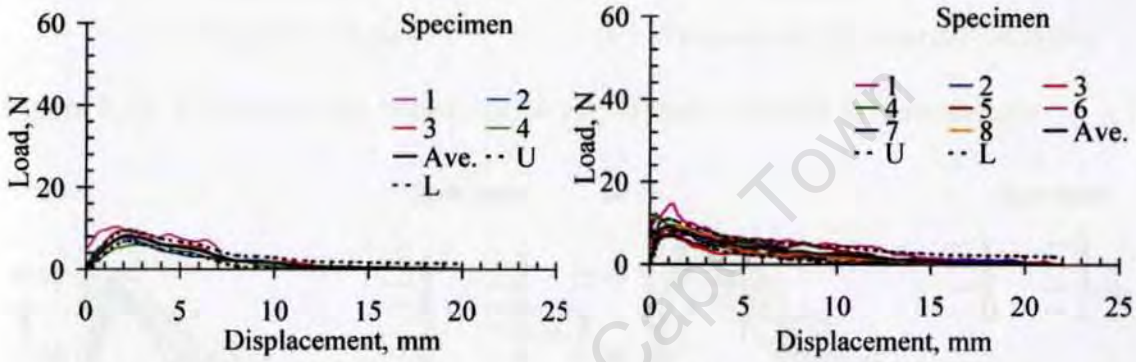

(a) Eight day old specimens (b) Six week old specimens

Figure 5.14: Fibre pull-out behaviour of control specimens

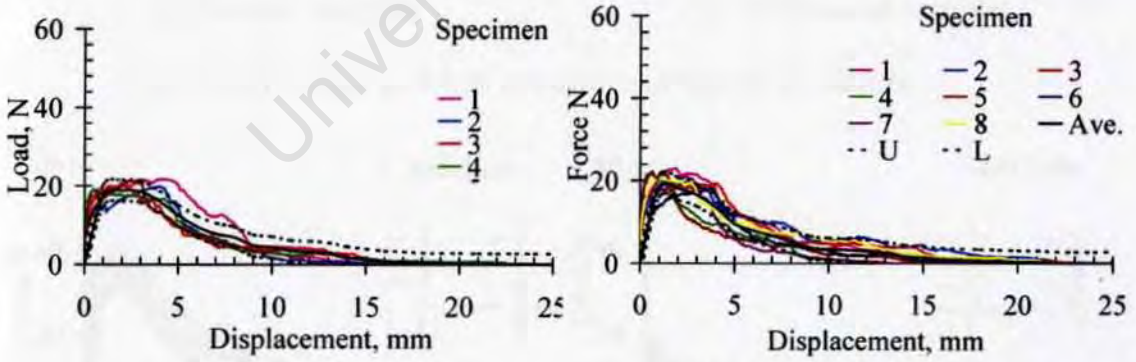

(a)Control samples (b) Hot/cold exposed samples

Figure 5.15: Fibre pull-out behaviour at age of five months- HC specimens

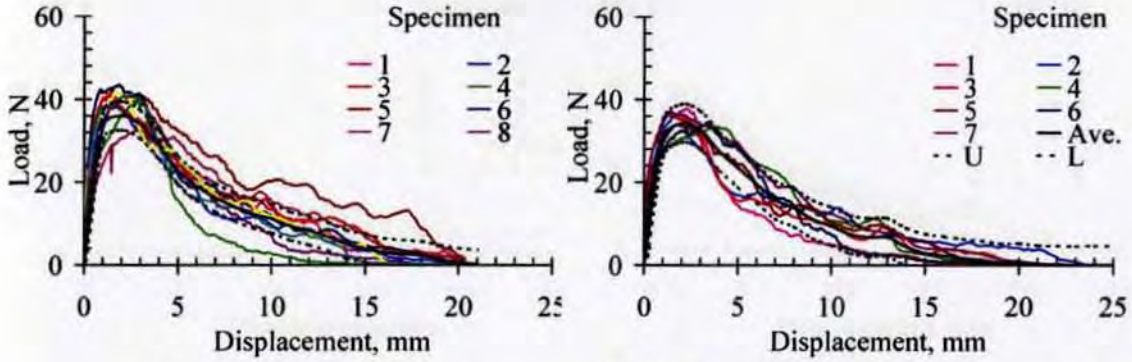

(a)Control samples (b) Wetting/drying exposed samples

Figure 5.16: Fibre pull-out behaviour at age of eight months-WD specimens

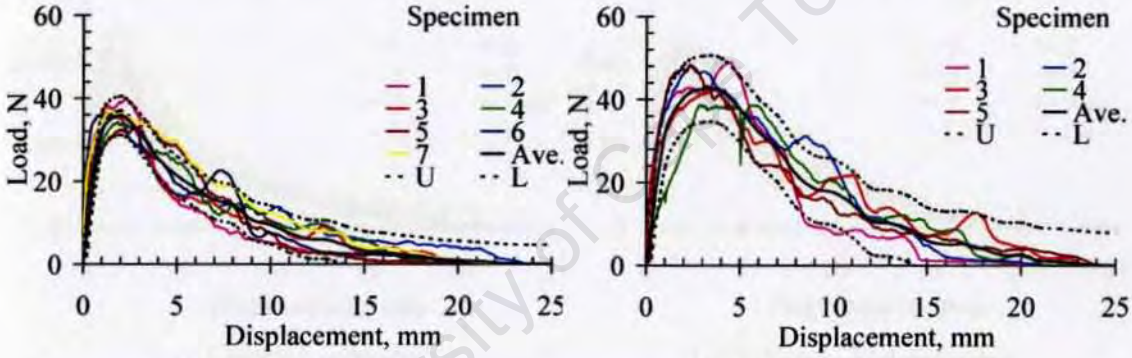

(a)Control samples (b) Carbonated samples

Figure 5.17: Fibre pull-out behaviour at age of 12 months

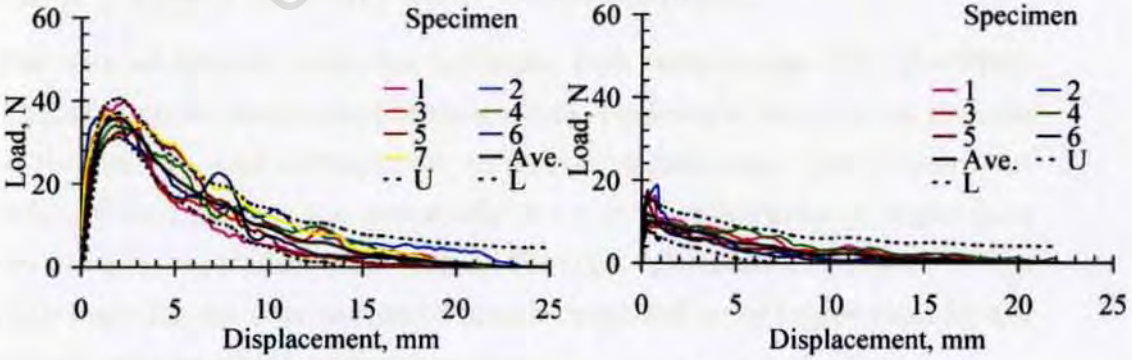

(a) Control samples (b) NM exposed samples

Figure 5.18: Fibre pull-out behaviour at age of 12 months

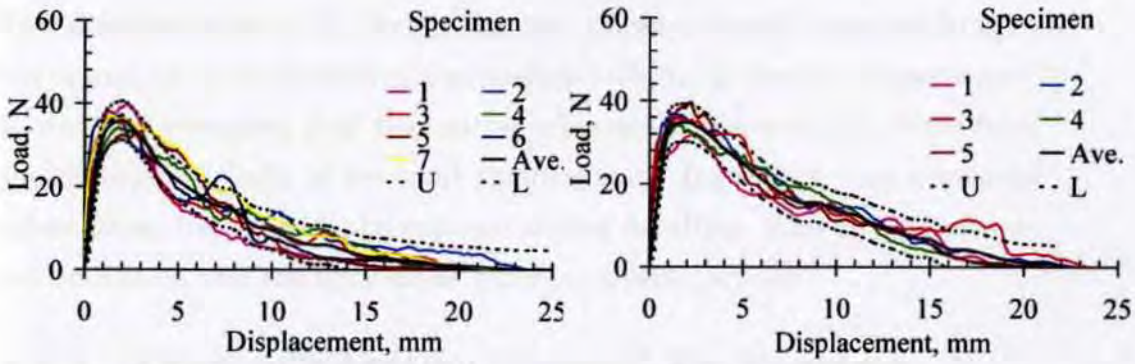

(a) Control samples (b) NM confirmatory tests

Figure 5.19: Fibre pull-out behaviour at age of 12 months

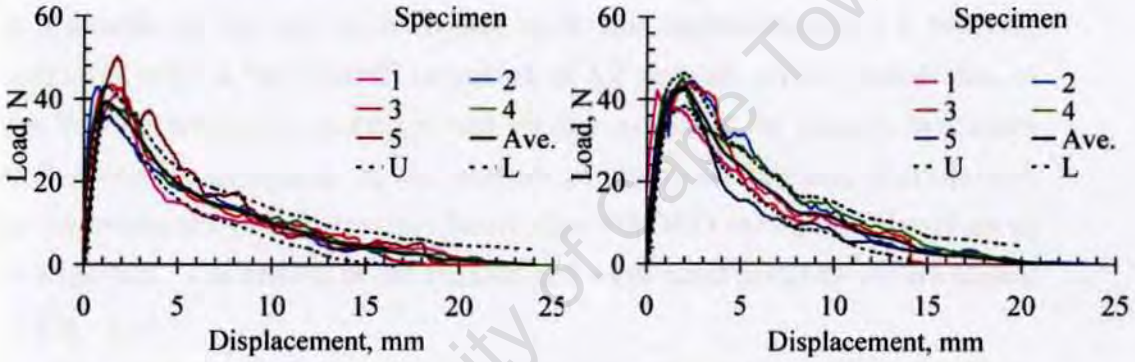

(a) Control samples (b) NT exposed samples

Figure 5.20: Fibre pull-out behaviour at age of 16 months

5.5.1 Effect of Hot/Cold Environment

The rate of cement hydration increases with temperature (Neville 2002). Therefore cyclic heating and cooling would be expected to cause an increase in the reaction and consequently to mortar densification. In addition, the hot/cold environment was essentially dry due to evaporation of water from the samples that takes place during heating. Therefore the results of the peak loads for the drier samples would be expected to be higher than for the control samples which were not as dry.

However, after hot/cold exposure there was no significant change in the peak loads in comparison with the control samples as shown in Fig. 5.15.

The possible cause of this behaviour was thermo-related micro-cracking in the matrix which counteracted the beneficial effects of elevated temperatures. It was also presumed that the mortar adequately protected the fibres from the damaging effects of hot/cold environment. Indeed, on rare occasions where fibres happened to be exposed during handling, then elongation was not consistent and the fibre broke before complete pull-out.

5.5.2 Effect of "Wetting/Drying" Environment

Samples exposed to 100 cycles of "Wetting/Drying" were tested at the end of the "Drying" (WD) cycle. As shown earlier in Fig. 4.21, the moisture content in a sample at the end of a Drying cycle was approximately 1.5 percent, compared with a "saturated" condition of 8.2 percent, which meant that in the WD environment, moisture was readily available for cement hydration and matrix densification. In the absence of any other physical degradation, an improvement in fibre/matrix bond after 100 WD cycles was therefore to be expected. The results of the control and weathered samples are are shown in Fig. 5.16.

The control samples were tested after 8 months in controlled conditions of temperature and moisture content, which was lower than in weathered samples. The fibre pull-out test results did not indicate a significant increase in peak load values that could be attributed to weathering. This was because again, there were competing effects: a wetting cycle in which the temperature was elevated and moisture was readily available caused progression of hydration and increase in bonding, cyclic drying conditions were detrimental to mechanical properties due to microcracking.

The results shown in Fig. 5.16(b) were a combined effect of the competing mechanisms of cement hydration and wetting, which were not easily separable in the study. Assessment of the degree of hydration is normally done through microscopic studies but this was not dealt with in this research.

5.5.3 Effect of Carbonation

A high CO_2 environment resulted in matrix densification due to deposition of carbonate species around the fibre as revealed in the micrograph in Fig. 6.6 in Chapter 6. Independent tests using phenolphthalein in dilute alcohol confirmed that samples were fully carbonated down to the fibre. The carbonate species deposited on the fine fibrils increased the inter-fibril as well as fibre/matrix interaction resulting in higher peak loads as shown in Fig. 5.17.

5.5.4 Effect of Natural Environments

Samples weathered naturally in a moderate climate (NM) had very poor load-displacement behaviour which was markedly different from the behaviour of the fibres and the matrix. Whereas the fibre stiffness and rigidity increased after weathering (see Table 5.2), the composite was characterised by significant decrease in peak loads. These results are therefore not included in this discussion.

Samples weathered naturally in a moderate climate had very poor load-displacement behaviour which was remarkably different from the behaviour of the fibres and the matrix. Whereas the fibre stiffness and rigidity increased after weathering (see Table 5.2), the composite was characterised by significant decrease in peak loads.

The results shown in Fig. 5.18(a) demonstrated good repeatability. Although NM-weathered fibre pull-out behaviour seemed to be atypical or unusual, good repeatability demonstrates that the results are legitimate. It was therefore, not fully understood why the NM environment caused such a poor performance. More tests were performed on NM-weathered samples and the results, shown in Fig. 5.21 were consistent with the original results shown in Fig. 5.18(a).

Exposure of individual fibres to a tropical climate caused embrittlement due to UV irradiation as illustrated earlier (Fig. 5.9). By casting the fibres in mortar, they were adequately protected and this is demonstrated by an

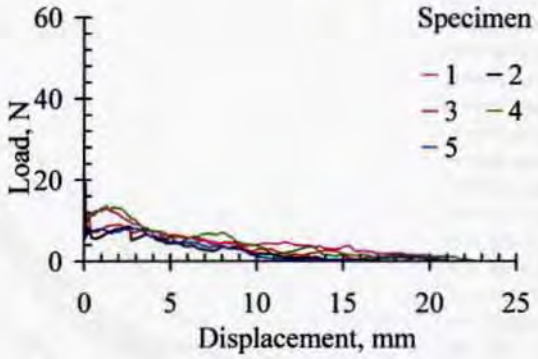

Figure 5.21: Confirmatory tests for NM-weathered samples

increase in peak load as shown in Fig. 5.19(b) and 5.20(b), which is an indication of improved fibre/matrix bonding. The analysis of the fibre pull-out behaviour is discussed further in the subsequent section.

5.5.5 Analysis of the Fibre Pull-out Behaviour

The results shown in Figs. 5.14 to 5.20 illustrate an increasing trend in the peak load with ageing, which is attributed to matrix densification caused by increased cement hydration with ageing at least for control specimens. For later age samples, the effects of drying and shrinkage are contributory to the observed densification. A denser matrix was essentially manifested in a stronger fibre/matrix bond. The manner in which ageing and weathering affected the load-displacement behaviour, is illustrated in Figs. 5.22 and 5.23.

Samples aged under controlled laboratory conditions showed a marked improvement in behaviour between five and eight months of air drying under controlled conditions. This can be explained possibly because after eight months, the critical region at the fibre/matrix interface had dried sufficiently for a change in fibre pull-out behaviour to be significant. The moisture condition at the critical region reduces the interfacial friction by a "lubricating" action, which would then lead to a reduction in bonding. Therefore, for the same age of specimens, the fibre pull-out performance is higher in dry than in wet samples.

From Fig. 5.23, carbonated samples and NT specimens at age of 16

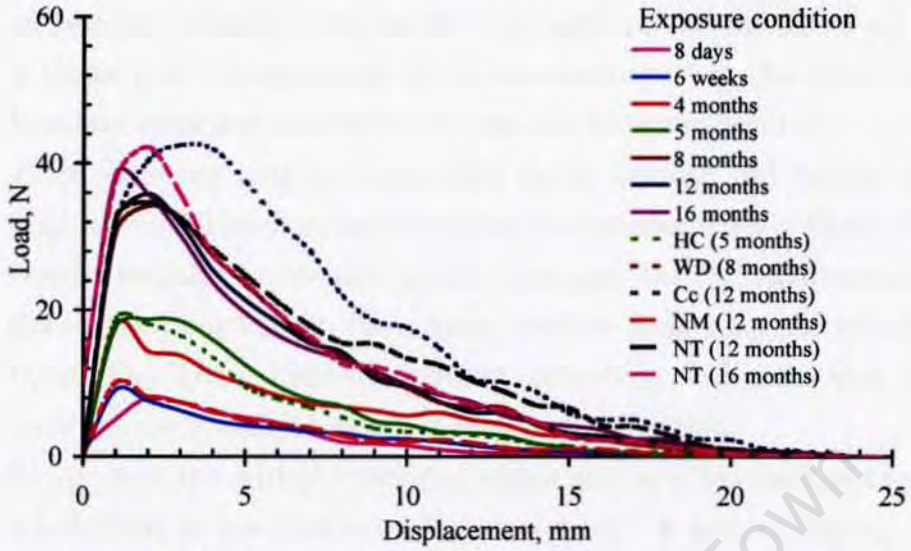

Figure 5.22: Average load-deflection curves for all samples

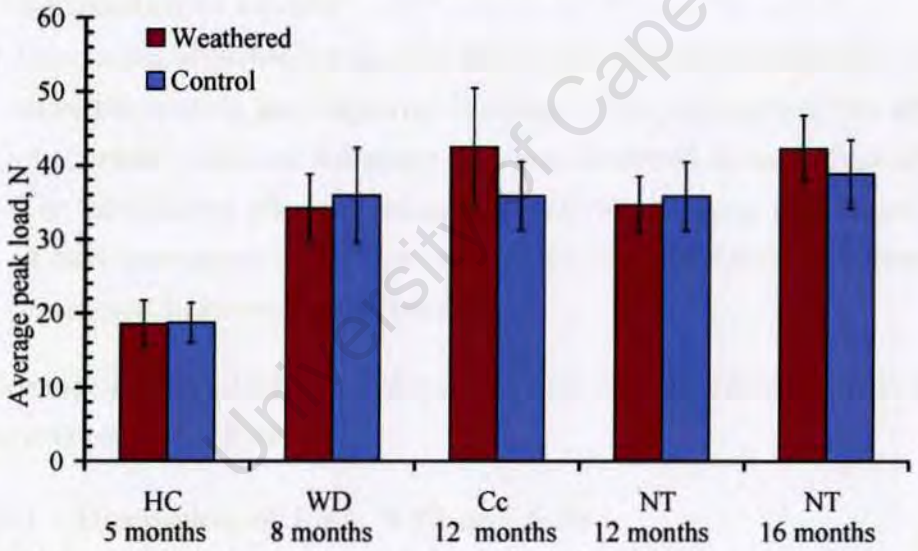

Figure 5.23: Variation of peak loads with exposure and ageing

months may be regarded as having undergone significant change after ageing.

From the preceding discussions, it is clear that the peak fibre pull-out loads were a function of the following mechanisms:

- Matrix densification that results from ongoing hydration is a basic mechanism in cement-based products and it depends on the age of samples and exposure conditions. At early ages, densification is mainly due

to cement hydration whereas at later ages, the effects of drying play a major role. Densification of the microstructure at the fibre/matrix interface increases interfacial friction and improves bonding.

- Fibre softening that occurred after cyclic heating and cooling (HC) together-with loss in strength had an adverse effect on the fibre/matrix bond strength. In addition to fibre damage, the HC environment induced microcracking in the matrix, further weakening the interfacial bond. This was a thermally-induced competing mechanism that counteracted the beneficial effects of matrix densification.
- Moisture at the critical interfacial region acts as a lubricant and causes a reduction in the interfacial frictional bond. A wetting/drying cycle did not dry this critical zone sufficiently for the benefits of matrix densification to be seen.
- Deposition of carbonate species within the microstructure further densifies the matrix and improves bonding. This counteracts the effects of thermally-induced softening that was observed in individual fibres. The cumulative effect of microstructure densification and deposition of carbonate species was that carbonated samples clearly manifested a significant improvement in bonding.

The average peak loads shown in Figs. 5.22 and 5.23 are discussed more fully in the section that follows.

5.5.5.1 Discussion of Figs. 5.22 and 5.23

The average curves in Fig. 5.22 envelop the overall behaviour of each set of samples. Although the initial slope, designated slope (i) in Fig. 5.1 is not obvious in the figure, the other four slopes are distinct for each set of samples. The variations in the pre-peak gradients illustrate how microcracking at the fibre/matrix interfacial region changes with ageing. At early age, specimens are relatively weaker and are therefore more prone to microcracking as clearly shown by reduced pre-peak gradients. Similarly, a stronger interface is relatively more brittle and is associated with a steeper post-peak gradient

which increases with ageing. A steep post-peak slope is indicative of a loss of a lot of bond stress without much pull-out.

For each specimen tested, fibre matrix bond strength τ was computed by substituting the average pull-out load P_{max} and the surface area of the embedded fibre length l_e (22 mm) into Eq. 3.1, which was presented earlier in Chapter 3 and is reproduced below.

$$\tau = \frac{P_{max}}{\pi d_f l_e} \tag{3.1}$$

A correlation between the post-peak slope (representing fibre debonding stage) and peak loads, which are directly related to τ, is illustrated in Fig. 5.24.

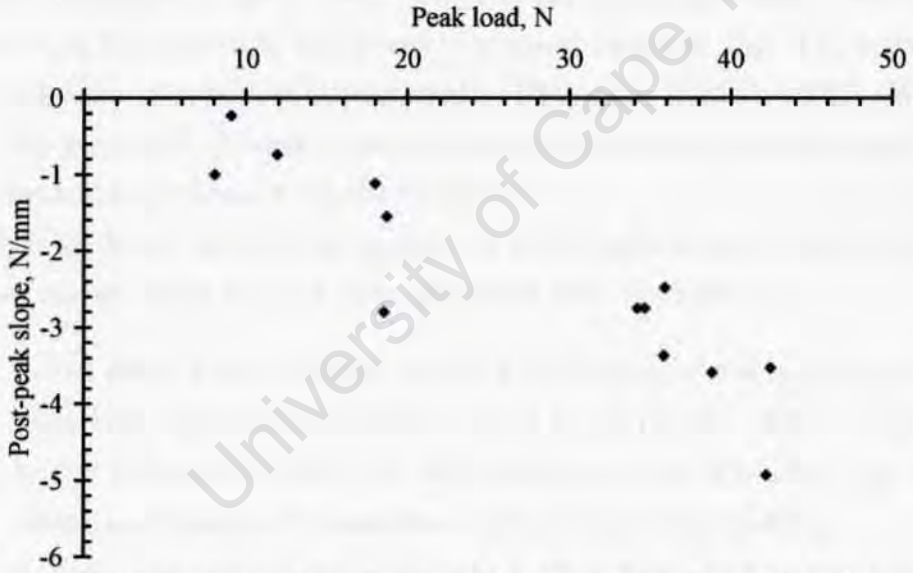

Figure 5.24: Correlation between peak load and slope at fibre debonding stage

The linear relationship between τ and P_{max}, represented by Eq. 3.1, means that the variations of these two parameters with ageing are the same. Values of τ for each set of specimens were presented in Table 5.5.

The average of the individual standard deviations that were computed for each set of samples (σ_{ave}) at peak load was an indication of the overall variability in the measurements and the conditions during the weathering

process. The variations were shown in the bar chart in Fig. 5.23. Low variability in the results was an indication of uniformity in weathering across specimens in the same batch (e.g. HC environment) as opposed to relatively higher variability in samples weathered by carbonation in which CO_2 penetration rate seemed to be less uniform. However, as the mechanisms in HC and carbonated environments were of very different nature, the variations in the two sets of results were not surprising.

5.5.5.2 Pre-Peak Gradients of the Load-Displacement Curves

The fibre pull-out load-displacement behaviour in cementitious materials has been studied in the past and the mechanisms of the pull-out process documented (Balaguru & Shah 1992). The general load-displacement behaviour observed in this research, which was illustrated earlier in Fig. 5.1, is similar to the behaviour reported in past studies (Balaguru & Shah 1992), (Wang, Li & Backer 1988). Therefore the discussions carried out here are based on theories and hypotheses from the literature.

The gradients used in the analysis of load-displacement behaviour were defined earlier using Fig. 5.1. The gradients were identified as:

- Initial steep linear gradient before mobilisation of the interfacial friction. Low displacement of the order of 1 mm characterise the slopes.
- In the region of 1-2 mm, the slope reduces at an increasing load indicating mobilisation of interfacial friction and microcracking.
- A steep post-peak negative slope with fibre debonding and pulling out of the matrix. The slope depends on the extent of damage to the fibre and the matrix.
- A final low negative slope that approaches asymptotic to the horizontal. This is due to stable crack propagation and final fibre pull-out of the damaged matrix.

The pre-peak gradients were obtained by taking the average of the tangents of the load-displacement curves at five points between the origin and the 2

mm displacement points. In all the samples tested, the initial gradient was uniform up to displacements in the vicinity of 1 mm, which represented a linear fibre matrix bond.

At this initial stage the load-displacement behaviour was mainly a matrix property. Beyond displacements of approximately 1 mm, a reduction in the gradient of the load-displacement curve occurred due to matrix microcracking and subsequent mobilisation of interfacial friction. The slopes are shown in Fig. 5.25 illustrating the variation in the initial load-deflection slopes with ageing, and from the curves, an increasing hardening trend in the matrix is indicated. For control fibres, the variations of the pre-peak slopes with ageing are shown in Figs. 5.26(a) and 5.26(b).

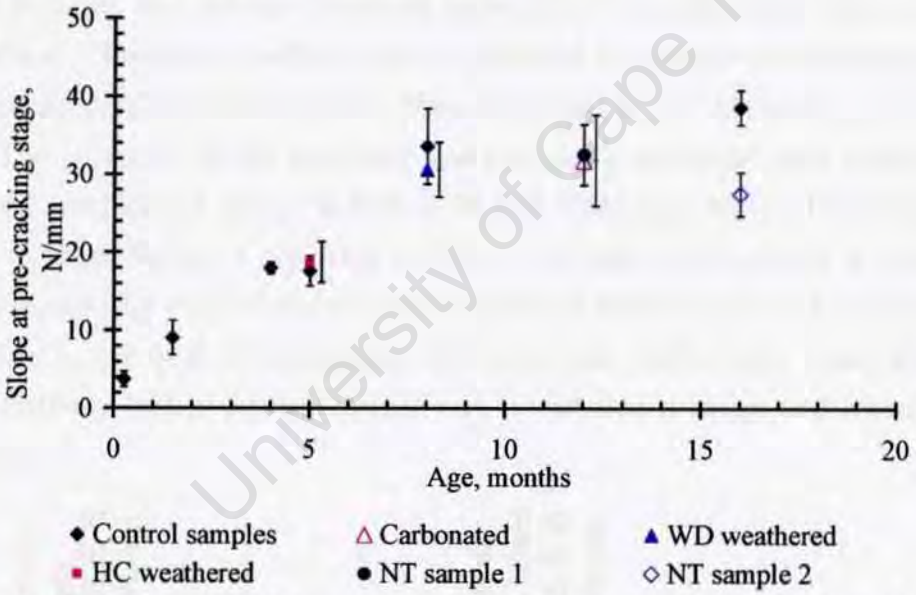

Figure 5.25: Variation of pre-cracking slope for control and weathered samples

The second stage in a typical load-displacement curve was between 1 mm and 2 mm. The behaviour at this stage was characterised by an abrupt reduction in the slope of the curve. This reduction indicated the onset of interfacial microcracking. As loading gradually increases, the interfacial frictional shear strength is mobilised and therefore microcracking progresses. Debonding of the embedded fibre is the activation of the interfacial frictional

slip (Lin & Li 1997).

5.5.5.3 Post-Peak Gradients of the Load-Displacement Curves

The post-peak slopes of the load-displacement curves gradually reduced up to displacements in the vicinity of 10 mm, indicating a change in the mechanism of fibre/matrix interaction: from fibre debonding and elastic deformation, which occurs at pre-peak conditions, to frictional sliding and major damage of the fibre/matrix interface.

The final gradient of the load-displacement curve was obtained from points beyond the 10 mm displacement point up to 22 mm, the approximate displacement at failure. The interactive mechanisms at this final stage were fibre pull-out and residual frictional resistance at the damaged fibre/matrix interface. Therefore, the final slope approached asymptotic to the horizontal end point at 22 mm, the length of fibre embedded in one side of the specimen.

The variation of the pre-peak and post-peak gradients with ageing for control samples are shown in Figs. 5.26 and 5.27 respectively. The information in these figures is repeated in Figs. 5.28 and 5.29 in which a uniform scale is used for ease of comparison. While the initial slope had a low scatter due to minimal microcracking, the post-peak slopes were characterised by relatively higher scatter mainly due to variable damage and interfacial friction.

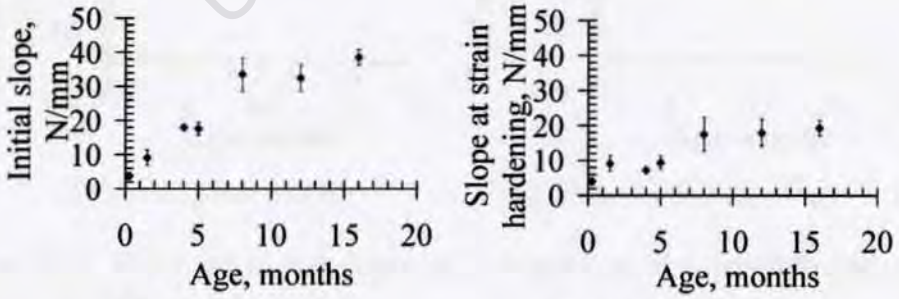

(a) Initial slope (b) Second slope

Figure 5.26: Variation of the slopes of the curves at pre-peak stage for Control samples

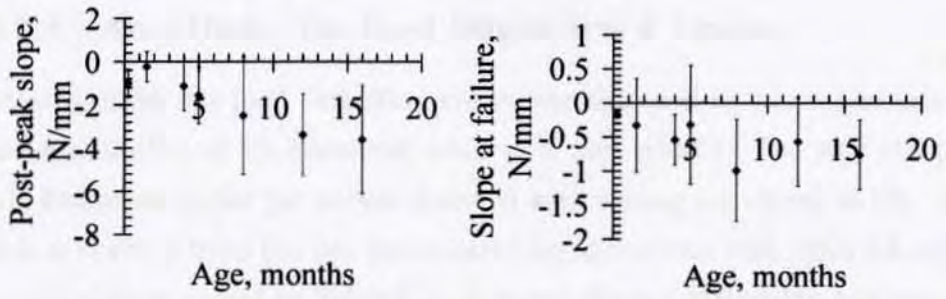

(a) Post-peak slope (b) Slope at failure stage

Figure 5.27: Variation of the slopes of the curves at the debonding stage for Control samples

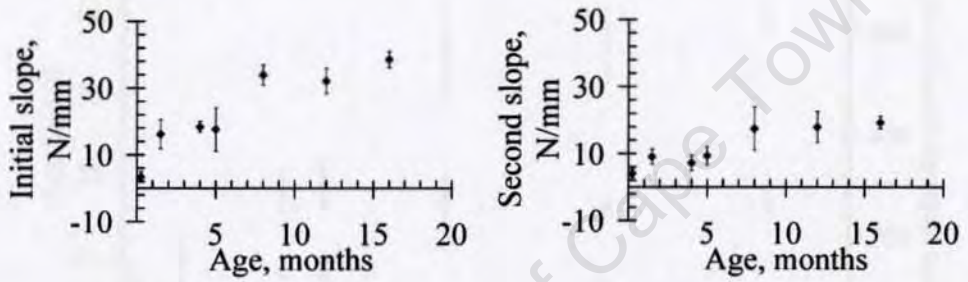

(a) Initial slope (b) Second slope

Figure 5.28: Variation of the slopes of the curves at pre-peak stage for Control samples

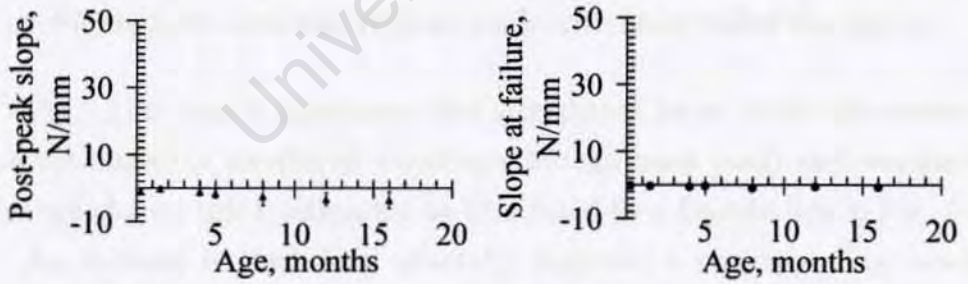

(a) Post-peak slope (b) Slope at failure stage

Figure 5.29: Variation of the slopes of the curves at the debonding stage for Control samples

5.5.5.4 Area Under the Load-Displacement Curves

The area under the load-deflection curve was obtained by numerical integration (summation of 25 elemental areas of 1 mm width). The way the peak loads and areas under the curves changed with ageing are shown in Fig. 5.30, which is derived from the key parameters for specimens with different ageing histories shown earlier in Table 5.5. A more direct relationship between the peak loads and areas under the curves is shown in Fig. 5.31.

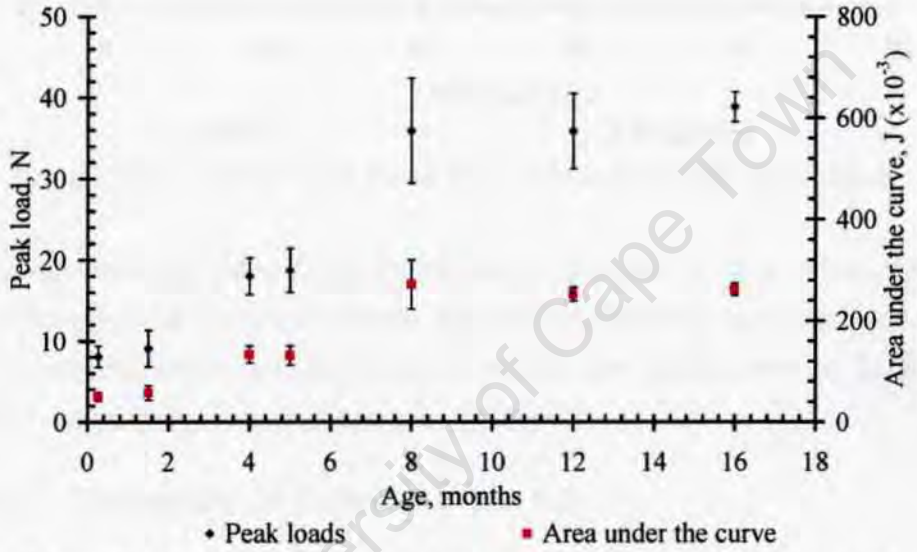

Figure 5.30: Contrast of peak loads with areas under the curves

Fig. 5.30 clearly illustrates that Toughness (area under the curve) is directly linked to interfacial bonding (through peak load) and weathering does not change this relationship as illustrated by a Best-fit line in Fig. 5.31.

An increase in peak load generally indicates a corresponding increase in bonding. The microstructural changes that accompany the increase in bonding were described earlier in section 5.5.5.1. Fig. 5.33 illustrated that substantial microcracking and damage to the interfacial zone that occurs at the post-peak stage of fibre pull-out process is a major contributor to toughness of a sample. It therefore follows from these discussions that the higher the bond, the higher the microcracking at the interfacial zone. Due to instrumental limitations in this research, it was not possible to monitor

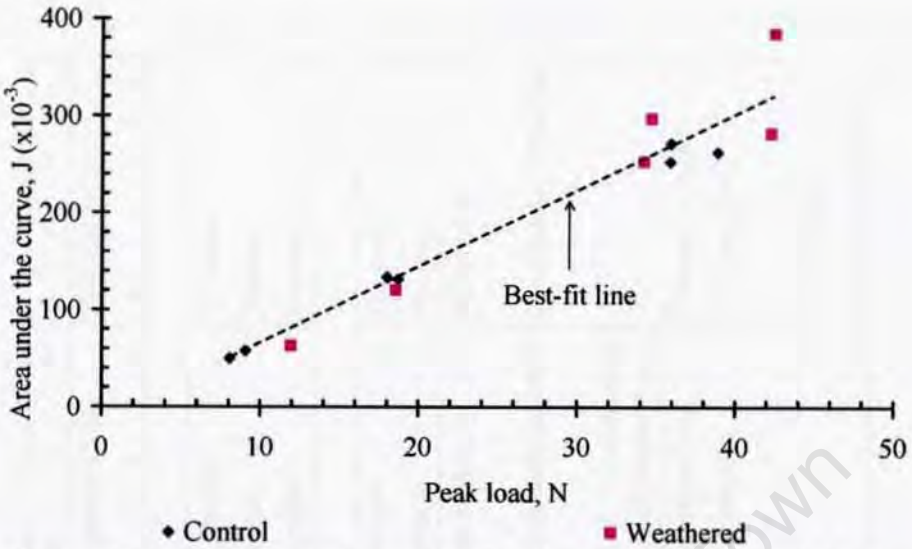

Figure 5.31: Variation of areas under the curves with peak loads

the progression and extent of microcracking. Therefore, for a better insight into this aspect of Textile Concrete, future investigations are suggested.

The mechanisms outlined earlier in section are summarised in Table 5.4 and the key parameters are shown in Table 5.5.

5.5.5.5 Discussion of Tables 5.4 and 5.5

There have been many investigations of plain fibre pull-out-behaviour and these have been comprehensively reported by Bentur and Mindess (Bentur & Mindess 1990), and more recently by Mu and co-workers (Mu et al. 2002). From the literature, the fibre pull-out bond strength is dependent on the fibre and matrix properties, age and geometry of the sample, and the loading conditions.

For cement-polypropylene fibre systems cured for 28 days, a maximum interfacial bond strength of approximately 0.8 MPa has been reported by Wang and co-workers (Wang, Li & Backer 1988) and similar values (between 0.3 MPa and 0.6 MPa) by Li and Stang (Li & Stang 1997).

Table 5.4: Environmental effects on individual fibres, and the pull-out behaviour

Characteristic behaviour	Exposure condition				
	hot/cold (HC)	Wetting and Drying (WD)	Carbonated (C_c	Moderate (NM)	Tropical (NT)
Fibre tensile behaviour					
Fibre failure load	Decrease	No change	Decrease	No change	Decrease
Fibre stiffness E_f	Decrease	Increase	Decrease	Increase	Increase
Fibre toughness	Increase	Decrease	Increase	Decrease	Decrease
*Fibre pull-out behaviour					
Bond strength	No change	No change	Increase	Decrease	Decrease
Toughness	Decrease	Decrease	Increase	Decrease	Decrease
Weakening mechanisms	Fibre softening Matrix micro-cracking	More brittle fibre/matrix interface	Fibre soft-ening	More brittle fibre/matrix interface Other mechanisms not fully understood	More brittle fibre/matrix interface
Strengthening mechanism(s)	Compliant fibre/matrix interface Increase in hydration rate	Matrix densification Favourable hydration conditions	Compliant fibre/matrix interface Matrix densification	Protection from UV radiation	Protection from UV radiation Densification Further hydration

*A summary quantitative Table giving the key parameters is shown in Table 5.5

Table 5.5: Characteristics of average fibre pull-out load-displacement curves

Sample	No. of tests	Peak Load $\pm 2\sigma$, N	Bond strength τ_{max}*, MPa	Slope of the curve: Second, N/mm	Third, N/mm	Fourth, N/mm	Fifth, N/mm	Area under the curve, J (x10^{-3})
8 days	4	8.08±1.30	0.18	4.02	3.39	-1.0	-0.17	49.93±8.00
6 weeks	8	9.08±1.89	0.21	16.18	9.08	-0.23	-0.33	57.51±14.31
4 months	8	18.0±2.26	0.42	18.4	7.21	-1.12	-0.54	133.55±16.82
5 months	4	18.72±2.72	0.44	17.63	9.35	-1.55	-0.32	131.41±19.11
8 months	13	35.92±6.46	0.84	33.91	17.46	-2.48	-0.99	271.55±48.79
12 months	7	35.86±4.64	0.84	32.11	17.93	-3.37	-0.57	252.53±13.68
16 months	5	38.86±1.84	0.91	38.56	19.28	-3.59	-0.76	262.42±12.40
hot/cold (5months)	4	18.56±3.20	0.43	18.76	18.56	-2.80	-0.30	120.02±20.70
wetting/drying (8 months)	6	34.22±4.60	0.78	30.6	17.12	-2.75	-0.608	252.74±34.02
Cabonation (12 months)	5	42.48±7.98	0.99	31.78	14.16	-3.53	-0.98	384.64±72.31
Moderate (NM) (12 months)	6	11.93±3.86	0.24	10.03	4.10	-0.74	-0.34	62.94±20.41
Tropical (NT) (12 months)	5	34.68±5.62	0.81	32.54	17.84	-2.75	-1.24	297.12±38.90
Tropical (NT) (16 months)	6	42.24±4.00	0.98	37.80	21.16	-4.93	-0.89	282.21±26.69

* The calculation of τ_{max} was explained earlier in Chapter 3

These values are comparable to the values of bond strengths shown in Table 5.5 ranging from 0.18 to 0.99 MPa. It is therefore clear that the results of this research are largely consistent with literature in terms of fibre pull-out bond strength. In addition, the various stages in fibre pull-out behaviour are consistent with the findings in the literature (Gopalaratnam & Shah 1987*a*), (Li & Chan 1994), (Li & Stang 1997).

There are typically five main gradients on the load-displacement curves described earlier in section 5.1; the corresponding mechanisms were identified as follows:

i. At the initial loading stage, the shear stresses at the fibre/matrix interface are elastic in nature resulting in a steep positive linear slope indicating that at this stage, the interfacial friction is not yet mobilised (Bentur & Mindess 1990).
ii. As loading progresses, the interface undergoes microcracking and the interfacial friction is mobilised (Bentur & Mindess 1990). The load is resisted by elastic shear stresses and interfacial friction, which is marked by a reduction in pre-peak slope.
iii. The peak load (P_{peak}) is attained when the whole embedded fibre length debonds from the matrix.
iv. Beyond P_{peak} as the fibre progressively pulls out of the matrix, the stresses within the interfacial microstructure are frictional in nature. The interaction of a damaged matrix and fibres causes cracking to propagate in an unstable manner. The magnitude of the negative gradient at the post-peak stage depends on the nature of the microstructure with a steeper slope corresponding to a more brittle interface.
v. As fibre slippage and pull-out progress and the microstructure has undergone substantial damage, cracking at the interfacial zone stabilizes. Therefore, the final slope is asymptotic to the horizontal.

Composite toughness represented by area under the curve in Table 5.5 is composed of: pre-peak microcracking, post-peak debonding, and fibre pull-out. The three processes are illustrated schematically and in bar-chart format

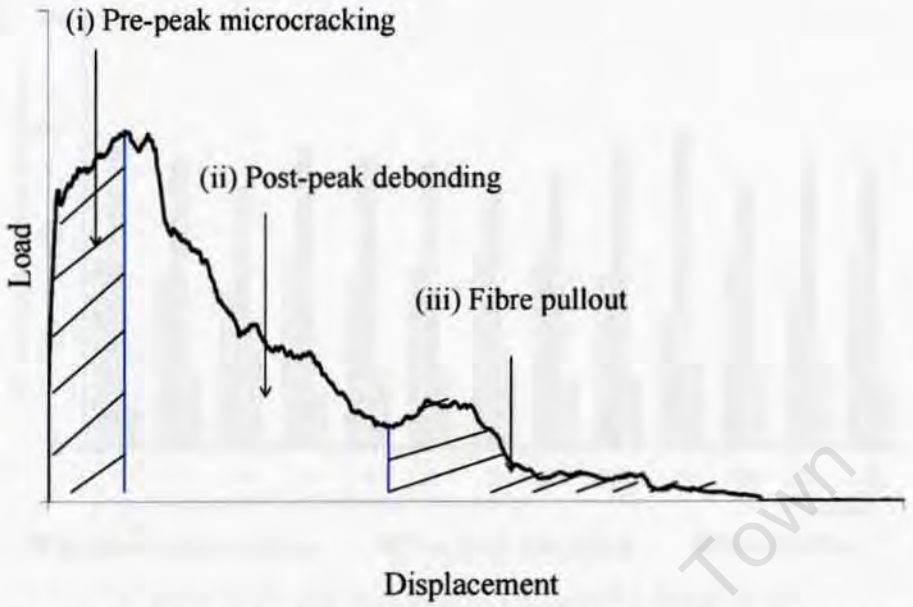

Figure 5.32: Illustration of different regions under a load-displacement curve

in Figs. 5.32 and 5.33 respectively. Fig. 5.33 shows that the highest proportion of energy is expended in debonding the fibre from the matrix to cause the associated damage to the microstructure. In contrast, lower energy is required to pull the fibre out of the damaged interface relative to microcracking an intact matrix.

5.6 Discussion of the Fibre Pull-out Behaviour

A discussion of various aspects that arise from the fibre pull-out test results is presented in this section. The discussion refers to the results shown in Tables 5.4 and 5.5, and Figs. 5.22 to 5.34.

5.6.1 Comparison of Peak Loads With Toughness

A general increase in the average peak loads was observed with ageing under controlled laboratory conditions. The increase was mainly due to development of a stronger fibre/matrix interfacial bond as the mortar matured. The

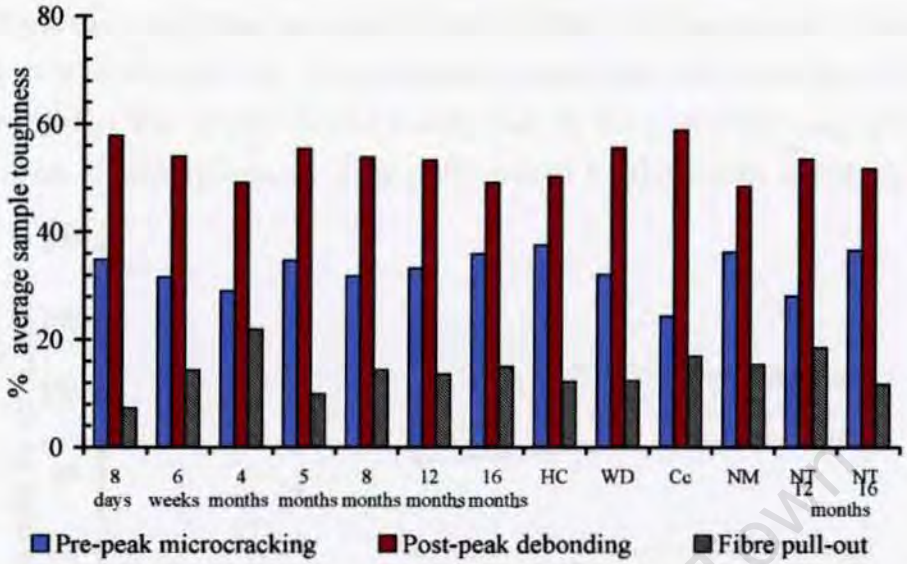

Figure 5.33: Percentages of composite Toughness

rate decreased with ageing and after about eight months, there was very little further increase as shown in Fig. 5.25.

The trend in the average areas under the load-displacement curves (toughness) varied slightly from peak loads in that after about eight months of ageing under controlled conditions, a minor decrease was observed. The differences in the two trends are illustrated by Figs. 5.34(a) and 5.34(b).

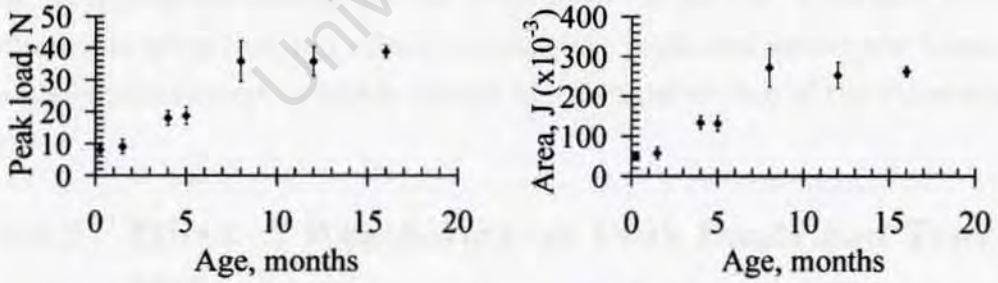

(a) Peak load versus ageing (b) Area under the curve versus ageing

Figure 5.34: Variation of peak loads and Toughness with ageing for Control samples

Although the decrease in toughness after eight months would be insignificant if the statistical variation of the data is taken into account, by separat-

ing the areas into initial, pre-peak cracking region, and post-peak debonding stage, it is illustrated that the reduction in toughness that was observed after eight months was mainly due to a reduction in the post-peak area, and was indicative of embrittlement. This is illustrated by the trends in Fig. 5.35.

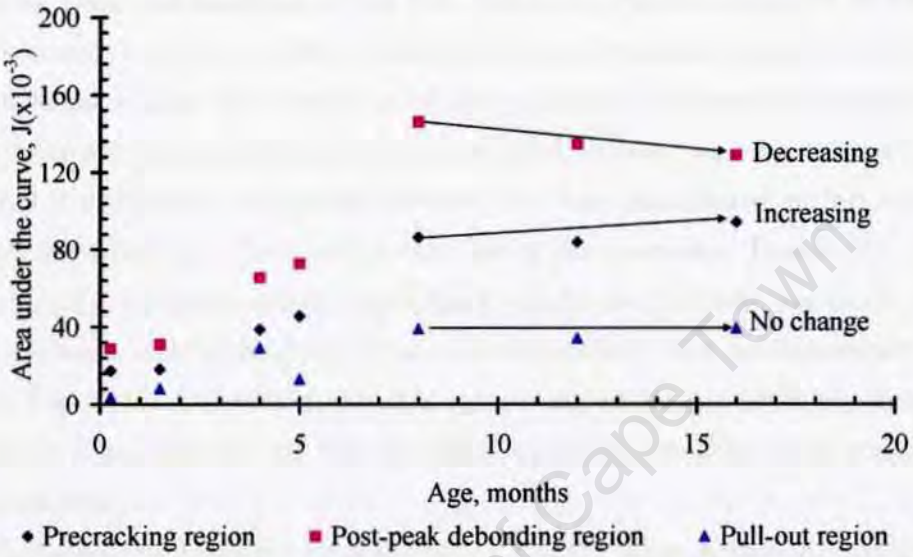

Figure 5.35: Variation of areas under different regions on the load-displacement curves

The area under the load-displacement curves represents the work done in debonding and pulling out the fibres from the matrix. Therefore, the reduction in areas that was observed from eight months of ageing was a sign of some embrittlement, possibly caused by effects of drying of the microstructure.

5.6.2 Effect of Weathering on Peak Loads and Toughness

With a denser matrix, a stronger bond and increase in the peak load will result as clearly shown in Fig. 5.30. It was observed that variations between the peak loads for specimens weathered by accelerated ageing in the laboratory, and the comparable controls, did not follow a clearly defined trend. For example, there was a nominal decrease of approximately 2 percent in the

peak loads after exposure of specimens to 100 hot/cold cycles, which was not considered significant. Similarly, although cyclic Wetting and Drying of the specimens was effective in matrix densification, it did not cause a significant change in the average peak loads.

The main mechanisms at the post-peak and failure stages on the load-displacement curves were the combined effects of complex processes involving interactions within the matrix particles (a degree of internal fracture) and fibre/fibre frictional effects at the micro level. These processes caused substantial fibre/matrix interfacial damage that was manifested in failure that always occurred by pull-out from one side of the specimen. Due to the interface damage, the proportion of specimen toughness that was due to the final fibre pull-out was much lower than the debonding part as illustrated earlier in Fig. 5.35. Samples underwent minor embrittlement after exposure to cyclic hot/cold and wetting/drying which was manifested in minor reduction in toughness.

Carbonation exposure caused matrix densification giving strength gain of approximately 18 percent in the bond. In addition, an improvement in toughness, which was more than what was observed in the other accelerated ageing mechanisms, characterised the fibre pull-out of specimens aged in a CO_2-rich environment. The change was attributed to deposition of carbonates in the matrix pores, and possibly due to a change in interface densification. It could be argued that CO_2 penetrated up the fibre/matrix interface relatively easily. Indeed, from the SEM images shown in Fig. 6.6 in the subsequent Chapter, carbonate species were observed all along the fibre interface. A phenolphthalein test (see section 4.5.4 in Chapter 4) similarly indicated a fully carbonated specimen after a six month exposure. An obvious observation is that the beneficial effects of carbonation are in the matrix and not in the fibres.

Specimens weathered naturally in a moderate climate (NM) suffered significant loss in strength as illustrated in Fig. 5.19, despite increased matrix densification. The weather in Cape Town during the exposure period was typ-

ically moderate but strong winds with wet and dry seasons were experienced throughout the year. The yearly average minimum and maximum temperatures were 11 °C and 41 °C respectively as shown in Table 4.8 in Chapter 4, and thus the samples were subjected to an average of 30°C temperature differential for the exposure period of close to one year. These conditions were comparable to the hot/cold (HC) cycles in the ageing facility. Therefore, the poor fibre pull-out performance observed in NM-weathered samples was not well understood and further investigations are to be suggested.

The load-displacement behaviour of specimens weathered by natural exposure in a tropical (NT) environment showed a different trend from NM-weathered samples, and this difference is clear from Fig. 5.20. A similar trend was observed for NT exposed specimens that were tested after 16 months of exposure in which an increase in the average peak load of approximately 10 percent was observed. The fibre pull-out behaviour of NT weathered specimens illustrated the ability of the matrix to sufficiently protect the embedded fibres against a medium altitude climate in Nairobi (in the tropics), which was attributed to an improvement in the fibre/matrix interaction despite serious embrittlement in the individual weathered fibres. From the results of the fibre pull-out test, no signs of embrittlement were observed in the pull-out specimen that was attributable to loss in fibre strength.

5.6.3 Effect of Weathering on Slopes of Load-Displacement Curves

The slopes referred to as "Third" and "Fourth" in Table 5.5, which correspond to slopes labeled C and D respectively in Fig. 5.13, are used for the discussion that follows.

The "Third" slope leading to the peak load (C) represents the pre-peak stage when interfacial shearing stresses are being mobilised along the fibre/matrix interface. At this stage, although the interface is undergoing significant micro-cracking, the fibre is still bonded to the matrix. The results shown in Table 5.5 indicate that cyclic heating and cooling in a dry environ-

ment increased the shearing stresses slightly along the interfacial zone. This phenomenon was not observed in the other accelerated ageing environments in which the presence of moisture acted as a lubricant within the interface microstructure and hence reduced the interfacial shear stresses. Conversely, accelerated ageing caused embrittlement to the samples and this was indicated by a general increase in the post-peak ("Fourth") slopes.

5.7 Summary of the Results of Fibre Pull-out Tests

There have been many characterisations of single fibre pull-out behaviour and the results of this research are largely consistent with literature particularly in the load-displacement curves, and bonding in polypropylene-cementitious matrix systems. What is new in this work is the influence of ageing on the physical and chemical processes that govern the fibre pull-out behaviour of Textile Concrete. The knowledge gained from fibre pull-out tests is presented in form of a "key summary" as follows:

- The mechanisms of cement hydration at early ages, and drying shrinkage at later ages influence fibre pull-out bond strength in a similar manner to mortar strength. A denser and stronger matrix means higher fibre/matrix bond strength.
- The mechanical behaviour of embedded PP fibres is different from the plain fibres, and varies according to the environmental conditions. The most significant change that was observed was the reduction of the effects of sunlight on fibre pull-out tests. The fibres are sufficiently shielded by the matrix from the damaging effects of UV irradiation .
- Various slopes on a load-displacement curve represent the effects of different mechanisms: initial slope represents an intact interface, second slope represents microcracking and mobilisation of shearing stresses along the interface, fibre debonding and interface damage is manifested

by a negative post-peak slope, and the slope at final failure represents pulling out of a fibre from the damaged matrix.

- The mobilisation of interfacial friction that takes place at the pre-peak stage is associated with microcracking of the fibre/matrix interface, which influences the bond.
- The more brittle the microstructure, the steeper the post-peak slope.
- During ageing, the following competing mechanisms contribute to the fibre pull-out behaviour: densification of the matrix and the fibre/matrix interface, microcracking of the microstructure, embrittlement, lubrication of the interfacial shearing stresses.
- A cyclic hot/cold environment induces drying shrinkage, embrittlement and microcracking of the matrix resulting in reduction in bonding.
- Moisture at the interfacial zone act as a lubricant resulting in reduction in the interfacial shearing stresses and fibre/matrix bonding.
- A CO_2-rich environment causes the highest increase in densification of the microstructure and gain in the interfacial bond strength due to deposition of carbonate species and subsequent densification of the microstructure.
- In general accelerated ageing causes matrix embrittlement.
- Fibre pull-out behaviour is governed by different competing mechanisms depending on the environmental conditions. For example, whereas matrix embrittlement occurred after exposure to all regimes under study in this research, it did not cause a loss in bond strength in carbonated samples implying that there was a contributory effect of other competing mechanisms.

5.8 Results of Tensile Tests on Composite Textile Concrete Specimens

The objectives of tensile testing of composite specimens were:

- To provide the basic generalised description of stress-strain behaviour.

- To identify the mechanisms at various stages up to final failure.
- To characterise the stress-strain (σ-ϵ) behaviour for representative samples from each environmental regime.
- To synthesise an understanding of the failure processes between the individual fibres, fibre pull-out, and composite tensile behaviour.
- To draw together the "key summaries" from each major set of tests, and look for the links and relationships.

The experimental process was developed from trial tests on specimens with a "Short" geometry (see Fig. 4.10 in Chapter 4). These specimens had a gauge length of only 25 mm which proved to be too short to facilitate the formation of enough number of cracks for meaningful crack quantitification, an aspect of multiple cracking that was part of this research. However, the "Short" samples underwent multiple cracking and failure was by crack localization and fibre rupture. Multiple cracking is a useful mechanistic property because it characterises the strain hardening capacity of the composite (Naaman & Reinhardt 2006). Conversely, "Long" specimens underwent multiple cracking (with several cracks on the gauge section) prior to final failure which was by crack localisation and fibre rupture. The stress-strain (σ-ϵ) curves for the two types of specimens illustrating the size effect are shown in Fig. 5.36.

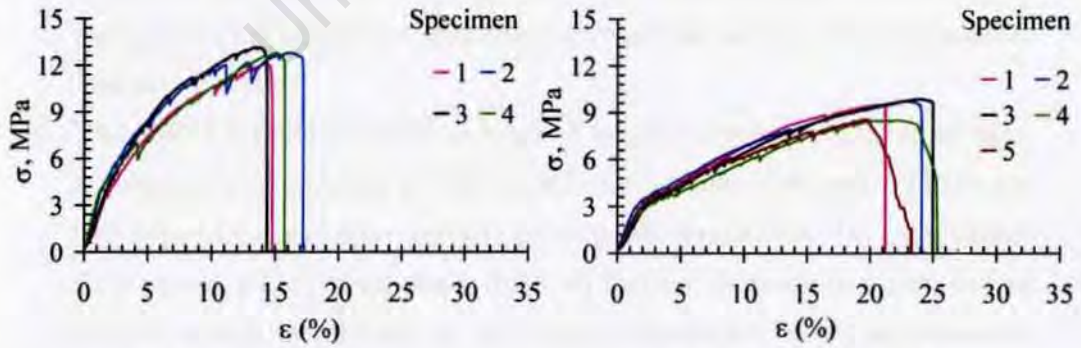

(a) Short specimens (b) Long specimens

Figure 5.36: Tensile behaviour of eight month old control specimens with gauge lengths (a) 25 mm and (b) 125 mm

5.8.1 Key Regions on Stress-Strain Curves

Stresses and strains at key points on the σ-ϵ curves were a useful means of characterising the overall tensile behaviour of TC. The average values of the key parameters for samples of ages ranging between eight and 24 months are shown in Table 5.6.

The stress-strain curve is characterised by six stages (with reference to Fig. 5.36) as follows:

i. The initial linear stage prior to matrix cracking. Since the strains at this stage are too low (below 0.02 percent), they are not shown on a typical σ-ϵ curve.

ii. A steep ascending linear stage up to about 2 percent strain that is characterised by microcracking, which is essentially the development of fine superficial cracks characterising composite behaviour rather than a simple matrix property.

iii. The region beyond about 2 percent strain is marked by a deviation of the σ-ϵ curve from linearity due to development of macro cracks. A macro crack is a crack that transects the specimen as opposed to microcracking which is fine superficial cracking (Naaman & Reinhardt 2004).

iv. After the first macro crack, a specimen typically undergoes strain hardening due to propagation of more macro cracks as the material exhibits "pseudo-ductility".

v. The end of pseudo-ductility is marked by peak stress and strain without an appreciable amount of "fibre pull-out" being observed. There are two types of composite properties at peak conditions: (a) composites that attain a high peak stress with no further increase in strain before failure, which is referred to as "composite failure", (b) achievement of relatively lower peak stress but a subsequent increase in strain at constant stress, or a progressively decreasing slope of the σ-ϵ curve up to final failure. This behaviour characterises composites that achieve the "full capacity" of multiple cracking.

vi. Final failure was caused by the opening up of a critical crack (crack localisation) and fibre rupture. This mechanism differed from pull-out tests in which the mechanism at failure was fibre pull-out implying that it was only the pre-peak behaviour of fibre pull-out tests that was relevant to the composite tensile behaviour.

5.8.2 General Description of Tensile Behaviour

As it was not possible to achieve saturated crack densities in Short samples, Long specimens were chosen for the analysis of the tensile behaviour of TC, and the behaviour of only Long specimens is dealt with subsequently.

Typically each curve had a linear portion up to matrix cracking, followed by a strain-hardening branch where multiple cracking developed.

An initial linear stage in cement-based materials occurs at low strains of less than 0.02 percent (Neville 2002), which was too low to be represented on the overall σ-ϵ curves in Fig. 5.36. Therefore, only the micro-cracking and multiple cracking stages will be considered in the analysis that follows. The translation between microcracking and multiple cracking stages will be referred to here as the "end of linear region".

Multiple cracking accounted for the strain hardening behaviour of the composite. An important feature of the σ-ϵ curves at this stage was the gradient both during multiple cracking and also just before final rupture. The key regions on the tensile stress-strain curve, and a general description of the mechanisms in these regions are illustrated in Fig. 5.37.

Samples that achieved the full multiple cracking capacity were characterised by curves which were asymptotic to the horizontal just before final failure. On the other hand, specimens exhibiting the so called composite failure exhibited steep σ-ϵ curves up to final failure (Naaman & Reinhardt 2006), (Kabele 2003*b*). The gradients of the curves at the multiple cracking stage varied with ageing and the environmental conditions. These variations and their relationships to other properties of the σ-ϵ curves form the basis of the discussions to follow. The key parameters on the σ-ϵ curves are shown in

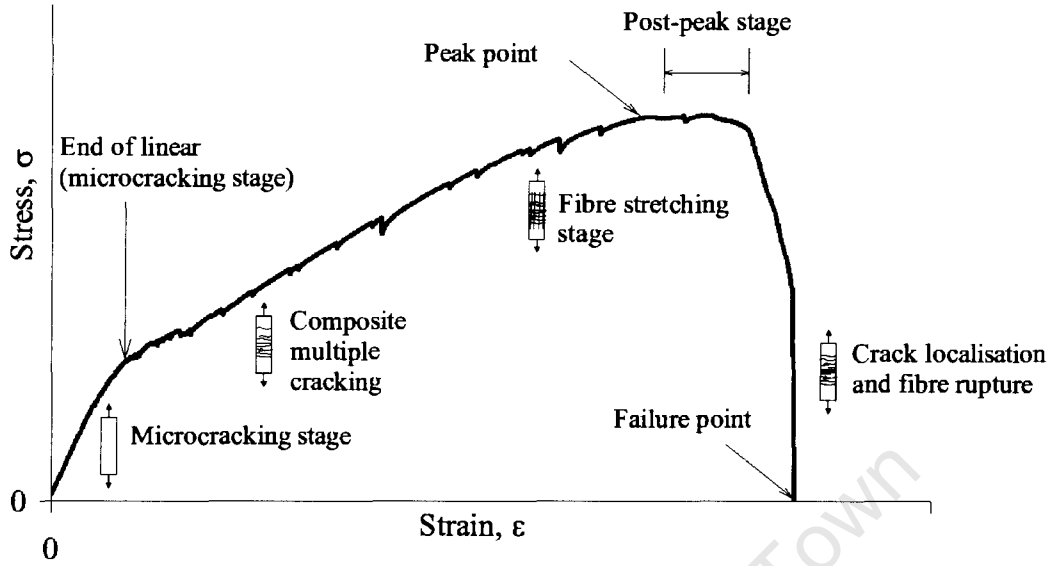

Figure 5.37: General description of the stress-strain behaviour

Table 5.6.

The strains at failure were fairly similar for all samples apart from the 16 month and Industry sample in which failure strains exceeding 30 percent. The high failure strain in the 16 month old sample, which seemed anomalous to other age specimens, was due to development of fine branching-off cracks in the vicinity of the major cracks which contributed to further extension of the specimens. On the other hand, a high failure strain in Industry samples was due to development of several closely spaced cracks that were fairly evenly distributed over the gauge length of the specimens.

The other key observation from Table 5.6 was that for control samples, there was an increasing trend in toughness with ageing. However, weathering under different environments causes embrittlement and loss in pseudo-ductility.

5.8.3 Effect of Hot/Cold Environment

Specimens weathered by cyclic heating and cooling demonstrated some increase in ductility and minor decrease in strength. There was also greater variability in failure strains as shown in Fig. 5.38(b).

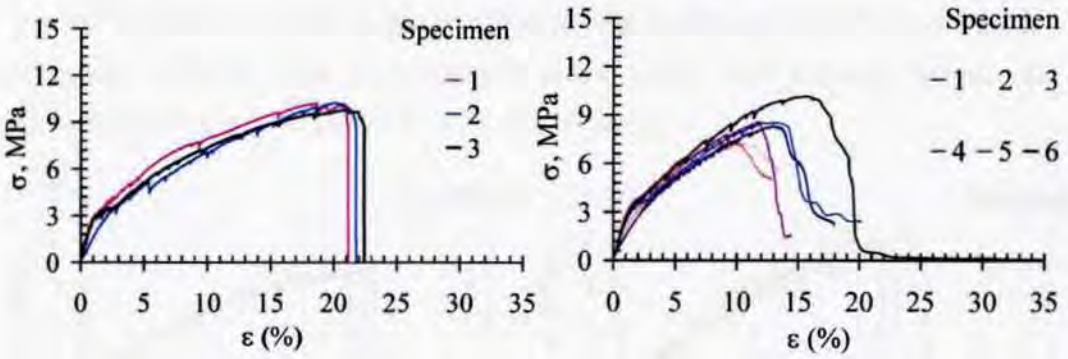

(a) Control sample (b) HC weathered

Figure 5.38: Behaviour of specimens after 12 months of ageing - hot/cold samples

The specimens displayed some post-peak ductility before failure in a manner similar to failure behaviour of the weathered HC fibres illustrated earlier in Fig. 5.7(a). The results also show that HC leads to a drop in peak loads, elongation, and the scatter goes up. The composite behaviour shows a contra-effect to fibre ductility which suggests that the matrix protects the fibres from direct effects of cyclic heating and cooling, hence the embedded fibres did not undergo the same degree of softening as was observed in plain fibres after exposure (see Fig. 5.7). Under this hypothesis, the composite behaviour is influenced more by matrix properties than the fibres.

The gradients of the σ-ϵ curves show that the weathered samples achieved the full multiple cracking capacity (Naaman & Reinhardt 2006). It was also observed that before failure occurred, fibres bridging the crack stretched excessively, a behaviour which was attributed to fibre softening. As loading progressed, the localised crack continuously widened until the stretched fibres failed by rupture.

5.8.4 Effect of Wetting/Drying on Tensile Behaviour

The tensile stress-strain behaviour after cyclic wetting/drying differed from hot/cold exposure particularly in the final failure stress, and strain hardening capacity. This is illustrated by a brittle failure in Fig. 5.39 that was char-

acteristic of the final fibre rupture. The tensile behaviour of WD-weathered composites differed from the relatively more ductile and variable failure of HC-weathered samples illustrated in Fig. 5.38(b).

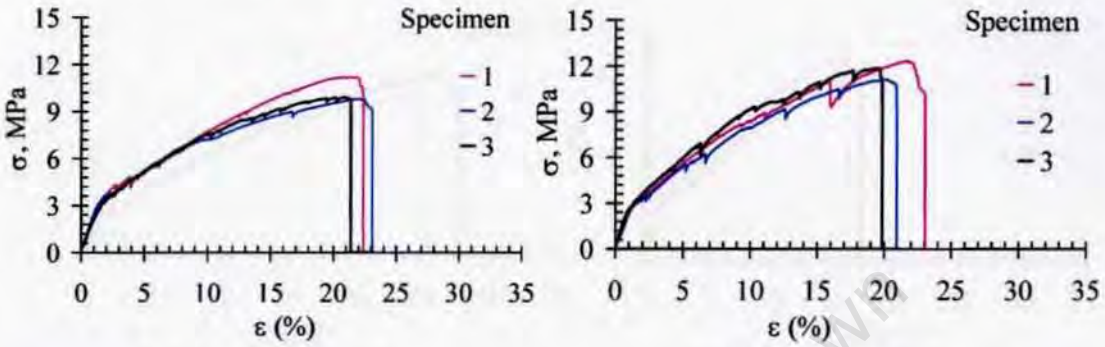

(a) Control sample (b) WD weathered

Figure 5.39: Behaviour of specimens after 14 months of ageing - wetting/drying samples

An improvement in the composite strength after weathering was observed as illustrated by a steeper σ-ϵ curve in Fig. 5.39(b) compared with Fig. 5.39(a). The full multiple cracking capacity was also achieved in WD-weathered samples, which was consistent with the behaviour of the weathered fibres and fibre pull-out specimens. A slight increase in fibre stiffness was observed in the weathered samples, and the effects of matrix embrittlement were manifested by reduction in toughness in the fibre pull-out behaviour (see Table 5.3).

An increase in the gradients of the σ-ϵ curves, and effectively in the composite strength, demonstrated that the wetting/drying environment, which essentially involved moisture movement within the specimen, had beneficial effects in that the samples exhibited multiple cracking prior to failure. The performance was similar to a class of fibre reinforced cementitious composites referred to as High Performance Fibre Reinforced Cementitious Composites (HPFRCC) which undergo multiple cracking and strain hardening, with failure occuring after the tensile load is fully transferred from the matrix to the fibres (Naaman & Reinhardt 2006).

5.8.5 Effect of Carbonation

The results of the tensile behaviour of 16 month old samples are shown in Fig. 5.40.

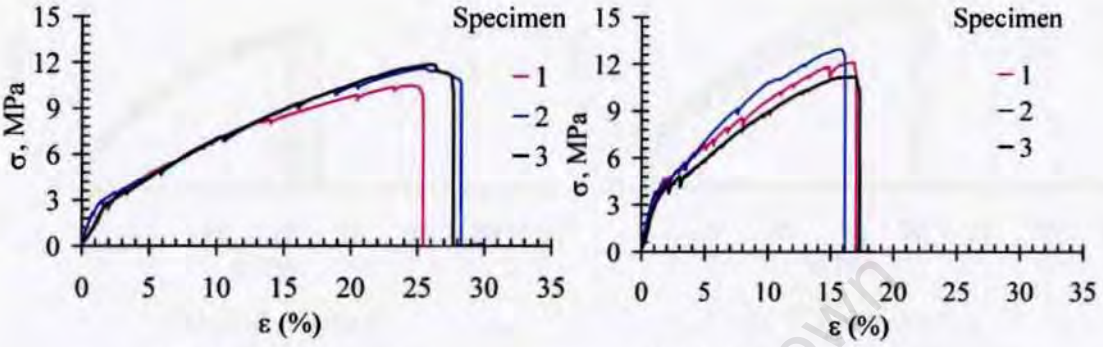

(a) Control sample (b) Carbonated specimens

Figure 5.40: Behaviour of specimens after 16 months of ageing - Carbonated samples

With regard to the gradients of the σ-ϵ curves at the multiple cracking phase, the behaviour of carbonated samples was similar to HC and WD-exposed samples in that the curves were steeper than for comparable control samples, and hence higher stresses were obtained for the same strains. However, carbonation resulted in the highest change in failure strength as shown in Fig. 5.40. This change was attributed to a remarkable increase in matrix densification as well as the bonding capacity (see Fig. 5.17 for fibre pull-out behaviour), and the combined effect of these two is demonstrated in a stronger composite. A brittle failure occurred with minimal post-peak ductility. In High Performance Fibre Reinforced Cementitious Composites (HPFRCC), this behaviour is attributed to attainment of the composite strength before the full multiple cracking capacity is exhausted (Naaman & Reinhardt 2006).

5.8.6 Effect of Natural Environment Weathering

In a manner similar to the behaviour of samples weathered by accelerated ageing, samples exposed to natural climates exhibited typical strain harden-

ing and multiple cracking behaviour as shown in Fig. 5.41. The σ-ϵ behaviour of control samples was shown earlier in Fig. 5.38(a).

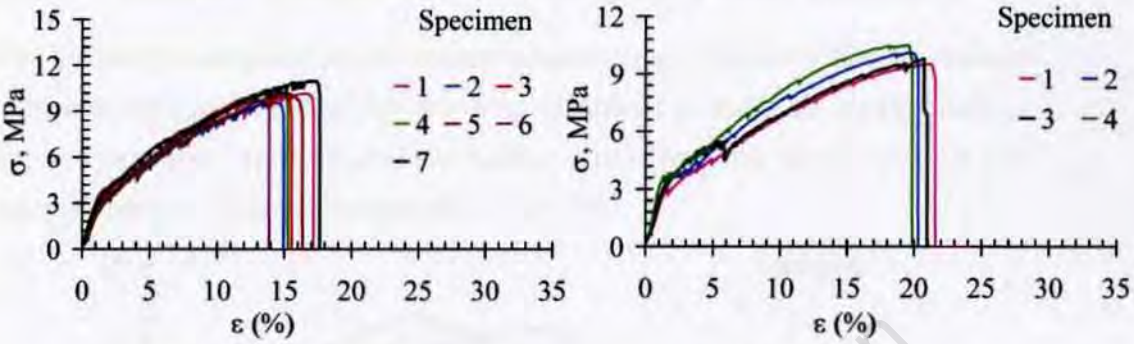

(a) NM exposed (b) NT exposed

Figure 5.41: Tensile behaviour of naturally weathered samples at age 12 months

The behaviour of specimens exposed to a moderate climate was in contrast to the poor performance in fibre pull-out behaviour (Fig.5.19(a)), again motivating the need for further investigation into the poor performance of fibre pull-out tests on NM-weathered samples.

The behaviour of samples weathered in a "tropical" (high altitude) climate (NT) was similar to NM samples particularly in strain hardening behaviour. However, NT-weathered samples developed the full multiple cracking capacity, which is illustrated by reduction of the slope of the σ-ϵ curve before final failure by fibre rupture.

Weathering in natural climates combines the ageing regimes that were simulated in the laboratory namely, hot/cold, wetting/Drying and carbonation. Measurements of the carbonation depth (see section 4.5.4.1 in Chapter 4) indicated that samples were carbonated to depths of less than 2 mm. Therefore, carbonation in natural environments was not considered to have contributed significantly to the mechanical behaviour. Although the natural exposure period was limited, the results were nevertheless useful in that the general tensile σ-ϵ behaviour including the end of the elastic region and multiple cracking stages were clearly manifested in the naturally weathered

samples.

5.8.7 Tensile Behaviour of Samples From Industry

The Industry material (I) was in many respects quite different from laboratory-prepared samples. Firstly, the material exhibited remarkable strain hardening and multiple cracking and the failure strain was the highest among the samples tested. This is illustrated in Fig. 5.42.

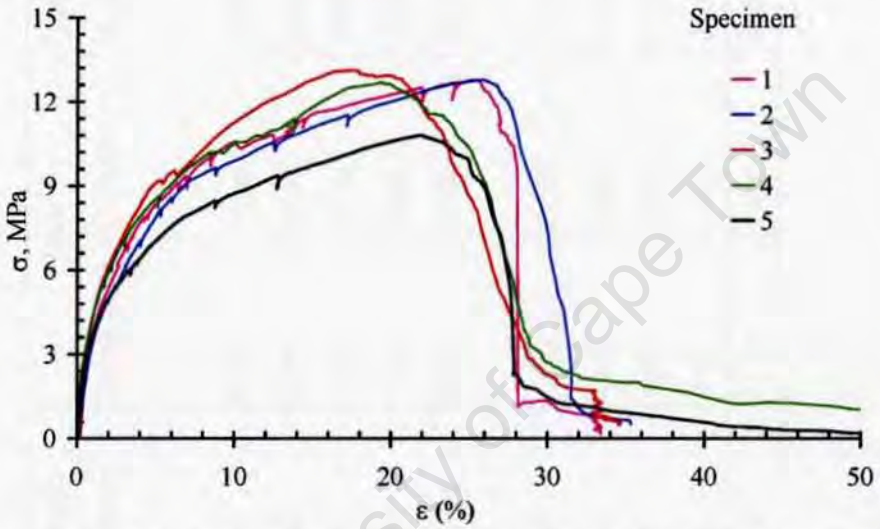

Figure 5.42: Behaviour of samples from industry (at age of 24 months)

Samples from Industry were characterised by high ductility with failure occurring at strains in the vicinity of 30 percent. Secondly, the samples developed closely distributed fine cracks over the gauge areas (achieved full multiple cracking capacity) which indicated that the applied tensile load had been fully transferred to the fibres (achieved full multiple cracking capacity) before crack localisation as manifested by a reduction in the the slope of the σ-ϵ curves near the peak stress.

Industry samples were four-layered with a thickness of approximately 6 mm in contrast with six-layered laboratory-produced samples with an average thickness of 8 mm. This meant that the two types of samples had different fibre volume fractions (V_f), which could have accounted for the difference in σ-ϵ behaviour.

Table 5.6: Key parameters of the stress-strain curves of composite specimens

Sample	Age, months	No. of tests	End of linear region		Peak		% Strain at failure	Area under the curve, J/m
			Stress, MPa	% Strain	Stress, MPa	% Strain		
Control	Earlier ages*							
Control	8	5	3.22	2.15	8.95	20.00	23.82	377.50
Control	12	5	3.25	2.00	9.91	20.34	22.34	413.00
Control	14	3	3.23	1.88	10.26	21.00	22.00	407.10
Control	16	3	2.83	1.98	11.22	25.00	30.07	521.40
Hot/Cold	12	3	3.77	2.19	8.73	12.00	20.04	299.68
Wetting/ Drying	14	3	2.99	1.36	11.43	19.00	21.00	397.53
Carbonated	16	3	3.95	1.79	12.33	15.95	17.95	320.56
Moderate	12	5	3.93	1.95	9.68	12.96	17.97	279.63
Tropical	12	4	3.35	1.51	9.78	18.97	20.96	351.22
Industry	24	5	2.91	0.49	12.08	19.96	30.29	695.30

Average values are stated within 15 percent of error

*No tests were carried out on samples at earlier ages

The matrix in samples from Industry ("I") had different properties from the laboratory-produced samples as illustrated by a relatively low strain at the end of the linear portion shown in Table 5.6. This low value was indicative of a higher level of microcracking in "I" samples than in the laboratory-produced samples.

The matrix in "I" samples was different from the mix used in this research work. The Industry utilises a premix (locally referred to as Cemcrete) specially manufactured for use in Textile concrete. The mix proportions together-with refined laminate production techniques contributed to the excellent pseudo-ductility observed in Industry samples. The role of the matrix composition in development of a "compliant" microstructure came out clearly from the results of the Industry samples.

The results illustrate the potential for production of TC composites with performance designed to suit a desired demand. The observations in Table 5.6 bring out certain key issues. Firstly, the stresses at the end of the linear region, marking the formation of the first macro crack, were remarkably similar and did not demonstrate much sensitivity to ageing or weathering. This could be explained by the fact that at the end of the linear stage, all composites had undergone substantial microcracking and the stress at this first "through" crack depended on the degree of microcracking rather than on the matrix strength. On the other hand, the strain at the end of the linear region reduces with age and weathering indicating hardening of the matrix and reduction in composite ductility.

5.8.8 Analysis of Results of Composite Tensile Tests

Typical σ-ϵ curves for control and weathered samples were obtained from averages of the curves in Figs. 5.38 to 5.42 and are presented as sets of "Composite curves" in Figs. 5.43 and 5.44.

From the results shown in Figs. 5.43 and 5.44, the following criteria were used in describing the failure of the specimens:

- Achievement of maximum composite strength (σ_c) but without the at-

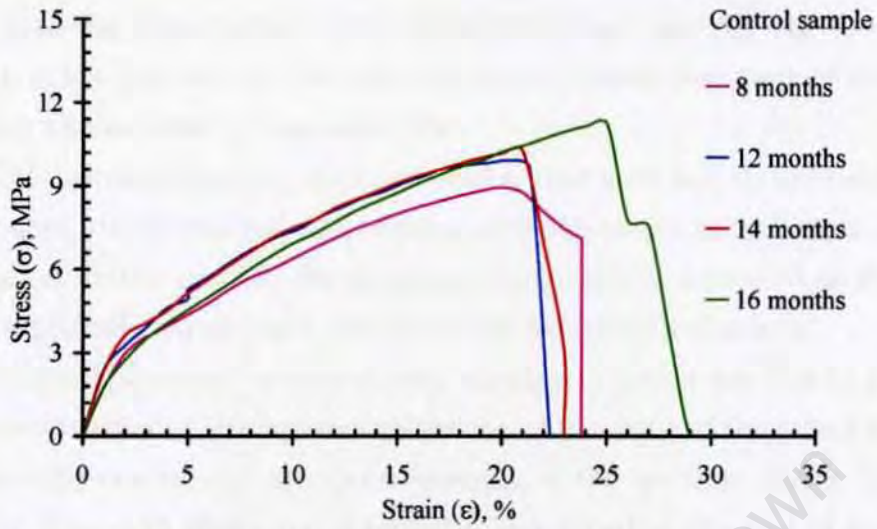

Figure 5.43: Typical stress-strain behaviour for control samples

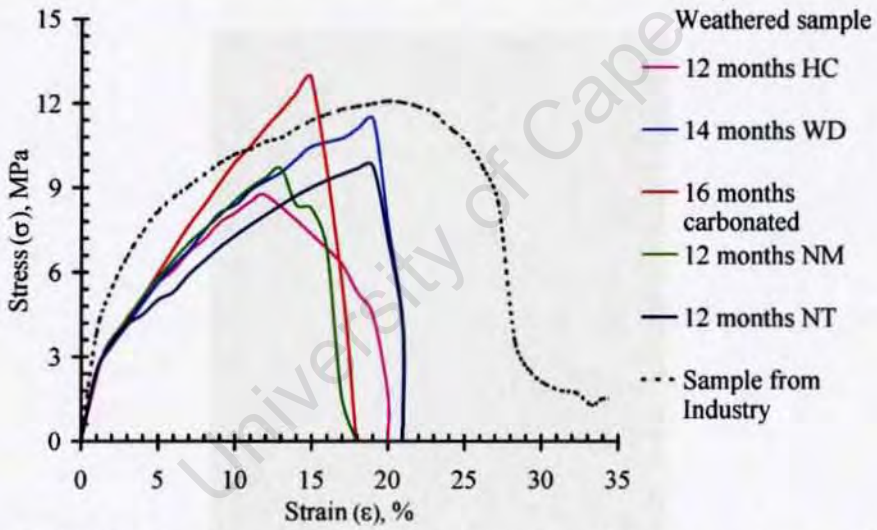

Figure 5.44: Typical stress-strain behaviour for different ageing conditions

tainment of full multiple cracking state.

- Attainment of full multiple cracking capacity with the failure mechanism being excessive opening up of cracks and exceeding of the fibre bridging capacity at a localised crack.

Beyond the linear region, the load is no longer carried predominantly by the matrix but rather it is distributed to the fibres as well. As the loading increased beyond approximately 3 MPa, there is deviation from linearity, and

also increasing participation of the fibres in the load carrying capacity. This stage is a key property of the material since it marks the onset of multiple cracking and so-called pseudo-ductility.

With increased loading, multiple cracks, that were not always uniformly distributed, developed and perpetuated over the entire gauge length of the specimens. In the process, the composite progressively extended as the material exhibited characteristic pseudo-strain hardening behaviour.

The gradual stress increase during multiple cracking was due to a complex combination of mechanisms consisting of straining of the intact matrix between the cracks, and opening/reopening of the multiple cracks (Kabele 2003*b*). Fig. 5.45 shows the cracks that developed at the end of multiple cracking in a typical TC specimen.

Figure 5.45: Typical very fine cracks on a post-loaded sample (scale on the extreme right is in cm and mm)

The figure illustrates the variability in crack spacing, which varies from very wide spacing of between 20 and 40 mm reducing to less than 10 mm. By comparison with Fig. 5.46, "I" specimens developed fine cracks at average

spacings of 4.8 mm. The figure further illustrates fibre elongation within the cracks as well as signs of fibre debonding from the matrix. The typical strain in a specimen with cracking pattern exemplified by Fig. 5.45 was approximately 20 percent.

Figure 5.46: Typical cracks on a post-loaded Industry sample (scale on the extreme right is in cm and mm)

The end of strain hardening leads to a peak condition of maximum post-cracking stress and strain. At the peak conditions, one crack becomes critical due to crack localisation caused by fibre elongation and local damage, opening of the cracks and mechanisms involving crack bridging by the fibres. These micro-mechanisms are typical of so-called High Performance Fibre Reinforced Cementitious Composites (HPFRCC) (Naaman & Reinhardt 2006).

Specimen failure is by ultimate fibre rupture as shown in Fig. 5.47, and the final failure stress is similar to failure stress of the fibres. The loads and strains at the peak and failure points were useful in computation of areas under the curves, which are a measure of toughness of the specimens.

5.8.8.1 Gradients of the Stress-Strain Curves

The gradient before initiation of the micro-cracks, which represents the modulus of elasticity of the matrix E_m, was not computed due to equipment

Figure 5.47: Crack localisation at final failure

limitations in precise measurements below 0.02 percent strain. However, the gradients of the σ-ϵ curves at the microcracking and multiple cracking stages of loading were readily computed, which represent the composite modulus of elasticity E_c.

The gradients of the curves at the microcracking stage E_c varied with ageing as illustrated in Fig. 5.48. From the figure, E_c varies between 0.5 GPa and 1.3GPa, which is very low in comparison with a plain matrix E_m of between 5-10 GPa (Hannant 1978), (Naaman & Reinhardt 2006), which indicates that the specimen is heavily microcracked at this stage.

The onset of multiple cracking occurred at strains of between 1 and 2 percent and the modulus of the composite is comparable to plain fibres that was measured as 1077 MPa (see section 5.4). At this stage, the composite load carrying capacity ceases to be matrix dominated but rather, the load is distributed into the fibres bridging the cracks resulting in the so called strain hardening behaviour which is associated with the so called multiple cracking. During strain hardening, the gradient of the curve progressively decreases with loading up to the peak conditions. The rate of this decrease de-

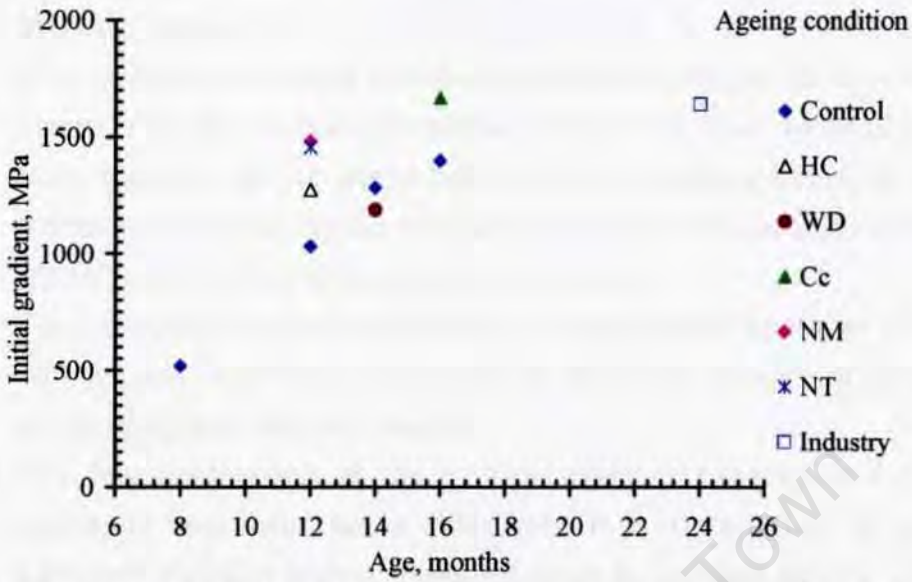

Figure 5.48: Gradient of the stress-strain curve at microcracking stage

pends on the extent of cracking (crack density and crack widths). Therefore, the gradient at multiple cracking and failure stages are composite material properties. The gradients are discussed further in section 6.4 in Chapter 6.

5.9 Summary of Stress-Strain Behaviour

- The tensile stress-strain behaviour of Textile Concrete is characterised by six main stages of loading: initial linear stage at low strains of less than 0.02 percent, microcracking stage which is between approximately 0.02 percent and 2 percent strain, strain hardening stage when the material exhibits pseudo-ductility, peak conditions, post-peak stage, and final failure.
- The mechanisms at different loading stages are: pure matrix tensile behaviour at low strains of less than 0.02 percent, microcracking after the matrix cracking strength is exceeded, development of the first crack which traverses the sample depth, which is accompanied by transfer of loading from the matrix to the fibres, propagation and widening of macro cracks up to peak conditions, crack localisation, and final failure

by fibre rupture.

- The mechanism of crack localisation involves widening of an existing macro crack due to fibre debonding at the crack plane (depending on bond strength) and/or stretching of the fibres bridging the crack. This mechanism accounts for the decreasing stress level that is observed after the full multiple cracking capacity is attained.
- The post-peak composite behaviour is characterised by either (a) full development of multiple cracking or (b) brittle failure upon attainment of the composite failure strength.
- The full development of the multiple cracking capacity is a strain hardening behaviour that is aimed for. It is characterised by minor post-peak ductility and/or stress reduction before final failure. This is consistent with the behaviour of High Performance Fibre Reinforced Cementitious Composites (Kabele 2003*a*), (Li, Wang & Wu 2001) described earlier in section 2.7.4 in Chapter 2
- Exposure to hot/cold, wetting/drying environments, and a high altitude climate in the tropics yield Textile Concrete specimens that exhibit multiple cracking behaviour.
- The strong fibre/matrix bonding and densification of the matrix observed after exposure of TC samples to to a CO_2-rich environment translates into loss in post-peak ductility (over the region shown as "Post-peak stage" in Fig. 5.37) before final failure. Carbonated samples exhibited high failure stresses and brittle failure.
- Moderate climatic conditions resulted in brittle composite failure, and the full multiple cracking capacity was not achieved.
- The results of samples from Industry illustrate the potential for production of TC composites with performance designed to suit a desired requirement.
- In all the samples studied in this research, final failure was by crack localisation and rupture that is illustrated earlier in Fig. 5.47. The failure strains were related to mechanisms of crack opening and the fibre bridging across the localised crack.

- The maximum failure load for a typical composite was approximately 2500 N, implying a stress of approximately 9±1 MPa, which was in the range of the total load-carrying capacity of 39 core fibres which crossed a crack in a typical specimen. The failure mode was consistent with the fibre rupture illustrated earlier by Figs. 5.6 to 5.9 in section 5.4.

5.9.1 Summary of the Results of Mechanical Tests

In this section, linkages and relationships are built up by drawing together the "key summaries" of the results of tests on mortar cubes, fibres, fibre pull-out, and composite tensile tests.

It was found that the matrix effects on fibre pull-out and composite tensile tests were more consistent than fibre effects because after the fibres are embedded in the matrix, the mechanisms that influence the tensile properties are modified substantially.

The mechanical behaviour of Textile Concrete is affected by the physical and chemical processes that take place within the microstructure. These processes were found to vary with ageing and the environmental conditions.

The mechanisms that influence the tensile behaviour of TC were found to vary with different stages of loading: ranging from intact matrix behaviour at strains below approximately 0.02 percent, to final failure by fibre rupture which occurs at strains in the range of 20 percent. The behaviour between these two extremes was dependent on the properties of the fibre/matrix bonding. Similarly, the mechanisms that govern the fibre pull-out behaviour are load dependent ranging from the intact matrix properties, to microcracking and mobilisation of shear stresses, fibre debonding and matrix damage, and failure by complete fibre pull-out.

The following is the consolidated summary of the results of the mechanical tests.

- The effects of ageing and weathering on the mechanical behaviour of Textile Concrete are best understood firstly from analysis of the mechanisms governing the various slopes of fibre pull-out load-displacement

curves. Secondly, an understanding is gained from analysis of different stages of stress-strain behaviour of composite Textile Concrete. These effects are subsequently related to matrix and fibre properties.

- The slopes of the fibre pull-out load-displacement curves are: initial slope representing an intact interface, second slope representing microcracking and mobilisation of shearing stresses along the interface, a negative post-peak slope that is manifested during fibre debonding and interface damage, and the slope at final failure representing pulling out of a fibre from a damaged matrix.

  Mobilisation of interfacial friction that takes place at the pre-peak stage is associated with microcracking of the fibre/matrix interface, which influences the bond. On the other hand, the gradient of the post-peak slope during fibre debonding and interface damage is related to matrix brittleness. The more brittle the microstructure, the steeper the slope.
- The mechanisms governing different stages of a typical composite tensile stress-strain behaviour are: pure matrix tensile behaviour at low strains of less than 0.02 percent, matrix microcracking up to strains of approximately 2 percent, development of first macro crack which traverses the sample depth and subsequent transfer of loading from the matrix to the bridging fibres, propagation and widening of macro cracks up to peak conditions, crack localisation, and final failure by fibre rupture.
- Densification and reduction in porosity of the microstructure was caused by cement hydration at early ages. At later ages, the effects of drying influenced the material properties. These two mechanisms were responsible for embrittlement of the matrix that was common in all samples investigated in this research work. Matrix embrittlement resulted in microcracking at low loading levels that characterised the pre-peak stages in both fibre pull-out and composite tensile tests.
- Densification in composite TC specimens is extended into the interfacial zone. Carbonation results in deposition of calcium carbonate ($CaCO_3$)

crystals in the microstructure, which is associated with a reduction in the average pore size of cementitious materials (Rendell et al. 2002). The effect of deposition of $CaCO_3$ in the fibre/matrix interface is that there is an increase in mechanical interaction between the fibres and the matrix. This mechanism accounts for an increase in bonding of approximately 18 percent which was observed in carbonated samples. Similarly, the extent of densification depends on ageing and exposure conditions, the greatest effect, of approximately 0.4 percent, was observed in carbonated samples. A denser matrix and a higher bond resulted in embrittlement of the composite manifested in post-peak brittle behaviour.

- In a Wetting/Drying environment, the products of hydration, calcium hydroxide (CH) and calcium silicate hydrates (C-S-H) are deposited in the microstructure which accounted for an increase of approximately 0.3 percent in matrix densification. For un-weathered samples, matrix densification leads to an increase in fibre/matrix bonding. However, a minor reduction of approximately 5 percent was observed in bonding after Wetting/Drying cycles indicating that the density of the microstructure at the fibre/matrix interface reduced after weathering. The reduction in density was possibly due to leaching of hydration particles at the fibre/matrix interface during Wetting.

  From the composite stress-strain behaviour, it was found that a Wetting/Drying environment was suitable for good hydration and suitable fibre/matrix bonding that resulted in excellent multiple cracking behaviour in the composite.
- The pre-peak behaviour in a fibre pull-out test is influenced by the matrix properties namely microcracking at the interfacial zone, and mobilisation of these cracks as the fibre debonds. This behaviour, rather than the post-peak behaviour, is relevant to composite tensile behaviour at the microcracking stage.
- The natural environment weathering of Nairobi (moderate altitude in

the tropics) combined the effects of hot/cold, Wetting/Drying and to a minor extent, carbonation. By embedding the fibres in the matrix, they were adequately protected from UV irradiation effects, which were accredited to loss of fibre strength and embrittlement. This environment resulted in multiple cracking behaviour in TC composites.

- Fibres weathered in a moderate environment exhibited minor loss in ductility without loss in strength whereas the pull-out samples exhibited markedly poor performance but the mechanisms contributing to this behaviour were not fully understood. Conversely composites weathered in a moderate climate had low post-peak ductility and failure was by fibre rupture.
- Exposure of Textile Concrete to the environment in Industry demonstrated excellent mechanical behaviour in terms of strain hardening and achievement of the full multiple cracking capacity. The behaviour was attributed to a suitable selection of the mix proportions and production techniques using customised machinery. This behaviour is an illustration of the potential for production of TC composites with performance designed to suit a desired requirement.

To substantiate the multiple cracking behaviour described here, the cracking patterns which developed on TC specimens after tensile testing are analysed in the section that follows.

5.10 Crack Features and Quantification

Firstly, specimens were visually examined soon after weathering for signs of damage and apart from the naturally weathered (NT) samples on which minor surface crazing was observed prior to mechanical testing, there was no significant damage in other samples. Fig. 5.49(a) shows surface crazing on a specimen after weathering.

Microcracking was characterised by fine cracks of the order of 20 μm as illustrated in Fig. 5.49(b). Although these cracks did not traverse the full

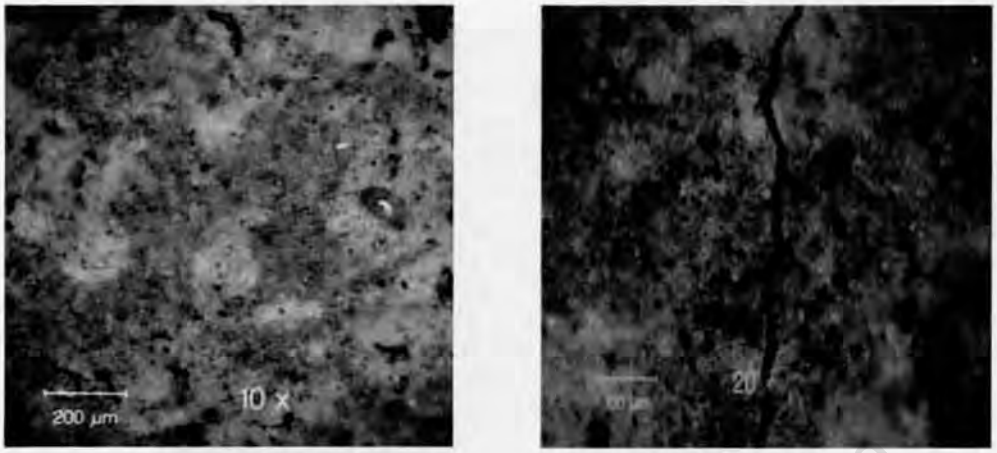

(a) Weathered surface (b) Typical micro crack (20μm)

Figure 5.49: Typical surfaces of tensile specimens (a) before and (b) after testing

width of samples, they nevertheless accounted for composite stiffness (see Fig. 5.48) that was much lower than would be expected in uncracked matrix. The results of the composite tensile test showed that the microcracking region is largely linear, meaning that the effects of these micro cracks on the overall matrix behaviour were not major.

Crack quantification involved characterisation of cracking patterns that developed on each set of samples after tensile testing. The technique employed was described earlier in section 4.7 in Chapter 4 in which the following measurements were taken:

- Crack density which was obtained by counting the number of visible cracks that traversed the full depth of the specimen's gauge length.
- The average crack spacings along the gauge length.
- Average crack widths of the full traversing cracks.

Multiple cracking, as exemplified by Fig. 5.50, characterised the cracking patterns after tensile behaviour and this was observed in all specimens. However, the pattern varied with the ageing conditions as shown in representative samples in Figs. 5.51 and 5.52.

Figure 5.50: Typical multiple cracking at strain hardening stage

Figure 5.51: Variation in cracking patterns

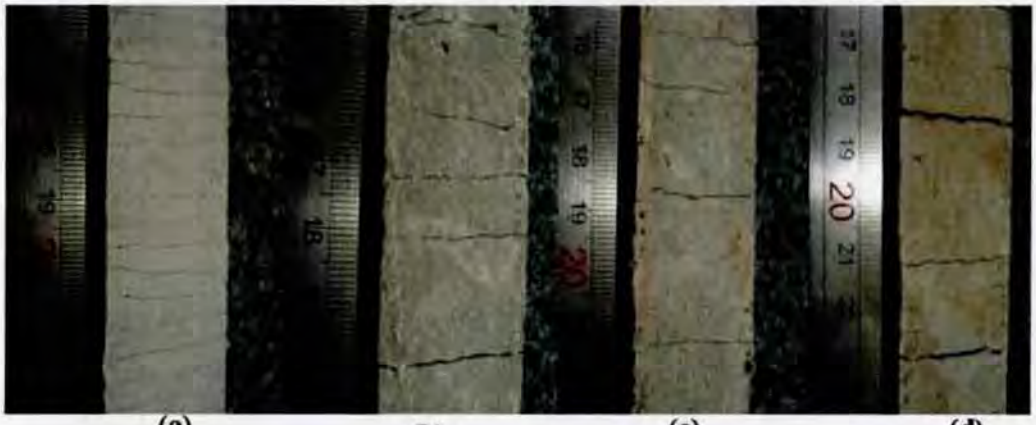

(a) (b) (c) (d)

Legend:
(a) Early-age control specimen loaded up to elastic stage
(b) Non-uniform crack widths and spacings in mature control specimen loaded to failure
(c) Multiple cracking on weathered specimen loaded to failure
(d) Several wide cracks interspersed by finer cracks on a naturally weathered specimen loaded to failure

Figure 5.52: Close-up of different cracking patterns

Despite all specimens being characterised by fully-traversing horizontal cracks, other fine cracks of sizes in the range shown in Fig. 5.49(b) were found to be branching off from the main cracks. This cracking mode made the measurements of crack spacings imprecise. To try and maintain consistency in crack spacings and densities, the branching cracks were therefore not measured. The results of crack quantification are shown in Table 5.7.

To try and gain insight into the correlation between the cracking patterns and stress levels, three samples were tested to strains between 1.0 and 2.4 percent, cracks were quantified and the results are included in Table 5.7.

5.11 Discussion of Crack Quantities shown in Table 5.7

The following are the main findings of the crack quantification represented in Table 5.7:

- Cracking on the Textile Concrete (TC) is a function of loading level, age and the environment. On rare occasions, weathering induced microcracks in the absence of load application (as shown by a single crack on NT samples before test).
- A controlled environment resulted in relatively uniform crack distribution over the gauge length. At early age (2 months), multiple cracking readily occurred but with ageing and strength increase, less multiple cracking was observed (see control 2 and 12 month old loaded up to elastic stage).
- The more mature samples exhibited more non-uniformity in crack widths (see control samples at ages 15 and 16 months in Table 5.7). In some of the samples, a major crack developed at one section over the gauge length but there were also several finer cracks traversing the specimen. This accounted for a higher value of crack spacing (and low values of crack width) for 16 month old control samples than was expected.
- Hot/cold (HC) exposure was characterised by fine multiple cracking at close spacing, which was consistent with the effects of HC-induced damage (softening) of Textile Concrete that has been highlighted as one of the main findings of this thesis.
- Whereas multiple cracking on samples weathered by Wetting/Drying were consistent with typical control samples at comparable age, carbonation resulted in a fewer but wider cracks accounting for the lower crack density shown in Table 5.7.
- Samples weathered in a natural environments developed several wide cracks interspersed by finer cracks thus accounting for high variation in crack widths. Conversely, fine closely spaced cracking characterised samples from Industry.

Table 5.7: Crack quantification data sheet

Exposure history	Age, months	No. of tests	Load and strain at failure		Crack quantities at end of test		
			Load,N	% Strain	Average crack density, /mm	Average crack spacing, mm	Average crack width, μm
Control*	2	5	901	2.4	0.12	8.6	141
Control	2	6	2900	25.7	0.12	8.5	202
Control	7	5	2670	20.4	0.18	5.5	124
Control	8	5	2670	23.8	0.18	5.8	141
Control	12	5	2550	22.3	0.19	5.7	141
Control*	12	5	901	1.7	0.08	12.2	33
Control	14	5	2921	22.0	0.16	6.7	147
Control	15	5	2969	25.0	0.21	4.9	152
Control	16	6	2848	30.1	0.07	14.6	86
Hot/Cold	12	5	1951	20.0	0.20	5.8	77
Wetting/Drying	14	5	2988	21.0	0.18	6.1	139
Wetting/Drying*	12	5	903	1.0	0.06	15.9	142
Carbonated	16	5	3331	18.0	0.10	10.8	167
Moderate	12	5	2696	18.0	0.20	4.9	198
Tropical	12	5	2475	21.0	0.22	4.8	108
Tropical	16	6	0	0	single	single	364**
(before test)					crack	crack	364**
Tropical	16	6	2980	21.0	0.05	20.7**	444**
Industrial	24	5	3020	30.2	0.21	4.8	130

* Samples were loaded up to elastic range

** There were several wide cracks interspersed by finer cracks hence the high values

See Table 5.8 for coefficients of variation

Due to the complex nature of the mechanism of cracking, the quantification process was inevitably characterised by high variability as illustrated in Table 5.8.

Table 5.8: Variability of crack quantities

Exposure condition	Age, months	Coefficient of variation of crack quantity, %			Loading state
		Density	Spacing	width	
Control	2	9.67	29.07	14.18	elastic
Control	2	44.44	30.91	30.64	failure
Control	8	44.44	39.66	41.84	failure
Control	12	47.37	36.84	21.99	failure
Control	12	11.22	22.95	42.42	elastic
Control	14	45.45	31.34	26.53	failure
Control	15	45.83	30.61	30.92	failure
Hot/Cold	12	45.00	39.66	32.89	failure
Wetting/Drying	12	75.00	62.89	54.76	elastic
Wetting/Drying	14	50.00	34.43	28.78	failure
Carbonated	16	45.45	59.26	27.54	failure
Moderate	12	44.44	26.53	51.52	failure
Tropical	12	45.45	31.25	42.29	failure
Tropical	16	23.33	28.50	58.78	failure
Industry	24	47.62	29.17	16.15	failure

Table 5.7 illustrates a trend in crack spacing with ageing for control samples. However, a deviation from this trend is seen with 16 month old control samples in which the average crack widths were lower than expected. This was because of the development of fine cracks that were branching off from the major cracks accounting for lower average crack widths. In addition, the additional microcracking accounted for a higher failure strain than expected.

It was observed that the samples weathered in a tropical climate developed several wide cracks interspersed by finer cracks at closer spacings hence the high values shown for these samples in Table 5.7. This behaviour, together-with the results of 16 month old control samples, was attributed to a dense microstructure and strong fibre/matrix bonding that was manifested by embrittlement of the microstructure in the vicinity of the widening cracks.

For a better insight into the trends of the results in Table 5.7, crack widths were analysed as a factor of loading and environmental conditions.

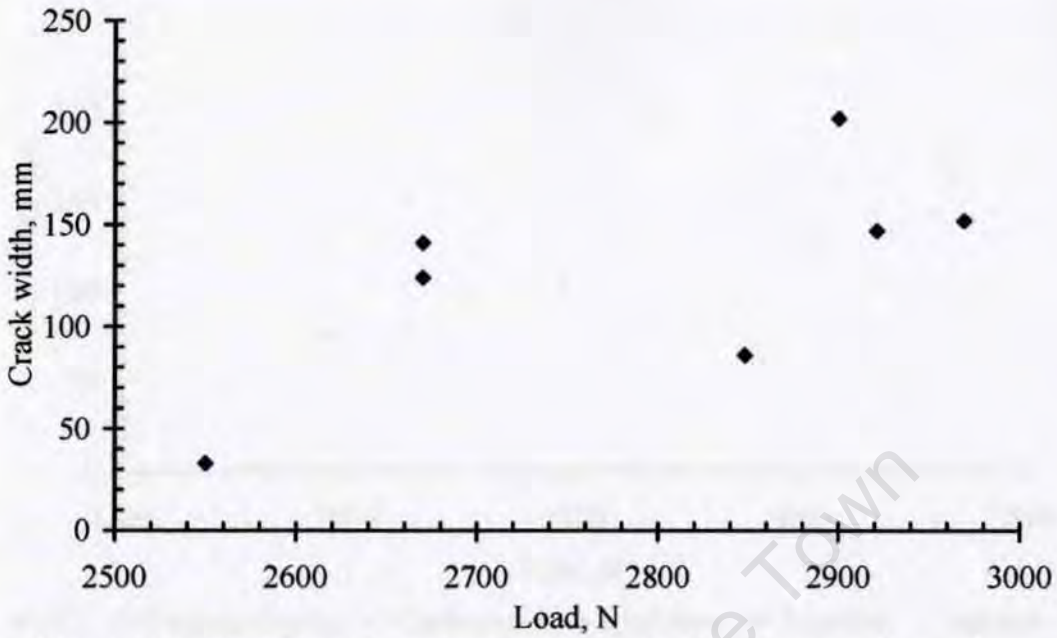

Figure 5.53: Variation of crack widths with loading for control samples

The trends are shown in Figs. 5.53 and 5.54. Specimens failing at higher loads developed wider cracks as illustrated for control samples in Fig. 5.53. A similar trend was found for crack widths in weathered samples as shown in Figs. 5.54.

The cracking behaviour of samples indicated that there was a correlation between crack density and ageing. For example, specimens cured for two months under controlled conditions developed cracks at spacings of approximately 5 mm after tensile testing as shown in Fig. 5.55(a). Conversely, specimens tested at a later age of approximately 16 months developed relatively wider cracks at wider spacings of between 8 mm and 20 mm as shown in Fig. 5.55(b).

Although the variation in crack widths was mainly accredited to ageing, the correlation was not linear as other factors such as the moisture state of the specimen and bonding nature could also have played a role. A strong bond and dense matrix (exemplified by carbonated samples) resulted in wide crack spacings compared with samples exposed to a hot/cold environment which had a weaker bond but developed closely spaced cracks. However, a

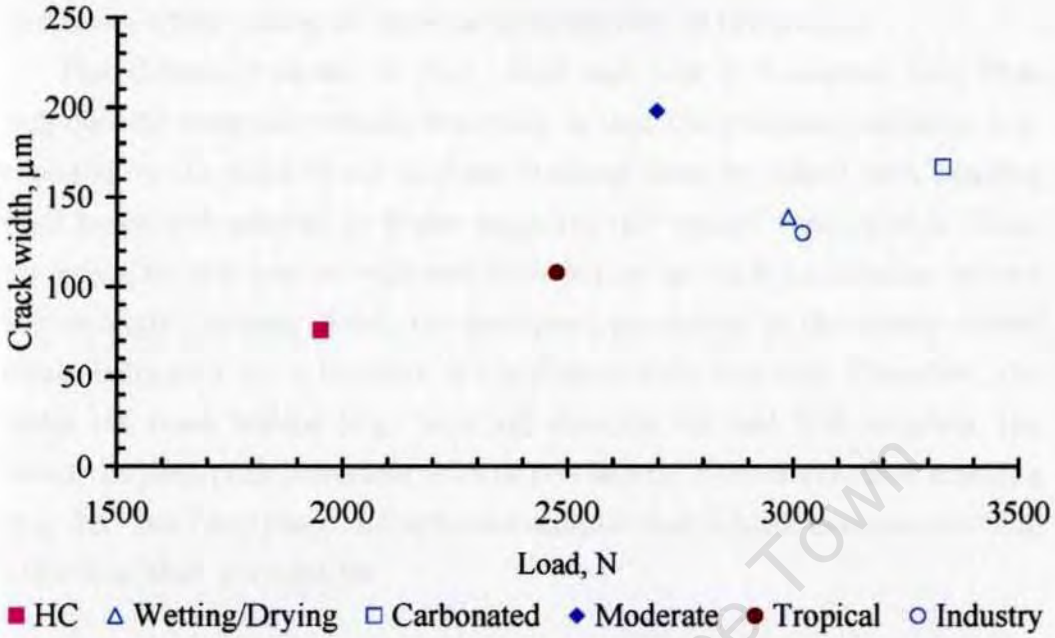

Figure 5.54: Variation of crack widths with loading for weathered samples

(a) Fine multiple cracking (b) Coarse multiple cracking

Figure 5.55: Typical cracking patterns at multiple cracking stage

general trend of increasing crack widths and crack spacing with ageing that characterised the multiple cracking of Textile Concrete was due to increased

hydration which causes an increase in brittleness of the matrix.

The behaviour shown in Figs. 5.53 and 5.54 is consistent with fibre pull-out and composite tensile behaviour in that the composite stiffness, represented by the slope of the multiple cracking zone, increased with bonding (and hence with ageing). It is also argued in the "model" developed in Chapter 6 that for composites evaluated after failure by crack localisation beyond the multiple cracking phase, the post-peak properties in the tensile stress-strain behaviour are a function of the fibre/matrix bonding. Therefore, the wider the crack widths (e.g. later age samples, Cc and NM samples), the closer the post-peak behaviour is to brittle failure. Conversely, finer cracking (e.g. HC and I samples), characterises samples that exhibit multiple cracking behaviour that is aimed for.

5.11.1 Synthesis of Separate Effects of Fibre, Matrix, and Composite

In an attempt to gain a better understanding of the mechanical behaviour of Textile Concrete, the "key summaries" of the results of mechanical tests are drawn together and represented in a Matrix Analysis format as shown in Table 5.9. On the figure, Fibre and Matrix Effects represent brief classification of effects of the main mechanical parameters; strength, slopes of the curves, and ductility. The effects are further elaborated in Table 5.10.

Table 5.10 is an attempt to link the different mechanisms that were described in this Chapter namely: bond strength, composite toughness, and cracking to the mechanical behaviour of TC.

Table 5.9: Synthesis of effects of fibre and matrix on the composite

			FIBRE EFFECTS				
			HC	WD	C_c	NM	NT
			Loss in strength, gain in ductility, increase in toughness	Minor loss in strength, increase in stiffness, minor embrittlement	Thermo-induced increase in ductility, loss in strength, increase in toughness	Minor embrittlement, and loss in strength, minor decrease in toughness	severe loss of strength and embrittlement, decrease in toughnes
MATRIX EFFECTS	HC	Microcracking due to a dry environment during a heating cycle	Minor loss in bond, reduction in pre-peak fibre pullout slope, major loss in toughness, achievement of full multiple cracking				
	WD	Strength increase due to favourable hydration conditions		Minor reduction in bonding and pre-peak fibre pullout slope, minor loss in toughness; achievement of full multiple cracking			

Continued on Next Page...

		FIBRE EFFECTS				
		HC	WD	C_c	NM	NT
C_c	Matrix densification and embrittlement due to deposition of carbonates			Gain in bond strength, strength gain, major increase in toughness, full multiple cracking capacity not achieved		
NM	Strength gain due to combined effects of HC, WD, and to a minor extent, C_c				Loss in bond (not fully understood), loss in toughness, full multiple cracking not achieved	
NT	Strength gain due to combined effects of HC, WD, and to a minor extent, C_c					Increase in bond with ageing, full multiple cracking achieved

Table 5.10: Linkage between constituent mechanical behaviours

Characteristic behaviour	Exposure condition				
	Hot/Cold (HC)	Wetting/Drying (WD)	Carbonated (C_c	Moderate (NM)	Tropical (NT)
Fibre tensile behaviour					
Fibre failure load	decrease	minor loss	decrease	minor loss	decrease
Fibre stiffness E_f	decrease	increase	decrease	increase	increase
Fibre toughness	increase	decrease	increase	decrease	decrease
Fibre pull-out behaviour					
Bond, τ	minor loss	minor reduction	increase	decrease	increase with age
Toughness	decrease	decrease	increase	decrease	minor increase with age
Composite tensile behaviour					
Hot/Cold	Weakening features	locally damaged fibrils; thermo-softening of fibres; matrix microcracking			
	Competing features	inter-fibril bonding, higher cement hydration rate			
Effects on behaviour		minor loss in bond strength and stiffness, toughness decreases			
Wetting/Drying	Weakening features	fibres weathered by hydrolysis and hardening, increased E_f			
	Competing features	favourable hydration conditions			
Effects on behaviour		no significant change in bond strength and stiffness, toughness decreases			
Carbonation	Weakening features	thermo-softening of fibres			
	Competing features	encrustation of fibres, favourable hydration conditions			
Effects on behaviour		significant increase in bond strength and stiffness, toughness increases			
Moderate climate	Weakening features	no clear understanding on mechanisms causing pre-mature debonding			
	Competing features	fibres protected from UV irradiation by the matrix			
Effects on behaviour		significant loss of bonding and stiffness, toughness decreases			
Tropical climate	Weakening features	combined effects of Hot/Cold and wetting/drying conditions			
	Competing features	fibres protected from UV irradiation by the matrix			
Effects on behaviour		decrease of bonding and stiffness, composite toughness decreases			

*Refer to Tables 5.3 and 5.4 in Chapter 5 for degradation mechanisms

5.12 Consideration of Errors in Experimental Measurements

The reliability and accuracy of the results of this research depended on the level of diligence during experimentation, and the precision of the equipment employed. Ordinarily, systematic errors are not detected by statistical analysis. Therefore, an attempt was made to minimise the effects of these errors from the outset. This was accomplished by careful design of the equipment, precise calibration of the instruments and employment of refined experimental techniques such as:

- Minimising variability in properties by uniformity of batching, mixing and curing.
- Specimen casting moulds which were made demountable thus ensuring minimal damage to the specimens
- Use of customised grips that were adjustable to the local testing conditions. The fibre grip had a special bracing device round which the fibres were wound and held in place without slippage or stress concentration. The composite specimen grips were modified according to the observed specimen response to the mechanical tests.
- The edges of the gripping areas of the tensile specimens which were smoothed with a fine sand-paper in order to eliminate stress concentrations at irregularities. The gripping areas were then re-cast in epoxy resin in order to arrest crack propagation in the gauge section and hence carry out the test to failure.
- Setting the testing machine input parameters specifically for each specimen tested.

These measures were carried to the limit of practicability. Any remaining sources of systematic errors were removed by selecting the specimens and the order of their preparation and testing on a random basis. Operator errors during experimentation were reduced by adequate training and super-

vision by skilled personnel. Therefore, the statistical measures stated here are considered to be related to random errors.

5.12.1 Uncertainties in the Measuring Equipment

Errors can be propagated from direct measurements into calculated values. Where the calculated value was the product or quotient of two measured quantities, the fractional uncertainty in the final value was obtained from the sum of the fractional uncertainties in the individual measurements (Taylor 1997*b*). Table 5.11 shows the uncertainties in the measuring equipment, and Table 5.12 shows the possible propagated errors in calculated quantities.

5.12.2 Limitations in Data Acquisition

The experimentation process involved taking measurements on several specimens, and therefore there were uncertainties due to random errors that are inherent in such measurements. The uncertainty was quantified by the standard deviation from the mean.

There was a possibility of other gross errors that were not necessarily related to the precision of the measuring equipment. These errors emanated from limitations in data acquisition particularly during the accelerated ageing process. Apart from the carbonation chamber which had a calibrated system of monitoring and controlling the environment, the Hot/Cold and wetting/drying systems were limited in this aspect, and the rate of progression of the damage was not quantified.

The experiment was carried out with the assumption that the extent of ingress of the damaging mechanisms was uniform for all specimens weathered in the same batch. However, it was likely that deterioration was variable within and between the specimens and this was a possible source of gross errors. Non-uniform weathering could have significant effects in material properties, and indeed did contribute to the scatter observed in the results of mechanical tests.

The consequences of the errors described here varied according to the

source. For example, batching errors were considered minor and could be neglected whereas errors in strain measurements had greater impact on the tensile test results and indeed were the main source of uncertainties in this research. Similarly, uncertainties in carbonation rate were negligible since the focus of the experimentation was more on complete penetration of specimens by CO_2 rather than the carbonation rate. On the other hand, errors in accelerated wetting and drying facility had a considerable impact on the results mainly due to the dependence of the weathering mechanisms on the effectiveness of moisture movement within the specimens. The other errors described in Tables 5.11 and 5.12 were minimised by repeating measurements and using mean values in the analysis of experimental data.

5.12.3 Use of Statistics in the Analysis

The experimental data presented in this Chapter was processed into a form that was representative of typical samples and then by use of the conventional statistics of mean values ($\overline{x}$)and standard deviation (σ), it was possible to assess the significance of variations in behaviour that could be accredited to exposure conditions. A change was considered significant if it exceeded σ of the mean. For example, the average cube crushing strength of mortar that was shown earlier in Fig. 5.1 was considered to be significant.

A statistical approach was found particularly useful in computing the peak load (P_{peak}) from the fibre pull-out test results. The peak loads, which were essentially "pseudo" average peak loads by virtue of having been computed as the averages of many samples, were used in computation of the fibre/matrix interface bond strength (τ).

Table 5.11: Uncertainties in measuring equipment

Measuring instrument	Random error, ±	Measurement affected by error	Relative uncertainty %	Risks/ consequences of errors
Weighing scale	Mix quantities, 5 g	batching	2	Cube density & crushing strength
Linear scale	1 mm	Spread of wet mortar	0.5	Mortar flow
Vernier callipers	0.02 mm	Diameter of silicone moulds	0.2	Fibre density
Thermometer	0.5°C	Conditions in the mixing room	2.5	Mortar flow
Universal Testing Machine (UTM)	Source: Table A.5 extracted from calibration certificate of 10 kN ZWICK load cell	Load measurements in mechanical tests	0.35 0.33 0.23 0.12	Loads up to: 40 N 50 N 100 N 4000 N
Extensometer	UTM	Variable: similar to measurements	Strain 0.35	Stiffness of the composite
Microscope	1 μm	Crack widths	2	Crack quantification
Research-based carbonation incubator	Temp.: 0.1°C CO_2 level: 0.1% Source: LEEC Technical manual	Carbonation rate	0.33 1	Extent of superimposed thermal effects

Table 5.12: Uncertainties in calculated values

Measurement	Random error, ±	Relative uncertainty,%
Mass of mix materials	5 g	0.71
Flow of mortar	1 mm	0.67
Specimen cross-sectional area	0.04 mm^2	0.02
Force, P: machine error + error due to repeated measurements	Based on load measurements using UTM (see Table 5.11)	Individual fibres: 6.39
		Fibre pull-out peak loads: 14.75
		Composite: 5.43
Strain, ϵ	Machine error+ error due to repeated measurements	Fibres: 6.3 Composite: 5.86
Crack widths	0.001 mm	2

The other key load-deflection parameters, which the statistics of standard deviation ($\overline{\sigma}$) was useful, was in assessing the variations in the pre-peak and post-peak gradients illustrated earlier in the quadri-linear representation in Fig. 5.1.

The tensile stress-strain (σ-ϵ) curves were statistically treated in a similar manner to the P-δ curves generated from the fibre pull-out tests. The standard deviation was used in testing for significance in the differences between results, based on the premise that variations in the measurements were of a random nature and thus resulted in a normal distribution. For example, to test the significance in differences between two results x_1 and x_2 with standard deviations $\overline{\sigma}_{x1}$ and $\overline{\sigma}_{x2}$ respectively, the average standard deviation $\overline{\sigma}_{ave}$ for the two values was firstly computed. Using $\overline{\sigma}_{ave}$, the number of standard deviations t by which the two results, x_1 and x_2 differed was then used as the measure of significance in the differences. This is described in Eq. 5.1.

$$t = \frac{|x_1 - x_2|}{\overline{\sigma}_{ave}} \tag{5.1}$$

At the 95 percent confidence level, $1.96\overline{\sigma}_{ave}$ was therefore the lower boundary for two results to be significantly different, that is, $t = 1.96$. This formed the basis for using a rounded value of $\pm 2\overline{\sigma}$ ($t = 2$) to enclose 95 percent of fibre pull-out test results. The statistical analysis was implemented in EXCEL.

5.13 Summary

The conclusions from Chapter 5 were that plain polypropylene (PP) fibres are damaged by exposure to "ambient" temperatures as illustrated in Table 5.9. The fibres suffered loss of strength and increase in ductility after exposure to a Hot/Cold (HC) environment. Similarly, carbonation at elevated temperature of 30°C induces thermo-related increase in ductility of the fibres.

The effects of Wetting/Drying (WD) to PP fibres was hydrolysis and "yellowing" which accounted for the minor embrittlement manifested in the tensile tests. It was further concluded that ultraviolet irradiation (UV) was a possible cause of severe loss of strength and embrittlement of the fibres exposed to a tropical climate.

By embedding PP fibres in a cementitious matrix they are sufficiently protected from environmental damage, and the performance of the composite is influenced more by the properties of the matrix and the less damaged embedded fibres as indicated in Table 5.10.

Ongoing cement hydration was beneficial in that it led to improvement of the fibre/matrix bond. The effects of different environments on the matrix were that whereas HC environment causes matrix microcracking, carbonation densifies the matrix and makes it brittle, and WD environment is a favourable condition for good cement hydration.

The composite behaviour after exposure to natural environments combined the effects of HC and WD but carbonation was not an influencing factor in these environments.

A major insight to new knowledge was that the mechanical properties of TC improve with ageing, and the new material is tolerant to a range of "ambient" surroundings without showing much degradation. In addition, the

important role of the matrix in composite behaviour was evident from the results of Industry samples. These results pointed to the need for design of mixes to meet specific applications and exposure conditions.

This Chapter has discussed the various aspects of the results of mechanical tests and associated information. The results were found to be repeatable within statistically accepted limits.

Arguments were developed around observed behaviour of four main sets of tests on the matrix (cube tests), fibres, fibre pull-out, and composite tensile tests. Similarities and consistencies in behaviour were sought with the aim of linking them to fundamental mechanisms. This was essentially a synthesis of the chemical and physical processes that affect the mechanical behaviour of Textile Concrete.

A "composite" behaviour was built up from the contributory behaviour of the constituents, which were not always complementary and contributory.

Based on the synthesis of the different tests, a better insight into the the mechanism of multiple cracking was gained and substantiated using crack patterns which were formed on TC samples after tensile testing. Using crack widths and spacings, the effect of ageing and weathering on the mechanical behaviour of TC was assessed. The results indicated that the behaviour was similar to so-called High Performance Fibre Reinforced Cementitious Composites (HPFRCC), is more likely to be found in composites with sufficiently weak fibre/matrix bonds. Conversely, strong bonding encourages reduction in post-peak ductility and failure before achievement of the full multiple cracking capacity.

For clarity, the interaction of the various mechanisms at the multiple cracking stage are linked in a flow chart format as shown in Fig. 5.56.

It was then possible to transform the information from experimental data into a more useful form and attempt to draw valid conclusions from the research. In addition, the data accorded a better insight into the effects of ageing on the performance of Textile Concrete. Micrographs from the SEM studies are presented in the subsequent Chapter.

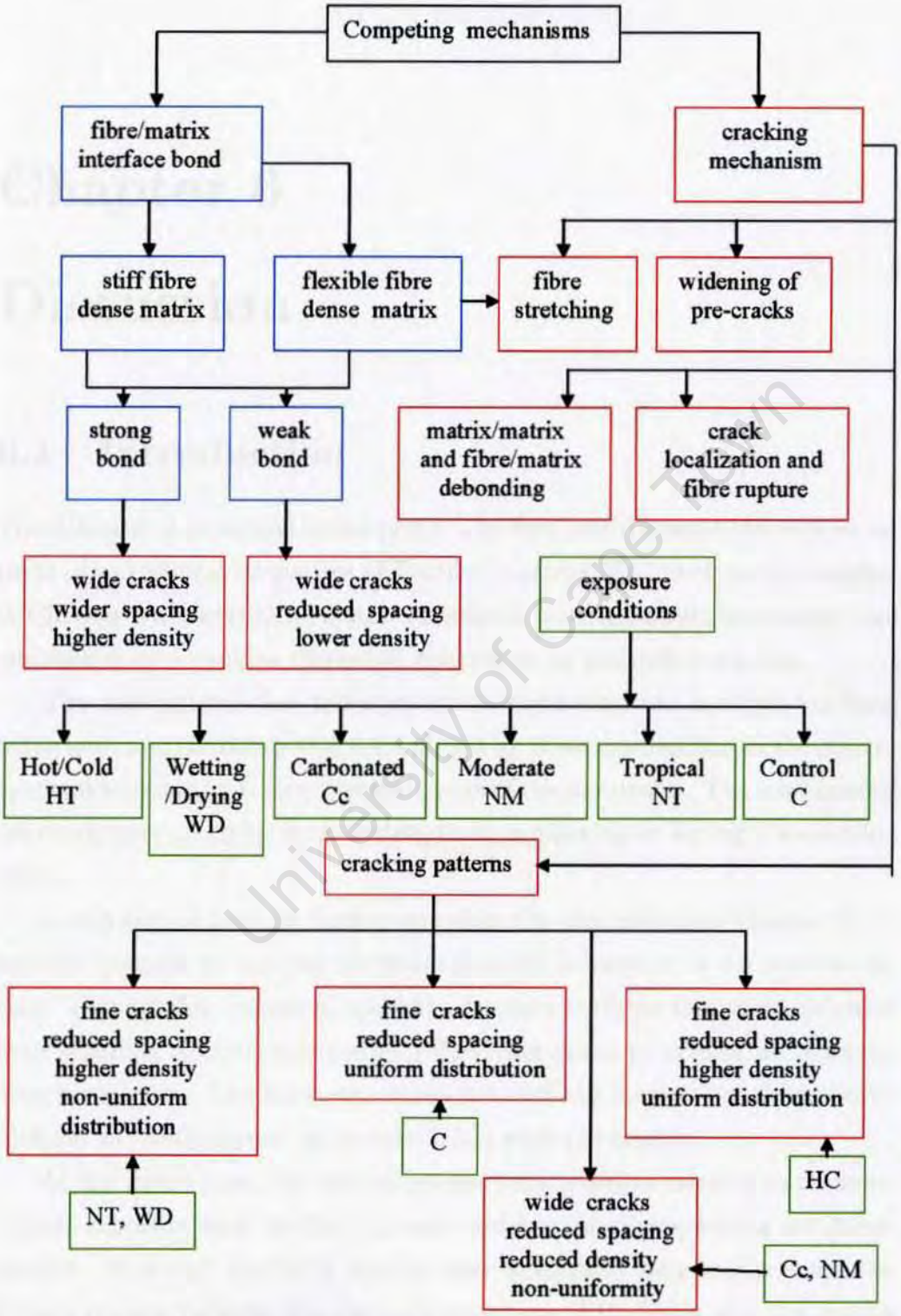

Figure 5.56: Linkage between mechanistic properties at micro and macro levels

Chapter 6

Discussion

6.1 Introduction

This Chapter is presented in two parts. The first part discusses the various aspects of mechanical properties of Textile Concrete (TC) that were presented in Chapter 5 namely; fibre/matrix interfacial bonding, strain hardening, and multiple macro-cracking (hereafter referred to as multiple cracking).

The mechanisms that influence strain hardening and multiple cracking behaviour, and the competing roles played by these mechanisms in the macro-mechanical behaviour, form the main part of the discussion. The mechanisms are categorised as either contributing to strengthening or having a weakening effect.

In the second part, to further elucidate the discussions in Chapter 5, an attempt is made to link the macro-mechanical behaviour to the microstructure. Topographic images of specimen fracture surfaces that were obtained from scanning electron microscopy (SEM) were used to present an independent perspective. The microstructures revealed the interaction of fine fibrils (defined as "fluffy layers" in section 2.7.1) with the matrix.

At the micro level, the key microstructural features relating to environmental exposure such as fibril damage and matrix microcracking are investigated. Although the SEM studies were essentially only exploratory, the critical regions between the fine polypropylene (PP) fibrils and the matrix

were clear. The key microstructural features characterising the interfacial region are linked to the macro-behaviour and to mechanisms that were hypothesised in Chapter 5.

The discussion in the first part of this Chapter forms the basis of the subsequent "model" of the mechanical behaviour of Textile Concrete. The second part of this Chapter provides a description of the model within an analytical framework. The analysis focusses on variations in bonding, cracking, stiffness, and toughness as a function of ageing and environmental exposure. The model is developed further into mathematical formulations that describe the tensile behaviour, leading to a prediction of a generalised stress-strain (σ-ϵ) relationship for TC.

The terminology used in the discussion includes "compliant microstructure" (non-linear stress-strain behaviour), which refers to a microstructure related to a matrix that easily mobilises full multiple cracking. Similarly, the term "shrinkage" refers to volume changes in the matrix that result from moisture movement during the process of cement hydration, which may improve bonding.

6.2 Fibre and Matrix Properties Affecting Performance of the Composite

The results of the composite tensile behaviour presented in Chapter 5 illustrate that the performance of Textile Concrete is a function of several factors namely: fibre properties, matrix strength and toughness, microstructure densification, and fibre/matrix bonding. The influencing factors were age and exposure conditions.

Fibre strength and stiffness were sensitive to weathering conditions. Indeed, significant variations were observed in fibre stiffness after exposure to a range of "ambient" surroundings commonly encountered in service. The stiffness varied from softening (e.g. after Hot/Cold and carbonation exposures) as shown earlier in Table 5.2, to increase in stiffness and embrittlement (e.g.

after exposure to a tropical environment). Embrittlement was attributed to ultraviolet (UV) irradiation.

By embedding the fibres in the matrix, the effects of weathering of the fibres were substantially reduced. Direct physical assessment of fibres and their interface characteristics, once embedded in the matrix, was not easily studied. Rather their effect was inferred from the mechanical tests results as described in Chapter 5 (i.e. fibre strength, fibre pull-out and tensile characteristics of the laminate composite). Together with the mechanical tests, an attempt to correlate fibre and interface features with mechanical behaviour was undertaken using SEM observations of the fibre composite area broken open and exposed for observation. This technique of SEM sample preparation was chosen because it caused minimal damage to the fibre/matrix interface.

A trend of increasing matrix strength was observed with ageing (as illustrated in Fig. 5.4 in Chapter 5) and was attributed to progression of cement hydration. This was beneficial to fibre/matrix bonding and was consistent with theoretical expectations.

A dry environment (in the Hot/Cold chamber) induced microcracking in the matrix. The major roles played by the microcracks associated with a dry environment are a decrease in elastic properties and a decrease in the mortar failure strength (Skoczylas, Burlion & Yurtdas 2007). In a Wetting/Drying (WD) environment, the Wetting regime counteracted the effects of drying (microcracking). Indeed, an increase in mortar failure strength was observed in WD weathered samples, contrary to a reduction of strength after Hot/Cold cycles.

Minor local debonding of fibres from the matrix was observed after tensile testing of the composite (see Fig. 5.47 in Chapter 5) but its effect in the strain hardening behaviour of the composite was not evaluated. All samples failed by fibre rupture at a localised macro crack.

Improved fibre/matrix bond was attributed to microstructure densification due to on-going hydration. Drying shrinkage was considered as causing

modifications in the physical state of the fibre/matrix interfacial zone, which improved the mechanical interaction (bonding) between the fibres and the matrix.

6.2.1 Strain Hardening and Multiple Cracking

The gradual strength increase that characterises the strain hardening phase (see Fig. 5.37 in Chapter 5) in a typical stress-strain relationship of TC is attributed to the following phenomena: matrix multiple cracking, opening of existing cracks and formation of new ones (multiple cracking), and stretching of fibres across the cracks (bridging action). During the application of a tensile load, the intact composite between cracks undergoes some straining, further increasing the overall strain. This behaviour is typical of TC and the general class of cementitious composites referred to as High Performance Fibre Reinforced Cementitious Composites (HPFRCC) (Kabele 2003*b*).

In HPFRCC, crack bridging action and fibre/matrix bonding are considered as the main mechanisms influencing strain hardening (strengthening) of the composites. Conversely, fibre debonding, elastic stretching of fibres between cracks, and fibre pull-out are the main softening (weakening) mechanisms in the multiple cracking phase (Naaman & Reinhardt 2006).

In the Textile Concrete composites investigated, the central core of PP fibres is longer than the critical embedment length (l_e) of 22 mm which was applicable for this research. Therefore fibre pull-out at failure was not a dominant factor but rather the effects of localised damage at the fibre/matrix interface and at the crack planes. These effects counteract strain hardening and cause reduction in composite stiffness at the multiple cracking phase leading to final failure, which is by brittle fibre rupture. Since the major influencing factor at failure was fibre strength, the failure loads for the composites (with approximately 39 fibres) were comparable to plain fibres. Composites failed at loads between 2200 N and 3000 N, which was consistent with the measured tensile strength of single fibres which ranged between 60 N and 80 N.

6.2.2 Microstructure of Typical Fibre Matrix Interface

SEM images provide useful information on the critical fibre/matrix interfacial region. Sample preparation, condition, and coating for SEM studies was described earlier in section 4.8.1.1 in Chapter 4. The preparation essentially involved notching (illustrated by Fig. 4.36) fibre pull-out samples on one of their surfaces in the direction of fibre orientation and by application of a nominal bending force, the fibre/matrix interface was sufficiently exposed. This technique of sample preparation caused minor damage to the interface due to minimal debonding of fibres from the matrix. However, the method sufficed for these preliminary investigations. Practical specimens of sizes of approximately 10x5x5 mm were prepared, and the specimens were coated with a thin layer of gold/palladium in order to reduce charging problems in the SEM chamber. The electron beam used to scan the specimens was operated with an accelerating voltage of 20.00 keV from a tungsten source.

Typical views of the critical fibril/matrix region are shown in Figs. 6.1 and 6.2. The figures illustrate typical microstructures of 16 month old samples, the first a control sample cured under laboratory conditions, and the second, sample weathered in a medium altitude in the tropics, respectively.

The following features are illustrated in the images:

i. Fig. 6.1 illustrates fine cement hydration products partially covering "whisker-like" fibrils which are still embedded in the matrix. The fibrils in the micrograph are approximately 20 μm in diameter. The matrix is homogeneous consisting of closely packed hydration products, with no signs of microcracking or macro porosity.

ii. Fig. 6.2 shows a fibril covered with cement hydration products and embedded in the matrix. The discontinuity in the figure marks out the boundaries of a sand particle (of diameter approximately 160 μm), and the matrix is solid.

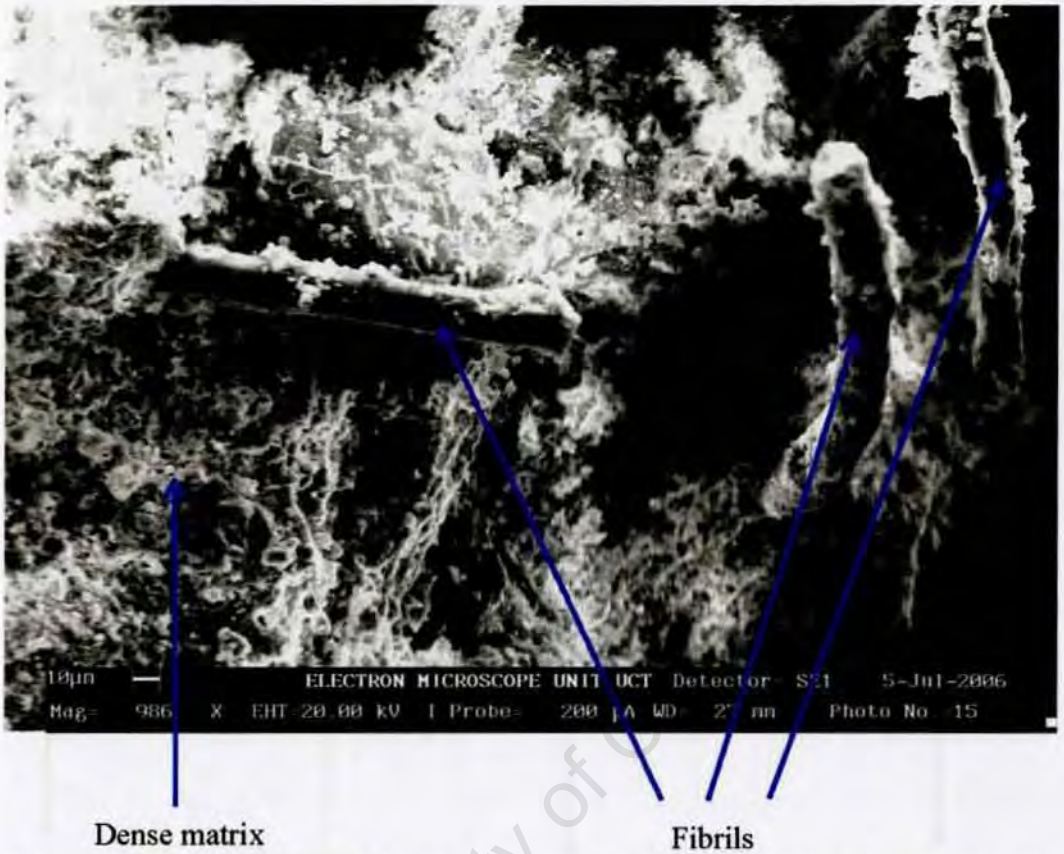

Figure 6.1: Typical view of interfacial region in a 16 month old mature control specimen

6.2.2.1 Microstructure of Mature samples

As is to be expected of cementitious products, mature samples exhibit dense microstructures attributed to ongoing cement hydration. This accounted for the good interaction between the matrix particles and the fine fibrils resulting in strong bonding typically of the form shown in Fig. 6.1. The figure illustrates good bonding revealed by fine fibrils still firmly embedded in the matrix.

Various features are seen in the microstructure, namely: fibril/matrix interaction, dense microstructure at the interfacial zone with no obvious signs of microcracking, and all these characteristics suggest good bonding. Although the relative differences in bonding are not quantified between dif-

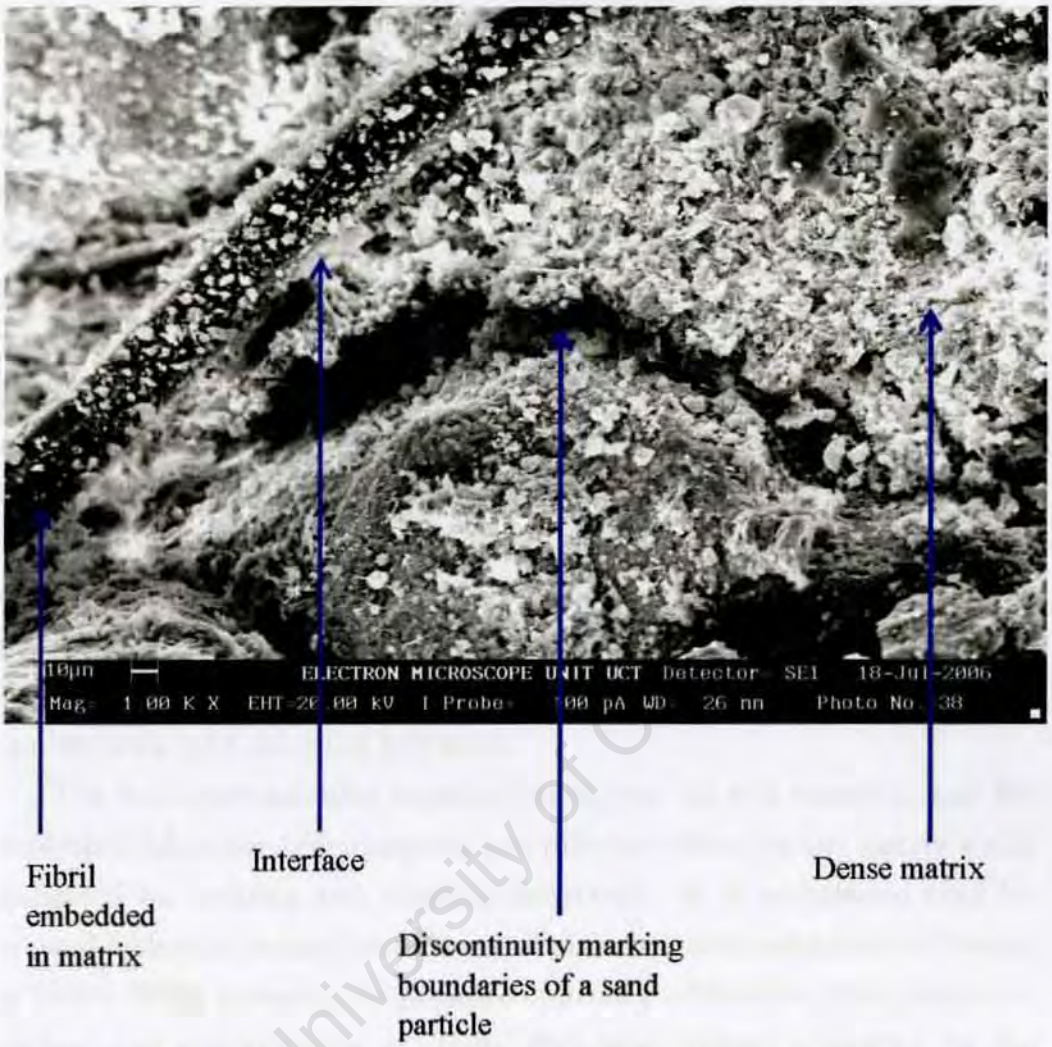

Figure 6.2: Typical features in a 16 month old sample weathered in a tropical climate

ferent microstructures, bonding between the fine fibrils and the matrix is clearly evident. In addition, the microstructure in Fig. 6.2 shows hydration products covering the fibril surfaces, further indicating good fibre/matrix bonding. Similarly, the results of fibre pull-out tests (shown earlier in 5.14 to 5.20 in Chapter 5) illustrate progressively increasing peak loads with ageing due to improvement in fibre/matrix bonding as samples mature.

6.2.2.2 Linkage of Fibre Pull-out and Composite Cracking

A close link exists between the fibre pull-out properties and composite cracking behaviour in that the factors that influence the fibre pull-out, that is matrix properties and fibre/matrix bonding, also affect the cracking behaviour. In addition, fibre pull-out and composite cracking behaviour are influenced by age and exposure conditions.

As discussed in the preceding section, since the fibres were sufficiently protected from severe damaging effects of the environment, the matrix had a bigger influence on fibre pull-out behaviour than the fibres. This was manifested in the variation between individual fibre behaviour and fibre pull-out in carbonated and naturally weathered (NT) samples. In these environments, the effects of exposure in the mechanical behaviour were more distinctive in plain fibres than in pull-out or composite behaviour. As expected of cement-based products, the common feature in all the environments was matrix densification with on-going hydration.

The five environmental regimes investigated in this research, and the controlled laboratory environment, had different effects on the matrix which impacted on bonding and cracking behaviour. It is understood that increased hydration reduces compliance of plain cementitious matrices (Bazant & Gettu 1992), however, the presence of fibres modified the fibre/matrix interface, and quantification of cracks after final rupture accounted for the composite behaviour observed in this research. A brittle matrix and a strong bond (similar to carbonated samples) causes fewer wider cracks whereas a microcracked matrix (HC), and well hydrated matrix (WD), both of which result in "compliant" matrices that mobilise the full multiple cracking.

The behaviour of composites with a "compliant" matrix is consistent with High Performance Fibre Reinforced Cementitious Composites (HPFRCC) because they achieve the full multiple cracking capacity, which is an important consideration in design (Naaman & Reinhardt 2006). On the other hand, microstructures that are not "compliant" may be characterised by high strength, but failure occurs prior to achievement of full multiple cracking ca-

pacity. This aspect of multiple cracking in relation to different environmental exposures, is further discussed in the sections that follow.

6.3 Environmental Effects on Mechanical Behaviour

The effects of exposure to five environmental regimes is dealt with in this section, from a microstructural perspective. These regimes are: cyclic Hot/Cold (HC), cyclic Wetting/Drying (WD), carbonation (Cc), natural weathering in moderate (NM), and tropical (NT) climates. For each regime, a brief discussion is given on the mechanisms of degradation of polypropylene (PP) fibres, the matrix, and the composite. A linkage between the features observed in the microstructure and the mechanical behaviour is the main subject of the discussion.

6.3.1 Effects of Cyclic Heating and Cooling

Cement hydration being a chemical reaction means that elevated temperatures normally accelerate the cement hydration reaction resulting in matrix densification within a relatively short time. However, the effect was not considered significant in this work since by the age of approximately 4 months when HC weathering was initiated, cement hydration was substantially well advanced. Moreover, the inclusion of Ultra-Fine Fly Ash enhanced early-age strength (up to approximately 28 days) development. The effects of HC exposure are investigated by studying the extent of microcracking in a weathered matrix exemplified by Fig. 6.3.

The microstructure of the weathered sample in the figure shows a homogeneous matrix with a few microcracks. Well dispersed cement hydration products of different sizes can be seen in the microstructure. A damaged fibril are also revealed in Fig. 6.3. The matrix is traversed by a discontinuity which was attributed to flaking of the specimen during sample preparation. Considering that all samples were prepared under similar conditions, flaking

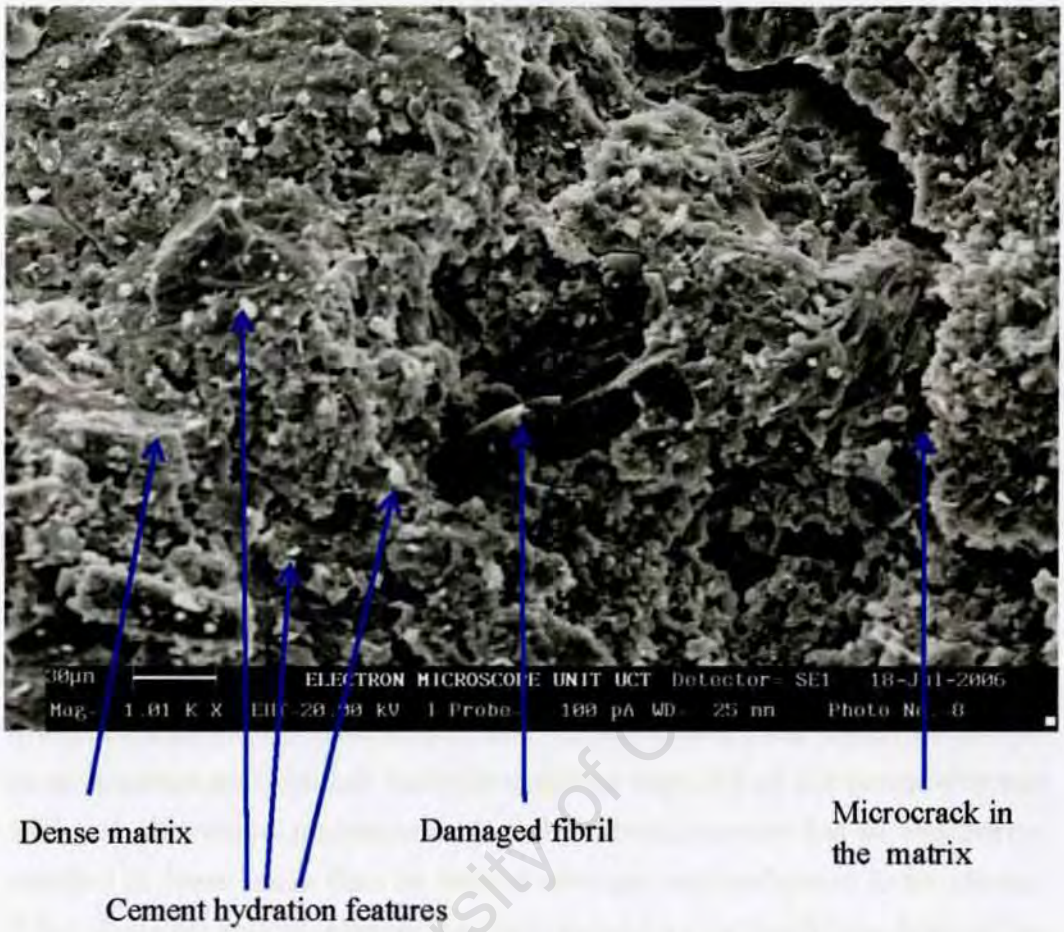

Figure 6.3: Microcracking due to cyclic heating and cooling

in the manner shown in Fig. 6.3 was indicative of a brittle matrix. This was to be expected of HC-weathered samples which were quite dry by virtue of the condition in the Hot/Cold facility that was employed for weathering of the samples. The minor matrix microcracking after heating and subsequent cooling was attributed to dimensional movements of expansion and contraction.

The reduction in the peak fibre pull-out load after HC-weathering was of a minor nature as illustrated in Fig. 5.15(a) and 5.15(b). This behaviour was evidence of effective protection of fibres by the matrix from direct effects of temperature on the fibre itself, and it also implied that dimensional movements (such as shrinkage) did not affect the bonding significantly.

The effects of fibre/matrix interface bonding on the tensile behaviour together-with the cracking patterns that developed after mechanical testing were dealt with earlier in section 5.11. To be able to correlate the cracking patterns in HC-weathered composite samples with the microstructure, the following competing mechanisms are considered: thermally-induced mechanisms of strengthening (matrix densification due cement hydration at elevated temperature, which will be limited due to drying out), and weakening mechanisms (matrix microcracking and localised fibre damage).

The microstructure of HC-weathered samples could perhaps best be described as composed of ductile fibres embedded in a microcracked matrix. These are the main properties characterising the so called "compliant" or "flexible" microstructure as opposed to a homogeneous matrix/stiff fibre TC composite. The tensile behaviour as well as the cracking patterns of HC-weathered samples were consistent with the consequences of dimensional movements in the microstructure, and ductile fibres. Fine cracks formed at close spacings and the full multiple cracking capacity of the composite was achieved. Increased microcracking of the microstructure due to weathering resulted in lower loads than in control samples, and reduction in toughness. Fibre ductility was manifested by high variability in the failure load of the composite (see Fig. 5.38 in Chapter 5).

6.3.2 Cyclic Wetting/Drying Environment

Polypropylene (PP) fibres undergo chemical degradation in a moist environment due to the mechanisms of oxidation and hydrolysis of molecular groups in the microstructure. This form of degradation takes place in aerated conditions (Moore 1996), (Azapagic et al. 2003). Most Polypropylene manufacturers use thermo-stabilisers to counteract softening. It was therefore inferred that physical changes related to hydrolysis occurred after WD exposure but this was not conclusive since no investigations were specifically undertaken in this regard.

In this research, the extent of degradation of the fibres after exposure to

the moisture movement as well as other "ambient" environments was evaluated from tensile tests. The results were presented in Fig. 5.7(b) in Chapter 5. The results indicated a modest increase in stiffness after approximately 3 months during which time the fibres were exposed to a warm damp environment and were aerated sufficiently during the wetting cycles.

At the end of Wetting/Drying, the fibres had discoloured due to degradation by "yellowing" (see section 2.3). This was consistent with the literature since it is known that degradation in PP by "yellowing" is mostly accelerated by exposure to light (Moore 1996).

Analogous to a typical solid polymer, PP undergoes loss in toughness after prolonged storage under hot damp conditions (Mills 1986). This was confirmed from a slight increase in stiffness observed in the weathered fibres. It is therefore argued that samples were fully penetrated by moisture at the end of each wetting cycle, and also after approximately 100 WD cycles, the fibres underwent a form of physical change. The fibre pull-out results indicated a minor reduction in bond (see Table 5.5 in Chapter 5) which meant that the mechanical properties of the composite were not affected significantly by the increase in fibre stiffness.

Favourable cement hydration conditions existed in the WD environment which enhanced cement hydration and consequently, matrix densification. The nature of physical changes in the fibres and the matrix can be suggested from the microstructure of the composite shown in Fig. 6.4.

Fig. 6.4 shows a typical microstructure of TC composite after cyclic Wetting/Drying. The porosity that appears in the foreground of the microstructure resulted from damage by minor fibre debonding at the sample preparation stage. Fine fibrils of diameter approximately 25 μm and with rough surfaces are clearly seen. The fibrils are covered with fine cement hydration products indicating good bonding, and the well dispersed matrix particles of variable sizes. In the background of Fig. 6.4 where the fibrils are still intact in the matrix, good fibril/fibril interaction as well as fibril/matrix bonding is evident. No visible damage was observed on the surfaces of the

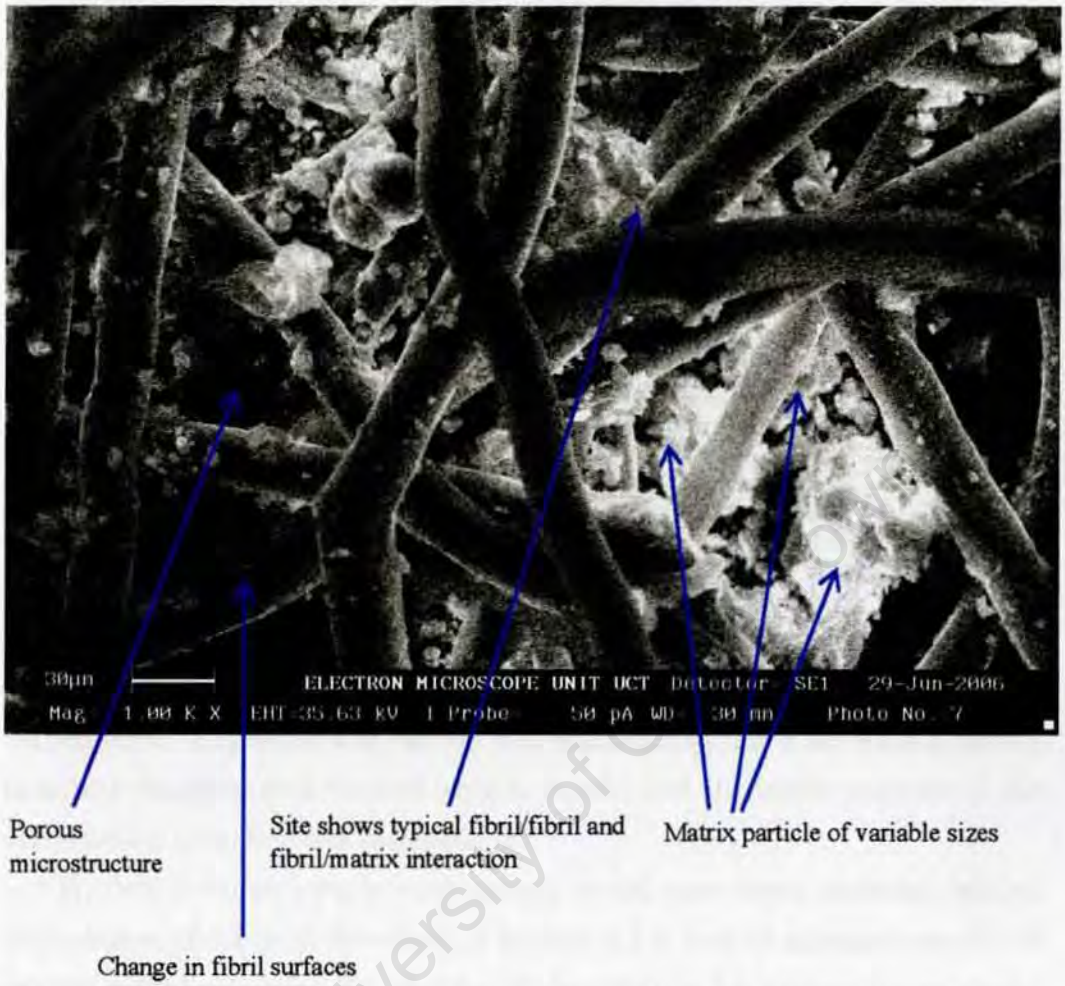

Figure 6.4: Typical composite microstructure after weathering by cyclic wetting and drying

embedded fibrils. The porosity that is seen in the foreground of Fig. 6.4 is due to debonding of some of the fibres during the sample preparation.

The means of assessing the effects of Wetting/ Drying in this research was by carrying out fibre pull-out tests while the composite performance was assessed by analysing the tensile behaviour. The analysis of the cracking patterns after the tensile tests indicated that WD environment caused fine and closely spaced cracks in the samples. This form of cracking is similar to the cracking mode in HPFRCC (Naaman & Reinhardt 2004), (Naaman & Reinhardt 2006). This performance was attributed to good bonding result-

ing from the presence of moisture and slightly elevated temperatures that were above 30°C (on average) in the WD environment, and a "compliant" microstructure that mobilised full multiple cracking.

6.3.3 Effects of Carbonated Environment

Carbonation was carried out at a CO_2 level of 10 percent with the chamber at a slightly elevated temperature of approximately 30° C. Although 10 percent was a relatively high CO_2 level considering that the normal level in the atmosphere is much lower at approximately 0.2 percent, a CO_2-rich environment was motivated by the need to accelerate the weathering process. As a result, thermally-related effects could not be fully eliminated but were superimposed on the carbonation mechanism.

The relative humidity in the chamber was manually controlled to vary between 50 and 70 percent making it a suitable environment for accelerating carbonation. Exposure was carried out continuously for a six month period in a dark chamber with limited oxygen supply, and the inside pressure of the carbonation chamber was atmospheric.

While a moist and warm environment would cause some moisture-related degradation of fibres as described in section 6.3.2, lack of adequate supply of oxygen would minimise the chances of degradation by hydrolysis, as would a relatively dry environment. On the other hand, exposure of PP fibres to a temperature of approximately 30° C over an extended period of six months had thermally-related effects. Indeed, the fibres became more ductile after carbonation exposure as illustrated earlier in Fig. 5.8(b) in Chapter 5.

After carbonation exposure, no physical damage was observed in the fibres as illustrated in Fig. 6.5. The figure illustrates SEM images of fine fibrils of diameter of approximately 20 μm. The fibril surfaces have trapped particles from the environmental chamber but there are no signs of cracking or flaking on the fibrils. Some of the particles on the fibre surfaces were likely to be carbonates from other concrete samples in the chamber. The presence of carbonates and possibly other species (such as silicates or aluminates) was

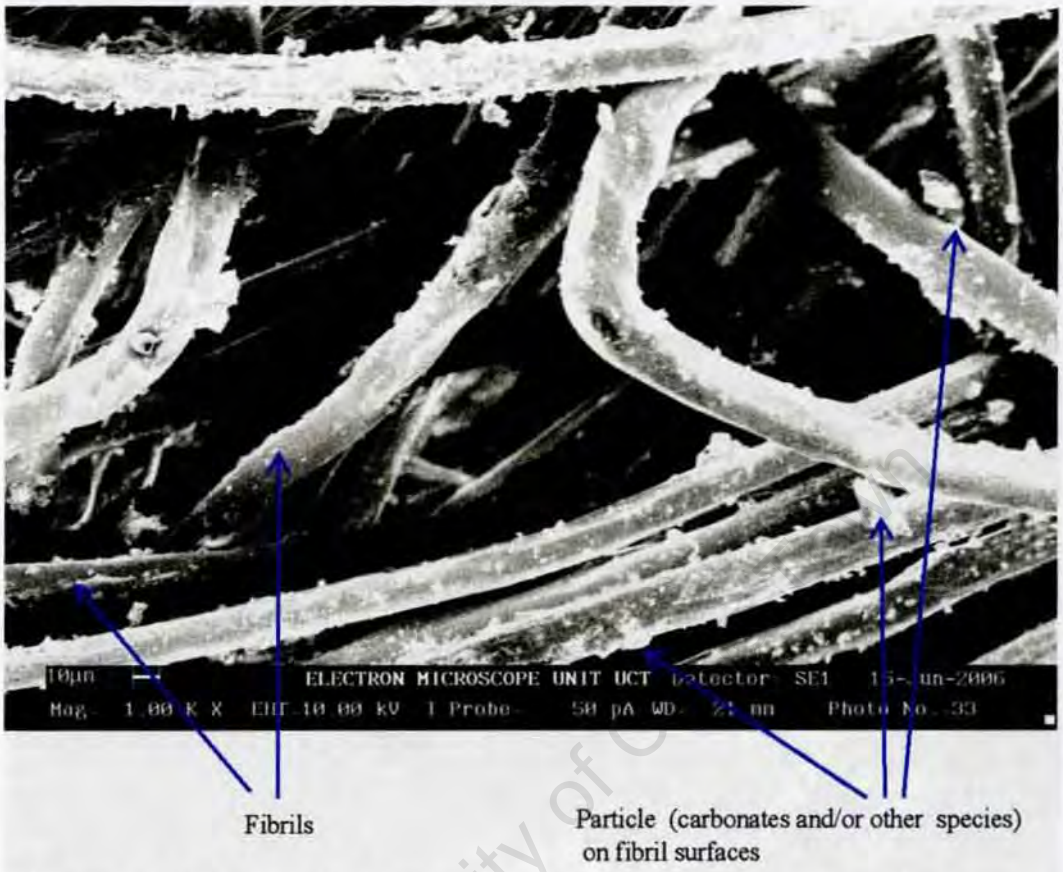

Figure 6.5: Fibril surfaces on a plain fibre after exposure to carbonation

confirmed from the simple phenolphthalein test described earlier in section 4.5.4 in Chapter 4. Carbonation exposure at elevated temperature resulted in loss in strength and stiffness in fibres in a manner similar to the effects of Hot/Cold exposure (see Figs. 5.8(b) and 5.7(a) respectively).

Absorption of CO_2 in semi-crystalline polymer such as PP above the glass transition temperature (T_g) of approximately -16^{o}C partly involves physical adsorption of the gas to form a monolayer on the surface of the polymer which increases with pressure (Mills 1986). As the pressure in the carbonation chamber was atmospheric, it was unlikely that the fibres underwent chemical changes as a result of CO_2 exposure.

In view of the foregoing, the effect of PP exposure to carbonation was not considered as a chemical change since for this to take place the temper-

ature needs to be elevated sufficiently (above 160°C for PP). In addition, the pressure needs be above 5 atmospheres for CO_2 to be absorbed in the PP molecule (Mills 1986). Therefore, the reduction in fibre stiffness after carbonation exposure was considered to be by thermally induced softening. The microstructure of a typical pull-out sample after carbonation exposure is shown in Fig. 6.6.

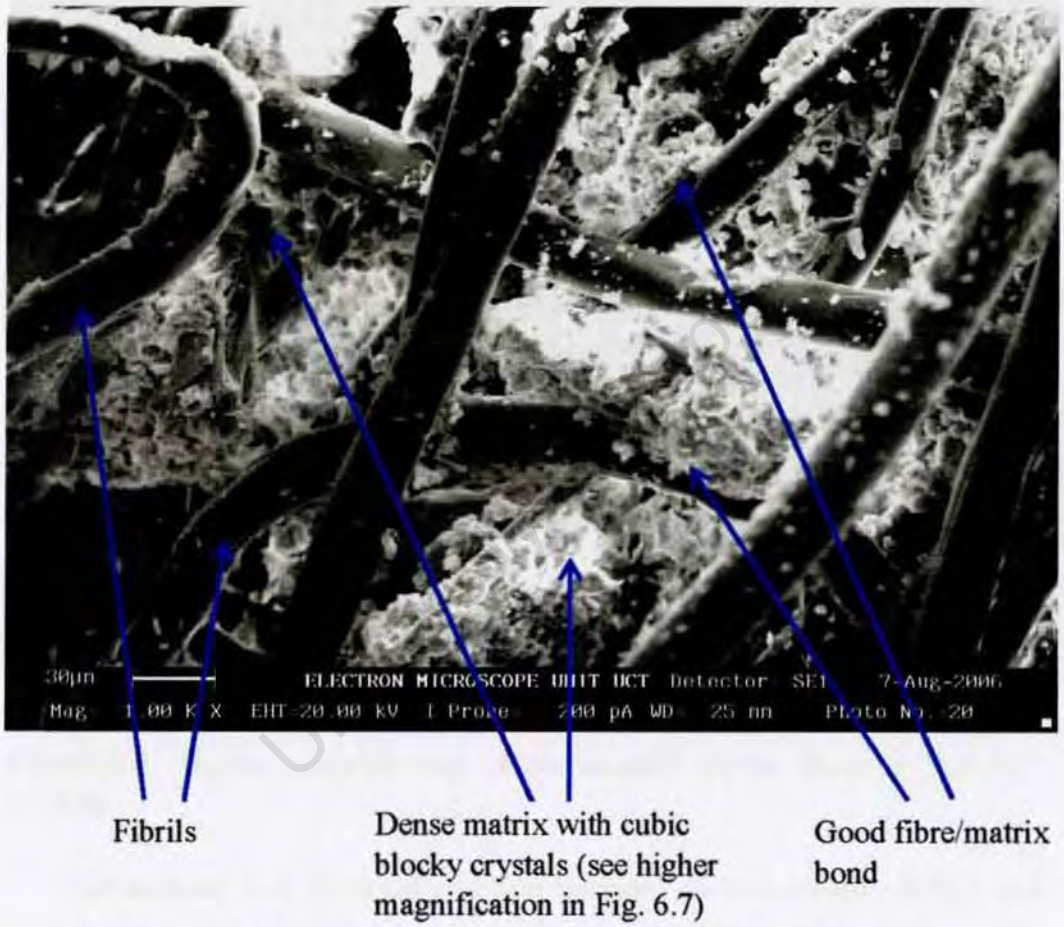

Figure 6.6: Fibre pull-out specimen weathered by carbonation

The micrograph illustrates presumed calcium carbonate ($CaCO_3$) and/or possibly other species on the fibril surfaces. The presence of these particles on the fibril surfaces enhances the fibril/fibril and fibril/matrix (inter-particle) interaction. This inter-particle interaction coupled with a homogeneous matrix was manifested by increased fibre/matrix bonding (see Fig. 5.17). Cu-

bic, blocky carbonate crystals in a dense homogeneous matrix are shown at a higher magnification in Fig. 6.7.

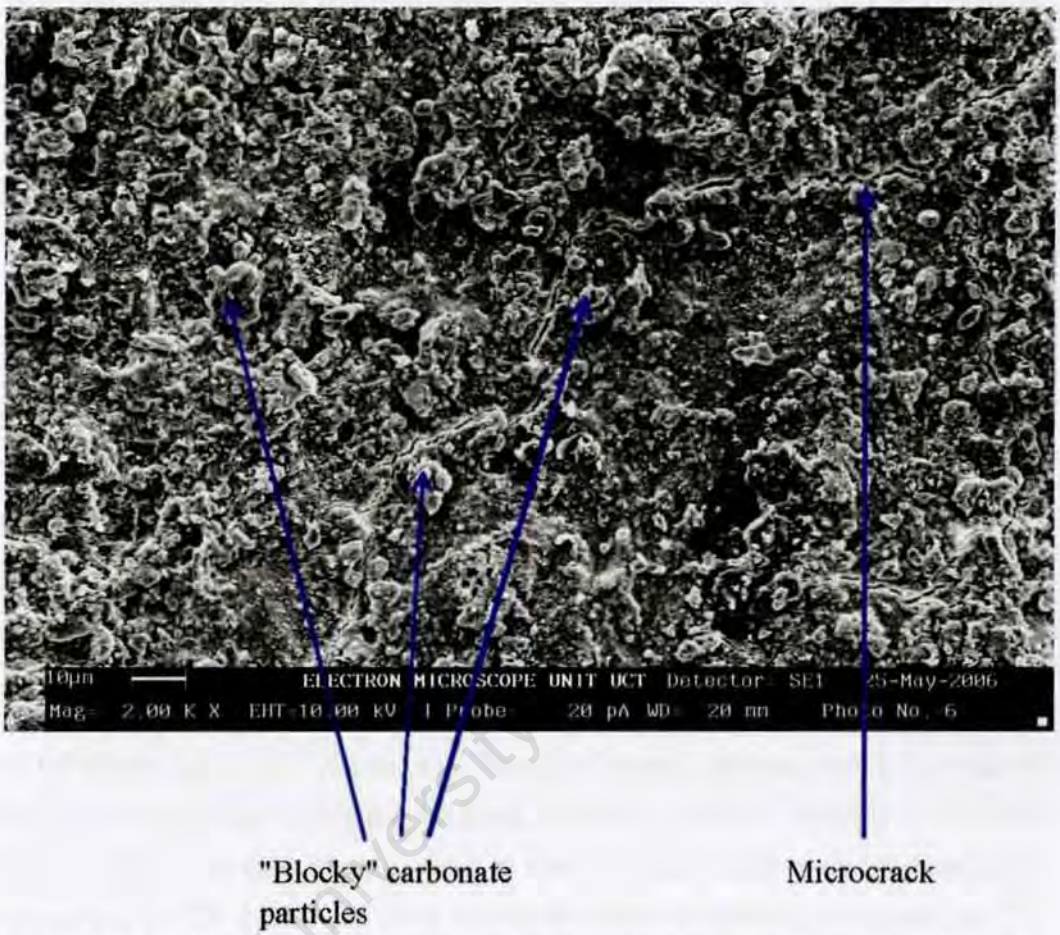

Figure 6.7: Higher magnification of carbonated matrix showing "blocky" crystals

Carbonation is a chemical reaction between carbon dioxide (CO_2) and calcium hydroxide ($CaOH_2$) to form calcium carbonate $CaCO_3$. The reaction proceeds according to Eqs. 2.1 to 2.2 in section 2.5.2 which were shown earlier in Chapter 2. The final reaction proceeds as follows:

$$CO_2 + Ca(OH)_2 \rightarrow CaCO_3 + H_2O \tag{6.1}$$

As the composite ages under a CO_2-rich environment, $CaCO_3$ crystals, hydration products (CH and C-S-H), and unhydrated cement particles contribute

to densification of the matrix. At the fibre/matrix interface, the particles get deposited on the fine fibril surfaces leading to an improvement in the mechanical interaction of the fibres with the matrix. This mechanism improves the fibre/matrix bond.

Strong fibre/matrix bonding due to carbonation accounted for high energy consumption which was consistent with a high pull-out load illustrated earlier in Fig. 5.17(b). The composite strength increased due to development of a strong bond, and a dense matrix increased brittleness of the matrix.

Due to strong bonding and brittle matrix in the carbonated samples, high peak stresses were attained but the development of full capacity of multiple cracking was impeded. The strong fibre/matrix bonding and a brittle matrix accounted for wide cracks and non-uniformity in crack spacings. The mode of final failure, as in specimens exposed to HC and WD environments, was by fibre rupture.

6.3.4 Effects of Exposure to Moderate Climate

Exposure to direct sunlight is known to cause degradation and embrittlement of PP fibres due to UV irradiation. Tensile strength decreases with the time of exposure according to Fig.6.8 (Joseph, Rabello, Mattoso, Joseph & Thomas 2002). The reduction in properties is due to chain scission and degradation occurring to PP molecules as a result of photo-oxidation promoted by UV irradiation.

Cape Town experiences a moderate climate (NM) with average temperatures of 7°C in winter and 30°C in summer and an annual average humidity of about 78 percent making it a favourable environment for cement hydration and matrix densification particularly during the winter season. The samples were exposed to weathering soon after curing for 28 days and therefore cement hydration took place under favourable conditions.

Minor reduction in stiffness was observed in NM-weathered fibres implying that the samples did not get enough exposure to sunlight for any UV effects to cause embrittlement and major loss in strength.

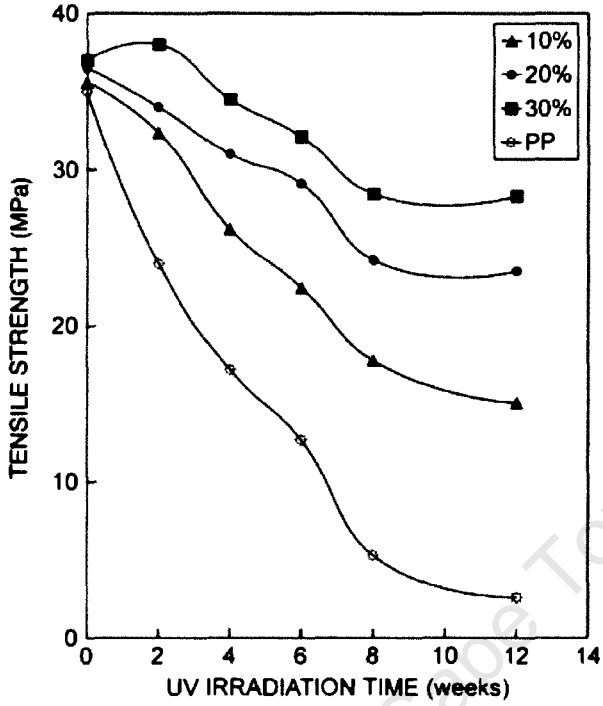

Figure 6.8: Loss of strength in PP (and PP composites) with exposure to UV irradiation (from Joseph *et al.* (2002))

The moderate climate caused an increase in cube crushing strength as shown in Fig. 5.5 in Chapter 5. The increase was attributed to combined effects of Hot/Cold, Wetting/Drying, and the beneficial effects of Ultra-Fine Fly Ash. Carbonation was not considered as having a major role in matrix densification because the fibre depth was not penetrated at the time of test, as illustrated by Fig. 4.25 in Chapter 4.

Low peak loads characterised the load-displacement behaviour in the fibre pull-out tests, contrary to performance of individual fibres, matrix and the composite. Additional tests which were carried out on the NM-weathered fibres confirmed the poor performance. Since it was not clear, from the fibre pull-out behaviour, what caused the apparent poor performance, further investigations into the possibility of environmentally-induced debonding is suggested. However, these results demonstrate that the mode of failure after composite tensile testing was not influenced significantly by fibre pull-out.

Microstructures of NM-weathered samples are shown in Fig. B.1 to B.4 in Appendix B.

Since the mode of composite failure did not allow for fibre pull-out, any environmentally induced debonding was not manifested in the composite tensile tests. The important properties were the matrix properties; strength, and brittleness. Due to a dense brittle matrix, the composite tensile behaviour of NM-weathered specimens (Fig. 5.41(a) in Chapter 5) was characterised by strain hardening with a brittle post-peak region, with failure occurring before attainment of full multiple cracking capacity.

NM-weathered composite samples developed major wide cracks interspersed by minor cracks due to a brittle matrix. The cracks were not uniformly spaced along the specimen's gauge length as illustrated earlier in Fig. 5.52. The composite failure mode was typical of microstructure that is not "compliant"; failure by by brittle fibre rupture which occurs before achievement of the full multiple cracking capacity.

In view of the performance of the NM-weathered samples discussed here, a great deal of understanding is still required with regard to environmentally induced debonding that caused the poor pull-out performance.

6.3.5 Effects of Exposure to Tropical Environment

In contrast to a moderate climate whereby individual fibres stiffened after weathering, a tropical (NT) climate caused a significant loss in fibre strength and embrittlement despite a notable increase in stiffness (see Fig. 5.9(b) in Chapter 5). The fibres exhibited significant degradation after approximately 12 months of continuous exposure to the tropical environment. A possible cause of the embrittlement was ultraviolet (UV) irradiation but this aspect was not tested in this research.

The other possible cause of damage to NT-weathered fibres was contamination as illustrated by the SEM images in Fig. 6.9. The figure shows fine fibrils of diameters of approximately 12 μm. Fine particles are seen on the fibril surfaces.

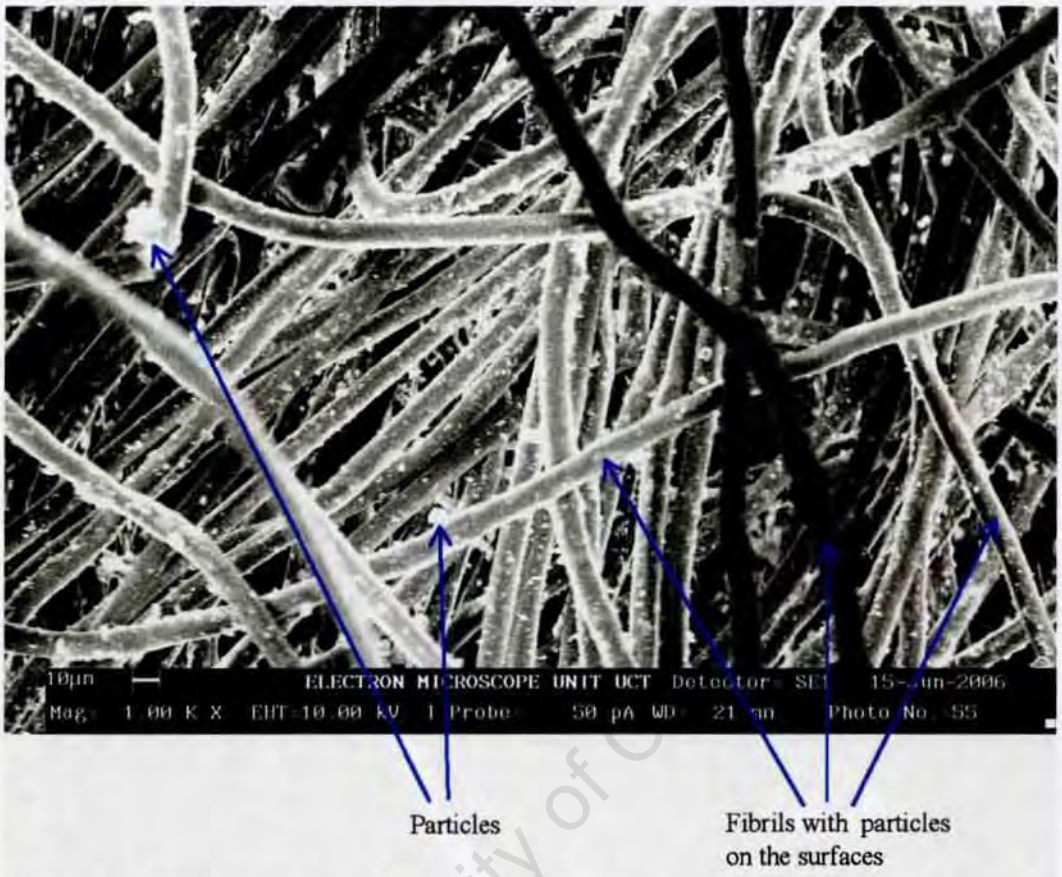

Figure 6.9: Fibril surfaces of a plain fibre after weathering by exposure in a tropical climate

The loss in strength after exposure to a tropical climate was not surprising because it is known that impurities, whether deliberately or adventitiously added to polymers (including PP) have a profound effect on fibre stability by accelerating or inhibiting the degradation reactions (Azapagic et al. 2003), (Joseph et al. 2002). This research suggests that the combined effects of UV irradiation and contamination accounted for the loss in fibre tensile strength.

Elemental analysis of the particles on the fibril surfaces was not carried out. Therefore the exact nature of contamination was not clearly understood from physical observations. However, by casting the fibres in mortar, protection from the damaging effects of the environment was provided. A minor increase in bonding on samples weathered for a period of 16 months

was observed. This increase in bonding was accredited to favourable cement hydration conditions.

The fibre/matrix bond strength was evaluated using the peak loads shown in Figs. 5.19 in Chapter 5. In an attempt to correlate the behaviour with the microstructure, the SEM image shown in Fig. 6.10 was examined.

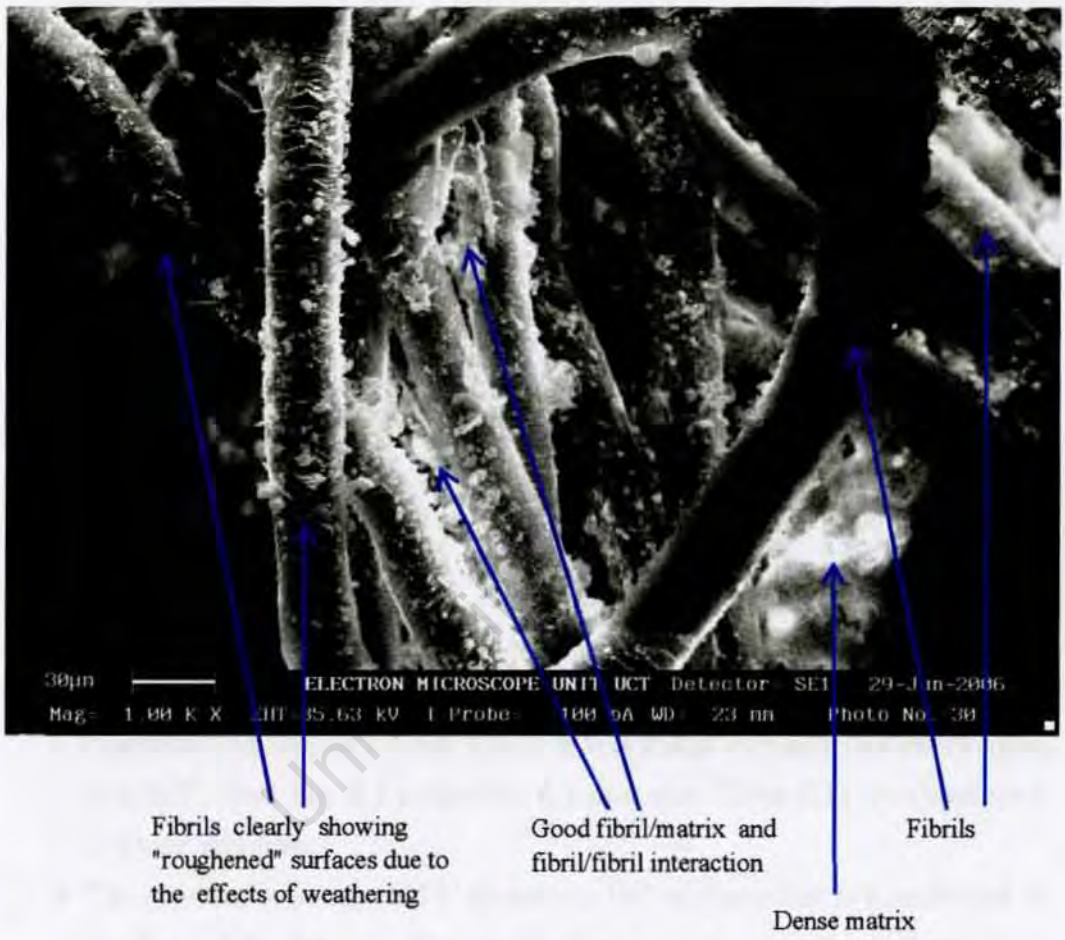

Figure 6.10: Fractured surface of NT-weathering specimen

The image shows fine fibrils embedded in the matrix illustrating that the fibrils underwent a form of weathering as shown by a series of "scale-like" features along the fibril surfaces. From the microstructure, good fibril/fibril interaction is revealed. The microstructure also shows fibril surfaces covered with cement hydration particles indicating bonding.

NT-weathered samples were subjected to the combined effects of the

mechanisms of HC and WD environments. These effects were competing in that HC environment induced microcracking whereas WD environment was well hydrated, which minimised shrinkage. Carbonation was not considered as having a significant influence in the mechanical behaviour because the specimen was not carbonated to the fibre depth level at the time of testing (see Fig. 4.26 in Chapter 4).

The cracking patterns that developed on the specimens after tensile testing illustrated that the combined effects of Hot/Cold and Wetting/Drying environments in a tropical environment were beneficial to the mechanical behaviour. The matrix microstructure was "compliant" in that it easily transferred the applied stresses across the interface resulting in attainment of full multiple cracking capacity.

6.3.6 Summary of Environmental Effects on Mechanical Behaviour

From the discussions presented here, the following evidence was put forward for the mechanisms of degradation of Textile Concrete:

- Good fibre/matrix interaction exists in mature Textile Concrete samples that have previously been water-cured for 28 days and aged under controlled laboratory conditions. Bond shear strengths of more than 0.40 MPa (see Eq. 3.1 in section 6.1 and also Table 6.1) are developed in these samples.
- The effect of exposure of PP fibres to a HC environment is manifested in localised fibril damage. The environment causes matrix microcracking.
- WD environment stiffens the fibres whereas in the matrix itself, this environment induces favourable hydration and subsequently, "compliant" microstructure.
- Carbonation results in deposition of carbonates and/or other species on the fibril surfaces, densification, and embrittlement of the matrix.
- Bond strength is a function of: fibril/fibre interaction, fibril/matrix interactions, and the physical condition of the matrix microstructure.

- The main property influencing strain hardening and multiple cracking properties of Textile Concrete is the fibre/matrix interaction. For multiple cracking to be described as similar to HPFRCC (e.g. HC, WD, and NT samples), the microstructure needs to mobilise full multiple cracking (to be "compliant").
- Full multiple cracking is induced by the following mechanisms:(a) when the applied stresses are transferred across the fibre/matrix interface (b) when the microstructure is accommodates the ensuing dimensional changes (c) fibre debonding at the crack planes is easily facilitated. These mechanisms result in sufficient crack propagation.
- There is still understanding needed regarding the apparent environmentally-induced debonding that was observed in NM-weathered fibre pull-out samples.

An attempt to relate different mechanisms of degradation in plain fibres, fibre/matrix bond, and the cracking patterns of TC composites is illustrated in Table 6.1.

These inter-relationships are used in describing strain hardening and multiple cracking behaviour of TC and are the subject of the discussions in the subsequent sections.

6.4 Analytical Behaviour

Based on the synthesis of the different mechanical tests described in Chapter 5, a "model" of the mechanical behaviour of Textile Concrete is developed. The mechanical behaviour of TC is characterised by distinct slopes on the tensile stress-strain (σ-ϵ) curves (as illustrated in Fig. 5.2 in Chapter 5). The following are the main features of a typical curve: initial linear (uncracked) stage, microcracking stage, strain hardening (multiple macro-cracking), peak point, post peak and final failure stages.

Table 6.1: Linkage of mechanical behaviour to the microstructure

Exposure history	Age, months	Change in stiffness		Bond strength τ, MPa		Cracking behaviour (qualitative)	Microstructure		
		Fibre E_f, MPa	Matrix E_m*, MPa	Absolute	% change		Fibrils	Matrix	Fibril/matrix interface
Control	8	control	0	0.84	+48†	control	control, smooth, no clustering	well hydrated, uniform and dense	good bonding,
Control	12	control	+33.7	0.84	+48	more crack wider crack spacings	control	dense matrix, hydration particles distinct	increase in matrix volume and more interaction
Control	14	control	+43.0	no test	no test	more cracks, wider spacing, and sizes	control	matrix clearly dense and and homogeneous	no clear difference in densification with age
Control	16	control	+14.1**	0.91	+52	a few major cracks, several fine cracks	control	signs of a dense matrix	excellent bonding, more matrix/fibril interaction
Hot/cold	5 (pull-out) 12 (composite)	-511.50	+9.6	0.43	-2††	dense cracking, fine cracks at low failure loads	localised damage, scorching and flaking	uniform, fine-grained microstructure, with signs of microcracking	clustering of fibrils, otherwise good bonding
Wetting/ Drying	8 (pull-out) 14 (composite)	+46.10	+48.1	0.78	-7	fewer and wider at reduced spacing	yellowing, roughened surfaces	lumps of dense matrix, sand grains are visible, debonding	fibrils in good contact with matrix, porous matrix
Carbonated	12 (pull-out) 16 (composite)	-465.50	+77.8	0.99	+18	few wide cracks, interspersed by fine cracks	carbonation and/or other species trapped on fibril surfaces	blocky hydration particles, homogeneous matrix	strong fibril/ matrix bonding
Moderate	12	+600.20	+57.5	0.24	-71	fewer and wider cracks, at wide spacings	a few particles trapped to surfaces but no obvious damage	a mould mark on surface, debonded damage matrix crystals	good interaction voids in matrix microstructure wide voids
Tropical	12	+214.80	+59.4	0.81	-4	dense, fine cracking at reduced spacing	contamination signs on fibril surfaces, rough surfaces	good hydration porous matrix around interface porosity	good interaction minor porosity at interfacial zone

*E_m was computed from stresses and strains at the end of the linear region (see Fig. 5.6)
**This reflects a non-linear rate of increase in matrix stiffness
† Values for control samples were based on the minimum value of 0.4 MPa
†† Values for weathered samples were based on control samples of comparable age

The effects of ageing and exposure of TC to different environments are manifested most clearly in the strain hardening and post-peak regions of the σ-ϵ curves. At the strain hardening stage, the behaviour is defined by the coordinates at the end of the linear microcracking region (σ_1,ϵ_1), and the peak point (σ_2,ϵ_2).

While (σ_1,ϵ_1) is a function of the matrix properties, (σ_2,ϵ_2) is dependent on ageing (t), environmental exposure of the composite, and the fibre stiffness (E_f). The rate of strain hardening is described by the slope of the stress-strain curve ($\frac{d\sigma}{d\epsilon}$), which is a function of age and factors related to environmental exposure $\{\frac{d\sigma}{d\epsilon}=f(t)\}$.

At the post-peak stage, the behaviour is characterised by either minor post-peak ductility manifested by reduction in the slope of the σ-ϵ curve ($\frac{d\sigma}{d\epsilon}<0$), or brittle failure ($\frac{d\sigma}{d\epsilon}\rightarrow-\infty$). The post-peak behaviour is influenced by the microstructure in that the less "compliant" the microstructure, the less the post-peak ductility and the material will fail before the full multiple cracking capacity is exhausted.

Conversely, a "compliant" microstructure results in sufficient fibre/matrix interfacial load transfer and crack propagation. These mechanisms enhance the development of a dense cracking patterns on TC composites, a behaviour that characterises High Performance Fibre Reinforced Cementitious Composites (HPFRCC).

The specific mechanisms for each of the different stages on the σ-ϵ curve are:

- At the initial linear uncracked stage, the behaviour is influenced by the elastic behaviour of the matrix.
- At the microcracking stage, the tensile behaviour is due to the composite action of the fine fibrils interacting with the matrix. Stresses are transferred from the matrix to the fibrils as the microcracks propagate.
- At the strain hardening stage, the existing cracks open up, the central cores of polypropylene fibres transfer the load to the matrix which cracks after attainment of the ultimate tensile stress.

- At the post-peak stage before final failure, the fibres stretch between the cracks thereby widening the existing cracks.
- The final failure occurs due to fibre rupture.

To further extend the understanding of the complex process of mechanical behaviour of Textile Concrete, an analytical framework is developed and subsequently used in proposing a prediction model of multiple cracking of TC.

The discussions in Chapter 5 illustrated that the underlying influencing factors in the stress-strain behaviour of Textile Concrete are: age, exposure and weathering, and the properties are fibre stiffness, matrix density, fibre/matrix interface bond, composite stiffness, composite failure stress and strain. A better understanding of the effects of the properties and influencing factors on the mechanical behaviour of TC are gained after the following inter-relationships are determined:

- Correlation between bond strength and toughness of the composite
- Cracking behaviour as a function of the applied stress level
- Effect of ageing on composite toughness
- Variation of composite stiffness with loading
- Variation of composite stiffness with ageing

These inter-relationships are used in describing strain hardening and multiple cracking behaviour of TC and are the subject of the discussions in the subsequent sections.

6.4.1 Correlation of Bond Strength With Toughness

Studies by Bentur and Mindess (Bentur & Mindess 1990) on interfacial property characterisation of polypropylene Fibre Reinforced Cementitious Composites (FRCC) indicates that prior to fibre rupture, increasing the interfacial bond τ accounts for an increase in the composite strength and toughness. These concepts were adopted later by Li et al. (Li et al. 1991*b*) in

characterisation of so called High Performance Fibre Reinforced Cementitious Composites (HPFRCC). By following a similar micro-mechanics-based approach, constitutive models have been suggested by different researchers which describe the tensile behaviour of HPFRCC (Kabele 2003*a*), (Kanda et al. 2000*b*).

Correlation of the interfacial bond strength with composite toughness was consistent with the findings of this research as shown in Fig. 6.11. The variation was similarly consistent with theoretical expectation in that a higher bond would essentially require higher energy to break the composite into blocks. However, as illustrated by the non-linear trend in Fig. 6.11, the correlation initially existing between bond and composite toughness changes when an optimum level is exceeded, the bond is sacrificed possibly due to increased microcracking that is associated with higher toughness.

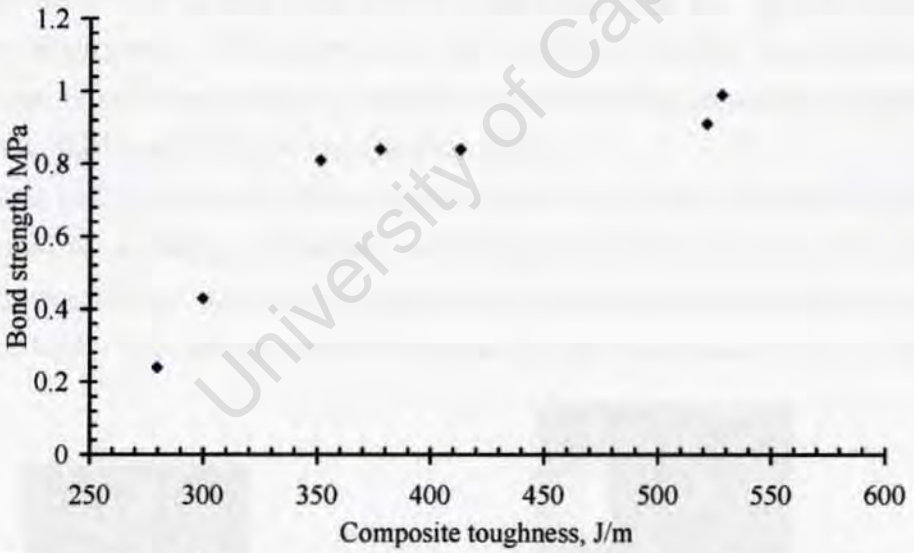

Figure 6.11: Variation of bond strength with composite toughness

6.4.2 Variation of Cracking With Stress Level

The basic theory of crack quantification in FRCC was developed by Aveston, Cooper, and Kelly (Aveston et al. 1971) and was subsequently extensively reviewed by Hannant (Hannant 1978). The assumption in the theory is that

after first cracking of the matrix, a linear transfer of stresses is mobilised from the matrix to the fibres bridging the cracks. As loading progresses, stresses are transferred back into the matrix and thus cracks are propagated in the composite at determinable spacings. Based on this theory, the relationship between crack spacings and the fibre traction stresses and strains is determined.

The mechanisms interacting during loading of FRCC are complex and therefore tensile $\sigma - \epsilon$ curves are better understood by analysing the mechanisms interacting at different stages of loading. These stages were described in section 5.8.2, and were incorporated in the model of mechanical behaviour that was described at the beginning of this section. The concepts introduced in the model are further elaborated on here.

Before the matrix reaches the cracking strength σ_m, the $\sigma - \epsilon$ curve is approximated by a linear function with elastic modulus E_m, which is a matrix material property. The upper limit of this initial loading stage represents the matrix cracking strain ϵ_m, which for cementitious matrices is typically between 0.01 and 0.02 percent (Neville 2002).

The end of the initial linear part of the σ-ϵ (matrix property) is characterised by a change in gradient and marks the onset of low density micro cracks that do not traverse the entire width of the specimen as illustrated in Fig. 6.12(a). The initial microcracking stage was illustrated in Fig. 5.2.

(a) Typical microcracking

(b) Macro cracks during strain hardening

Figure 6.12: Typical cracking patterns at different loading stages

As loading progresses, some micro cracks extend and open up (becoming macro cracks) while at the same time new cracks are formed at different locations along the gauge section.

The third region on the $\sigma - \epsilon$ curve characterises the strain hardening phase when existing macro cracks, which are essentially perpendicular to the loading axis, widen and new ones form and propagate along the specimens as shown in Fig. 6.12(b). During this stage, the crack density increases until either: the multiple cracking capacity of the material is achieved and material strains increase rapidly at very low stresses, or stress increases and failure occurs before full multiple cracking capacity is exhausted. The condition when the full multiple cracking capacity is attained is commonly referred to as crack "saturation" which characterises HPFRCC (Kabele 2003*a*). Strain hardening is not unique to the uniaxial loading mode as it has also been reported in thin TC laminates loaded in flexure (Tait, Mumenya, Alexander & Hourahane 2004).

The mechanism of multiple cracking in HPFRCC was described earlier in 2.7.4 in Chapter 2 where multiple cracking was shown to be influenced by the counteracting actions of fibre bridging traction σ_b, and crack opening displacement (COD) (Lin & Li 1997). Since the composite toughness takes into account the effects of crack opening, which in turn are related to the final failure strains, toughness is therefore investigated as a function of ageing in the section that follows, in an attempt to gain more insight into the multiple cracking behaviour of TC.

6.4.3 Effect of Ageing on Toughness

The area under the σ-ϵ curve represents the energy required to firstly, crack a specimen and secondly, to ultimately fracture it into blocks. A distinction is made between toughness in the multiple cracking zone (see Fig. 5.50), which is the zone where the composite can perform adequately, to the overall toughness obtained beyond this stage, when energy is consumed by the local opening of a localised single crack, as seen for example in Fig. 5.47. The

discussion in this research refers to the overall toughness because samples were tested to final rupture.

The capacity to develop a bigger block of matrix is an indication of brittleness. On the other hand, toughness of the composite is influenced not only by the crack spacings, but by the crack widths, which are a function of local debonding and extension of the fibres bridging the cracks. Conversely, loss in toughness is indicative of reduction in the fibre/matrix bonding capacity implying that less energy would be required for cracking the specimens. Based on this premise, it is expected that composites with wider and more frequent macro cracks would also exhibit high toughness.

Toughness is defined as the area under a σ-ϵ (or load-displacement) curve. When the areas under the σ-ϵ curves were investigated in this research, an increase in toughness of approximately 38 percent over an eight month period of ageing under controlled conditions was observed.

The increase in toughness was attributed to multiple cracking and subsequent opening of the cracks. Fig. 6.13 shows the variation of toughness of fibre pull-out samples (see area under the curve in Table. 5.5) with the average crack spacing of a composite specimen of comparable age. The trend shown in Fig. 6.13 illustrates that samples could have few cracks, but if these cracks open up sufficiently (under loading), the composite is able to sustain loads at strains well beyond those at which cracking first appears in the matrix, hence manifest high toughness. Higher crack spacing gives a higher toughness because of wider crack opening. As would be expected, the variation of bond strength with cracking followed a similar trend and this was substantiated in Fig. 6.14. These observations were consistent with the theoretical expectations.

6.4.4 Variation of Composite Stiffness

The initial gradient of the $\sigma - \epsilon$ curve (strains <0.02 percent) is a measure of the matrix stiffness. At this stage, the matrix is still intact until the first-crack strength is exceeded and microcracking is initiated.

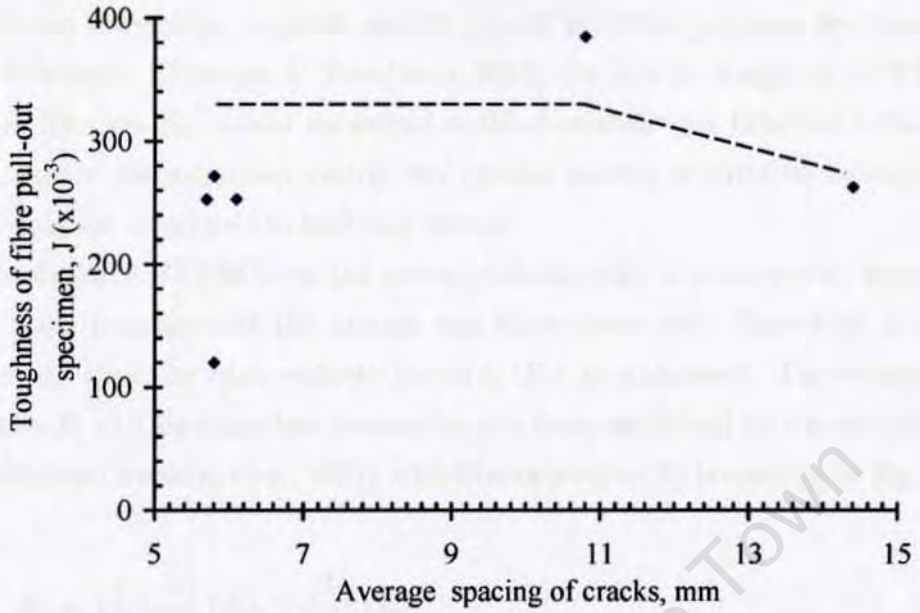

Figure 6.13: Variation of toughness with cracking

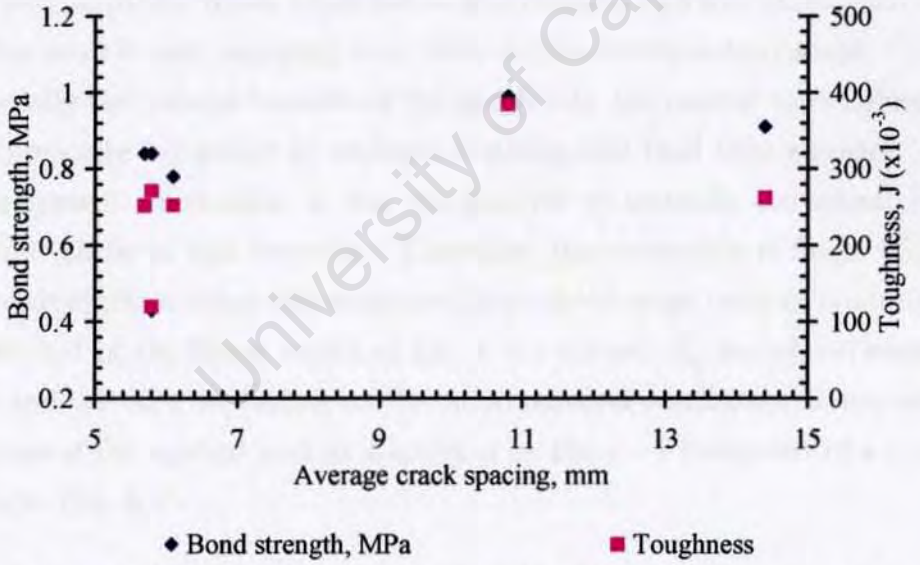

Figure 6.14: Linkage of bond strength with composite cracking

The "first" linear portion shown in Fig. 5.2 (and Fig. 6.15) represents a microcracked matrix with stiffness hereafter referred to as E_m. The variation of E_m was found to be essentially age related. In this research, E_m of tensile specimens typically ranged between 0.5 GPa and 1.6 GPa (see Fig. 5.48),

which are lower than a plain matrix E_m of 10 GPa proposed by Naaman and Renhardt (Naaman & Reinhardt 2004) for use in design of HPFRCC mixes. The low E_m values measured in this research were believed to be due to a heavily microcracked matrix but further testing is required before such materials are employed in building design.

Stiffness of HPFRCC at the microcracking stage is a composite property that takes into account the matrix and fibre properties. Therefore, it is at this stage that the fibre volume fraction (V_f) is addressed. The composite stiffness E_c at this stage has conventionally been described by the simple law of mixtures (Aveston et al. 1971) which incorporates V_f according to Eq. 6.2.

$$E_c = \{\frac{1 - V_f}{V}\}E_m + \{\frac{V_f}{V}\}E_f \tag{6.2}$$

The polypropylene fibres employed in this research had fine fibrils surrounding the central tape implying that while at the microcracking stage, V_f was essentially the volume fraction of the fine fibrils, the central tape influenced the composite behaviour at multiple cracking and final failure stages. Due to equipment constraints, it was not possible to quantify the actual V_f of the fine fibrils in this research. Therefore, the composite stiffness (E_c) at the microcracking stage was estimated from the average tangent modulus up to the end of the linear region of the $\sigma - \epsilon$ curves. E_c varied between 0.2 GPa and 0.5 GPa depending on the environmental conditions. It was also a function of the applied load as illustrated by the $\sigma - \epsilon$ behaviour of a typical curve in Fig. 6.15.

6.4.4.1 Variation of Composite Stiffness with Loading

To determine the variation of composite stiffness with loading at the multiple cracking stage, an empirical approach was adopted. Firstly the experimental data for each exposure condition were used to determine a relationship by curve fitting using a second order polynomial as exemplified in Fig.6.16. Typical hypothetical curves were thus obtained.

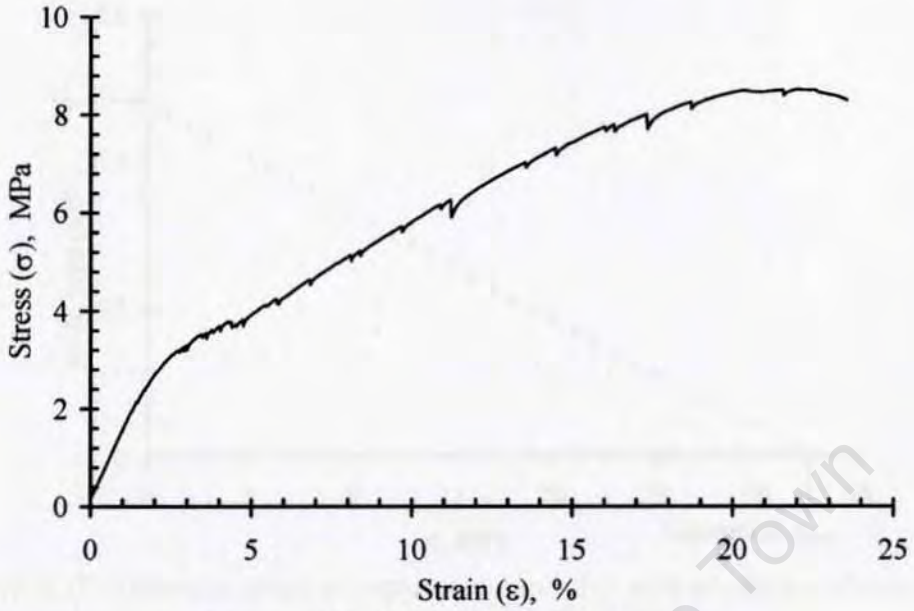

Figure 6.15: Typical tensile behaviour

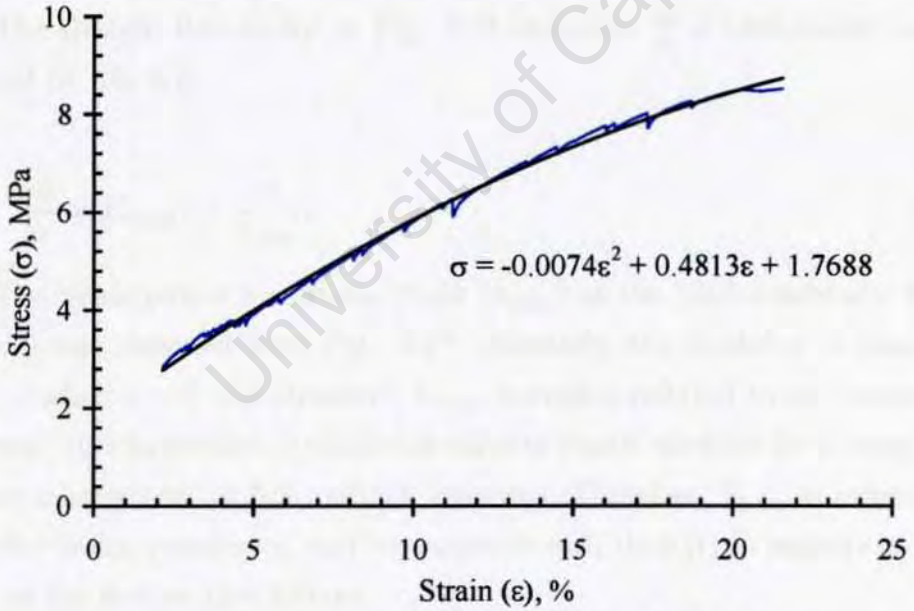

Figure 6.16: Curve fitting to experimental data

For each exposure condition, the gradient of the hypothetical curve ($\frac{d\sigma}{d\epsilon}$) was computed and the modulus E_c at the start of strain-hardening region obtained by plotting $\frac{d\sigma}{d\epsilon}$ against σ as shown in Fig. 6.17.

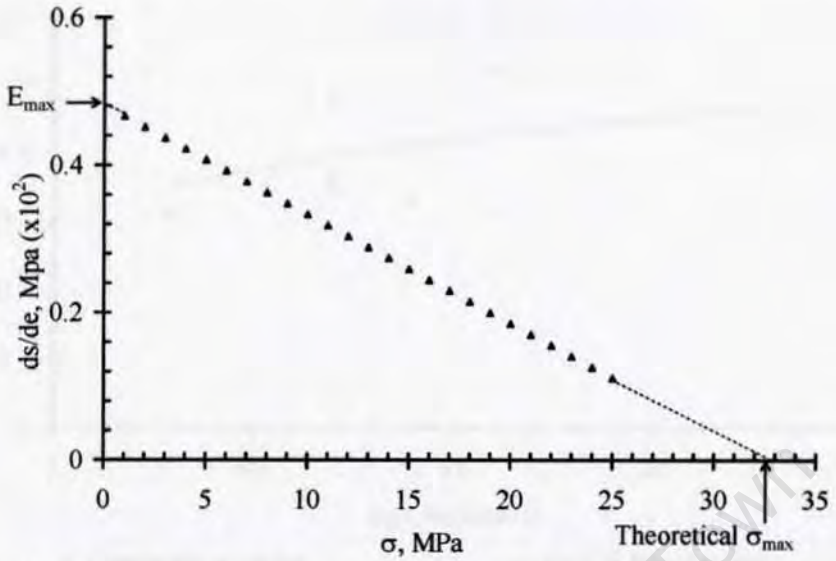

Figure 6.17: Determination of composite modulus and maximum theoretical stress: representing the gradient of curve in Fig. 6.16

The straight line shown in Fig. 6.17 describes $\frac{d\sigma}{d\epsilon}$-$\sigma$ relationship and is defined by Eq. 6.3.

$$\frac{d\sigma}{d\epsilon} = E_{max}[1 - \frac{\sigma}{\sigma_{max}}] \tag{6.3}$$

The hypothetical maximum stress (σ_{max}) at the peak conditions when $\frac{d\sigma}{d\epsilon} = 0$ was obtained from Fig. 6.17. Similarly, the modulus of elasticity (E_{max}) when $\sigma = 0$ was obtained. E_{max}, hereafter referred to as "composite stiffness", is a hypothetical maximum value of elastic modulus for a composite before achievement of full multiple cracking. Therefore, E_{max} is considered a useful design parameter, and its variation with time (t) in months is dealt with in the section that follows.

6.4.4.2 Variation of Composite Stiffness with Ageing

Composite stiffness (E_{max}) is dependent on age (t) and environmental conditions. As the composite ages, E_{max}-t relationship follows the trend shown in Fig. 6.18.

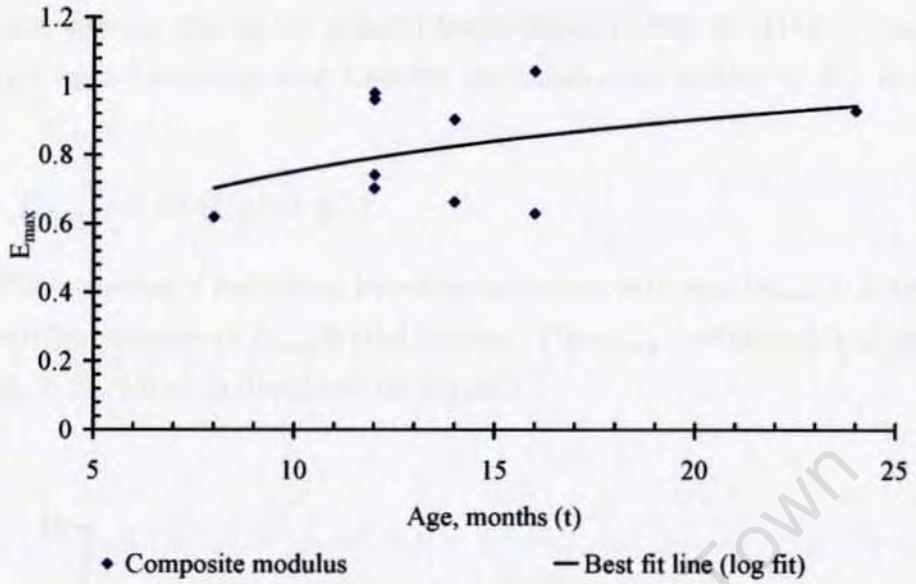

Figure 6.18: Variation of composite stiffness with age

A high scatter in results is observed in the trend shown in Fig. 6.18 but by computing the average value of E_{max} for specimens of the same age, a better approximation of the E_{max}-t relationship is obtained as shown in Fig. 6.19.

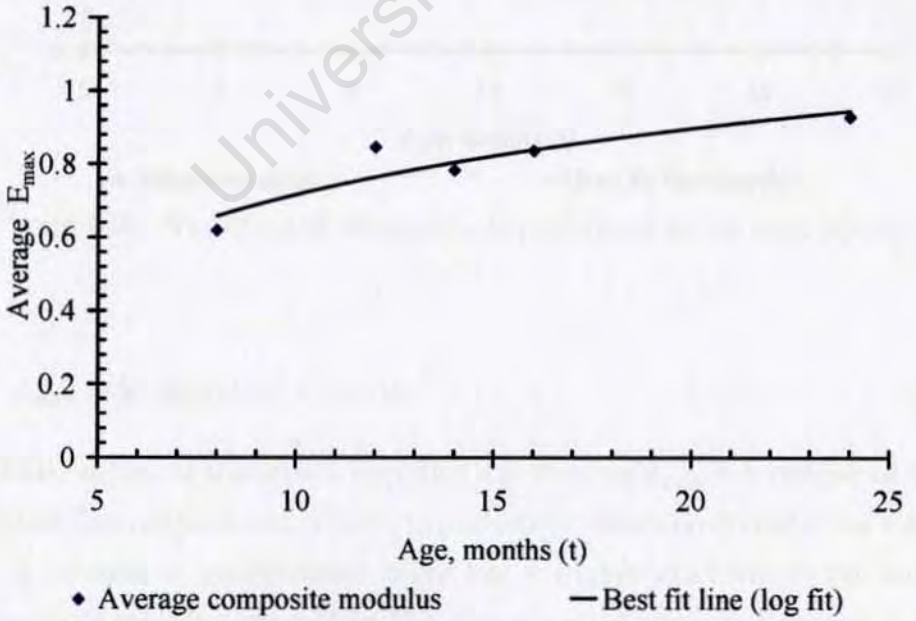

Figure 6.19: Prediction of maximum composite stiffness

One way of defining the general trend shown in Fig. 6.19 is by using the logarithmic relationship that best fits the trend as described by Eq. 6.4.

$$E_{max} = 0.600(log)t + 0.247 \tag{6.4}$$

The variation of maximum hypothetical stress with age, (σ_{max}-t) is treated in a similar manner to E_{max}-t relationship. The σ_{max}-t relationship is shown in Fig. 6.20, which is described by Eq. 6.5.

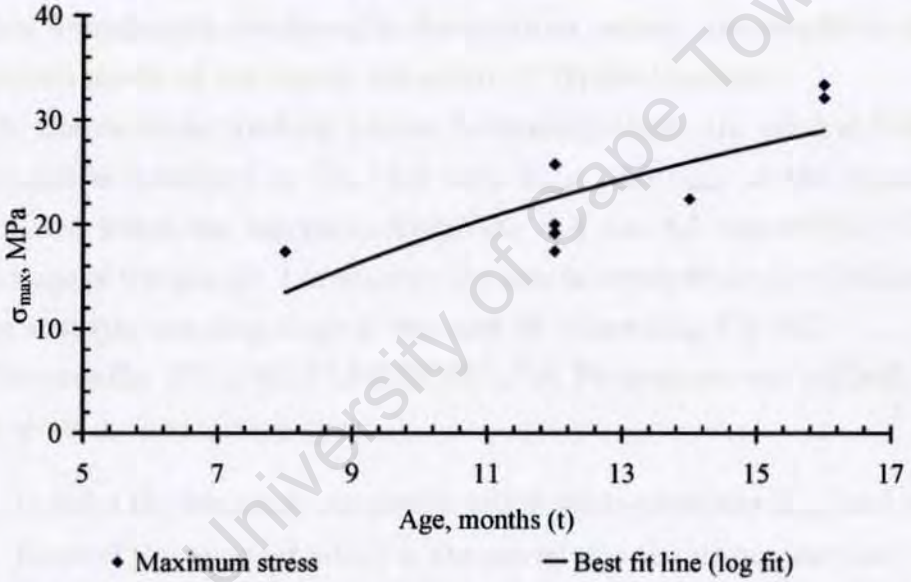

Figure 6.20: Variation of maximum hypothetical stress with ageing

$$\sigma_{max} = 51.569(log)t - 33.115 \tag{6.5}$$

When values of maximum hypothetical stresses σ_{max} are compared with the values from experimental data, hypothetical values are found to be higher. This is because a hypothetical curve has a higher gradient at the end of the multiple cracking zone than the experimental curve (as shown in Fig. 6.16). However, to make a prediction of the maximum elastic modulus of a

composite, which would be required for design, the hypothetical maximum stress σ_{max} also needs to be determined (as illustrated by Eq. 6.3).

The parameters described in sections 6.4.1 to 6.4.4 illustrate that composite stiffness is a function of ageing (time related) and loading. In addition, an important parameter in the analytical predictions is the loading rate of the composite specimens.

6.4.5 Simulation of Tensile Behaviour of Textile Concrete

The relationships described in the first part of this Chapter, and the mathematical formulations developed in the previous section, are simplified into a prediction model of the tensile behaviour of Textile Concrete.

At the multiple cracking (strain hardening) stage, the general form of the model is described by Eq. 6.3 with E_{max} and σ_{max} as the boundary conditions, which are computed from Eqs. 6.4 and 6.5 respectively. For a known age of the sample, t in months, the tensile stress-strain (σ-ϵ) behaviour at the multiple cracking stage is obtained by integrating Eq. 6.3.

To solve Eq. 6.3, a MATLAB/SIMULINK Programme was utilised. The main steps in the solution were:

i. Input of the boundary conditions which were essentially E_{max} and σ_{max}.
ii. Input of the constant which in the model was the strain rate (snr) used in the composite tensile test.
iii. Linking the boundary conditions with the constant in a logical manner that represents Eq. 6.3.

Eq. 6.3 and the strain rate were translated into a Block Diagram from which stress-strain (σ-ϵ) values were simulated. The SIMULINK Block Diagram used in simulation of the muitiple cracking stage is shown in Figs. 6.21.

The predictive capability of the model was tested on experimental data of a typical TC specimen that had been aged under laboratory conditions for eight months. The input values for the model were:

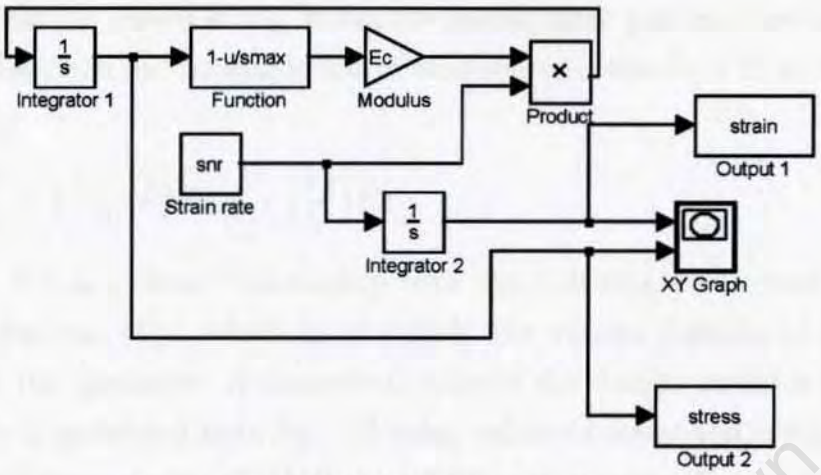

Figure 6.21: SIMULINK Block Diagram

E_{max}	65.86 MPa
σ_{max}	13.45 MPa
Strain rate	(10/125) per minute

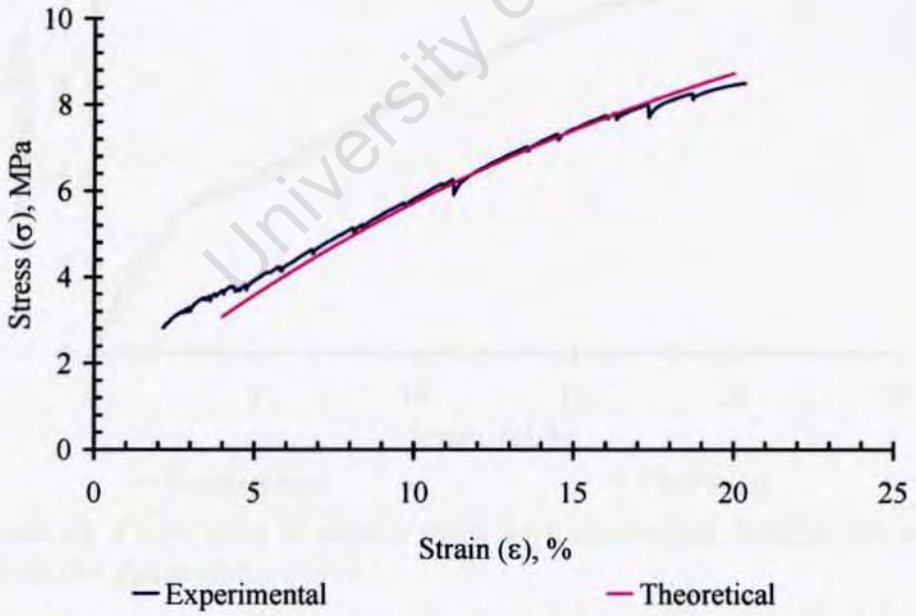

Figure 6.22: Correlation of experimental with theoretical data over the multiple cracking region

The predicted values of stress and strain correlated well with the exper-

imental data as shown in Fig. 6.22. The initial linear portion shown on Fig. 6.15 is described by the simple law of mixtures (see also Eq.6.2) as follows:

$$\frac{d\sigma}{d\epsilon} = \{\frac{1 - V_f}{V}\}E_{max} + \{\frac{V_f}{V}\}E_f \tag{6.6}$$

Eq. 6.6 is a linear relationship with the following parameters: Fibre volume fraction (V_f), which is essentially the volume fraction of the fine fibrils in the specimen. A theoretical value of the matrix modulus E_{max} of 112 MPa is generated from Eq. 6.3 using values of stress and strain at the end of the linear region (2.2 MPa and 2.2% respectively), E_f was measured for non-bonded fibres as approximately 1077 MPa (see section 5.4). These parameters can be used to solve equation 6.6 and hence get the modulus of the microcracked matrix ($\frac{d\sigma}{d\epsilon}$).

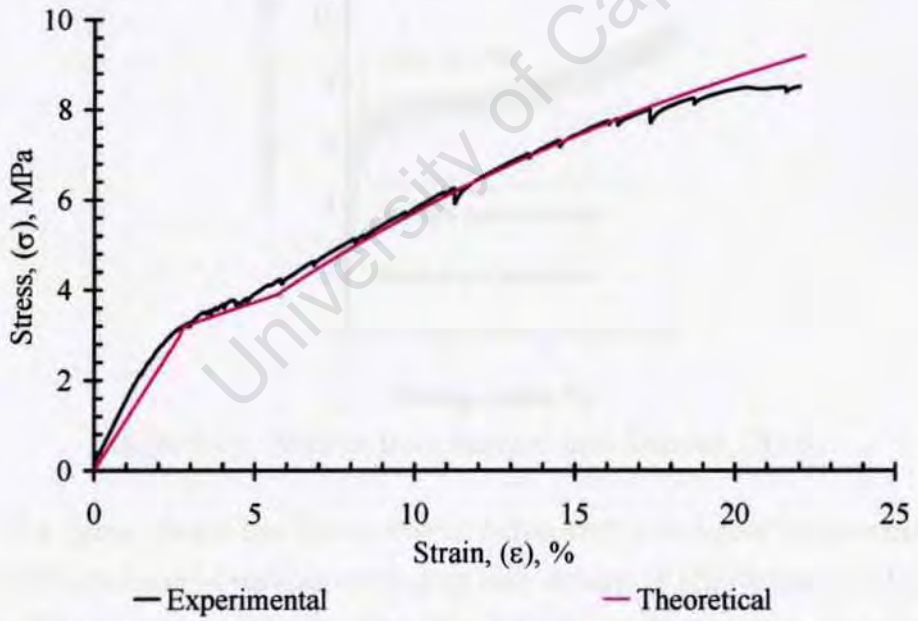

Figure 6.23: Correlation of experimental with theoretical data for the whole range of the stress-strain curve

An approximation of the value of $\frac{d\sigma}{d\epsilon} = 112$ was used to model the linear region of the stress-strain curve. The whole range of the stress-strain curve was thus modelled as shown in Fig. 6.23.

The figure shows that for the initial region, the simplified assumption of a linear relationship overestimated the strains developed for a given stress level. A better agreement would be achieved if the fibre volume fraction of the fine fibrils was known hence Eq. 6.6 would be solved.

6.4.6 Testing of the Model on Independent Data

The model was tested using independent data from literature. Fig. 6.24 shows the results of macroscopic material behaviour of Textile Reinforced Concrete (TRC) by Richter and Zastrau (Richter & Zastrau 2006).

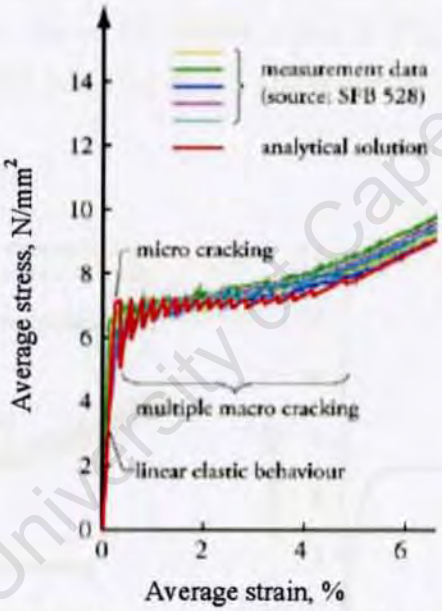

Figure 6.24: Results from Richter and Zastrau (2006)

The figure shows the linear elastic behaviour, non-linear micro-cracking and multiple macro-cracking extending over strains of approximately 4.5 percent. The terms used to describe the different regions on the stress-strain curve in Fig. 6.24 are consistent with the terms used in this thesis. The strain hardening stage shown on the figure extending beyond strains of approximately 4.5 percent is due to loading of rovings (a bundle of huge number of continuous filaments) which had an elastic modulus (E_f) of 76,000N/mm^2.

The applicability of the proposed model up to the end of multiple cracking stage is demonstrated in Fig. 6.25(b). The curve was simulated from the results of Richter and Zastrau (Richter & Zastrau 2006) by substituting the following parameters (quoted in the literature) into Eq. 6.3:

E_{max}	30,000 MPa
σ_{max}	7 MPa
Strain rate	(0.9/200) per minute

The results from Richter and Zastrau (Richter & Zastrau 2006) and the model simulation were placed on similar scales in Fig. 6.25. It is illustrated that within the multiple cracking stage, the model is in fair agreement with the independent data.

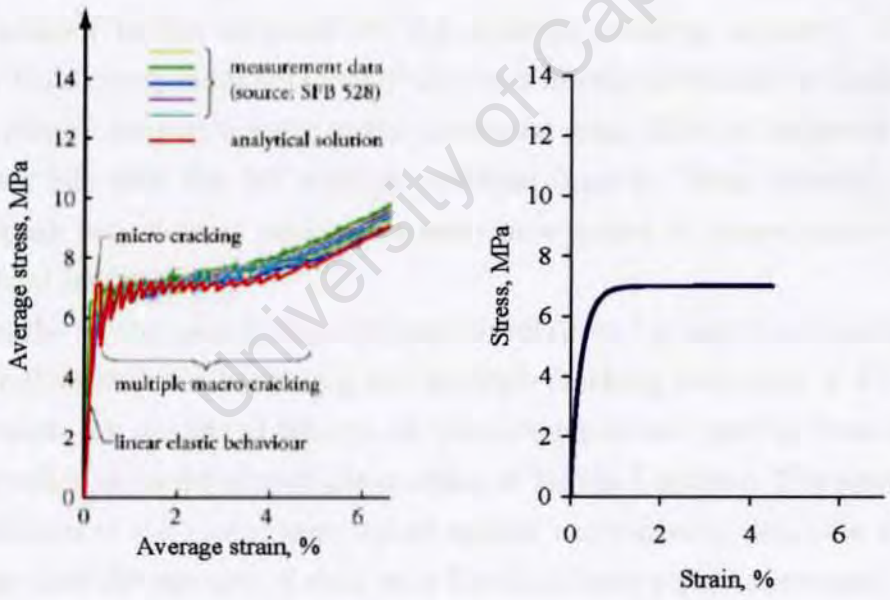

(a) Results from Richter and Zastrau (2006)

(b) Theoretical curve

Figure 6.25: Comparison of independent data with the model solution up to multiple cracking stage

6.5 Summary

It was illustrated from a mechanical behaviour as well as microstructural perspective that apart from good fibre/matrix interaction, there are other competing mechanisms that influence the fibre/matrix bond strength. These mechanisms influence the manner in which fibres pull-out from the matrix. Among these mechanisms, the nature of the matrix microstructure at the interfacial zone was found to play a key role in the fibre pull-out behaviour. The microstructure at the critical interfacial zone also influences multiple cracking and post-peak behaviour of TC.

It was clear from the discussions that full multiple cracking was not achieved in all TC composites used in this research study. Samples with strong fibre/matrix bonds and a dense microstructure at the critical interfacial zone failed at high stresses after attainment of the composite strength but without having achieved the full multiple cracking capacity. On the other hand, composites with relatively lower interfacial bonds but with more "compliant" microstructures at the interfacial zone, failed at relatively lower stresses but with the full multiple cracking capacity being achieved. The post-peak behaviour of composites was characterised by minor ductility before final failure.

In the second part of this Chapter, correlations between the mechanisms that influence strain hardening and multiple cracking behaviour of TC were discussed. An analytical framework was developed and used in formulation of a prediction model of multiple cracking of Textile Concrete. The predictive capabilities of the model were tested against experimental data of a typical sample and the two sets of data were found to have a good agreement.

Chapter 7

Conclusions and Recommendations

7.1 Conclusions

This thesis has been concerned with a mechanical evaluation of environmental weathering of Textile Concrete. To facilitate this, investigations were undertaken on the mechanical behaviour of polypropylene (PP) fibres, the matrix, fibre pull-out, and Textile Concrete (TC) composites, as a function of various environmental regimes.

An experimental programme was developed involving subjecting samples to "ambient" environments which are commonly encountered in service. These environments were: cyclic Hot/Cold (HC), Wetting/Drying (WD), carbonation (C_c), and natural environments (tropical (NT) and moderate (NM) climates). Parallel investigations involving ageing of samples under controlled laboratory conditions (C) for several months, as well as tensile testing of Textile Concrete samples obtained from Industry (I). The effects of ageing on strength and toughness were complemented by undertaking observations of fibre and interface features using a scanning electron microscope (SEM).

The tensile behaviour of plain PP fibres was found to be influenced by different environmentally-related mechanisms, the following being the main effects:

- Thermal-related softening and loss of strength in HC-weathered and carbonated fibres.
- Minor loss in toughness after exposure to a warm, damp WD environment.
- Embrittlement and loss of strength after exposure to sunlight in a tropical climate.

For the cementitious matrix itself, it was found that on-going cement hydration densifies the matrix but there were other environmentally-related factors which were manifested at the microstructure level. These effects were: embrittlement of the matrix due to carbonation, minor microcracking after HC exposure, increased hydration in WD environment which counteracted microcracking of the matrix.

The following were the main findings of mechanical characterisation of the fibre/matrix interfacial properties, and composite tensile behaviour:

- The main contribution to knowledge was that despite exposure to a range of "ambient" surroundings, TC does not show much degradation. Although this may not be surprising, mechanical evaluation of the effects of exposure to five different environmental regimes has not been documented in the past.
- By embedding the fibres in the matrix, the effects of environmental exposure of plain PP fibres were substantially reduced.
- The fibre/matrix bond strength increased with ageing. Among the environmental regimes investigated, carbonation caused the highest gain in bond strength whereas no significant variation occured due to HC, WD, and NT exposures. Poor performance in NM-weathered fibre pull-out was not well understood but was considered as an outlier.
- Textile Concrete exhibits a "pseudo-ductile" (strain hardening) nonlinear stress-strain tensile behaviour due to multiple cracking with load softening and significant toughness. In the range tested, TC exhibited two modes of strain hardening (see the summary in Table 7.1):

(a) achievement of the maximum composite strength (σ_c), but failure occurring before the full multiple cracking state is attained, and (b) achievement of the full multiple cracking capacity due to a "compliant" microstructure. This type of composite behaviour was characterised by minor post-peak ductility prior to final failure. The performance of composites with "compliant" microstructures is similar to High Performance Fibre Reinforced Cementitious Composites (HPFRCC) in that they are tough and strong enough for their application.

- A dense matrix and strong fibre/matrix bond (similar to carbonated samples) mitigated against mobilisation of the full multiple cracking capacity.

Table 7.1: Failure modes in samples weathered under different conditions

Strength> 10 MPa		Strength ≤ 10 MPa	
Full multiple cracking capacity achieved	Full multiple cracking capacity not achieved	Full multiple cracking capacity achieved	Full multiple cracking capacity not achieved
16 months control Industry Wetting/Drying	Carbonated 14 months control	8 months control Hot/Cold Tropical climate	12 months control Moderate climate

Table 7.1 illustrates that full multiple cracking capacity was achievable at different stresses, and apart from 16 month old control samples, which were considered as outliers, achievement of the full multiple cracking was more common in the earlier-age control samples. The following were the conclusions from the findings of this research:

- The matrix used for the study was effective in protecting polypropylene (PP) fibres from ultraviolet (UV) irradiation.
- For TC composites, the beneficial effects of "compliant" microstructures due to the combined effects of Hot/Cold and Wetting/Drying environments were realised in a tropical environment (NT) but not in a moderate climate (NM).

- The satisfactory weathering performance of TC composite from this research suggests that potential for production of TC composites with performance designed to suit a desired demand is achievable. Already the South African Textile Concrete Industry has gone a long way in optimising mix proportions and production techniques.
- The mechanical performance of Textile Concrete is, by and large, not adversely affected by "ambient" environmental exposures. However, if the prediction of its engineering performance, such as strength and toughness is to be possible, there is need for a suitable choice of material that should include an environmental parameter. The factor would be useful in design if incorporated in the composite stiffness (E_{max}) and the predicted maximum failure stress (σ_{max}).
- An analytical framework that was developed and used in formulation of a prediction model of tensile behaviour of Textile Concrete had good predictive capabilities. The possibility of such a prediction would then lead to the design of "fit for purpose" Textile Concrete products.

7.2 Research Limitations

- A single mortar mix was optimised (customised) to suit sample production for this research study. Therefore it was not established how the microstructure was related to the mix composition, and subsequently how the mechanical behaviour would change with matrix composition. If the prediction of the engineering performance of Textile Concrete, such as strength and toughness is to be possible, choosing of a suitable matrix through a standardised mix design process is necessary.
- The facility used for accelerated ageing was operated in a semi-automated manner. This was mainly because a discrepancy existed between the Hot/Cold and Wetting/Drying cycle times. The next step in development of the facility is to modify the design with the aim of synchronising Wetting/Drying with the Hot/Cold cycle times, and thus run the system as a fully automated facility. Potential for modification of

the facility is by improving its drying capabilities at room temperatures rather than Drying at elevated temperatures. In addition, since the accelerated ageing facility comprised of relays and timer, there is potential for computer interfacing and the possibility of running the integrated facility as a Programmable Logic Controlled (PLC) system.

- The mechanical characterisation undertaken in this research was limited to the behavioral level with no attempt being made to model the mechanics of load transfer, fibre/matrix interaction, and final composite failure. Numerical modeling, would provide a better insight into the composite behaviour and the information, particularly the limiting crack widths for multiple cracking, would be useful in material and structures design. Although it is acknowledged that this is certainly a current international focus area which is essential for introduction of new materials into the industry, numerical modeling was not undertaken in this research study.
- The evaluation of how mechanical properties of Textile Concrete change with the effects of fatigue and creep were not undertaken in this study. However, for a better insight into the long-term behaviour and structural performance of this new material, a better understanding of these aspects of mechanical properties of TC are to be recommended.

7.3 Recommendations

Due to equipment constraints in this research, it was not possible to carry out independent mechanical tests on fibres in their embedded state and hence observe the direct effects of ageing on the fibres. Investigations into this aspect of fibre properties are therefore suggested.

The level of interaction of fine fibrils with the matrix could not be quantified within the scope of this research. Therefore the fibre volume fraction (V_f) at the microcracking stage could not be stated precisely. Independent tests to establish V_f of CemForce in the matrix are suggested.

As a means of improving the ageing performance of Textile Concrete, it is suggested that design mixes be branded to suit different environments.

It was not clear from the fibre pull-out behaviour, or the microstructure of the matrix, how different weathering mechanisms affect the frictional shear forces at the fibril/matrix contact surfaces. In addition, the mechanisms of fibre debonding and the subsequent crack initiation and propagation were not directly investigated in this research. Extension of the study into these two aspects of fibre/matrix interfacial mechanics is suggested.

The tensile specimen production technique that was developed in this research was labour intensive thus posing serious limitations on the sample size that could be produced in a single batch. Future improvements to mechanise the production process and hence increase the sample size for a given set are suggested. This way, a robust statistical analysis of the experimental data would be possible leading to a broader and more representative contribution to knowledge.

The gradients of the composite stress-strain curves at the micro-cracking stage (strains of less than 2 percent) represented the modulus of the composite (E_c). The average values of E_c were in the vicinity of 0.5 GPa, which were very low in comparison with the modulus of a "pure" matrix (E_m) that typically varies between 5 GPa and 10 GPa (Hannant 1978), (Naaman & Reinhardt 2006). The low values of composite modulus indicate substantial microcracking at low strain levels up to 2 percent. This aspect of TC tensile behaviour would be worthy of further study.

A limitation in the method of crack quantification adopted in this thesis was that the quantification was undertaken on specimens in the unloaded state after final specimen fracture. However, at the end of composite tensile test, the cracks had undergone substantial "healing" and had subsequently closed up considerably after unloading at the end of the test. Therefore the measured crack widths did not strictly represent the specimens' stress state meaning that the stated crack quantities had inherent uncertainties which were not determined. An improvement in the accuracy of crack quantification

technique is suggested possibly taking the measurements during multiple cracking of the specimens at pre-determined loading intervals.

The techniques employed for composite tensile testing did not facilitate clear observations and evaluation of the extent of local matrix debonding at the crack planes to be made. For a better insight into the nature of crack initiation and propagation, future investigations into this aspect, possibly utilising ultrasound-based techniques, are suggested.

Severe fibre damage in NT-exposed fibres was accredited to the amount of sunshine in a medium altitude in the tropics (Nairobi) where the specimens were weathered. Ultra-violet (UV) irradiation was considered as playing a key role in the damage to plain PP fibres. However, UV damage to the fibres was not as severe in a moderate climate in Cape Town indicating that UV irradiation rate could be lower in Cape Town than in Nairobi. This was however not validated in this research but is recommended for further investigations.

Microstructural studies were undertaken up to a preliminary level only which involved topographic images of fracture surfaces observed under a scanning electron microscope (SEM). The study needs to be extended to cover "in situ" observations of the mechanisms of fibre/matrix interactions, debonding, and crack propagation during loading. To gain a better understanding of the chemical processes that lead to changes in mechanical properties of TC after exposure, an extension of microstructural studies to differential thermal analysis (DTA) would be useful.

Further evaluation of mechanisms of fibre/matrix bonding, and cracking behaviour in Textile Concrete composites, possibly using numerical techniques, is to be suggested. The evaluation would then lead to quantification of the damage that occurs at the interfacial microstructure during fibre pull-out and debonding and hence quantify more fully the changes that occur after different environmental exposures. In addition, a numerical approach would create a better understanding of the bond quality distribution along the embedded sections of fibres. This way, advancements in Textile Con-

crete technology could be significantly advanced. The key to the next step is testing of bonded (i.e. welded) fibres.

References

Addis, B. & Owens, G. (2001), *Fulton's concrete technology*, Cement and Concrete Institute, Midrand.

Agopyan, V., Savastano, H., John, V. & Cincotto, M. (2005), 'Developments on vegetable fibre-cement based materials in Sao Paulo, Brazil: an overview', *Cement and Concrete Composites* **27**(27), 527–536.

Ajiwe, V., Okeke, C. & Akigwe, F. (2000), 'A preliminary study of manufacture of cement from rice husk ash', *Bioresource Technology* **73**, 37–39.

Akers, S. & Studinka, J. (1989), 'Ageing behaviour of cellulose fibre cement composites in natural weathering and accelerated tests', *Journal of Cement and Concrete Composites* **11**(2), 93–97.

Akers, S., Tait, R. & Hourahane, D. (2003), Non-woven Textile Reinforced Composite Concrete, *in* M. Acar, ed., 'Fibre Society Conference, Engineered with Fibres', Loughborough, pp. 75–76.

Alcock, B., Cabrera, N., Barkoula, N., Reynolds, C., Govaert, L. & Peijs, T. (2007), 'The effect of temperature and strain rate on the mechanical properties of highly oriented polypropylene tapes and all-polypropylene composites', *Composites Science and Technology (Alticle in press)* .

Alwan, J., Naaman, A. & Guerrero, P. (1999), Effect of mechanical clamping on the pullout response of hooked steel fibres embedded in cementitious matrices, Technical report, RILEM Publications S.A.R.L.

Ashby, M. & Jones, D. (1986), *Engineering Materials 2: An Introduction to Microstructures, Processing and Design*, Pergamon Press, Oxford, UK.

Aspiras, F. & Manalo, J. (1995), 'Utilisation of textile waste cuttings as building material', *Journal of Materials Processing Technology* **48**, 379–384.

ASTM C 109/C 109M-05 (2005), *Compressive Strength of Hydraulic Cement Mortars (Using 2-in. or 50-mm Cube Specimens).*

ASTM C136-01 (1993), *International Test Method for Sieve Analysis of Fine and Coarse Aggregates.*

ASTM C1362 (1997), *International Standard Test Method for Flow of Freshly Mixed Hydraulic Cement.*

ASTM C1437-01 (2001), *Test Method for Flow of Hydraulic Cement Mortar.*

ASTM C150-07 (2007), *Specification for Portland Cement.*

ASTM C192/C192M-00 (2000), *International Standard for Making and Curing Concrete Test Specimens in the Laboratory.*

ASTM C230 (1990), *International Standard on Specification for Flow Table for Use in Tests of Hydraulic Cement.*

ASTM C494 (2005), *International Standard Specification for Chemical Admixtures for Concrete.*

ASTM C642-97 (1997), *Standard Test Method for Density, Absorption, and Voids in Hardened Concrete.*

ASTM C94/C94M-00e2 (2000), *Standard specification for Ready-Mixed Concrete.*

ASTM D4065-93 (1993), *International Standard for Determining and Reporting Dynamic Mechanical Properties of Plastics.*

Aveston, J., Cooper, G. & Kelly, A. (1971), Single and multiple fracture, *in* 'The Properties of Fibre Composites', IPC Science and Technology Press, Surrey, U.K., pp. 15–26.

Azapagic, A., Emsley, A. & Hamerton, I. (2003), *Polymers, the Environment and Sustainable Development*, John Wiley.

Balaguru, P. & Shah, S. (1992), *Fiber-Reinforced Cement Composites*, McGraw-Hill.

Banholzer, B., Brameshuber, W. & Jung, W. (2005), 'Analytical simulation of pull-out tests - the direct problem investigations', *Cement and Concrete Composites* **27**, 93–101.

Banholzer, B., Brockmann, T. & Brameshuber, W. (2006), 'Material and bonding characteristics for dimentioning and modelling of textile reinforced concrete (trc) elements', *Materials and Structures* **39**, 749–763.

Banthia, N. & Trottier, J. (1994), 'Concrete reinforced with deformed steel fibers, *part* 1: Bond slip mechanisms', *ACI Materials Journal* pp. 435–446.

Baoju, L., Youjun, X., Shiqiong, Z. & Jian, L. (2001), 'Some factors affecting early strength of steam-curing concrete with ultrafine fly ash', *Cement and Concrete Research* **31**, 1455–1458.

Bazant, Z. (1979), Advanced topics in inelasticity and failure of concrete, Technical report, Swedish Cement and Concrete Research Institute, CBI.

Bazant, Z. & Gettu, R. (1992), 'Rate effects and load relaxation in static fracture of concrete', *ACI Materials Journal* **89, No. 5**, 456–468.

Bentur, A. & Akers, S. (1989), 'The microstructure and ageing of cellulose fibre reinforced cement composites cured in a normal environment', *The*

International Journal of Cement Composites and Lightweight Concrete **11**(2), 99–109.

Bentur, A. & Mindess, S. (1990), Fibre reinforced cementitious composites, Elsevier Applied Science, New York.

Bentur, A., Mindess, S. & Vondran, G. (1989), 'Bonding in polypropylene fibre reinforced concretes', *The International Journal of Cement Composites and Lightweight Concrete* **11**(3), 153–158.

Bergstrom, S. & Gram, H. (1984), 'Durability of alkali-sensitive fibres in concrete', *The International Journal of Cement Composites and Lightweight Concrete* **6**(2), 75–80.

Bouzoubaa, N., Zhang, I. & Malhotra, V. (1998), 'Superplasticised portland cement: Production and compressive strength of mortars and concrete', *Cement and Concrete Research* **28**, 1783–1796.

Broutman, J. & Krock, H. (1975), Structural design and analysis, part 1, *in* C. Chamis, ed., 'Composite materials', Vol. 7, Academic press.

Browne, M., Varadarajulu, D., Lewis-Michla, E. & Fitzgeralda, E. (2005), 'Cancer incidence and asbestos in drinking water, town of Woodstock, NewYork, 1980-1998', *Environmental Research* **98**(224-232).

Bruckner, R., Ortlepp, R. & Curbach, M. (2006), 'Textile reinforced concrete for strengthening in bending and shear', *Materials and Structures* **36**, 741–748.

Brydson, J. (1975), *Plastic Materials*, London Newnes-Butterworths.

Burrows, R. (2007), 'The life and death of type II cement', *Concrete Construction Magazine* .

Callec, P. (2003), Textile reinforced concrete, Technical report, RILEM Publications.

Campell, I. (2000), *Introduction to Synthetic Polymers*, 2nd edn, Oxford University Press.

Chang, C.F. Chen, J. (2005), 'Strength and elastic modulus of carbonated concrete', *ACI Materials Journal* **102, No. 5**, 315–321.

Chen, J., Thomas, J. & Jennings, H. (2006), 'Decalcification shrinkage of cement paste', *Cement and Concrete Research* **36**, 801 809.

Coutts, R. (2005), 'A review of Australian research into natural fibre cement composites', *Cement and Concrete Composites* pp. 518–526.

Currie, B. & Gardner, T. (1989), 'Bond between polypropylene fibres and cement matrix', *The International Journal of Cement Composites and Lightweight Concrete* **11**(1), 3–9.

Demortier, G. (2004), 'PIXE, PIGE and NMR study of the masonry of the pyramid of Cheops at Giza', *Nuclear Instruments and Methods in Physics Research* **B 226**, 98–109.

Dhir, R., Jones, M., McCarthy, M., Zheng, L., Chittirattnakorn, P. & Scorey, V. (2002), Optimizing the use of portland cement in concrete by void minimization using fillers and non-portland binders, Technical report, Department of the Environment, Transport and Regions.

Dhir, R., McCarthy, M., Zhou, S. & Tittle, P. (2004), 'Role of cement content in specifications for durability: Cement content influences', *Structures and Buildings* **157**, 113–128.

Diamond, S. (2004), 'The microstructure of cement paste and concrete - a visual primer', *Cement and Concrete Composites* **Vol. 26, No. 8**, 919–933.

Dransfield, J. (2003), *Advanced Concrete Technology Constituent Materials*, Elsevier.

EN 197-1 (2000), *European or International Standard, Code of Practice for Portland cement CEM-1 class 42.5 N.*

EN197-4 (2004), *Composition, specifications and conformity criteria for low early strength blastfurnace cements.*

Ferraris, C., Obla, K. & Hill, R. (2001), 'The influence of mineral admixtures on the rheology of cement paste and concrete', *Cement and Concrete Research* **31**, 245–255.

Fulton, F. & Crawfold, P. (1982), *Cement and Concrete*, Portland Cement Institute.

Galloway, J., Williams, R. & Raithby, K. (1981), Mechanical properties of polyolefin reinforced cement sheet for crack control in reinforced concrete, Technical Report 658, Crowthorne Transport and Road Research.

Gardner, T. & Currie, B. (1983), 'Flexural behaviour of composite cement sheets using woven polypropylene mesh fabric', *International Journal of Cement Composites and Lightweight Concrete* **5**, 193–197.

Gardner, T., Currie, B. & Green, H. (1983), Performance of Civil engineering products made from a cement matrix reinforced with polypropylene matting, *in* 'Third International Conference on Polypropylene Fibres and Textiles', University of York, pp. 1–39.

Gilbert, G. (2004), GFRC-30 years of High Fiber Cement Composite applications worldwide, *in* A. Dubey, ed., 'Thin Reinforced Cement-Based Products and Construction Systems', number SP.224, American Concrete Institute, pp. 1–20.

Gopalaratnam, V. & Shah, S. (1987*a*), Failure mechanism and fracture of fibre reinforced concrete, Technical report, American Concrete Institute.

Gopalaratnam, V. & Shah, S. (1987*b*), 'Tensile failure of steel fiber-reinforced mortar', *Journal of engineering mechanics* **113**(5), 635–652.

Grabiec, A. (1999), 'Contribution to the knowledge of melamine superplasticizer effect on some characteristics of concrete after long periods of hardening', *Cement and Concrete Research* **29**, 699–704.

Gray, B. (1972), Fibre reinforced concrete- a general discussion of field problems and applications, *in* 'Proceedings of Conference on New Materials in Concrete', University of Illinois ant Chicago Circle, pp. 1–14.

Hannant, D. (1978), *Fibre Cements and Fibre Concretes*, John Wiley.

Hannant, D. (1980), Polymer fibre reinforced cement and concrete, Boston.

Hannant, D. (1998), 'Durability of polyproylene fibers in portland cement-based composites: Eighteen years of data', *Journal of Cement and Concrete Research* **28**(12), 1809–1817.

Hannant, D. & Hughes, D. (1986), Durability of cement sheets reinforced with layers of continuous networks of fibrillated polypropylene film, *in* R. N. Swamy, R. Wagstaffe & D.R.Oakley, eds, 'RILEM Symposium FRC 86 Third International Symposium on Developments in Fibre Reinforced Cement and Concrete', Vol. 2.

Hannant, D. & Zonsveld, J. (1978), 'Polyolefin fibrous networks in cement'.

Hannant, D., Zonsveld, J. & Hughes, D. (1978), 'Polypropylene film in cement based materials', *Composites* pp. 83–87.

Hegger, J., Schneider, H., Sherif, A., Molter, M. & Voss, S. (2004), Exterior Cladding Panels as an Application of Textile Reinforced Concrete, number SP-224, American Concrete Institute, pp. 55–69.

Hegger, J., Sherif, A., Brukermann, O. & Konrad, M. (2004), Textile Reinforced Concrete: Investigations at Different Levels, *in* A. Dubey, ed., 'Thin Reinforced Cement-Based Products and Construction Systems', number SP-224, American Concrete Institute, pp. 33–44.

Hegger, J., Will, N., Bruckermann, O. & Voss, S. (2006), 'Load-bearing behavior and simulation of textile reinforced concrete', *Materials and Structures* **36**, 765–776.

Hein, M. (2001), Historical time line of concrete, Technical Report BSCI 3450, Urburn University Building Science Department.

Hibbert, A. & Hannant, D. (1982), 'Toughness of cement composites containing polypropylene films compared with other fibre cements', *Composites, The International Journal of Science and Technology of Reinforced Materials, Plastics, Cement, Metals, Ceramics* (Specila Issue), 393–399.

Isaia, G., Gastaldini, A. & Moraes, R. (2003), 'Physical and pozzolanic action of mineral additions on the mechanical strength of high-performance concrete', *Cement and Concrete Composites* **25**, 69–76.

Jasper, S., Bush & Henrick, S. (1989), Mechanical behaviour of FRC materials with added micro filler, *in* R. Swamy & B. Barr, eds, 'Fibre Reinforced Cements and Concretes: Recent Developments', University of Wales, Cadiff, pp. 42–49.

Joseph, P., Rabello, M., Mattoso, L., Joseph, K. & Thomas, S. (2002), 'Environmental effects on the degradation behaviour of sisal fibre reinforced polypropylene composites', *Composites Science and Technology* **62**, 13571372.

Kabele, P. (2003*a*), Analytical model of multiple cracking in fibre reinforced cementritious composites under uni-axial tension, *in* 'Internatioanal Conference on Structural Health Monitoring and Intelligent Intrastucture', Tokyo, Japan.

Kabele, P. (2003*b*), 'New developments in analytical modeling of mechanical behavior of ECC', *Journal of Advanced Concrete Technology* **1**(3), 235–264.

Kanakubo, K., Shimizu, K., Katagiri, M., Kanda, T., Fukuyama, H. & Rokugo, T. (2005), Tensile characteristics evaluation of DFRCC-Round Robin test results, Technical report, JCI-TC; RILEM Technical Commitee TC 182 HFC , Hawaii.

Kanda, T., Lin, Z. & Li, V. (2000*a*), 'Modeling of tensile stress-strain relation of pseudo strain hardening cementitious composites', *ASCE Journal of Materials in Civil Engineering* **12**(2), 147–156.

Kanda, T., Lin, Z. & Li, V. C. (2000*b*), 'Tensile stress-strain modeling of pseudostrain hardening cementitious composites', *Journal of Materials in Civil Engineering* **12**(2), 147–156.

Katz, A., Li, V. & Kazmer, A. (1995), 'Bond properties of carbon fibres in cementitious matrix', *Journal of Materials in Civil Engineering* **7**(2), 125–128.

Kayali, O. (2004), 'Effect of high volume fly ash on mechanical properties of fiber reinforced concrete', *Materials and Structures* **37**, 318–327.

Keer, J. & Hannant, D. (1986), The prediction of the load-deflection behaviour of a fibre reinforced cement composite, *in* 'RILEM Symposium', Sheffield.

Kelly, A. (1995), Micromechanics foundations and challenges, *in* 'The Tenth International Conference on Composite Materials: Fatigue and Fracture', Vol. Volume 1, Woodhead Publishing.

Kenai, S. (1994), Tensile, flexural and impact behaviour of ferrocement with chicken wire mesh reinforcement, *in* P. Dedwell & R. Swamy, eds, 'Fifth International Symposium of Ferrocement', Cahpman &Hall: E& FN Spon,, UMIST, Manchester, pp. 343–357.

Kenai, S. & Brooks, J. (1993), Impact and tensile properties of a thin cement sheet reinforced with geotextile meshes, *in* 'Concrete 2000, Economic

and Durable Construction through Excellence', University of Dundee, Scotland, U.K.

Kenai, S., Brooks, J. & Dalton, D. (1987), Properties of polypropylene-mesh reinforced cement composites, *in* 'Fourth International Symposium on Polypropylene Fibres', Nottingham, UK, pp. 51/1–51/6.

Kenai, S., Refai, A. & Brooks, J. (1995), The use of polymer grids as surface reinforcement to plain and reinforced concrete, *in* 'New Development in Concrete Science and Technology', Southeast University, Nanjing, China.

Kim, J., Wu, H., Lin, Z., Li, V., deLhoneux, B. & Akers, S. (1999), 'Micromechanics based durability study of cellulose cement in flexure', *Cement and Concrete Research* **29**, 201–208.

Klos, G. (1975), *Properties and testing of asbestos fibre cement*, Fibre reinforced cement and concrete, RILEM Construction Press.

Konrad, M., Chudoba, R., Butenweg, C. & Brukermann, O. (2003), Textile reinforced concrete part ii: Multilevel modeling concept, *in* 'International Conference on the Applications of Computer Science and Mathematics in Architecture and Civil Engineering', Weimer.

Labour, T., Gauthier, C., Seguela, R., Vigier, G., Bomal, Y. & Orange, G. (2001), 'Influence of the Beta crystalline phase on the mechanical properties of unfilled and $CaCO_3$-filled polypropylene. I. structural and mechanical characterisation', *Polymer* **42**, 7127–7135.

Lewis, R., Sear, L., Wainwright, P. & Ryle, R. (2003), *Advanced Concrete Technology Constituent Materials*, Elsevier.

Li, C. & Mobasher, B. (1998), 'Finite element simulations of fiber pullout toughening in fiber reinforced cement based composites', *Advance Cement Based Materials* **7**, 123–132.

Li, V. (1992), 'Postcracking scaling relations for fiber reinforced cementitious composites', *ASCE Journal of Materials in Civil Engineering* **4**(1), 41–57.

Li, V. C., Wang, S. & Wu, C. (2001), 'Tensile strain-hardening behavior of polyvinyl alcohol engineedre cementitious composites (pva-ecc)', *ACI Materials Journal* **98**(6).

Li, V. C., Wang, Y. & Backer, S. (1991*a*), 'A micromechanical model of tension-softening and bridging toughening of short fiber reinforced brittle matrix composites', *Journal of Mechanics and Physics of Solids* **39**(5), 607–625.

Li, V. & Chan, Y. (1994), 'Determination of interfacial debond mode for fiber-reinforced cementitious composites', *Journal of engineering mechanics* **120**(4), 707–719.

Li, V. & Stang, H. (1997), 'Interface property characterization and strengthening mechanisms in fiber reinforced cement based composites', *Advanced cement based materials* **6**, 1–20.

Li, V., Wang, Y. & Backer, S. (1991*b*), 'A micromechanical model of tension softening and bridging toughening of short random fibre reinforced brittle matrix composites', *Journal of Mechanics and Physics of Solids* **39**(5), 607–625.

Lin, Z. & Li, V. (1997), 'Crack bridging in fiber reinforced cementitious composites with slip-hardening interfaces', *Journal of Physics and Solids* **45**(5), 163–181.

Maage, M. (1978), Fibre bond and friction in cement and concrete, *in* 'Testing and Test Methods of Fiber Cement Composites, RILEM Symposium', The Construction Press, pp. 329–336.

Matsushita, F., Aono, Y. & Shibata, S. (2004), 'Calcium silicate structure and carbonation shrinkage of a tobermorite-based material', *Cement and Concrete Research* **34**, 12511257.

McGovern, M. (2001), 'Concrete technology today', *Portland Cement Association* **22**(3), 1–5.

Metha, P. & Burrows, R. (2001), 'Building durable structures in the 21st century', *The Indian Concrete Journal* pp. 437–443.

Miguel, A. & Amparo, M. (1997), 'Polypropylene fibre reinforced mortar mixes: Optimization to control plastic shrinkage', *Composites, Science and Technology Journal* **57**, 655–660.

Mills, N. (1986), *Plastics, Microstructure, Properties and Applications*, Edward Arnold.

Moore, E. (1996), *Polypropylene Handbook*, Hunser Publishers.

Moropoulou, A., Bakolas, A. & Anagnostopoulou, S. (2005), 'Composite materials in ancient structures', *Cement and Concrete Composites* **27**, 295–300.

Mu, B., Meyer, C. & Shimanovich, S. (2002), 'Improving the interface bond between fiber mesh and cementitious matrix', *Cement and Concrete Research* **32**, 783–787.

Mumenya, S., Tait, R. & Alexander, M. (2003), Textile concrete, characterisation of a new ductile material, *in* 'Second MRS Conference, University of Witwatersrand, Johannesburg, South Africa'.

Mumenya, S., Tait, R. & Alexander, M. (2006), An appropriate specimen geometry for direct tensile testing of Textile Concrete, *in* 'Young Engineers Conference, Midrand, South Africa'.

Naaman, A., Namur, G., Alwan, J. & Najm, H. (1991*a*), 'Fiber pullout and bond slip i: Analytical study', *Journal of structural engineering* **117**(9), 2769–2790.

Naaman, A., Namur, G., Alwan, J. & Najm, H. (1991*b*), 'Fiber pullout and bond slip ii: Experimental validation', *Journal of structural engineering* **117**(9), 2791–2800.

Naaman, A. & Reinhardt, H. (2004), 'High performance fiber reinforced cement composites HPFRCC-4: International workshop ann arbor, michigan', *Cement and Concrete Composites* **26**, 754–759.

Naaman, A. & Reinhardt, H. (2006), 'Proposed classification of HPFRC composites based on their tensile response', *Materials and Structures* **39**, 547–555.

Nehdi, M., Duquette, J. & Damatty, A. (2003), 'Performance of rice husk ash produced using a new technology as a mineral admixture in concrete', *Cement and Concrete Research* **33**, 1203–1210.

Neville, A. (1971), 'Hardened concrete: Physical and mechanical aspects', *American Concrete Institute* .

Neville, A. (2002), *Properties of Concrete*, 4th edn, Prentice Hall.

Owens, G. (2002), 'Concrete trends - annual cement and concrete review', *Journal of Cement and Concrete Institute* pp. 4–11.

Pala, M., Ozbay, E., Oztas, A. & Yuce, M. (2005), 'Appraisal of long-term effects of fly ash and silica fume on compressive strength of concrete by neural networks', *Construction and Building Materials* **Article in Press**, 1–11.

Papadakis, V., Vayenas, C. & Fardis, M. (1991), 'Physical and chemical characteristics affecting the durability of concrete', *ACI Materials Journal* **88**(2), 186–196.

Park, C., Noh, M. & Park, T. (2005), 'Rheological properties of cementitious materials containing mineral admixtures', *Cement and Concrete Research* **35**, 842–849.

Pei, M., Wang, D., Hu, X. & Xu, D. (2000), 'Synthesis of sodium sulfanilate-phenol-formaldehyde condensate and its application as a superplasticizer in concrete', *Cement and Concrete Research* **30**, 1841–1845.

Perrie, B. & Butler, R, J. (1994), *Fulton's Concrete Technology*, Portland Cement Institute, Midrand, South Africa.

Rendell, F., Jauberthie, R. & Grantham, M. (2002), *Deteriorated Concrete Inspection and physicochemical analysis*, Thomas Telford.

Richardson, I. & Cabrera, J. (2000), 'The nature of C-S-H in model slag-cements', *Cement and Concrete Composites* **22**, 259–266.

Richter, M. & Zastrau, B. (2006), 'On the nonlinear elastic properties of textile reinforced concrete under tensile loading including damage and cracking', *Materials Science and Engineering A* pp. 278–284.

SABS Method 1245 (1994), *Potential Reactivity of Aggregates With Alkalis (Accelerated Mortar Prism Method).*

Sahmaran, M. & Yaman, O. (2005), 'Hybrid fiber reinforced self compacting concrete with a high-volume coarse fly ash', *Construction and Building Materials* **On line edition**.

Salicimen, H., Shameem, M., Barry, M., Ibrahim, M. & Abbasi, T. (2003), 'Durability of proprietary cementitious materials for use in wastewater transport systems', *Cement and Concrete Composites* **25**(4-5), 421–427.

SANS 5863 (SABS SM 863 1994) (2006), *860-2: Specifications for Cube Test Apparatus and Test Procedures.*

Savastano, H., Warden, P. & Coutts, R. (2003), 'Potential of alternative fibre cements as building materials for developing areas', *Journal of Cement and Concrete Composites* **25**(6), 585–592.

Savastano, H., Warden, P. & Coutts, R. (2005), 'Microstructure and mechanical properties of waste fibre-cement composites', *Cement and Concrete Composites* **27**, 583–592.

Scrivener, K., Cabiron, J. & Letourneux, R. (1999), 'High-performance concretes from calcium aluminate cements', *Cement and Concrete Research* **29**, 1215–1223.

Segre, N., Tonella, E. & Joekes, I. (1998), 'Evaluation of stability of polypropylene fibres in environments aggressive to cement-based materials', *Cement and Concrete Research* **28**, 75–81.

Skoczylas, F., Burlion, N. & Yurtdas, I. (2007), 'About drying effects and poro-mechanical behaviour of mortars', *Cement & Concrete Composites* .

Stutzman, P. (2004), 'Scanning electron microscopy imaging of hydraulic cement microstructure', *Cement and Concrete Composites* **26**, 957–966.

Subramanian, V. & Madhavan, N. (2005), 'Asbestos problem in India', *Lung Cancer* **49S1**, S9–S12.

Swaddiwudhipong, S., Lu, H. & Wee, T. (2003), 'Direct tension test and tensile strain capacity of concrete at early age', *Cement and Concrete Research* **33**, 2077–2084.

Swamy, R. (1980), 'Influence of slow crack growth on the fracture resistance of fibre cement composites', *The International Journal of Cement Composites* **Vol. 2, No.1**, 43–53.

Swamy, R. & Falih, F. (1985), Development of a small aggregate concrete for structural similitude of slab-column connections, *in* 'Design of Concrete Structures', Elsevier Applied Science Publishers, pp. 25–34.

Swamy, R. & Hussin, M. (1986), Effect of curing conditions on the tensile behaviour of fibre cement composites, *in* 'RILEM Symposium, Developments in Fibre Reinforced Cement and Concrete', Vol. 1, RILEM Publications.

Swamy, R. & Hussin, M. (1989), Woven polypropylene fabrics- an alternative to asbestos for thin sheet applications, *in* R. Swamy & B. Barr, eds, 'International conference on fibre reinforced concrete', University of Wales, Cardiff, UK, pp. 90–99.

Swift, D. & Smith, R. (1978), Sisal fibre reinforcement of cement paste and concrete, *in* 'International Conference on Building Materials', Bangkok.

Szabo, L., Hidalgo, I., Ciscar, J. & Soria, A. (2006), 'CO_2 emmission trading within the European Union and Annex B countries: the cement industry case', *Energy Policy* **34**, 72–87.

Tait, R. & Akers, S. (1989), 'Micromechanical studies of fresh and weathered fibre cement composites. part 2: Wet testing', *The International Journal of Cement Composites and Lightweight Concrete* **11**(2), 125–131.

Tait, R. & Guddye, C. (2002), Textile concrete-mechanical characterisation of a unique fibre system for cement composites, *in* 'Concrete for 21st Century Conference', Johannesburg.

Tait, R., Mumenya, S., Alexander, M. & Hourahane, D. (2004), Textile composite concrete provides special architectural and permanent shuttering opportunities, *in* 'Conference Proceedings, Developing Concrete to Serve Practical Needs', Mindrand, South Africa, pp. 281–288.

Takahashi, K., Case, B., Dufresne, A., Fraser, R., Higashi, T. & Siemiatycki, J. (1994), 'Relation between lung asbestos fibre burden and exposure

indices based on job history', *Occupational and Environmental Medicine Online* **51**, 461–469.

Taylor, H. (1997*a*), *Cement Chemistry*, Thomas Telford Publishing.

Taylor, J. (1997*b*), *An Introduction to Error Analysis*, 2nd edn, University Science Books, Sausalito, Califonia.

Taylor, P., Mostert, H. & Hourahane, D. (1997), The evolution of cellular cement mortar fibre and fabric for reinforced precasts in South Africa, *in* 'ACI Spring Conference', Seattle.

Van Mier, J. & Van Vliet, M. (2002), 'Uniaxial tension test for the determination of fracture parameters of concrete:State of the Art', *Engineering Fracture Mechanics* **69**, 235–247.

Vittone, A. (1986), Industrial development of the reinforcement of cement based products with fibrillated polypropylene networks as replacement of asbestos, *in* 'RILEM Symposium, Developments in Fibre Reinforced Cement and Concrete'.

Wang, S. & Li, V. (2003), Tailoring of pva fibre/matrix interface for engineered cementitious composites (ECC), *in* M. ACar, ed., 'Fibre Society Conference: Engineered with Fibres', Loughborough, pp. 91–92.

Wang, Y., Backer, S. & Li, V. C. (1988), 'A special technique for determining the critical length of fibre pull-out from a cement matrix', *Journal of Materials Science Letters* **7**, 842–844.

Wang, Y., Li, V. & Backer, S. (1988), 'Modelling of fibre pullout from a cement matrix', *International Journal of Cement Composites and Lightweight Concrete* **10**, 143–149.

Wang, Y., Li, V. & Backer, S. (1990), 'Tensile properties of synthetic fiber reinforced mortar', *Cement and Concrete Composites* **12**, 29–40.

Wee, T., Matsunaga, Y.and Watanabe, Y. & Sakai, E. (1995), 'Production and properties of high strength concretes containing various mineral admixtures', *Cement and Concrete Research* **25,No. 4**, 709–714.

Wiliams, L. (1975), *Polymer Engineering*, Elsevier.

World Wide Web (2006*a*), 'The meteorogical department, nairobi, kenya: http://www.meteo.go.ke/customer/climat/index.html'.

World Wide Web (2006*b*), 'South african weather service: http://www.weathersa.co.za/climat/climstats/capetownstats.jsp'.

World Wide Web (2006*c*), 'Standerton mills: http://www.cottonafrica.com'.

World Wide Web (2006*d*), 'Textile concrete consultants: http://www.textileconcreteconsultants.com/news.html'.

World Wide Web (2007), 'Micro concrete roofing tiles: http://www.dainet.org/enterprise/mcr.htm'.

Xu, G., Magnani, S., Mesturini, G. & Hannant, D. (1996), 'Hybrid polypropylene glass cement corrugated sheets', *Composites Part A* pp. 459–466.

Yang, J. & Fischer, G. (2005), Investigation of the fiber bridging stress-crack opening relationship of Fiber Reinforced Cementitious Composites, Technical report, RILEM Technical Commitee TC 182, Hawai.

Zhandarov, S. & Mader, E. (2005), 'Characterization of fibre/matrix interface strength:applicability of different tests, approaches and parametersitives', *Composites Science and Technology* **65**, 149–160.

Appendices

Appendix A

A.1 Preliminary Characterisation of Textile Concrete

Figure A.1: Configuration of three-point bending test

Failure was characterized by multiple cracking as shown in Fig.A.2. The 28 days flexural behaviour of textile concrete is given in Fig.A.3 and Fig.A.4.

The crack spacing of textile concrete specimens varied with the textile specification, and the amount of pressure applied during production. This is illustrated by Fig.A.5.

Figure A.2: Multiple cracks after specimen failure

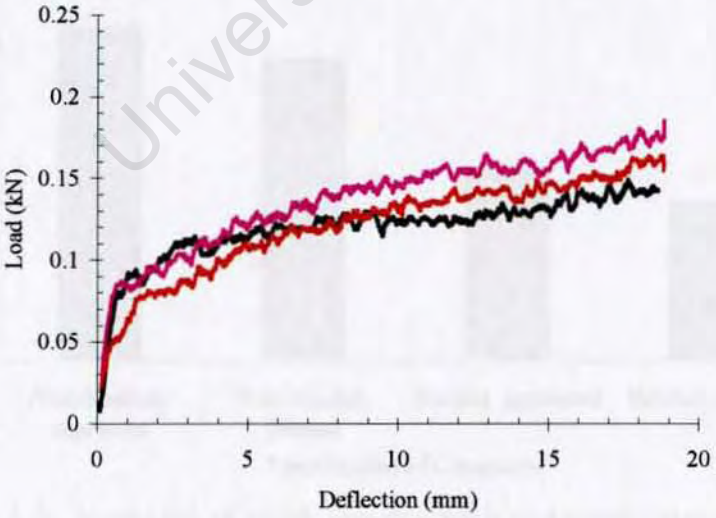

Figure A.3: Unbonded and pressed specimens

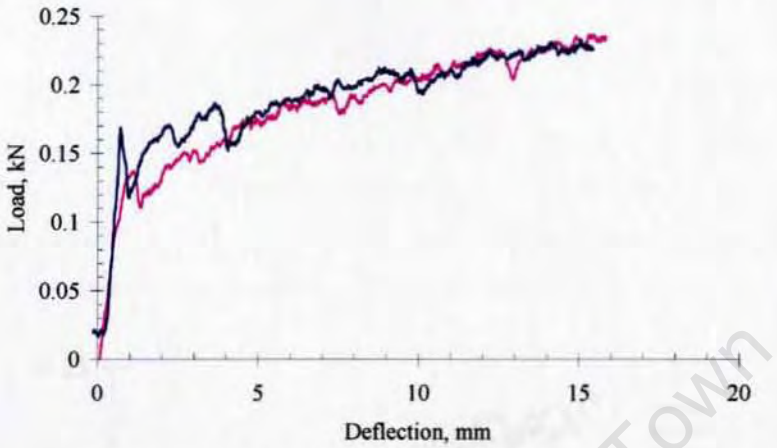

Figure A.4: Bonded and pressed specimens

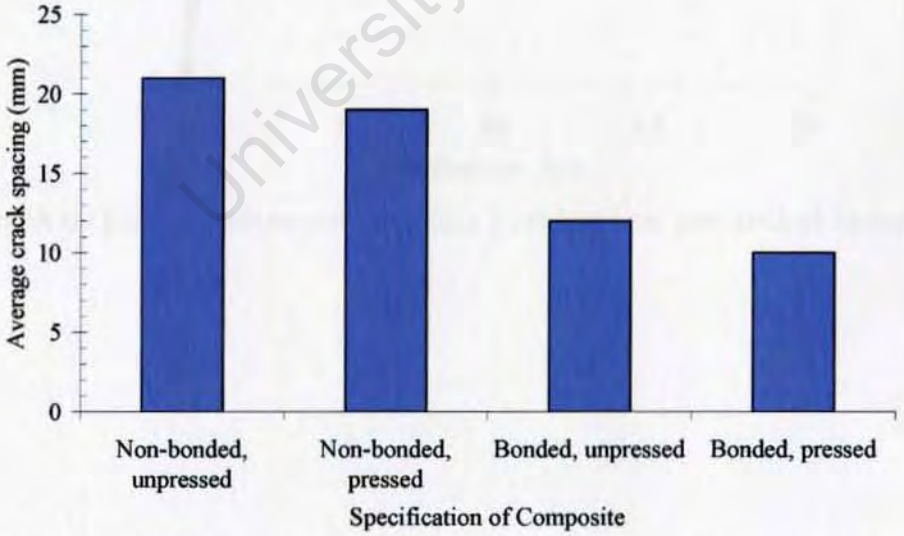

Figure A.5: Variation of crack spacing with composite specification

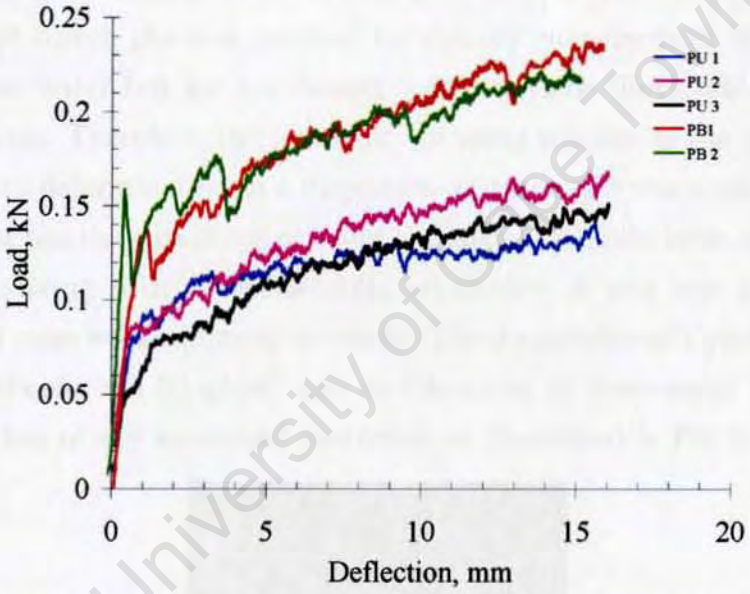

Figure A.6: Effect of ultrasonic bonding (welding) on mechanical behaviour

A.2 Density of Polypropylene Fibres

The physical properties of fibres are conventionally characterised by density, cross-sectional area, or mass per unit length. For polypropylene fibres, the cross-sectional dimensions could not be determined accurately from direct measurements using a micrometer or vernier due to the fibrillated nature of the yarn. Moreover, the presence of fine fibrils spun round the inner tape made direct measurements of the cross-sectional dimensions imprecise. Therefore, a volume displacement-based method was devised to indirectly measure the fibre density. The water displacement method is the most commonly used direct physical method for density measurement of materials denser than water but for low density polypropylene fibres, the method is inappropriate. Therefore, the possibility of using silicone as the medium for fibre density determination in a displacement technique was explored.

Silicone has the advantage of being available in a liquid form, it is viscous and after mixing with an accelerating admixture, it sets into a uniformly dense solid mass with minimum air voids. The manufacturer's quoted density of liquid silicone is 1.00 g/cm^3 and in this state, it flows easily infiltrating the interstices of any embedded materials, as illustrated in Fig A.7.

Figure A.7: Fibrils through a section of a "silicone-fibre" specimen

Silicone sets after approximately 12 hours. Due to its many advantages,

silicone was considered as the appropriate material to use for estimation of fibre density, and therefore, a simple test was devised.

The first step in the test involved casting regular shaped "silicone-only" control specimens in identical moulds for estimation of the density of plain silicone in the hardened state (ρ_{si}). The moulds were in form of circular rings of internal and external diameters 25.6 mm and 44.5 mm respectively, which were cored out of a rigid plastic mould. The mould had a nominal thickness of approximately 14 mm and had provision for a smooth flat base. Silicone and the accelerating admixture were firstly mixed in a syringe after which the moulds were evenly filled with the viscous mixture. The specimens were allowed to set undisturbed for approximately 12 hours after which they were carefully removed from the moulds. Fig. A.8 shows a "silicone-only" control specimen after removal from the mould.

Figure A.8: Typical silicone specimen

The thickness of each specimen was measured after setting and the mass was taken. The average thickness for the "silicone-only" control specimens was 13.40 mm. Since the specimen was denser than water, the volume of the specimens was easily measured using conventional water displacement technique. The average volume of the "silicone-only" specimens was 14.77 and therefore, the average density of plain silicone in the hardened state was estimated as 1.050 g/cm^3 with a standard deviation from the mean of 0.013 g/cm^3. Fibres were also weighed on a scale with an accuracy of 10^{-6} g and

the average mass obtained from the masses of ten pieces. The average mass for the non-bonded types of fibres was approximately 0.286 g, and for the bonded type, the average mass was 0.349. The masses for the non-bonded and bonded types of fibre had standard deviations from the mean of 0.005g and 0.008 g respectively.

The contribution of the fibres to the specimen density was determined from the weight of composite silicone rings that were cast with inclusions of fibres of pre-determined length and mass. For each specimen, three fibres were found to be optimum for casting the composite "silicone-fibre" specimens mainly due to the small volume of the specimens. In addition, for a significant difference between the two specimen types, it was important that the embedded mass of the fibres be as high as possible.

To cast the composite specimens, the plastic moulds were carefully lined with three fibres of total length of three metres and mass of approximately 0.858 g. The moulds were then filled with the silicone/accelerator mixture using a syringe while gently tapping the sides for the moulds to ensure effective infiltration of the fibres with the silicone mixture. The composite was thereafter allowed to set for 24 hours, and since the cast-in mass of non-bonded fibres was known, its contribution to the density of the specimen could easily be estimated. Any differences in the masses of the two types of specimens was attributed to the presence of fibres and not due to statistical errors. Fig. A.9 shows the composite "silicone-fibre" specimen before removal from the mould.

After setting, the mass and volume of each specimen was taken. For five "silicone-fibre" specimens, the average mass and volume were 15.801 g and 15.095 cm^3 respectively, hence the density of the composite specimen was 1.047 g/cm^3 with a standard deviation from the mean of 0.047 g/cm^3. As would be expected, the presence of fibres reduced the density of the control specimen by approximately 0.030 g/cm^3. Since the densities of the "silicone-only" (ρ_{si}) and "silicone-fibre" (ρ_{si+f})were known from the test, the volume and density (ρ_f)of the fibre were calculated. ρ_f was evaluated as

Figure A.9: Silicone-fibre specimen inside a mould

approximately 0.94 g/cm^3.

A.3 Calibration of the Mechanical Mixer

Table A.1: Mixer rotating about the bowl axis

Test No.	For each speed range time taken in seconds, per 100 revolutions about the bowl axis		
	Position 1	Position 2	Position 3
1	86	81	44
2	82	73	44
3	86	82	45
4	82	81	45
5	82	81	44
6	83	81	44
7	81	81	45
Average time, s	83	80	44
Average speed, revolutions/second	1.20	1.25	2.27

Table A.2: Mixer revolving about the hook axis

Test No.	For each speed range time taken in seconds, per 100 revolutions about the bowl axis		
	Position 1	Position 2	Position 3
1	31	32	57
2	41	43	76
3	35	36	65
4	38	39	70
5	38	39	70
6	38	39	70
7	38	39	70
Average time, s	37	38	69
Average speed, revolutions/second	2.7	2.8	5

A.4 Flow of Fresh Mortar

Table A.3: Flow of mortar

Time		Mix type								
Mixing time, s	Time at test, min.	1	2	3	4	5	6	7	8	9
30	0	144	172	140	155	150				
	15	127	149	114	124	124				
	30	121	143	108	119	116				
	45	116	140	105	115	110				
60	0	140	143	147	147	145	143			
	15	120	124	137	137	115	120			
	30	110	118	132	132	109	112			
	45	105	115	125	125	105	105			
120	0	165	172	160	155	150	149	150	158	149
	15	143	152	149	145	138	137	139	146	136
	30	136	148	143	140	133	134	136	142	133
	45	132	145	140	136	130	127	132	132	130

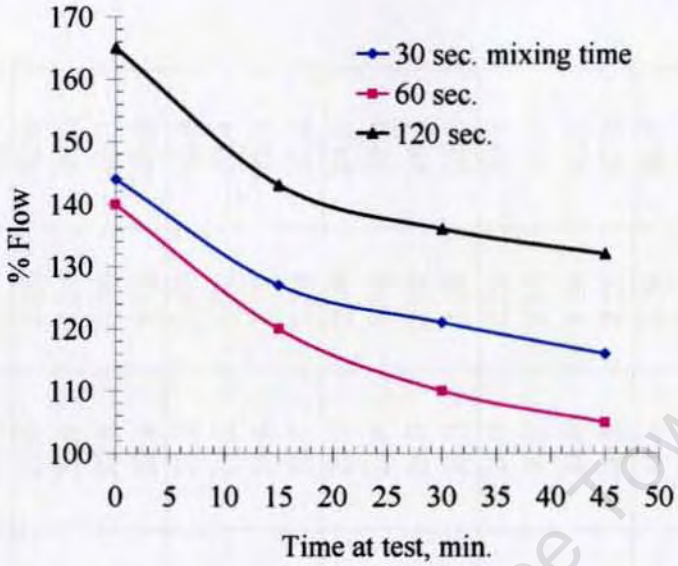

Figure A.10: Flow of mix type 1

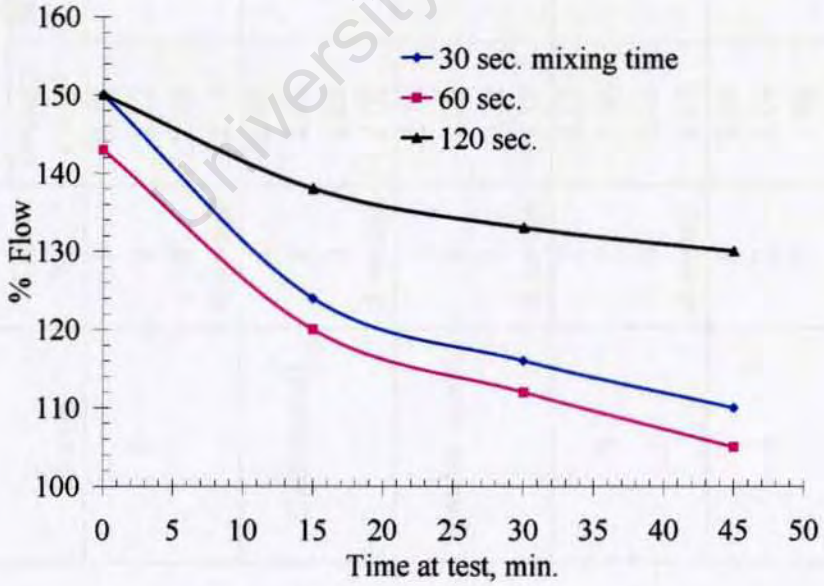

Figure A.11: Flow of mix type 5

Table A.4: Early age cube crushing strength of mortar

Mortar	Test No.	3 Days		7 Days		28 Days	
		Density, g/cm^3	Strength, MPa	Density, g/cm^3	Strength, MPa	Density, g/cm^3	Strength, MPa
1	1	2.16	14.4	2.16	20.8	2.20	40.0
	2	2.12	14.4	2.16	23.6	2.16	40.0
	3	2.16	14.0	2.24	22.8	2.20	40.0
	Average	2.14	14.4	2.18	22.4	2.18	40.0
2(air cured)	1	2.08	7.2	2.16	17.2	2.00	36.4
	2	2.04	6.4	2.16	17.2	1.92	32.4
	3	2.04	7.2	2.04	15.6	1.92	32.4
	Average	2.06	6.9	2.11	16.7	1.94	33.6
2(water cured)	1	2.16	13.2	2.00	25.2	2.08	24.8
	2	2.22	14.0	2.04	24.8	1.92	32.0
	3	2.22	12.0	2.00	26.0	2.00	28.4
	Average	2.18	13.1	2.04	25.3	2.00	28.4
3	1	2.12	20.0	2.12	28.0	2.16	50.0
	2	2.08	18.8	2.12	30.0	2.16	49.6
	3	2.12	18.8	2.16	34.0	2.16	45.6
	Average	2.14	19.2	2.14	30.8	2.20	47.2
4	1	2.04	10.4	2.08	18.8	2.04	36.0
	2	2.04	10.0	2.08	20.8	2.08	32.0
	3	2.08	12.0	3.12	22.8	2.08	37.6
	Average	2.05	10.8	2.09	20.8	2.06	35.2

A.5 Cube Crushing Strength

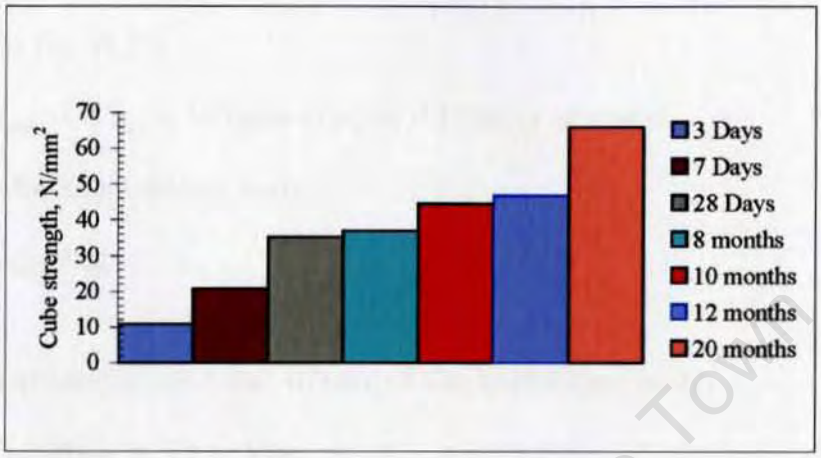

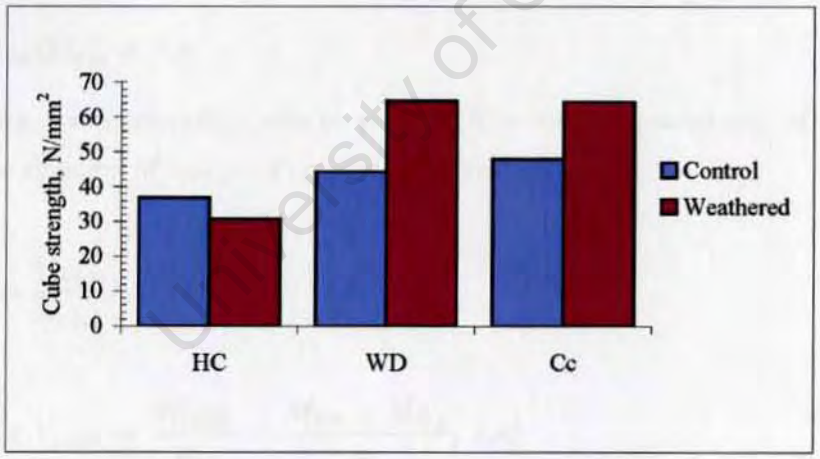

Figure A.12: Cube crushing strength of mix type 4 at different ages

A.6 Determination of Porosity

$$\text{Up thrust} = \mathrm{W}_{sat} - \mathrm{W}_{sus} \tag{A.1}$$

From Eq. A.1,

$$\mathrm{W}_{sat} - \mathrm{W}_{sus} = \text{Volume of solid} \times \text{Density of water} \tag{A.2}$$

But for a suspended body,

$$\mathrm{W}_{sat}\text{-}\mathrm{W}_{sus} \tag{A.3}$$

also quantifies the total volume of the submerged body:

$$\mathrm{W}_{sat}\text{-}\mathrm{W}_{sus} = \mathrm{V}\gamma = \mathrm{V}g\rho \tag{A.4}$$

Therefore, for a given body suspended in water,

$$\mathrm{M}_{sat}\text{-}\mathrm{M}_{sus} = \mathrm{V}\rho_w \tag{A.5}$$

where, g=acceleration due to gravity, V= volume,ρ=density of the fluid and ρ_w= density of water. Porosity, η is defined as:

$$\eta = \frac{V_{voids}}{V_{total}} \tag{A.6}$$

$$\text{But,} V_{voids} = \frac{M_{voids}}{\rho_w} = \frac{M_{sat} - M_{dry}}{\rho_w}, \text{ and} \tag{A.7}$$

$$\mathrm{V}_{total} = \frac{M_{sat} - M_{sus}}{\rho_w} \tag{A.8}$$

Therefore, porosity,

$$\begin{aligned} \eta = \frac{V_{voids}}{V_{total}} &= \frac{M_{sat} - M_{dry}}{\rho_w} \div \frac{M_{sat} - M_{sus}}{\rho_w} \\ &= \frac{M_{sat} - M_{dry}}{M_{sat} - M_{sus}} \end{aligned} \tag{A.9}$$

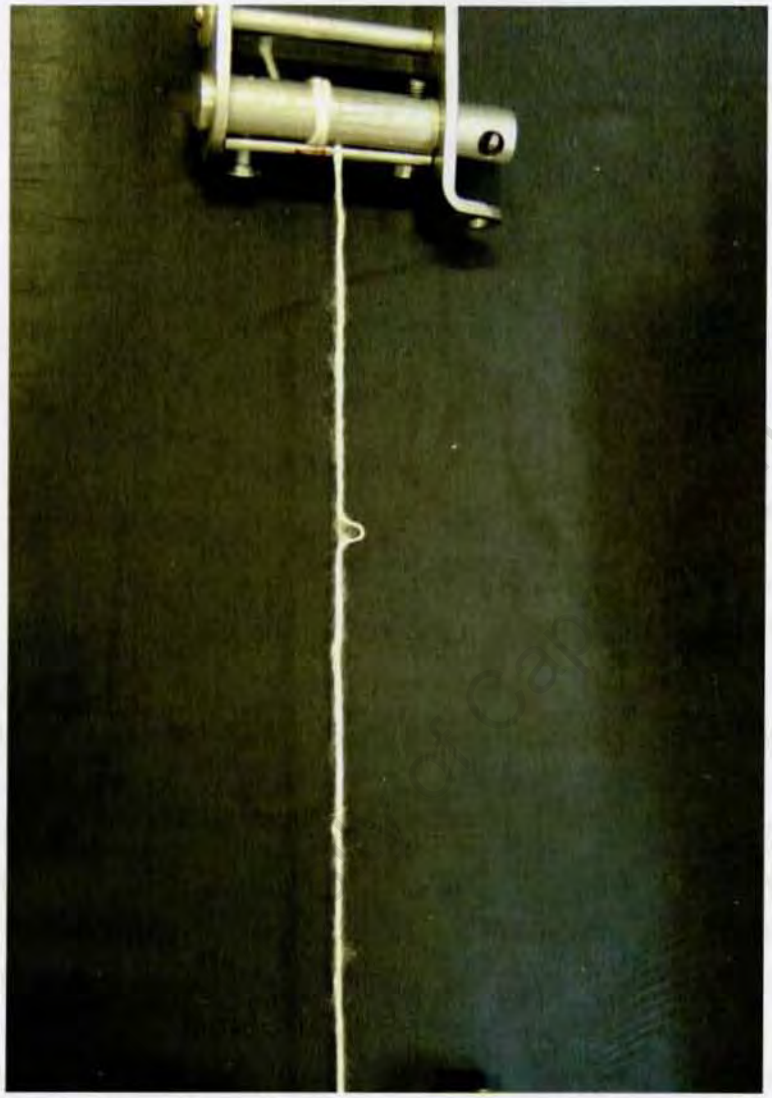

Figure A.13: A single fibre in tension showing behaviour of fine fibrils before failure

A.7 Wetting and Drying Studies

Preliminary trials were firstly carried out to determine the extent of wetting and drying of the specimens using basic physical techniques; for wetting, submersion in water; and for drying, using an oven at 50°C. Specimens were sufficiently wetted after 15 minutes of complete submersion in water. At the wet state, a moisture content of approximately 8 per cent for the composites

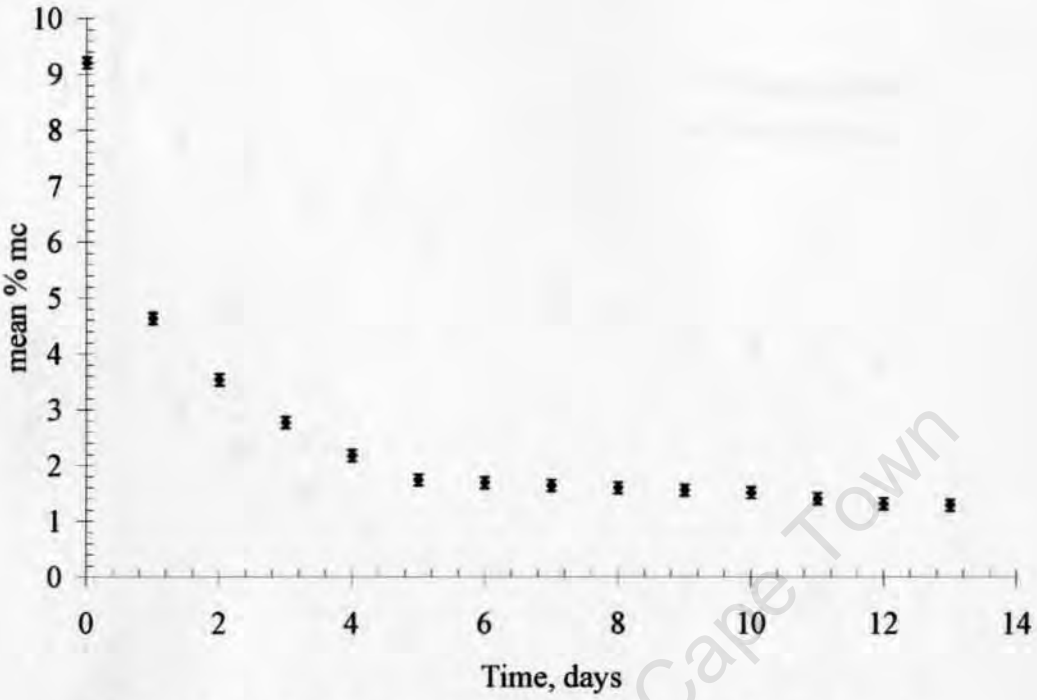

Figure A.14: Air drying characteristics for tensile specimens

and 12 per cent for the pullout specimens was achieved. "Wetness" of the specimens was therefore defined as the moisture content of at least 8 per cent for the laminates, and 12 per cent for the pullout specimens. Drying was investigated by exposing ten specimens to an open environment for 13 hours at ambient temperature of 24^{o}C. The open air drying rate over a 13 hour period is shown by Fig. A.14. As would be expected drying of in cementitious materials is a much slower process than wetting. It was therefore necessary to accelerate the drying process and to do this, further investigations were carried on oven drying. As expected, oven drying at 50^{o}C was much faster than than air drying. Oven drying for 13 hours at 50^{o}C reduced the specimens' moisture content to approximately 2.5 per cent. Therefore, this was taken as the lower limit of "dryness" of the specimens.

There was the concern that oven drying would damage the specimens. Therefore, vacuum drying was investigated. Vacuum drying was carried out in a 0.05 m^3 capacity vacuum chamber with approximately 500 g of silica gel

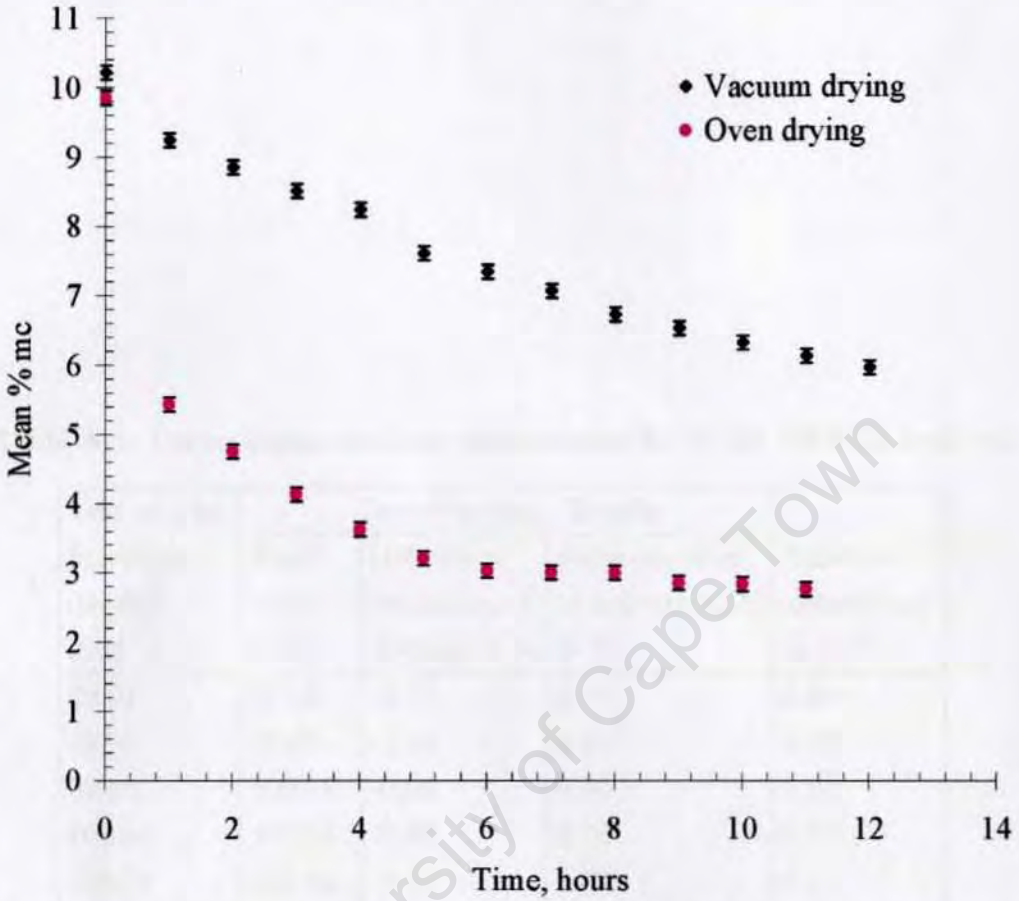

Figure A.15: Comparative of vacuum and oven drying for tensile specimens

crystals placed at the bottom. A vacuum of -100 kPa was then drawn and maintained for eight hours. This dried the specimens at a rate much higher than air drying but the rate was however, still half of oven drying as shown in A.15. For all specimens investigated, a moisture content reduction of over 70 per cent was achieved after five hours of vacuum drying, a level that was not achievable through open air drying for the same period.

Table A.5: Uncertainties in force measurement by 10 kN ZWICK load cell

Test results:	Test direction: Tensile			
Machine display in N	Real value in N	Relative deviation of display in %	Relative error of repeatability in %	Relative uncertainty in ± %
39.93	40.00	-0.18	0.04	0.35
49.95	50.00	-1.10	0.20	0.33
99.94	100.00	-0.06	0.04	0.23
100.00	100.09	-0.09	0.04	0.15
200.00	200.14	-0.07	0.07	0.12
500.00	499.77	0.05	0.00	0.12
1000.00	999.47	0.05	0.01	0.12
2000.00	1998.73	0.06	0.01	0.12
2000.00	1999.17	0.04	0.01	0.12
4000.00	3997.74	0.06	0.00	0.12

Appendix B

Microstructural Studies

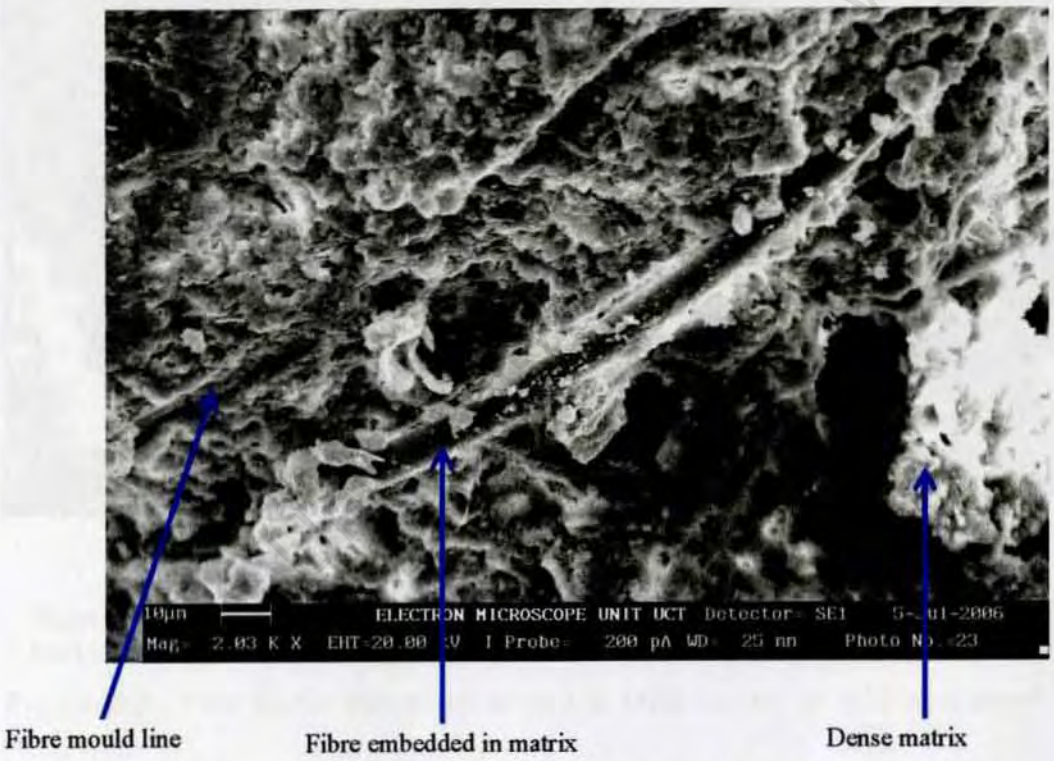

Figure B.1: Dense matrix and mould mark on NM-weathered surface

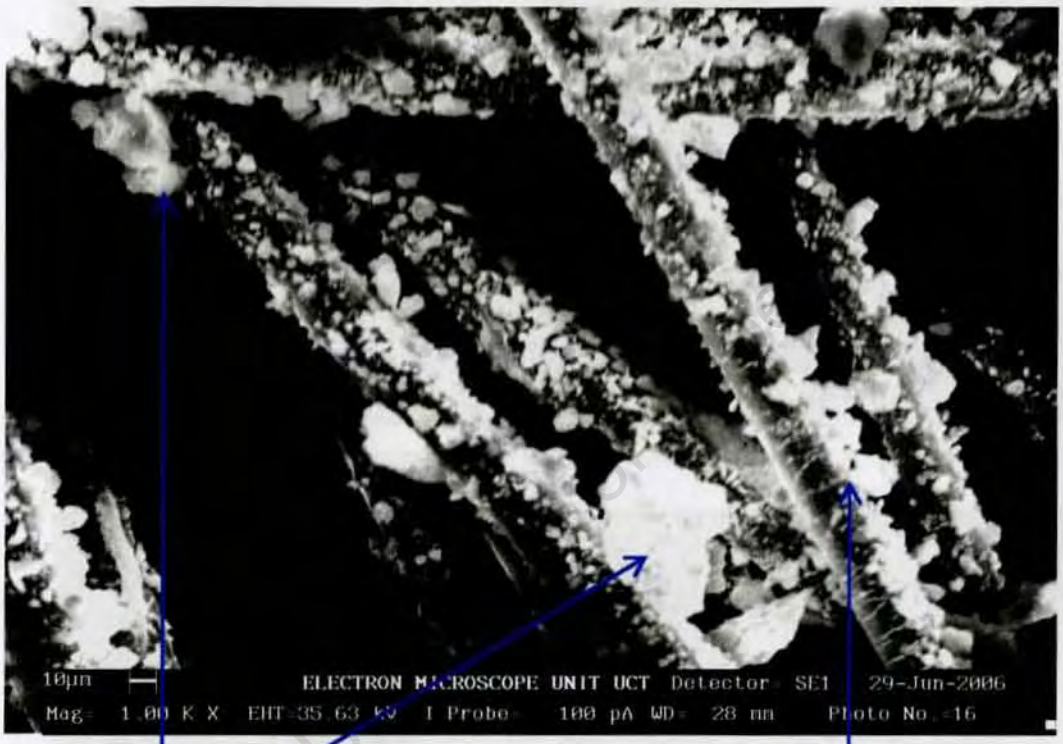

Figure B.2: Fine fibrils debonded from the bulk matrix in NM-weathered composite

Figure B.3: Enlarged view of fine fibrils illustrating separation from matrix

Figure B.4: Fibre pull-out test specimen with a matrix lump on a fibril